

**Best
Available
Copy**

UNCLASSIFIED

AD 257 824

*Reproduced
by the*

**ARMED SERVICES TECHNICAL INFORMATION AGENCY
ARLINGTON HALL STATION
ARLINGTON 12, VIRGINIA**



UNCLASSIFIED

NOTICE: When government or other drawings, specifications or other data are used for any purpose other than in connection with a definitely related government procurement operation, the U. S. Government thereby incurs no responsibility, nor any obligation whatsoever; and the fact that the Government may have formulated, furnished, or in any way supplied the said drawings, specifications, or other data is not to be regarded by implication or otherwise as in any manner licensing the holder or any other person or corporation, or conveying any rights or permission to manufacture, use or sell any patented invention that may in any way be related thereto.

257824

TRANSLATION

HYDRAULICS OF GAS-LIQUID SYSTEMS

By S. S. Kutateladze and M. A. Styrikovich

September 1960

305 Pages

AD No. —
ASTIA FILE COPY

FILE COPY

Return to

ASTIA

ARLINGTON HALL STATION
ARLINGTON 12, VIRGINIA

Attn: TISS

N-61-3-Y

XEROX

17575

\$19.75

PREPARED BY
LIAISON OFFICE
TECHNICAL INFORMATION CENTER
MCLTD
WRIGHT-PATTERSON AIR FORCE BASE, OHIO

F-TS-9814/V

ASTIA

JUN 20 1961

TPOR

This translation was prepared under the auspices of the Liaison Office, Technical Information Center, Wright-Patterson AFB, Ohio. The fact of translation does not guarantee editorial accuracy, nor does it indicate USAF approval or disapproval of the material translated.

Comments pertaining to this translation should be addressed to:

**Liaison Office
Technical Information Center
MCLTD
Wright-Patterson Air Force Base, Ohio**

S. S. Kutateladze and M. A. Styrikovich

GIDRAVLIKA GASO-ZHEIDKOSTIYKH SISTEM

Gosudarstvennoye Energeticheskoye Izdatel'stvo

Moscow

1958

Leningrad

232 pages

P-TS-9814/V

AN is made

~~The present book is the first attempt~~ at a systematic description of the most essential laws governing the combined motion of a gas and a liquid. As a basic subject of research, the problems considered are: the motion of a gas-liquid mixture in pipes, bubbling, atomization of a liquid by mechanical and pneumatic spray nozzles, critical regimes of boiling, and several other problems.

The book is designed for scientific workers, engineers, and students specializing in the fields of physical-heat engineering, power engineering, hydromechanics, chemical processes, and equipment.

Samson Semenovich Kutadeladze and Mikhail Adol'fovich Styrikovich

HYDRAULICS OF GAS-LIQUID SYSTEMS

Editor: L. A. Vitman

Technical Editor: A. A. Zabrodina

FOREWORD

The engineering fields in which we often must deal with the combined motion of a gas and a liquid are very extensive, and their number continues to increase. Numerous operations in power-engineering, chemical, metallurgic, and other equipment give rise to gas-liquid mixtures, or are based on their utilization. Related to this type of process are: motion of vapor-liquid mixtures in the tubes of steam boilers and in various heat exchange equipment; motion of gas-liquid mixtures in gas lifts (air lifts); atomization of a liquid by spray nozzles; operation of various types of bubblers, wetted-wall towers, and other equipment directly contacting gases and liquids; breakup and entrainment of a liquid by a stream of gas, etc.

All these and other problems of the hydraulics of two-phase flow have received comparatively extensive treatment only during the last 15 to 20 years, when the urgent need arose in engineering (above all in thermal-power engineering, and the petroleum and chemical industries) for a rapid and sufficiently accurate solution of the computational problems of the above-mentioned and other processes, and after the basic methods of their investigation had been developed.

The material now accumulated in this field is so large that we may speak of a new broad field of hydrodynamics: the hydraulics of two-phase flow. To a considerable or, more accurately, a major degree, this field of hydrodynamics originated and develops through

the efforts of Soviet scientists and engineers.

During the last 25 years, the authors participated in the formulation and development of the problem under consideration. The present book is, to a certain extent, an account of that approach to the investigation and the calculation of flows of gas-liquid systems, which they developed in their own works as well as in the works of their collaborators, mainly at the Tsentral'nyy Kotloturbinnyy Institut im. I. I. Polzunov (I. I. Polzunov Central Turbine and Boiler Institute), at the Energeticheskiy Institut im. G. M. Krzhizhanovskiy AN SSSR (G. M. Krzhizhanovskiy Power Engineering Institute of the USSR Academy of Sciences), and at the Moskovskiy Energeticheskiy Institut (Moscow Power Engineering Institute).

At the same time, the authors used the material of other research workers studying the field in question (D. F. Peterson, A. A. Armand, V. G. Levich, S. G. Teletov, O. M. Baldina, K. F. Poddatis, B. D. Katsnel'son, L. A. Vitman, and others). In addition to purely hydraulic problems, the book also deals with several heat-transfer problems closely associated with the peculiarities of motion in two-phase flows.

In this attempt to write the first monograph on the hydraulics of gas-liquid systems, the authors did not cover as fully as possible all the specific solutions available at the present time. The basic aim of the book is to formulate the problem as a whole on the basis of a certain general method of investigation of this kind of process and an examination of a series of problems sufficiently general in character.

The specific problem of motion of a gas and a liquid in porous bodies, developed in the works of L. S. Leybenzon and others, is not

considered here.

The bibliography at the end of this book lists reference sources pertaining to the topics touched upon here, as well as to the contiguous problems we have not considered.

V. N. Moskvicheva, candidate of technical sciences, to whom the authors express their gratitude, participated in the preparation of the manuscript for publication.

The authors are also grateful to the reviewer of the manuscript, V. G. Levich, and the editor, L. A. Vitman.

The authors will be indebted to those readers who find it possible to send to the Editors (Leningrad, Marsovo Pole 1, L/O Gosenergoizdata) their advice, comments, and wishes with respect to this book.

The Authors

FUNDAMENTAL NOTATIONS

l [m]	linear dimension
δ [m]	thickness
Ω [m ²]	cross-sectional area of flow
F [m ²]	surface area wetted by the flow
V [m ³]	volume
τ [sec]	time
τ [kg-force/m ²]	tangential stress
σ_n [kg-force/m ²]	normal stress
p [kg-force/m ²]	pressure
t, T [°C, °K]	temperature
w [m/sec]	velocity
w'_0 [m/sec]	reference velocity of heavy phase
w''_0 [m/sec]	reference velocity of light phase
$w_m = w'_0 + w''_0$	"velocity of mixture"
$w_0 = w'_0 + \frac{\gamma''}{\gamma'} w''_0$	flow velocity of two-phase stream ("velocity of circulation")
$v^* = \sqrt{\frac{\tau}{\rho}}$	"velocity of tangential stress"
\dot{Q} [kg/sec]	mass flow rate
q [kcal/m ² degree · hr]	heat-flux density
Q [kcal/hr]	heat flux
ρ [kg · sec ² /m ⁴]	density of medium
γ [kg/m ³]	density of medium (length-time-force, system)

μ [kg-force · sec/m ²]	dynamic viscosity
$\nu = \frac{\mu}{\rho}$ [m ² /sec]	kinematic viscosity
g [m/sec ²]	gravitation acceleration
σ [kg-force · m]	surface tension
λ [kcal/m · degree · hr]	heat conductivity
c_p [kcal/kg · degree]	specific heat
$\alpha = \frac{\lambda}{c_p \rho}$ [m ² /sec]	thermal diffusivity
h [kcal/kg]	heat content (enthalpy)
r [kcal/kg]	latent heat of change of phase
C_D	drag coefficient
ϕ	fraction of stream cross section occupied by the light phase
$\rho = \frac{\gamma}{\gamma_t}$	relative density of mixture
$\beta = \frac{w_O^n}{w_O^n + w_O^n}$	volumetric flow fraction of gas in the mixture
L [kg-force · m]	work
x, y, z	coordinates
$R; D = 2R$	radius and diameter

PRIMES AND SUBSCRIPTS

'	heavy phase	$\frac{1}{2}$	layer
"	light phase	cr	critical
w	wall	eq	equivalent
t	turbulent	m	mixture
f	friction	ac	acceleration
r	relative	b	boundary
O	scale quantity	n	external normal

TABLE OF CONTENTS

Foreword	111
Fundamental Notations	vi
Primes and Subscripts	viii
Introduction	1

CHAPTER ONE. FUNDAMENTAL PARAMETERS AND EQUATIONS

1-1 Conditions Uniquely Defining a Hydrodynamic Process in an Isothermal Gas-Liquid System	4
1-2 Reference Phase Velocities, True and Average Fraction of Gas in the Stream	5
1-3 Average Density of the Mixture	8
1-4 Fundamental Dimensionless Parameters of a Two-Phase Flow	9
1-5 Fundamental Equations of Hydrodynamics	10
1-6 Mechanical Interaction of the Phases at Boundaries	14
1-7 Pressure Jump at the Phase Boundary	18
1-8 Thermal Interaction of the Phases at Their Boundary	20
1-9 Equation of Averaged One-Dimensional Motion of a Gas- Liquid Mixture in a Circular Tube	21
1-10 Heat Balance Equation for the Flow of a Gas-Liquid Mixture in a Tube	26
1-11 Method of Dimensional Analysis and Similarity	28

CHAPTER TWO. MOTION OF DISCRETE BUBBLES AND DROPS IN THE ENTRAINING MEDIUM

2-1	Steady Motion of a Small Bubble	31
2-2	Law of Drag for a Sphere with a Motionless Surface. . . .	34
2-3	Free Motion of Gas Bubbles in a Liquid.	35
2-4	Effect of the Finite Dimensions of the Vessel	39
2-5	Generalization of Experimental Data on the Ascent Velocity of Single Bubbles.	40
2-6	Relative Motion of Single Drops	45
2-7	Release Diameter of a Gas Bubble Growing on a Solid Wall.	48
2-8	Formation of a Vapor Bubble on a Heating Surface.	49
2-9	Equation of Motion for a Bubble (Drop) in an Entraining Stream.	51

CHAPTER THREE. DOWNFLOW OF LIQUID FILMS

3-1	Flow Regimes in Thin Films.	54
3-2	Equations of Motion for a Film.	55
3-3	Laminar Flow of a Film of Constant Thickness on a Vertical Wall	57
3-4	Wave Flow of Film at $w \approx 0$	60
3-5	Turbulent Flow of a Film of Constant Thickness on a Vertical Wall	65
3-6	Laminar Flow of a Film When Condensation and Evaporation Occur	70
3-7	Heat Transfer between a Turbulent Film and a Vertical Wall.	72

CHAPTER FOUR. DISCHARGE OF A GAS INTO A LIQUID

4-1	Peculiarity of the Discharge of a Gas into a Liquid . . .	74
4-2	Dimensions of a Bubble Released from an Orifice	74
4-3	Velocity of Discharge through a Rather Large Orifice. . .	76
4-4	Formation of a Stable Gas Cushion Under the Orifice of a Perforated Plate.	82
4-5	Comparison of Theory with Experimental Data	84
4-6	Discharge into a Viscous Medium	86
4-7	Thickness of a Gas Cushion Under a Horizontal Perforated Plate	88

CHAPTER FIVE. DYNAMIC TWO-PHASE LAYERS

5-1	General Information	90
5-2	Dimensionless Parameters of a Dynamic Layer	92
5-3	Structure of a Two-Phase Dynamic Layer.	97
5-4	Effect of Geometric Factors on the Hydrodynamics of the Layer	102
5-5	Experimental Data on the Relationship Between ψ and w_0'' in a Gas-Liquid System	106
5-6	Effect of Admixtures on the Dynamic Layer in a Gas-Liquid System.	111
5-7	Experimental Data on the Relationship Between ψ and w_0'' in a Liquid-Liquid System.	114
5-8	Dynamic Layer with Crossflow of Phases.	116

CHAPTER SIX. TWO-PHASE FLOW IN CIRCULAR TUBES

6-1	General Information	118
-----	-------------------------------	-----

6-2	Flow Regimes in a Gas-Liquid Mixture in Straight Tubes . .	122
6-3	Symmetrical Laminar Flow of a Liquid Layer	130
6-4	Re' and Re" Numbers as Characteristics of the Phase-Flow Regime in an Annular Liquid Film	138
6-5	Experimental Data on Head Losses in a Two-Phase Flow with a Laminar Layer of Liquid	139
6-6	Symmetrical Turbulent Flow of a Liquid Layer	145
6-7	Certain Peculiarities of the Emulsion Flow Regime of a Gas-Liquid Mixture	154
6-8	Head Losses Due to Friction in a Quasi-Homogeneous Mixture.	157
6-9	Head Losses Due to Acceleration of the Mixture	158
6-10	Head Losses in Vertical and Inclined Tubes. * for Design Purposes.	159
6-11	Local Drags.	167
6-12	Formation of Vortexes During Free Discharge into a Tube. .	173

CHAPTER SEVEN. HYDRODYNAMIC THEORY OF CRITICAL CHANGES IN HEAT TRANSFER DURING BOILING ON HEATING SURFACES

7-1	Two Fundamental Regimes of Boiling	177
7-2	The Hydrodynamic Nature of Critical Changes in the Liquid Boiling Mechanism.	180
7-3	Derivation of a Formula for the First Critical Heat-Flux Density for Natural Convection of a Boiling Liquid (First Critical Change in the Regime of Boiling)	182
7-4	Effect of the Condition of the Heating Surface and of the Method of Heating on Quantity q_{cr}	192

7-5	Transition from the Film-Boiling Regime to the Bubble-Boiling Regime (Second Critical Change in the Boiling Regime)	193
7-6	Effect of a Subcooled Liquid (i.e., Below Saturation Temperature) on the Critical Heat-Flux Density.	197
7-7	Some Experimental Data on the Effect of a Subcooled (Below Saturation Temperature) Liquid on the First Critical Heat-Flux Density.	203
7-8	Effect of Flow Velocity, Channel Dimensions, and Vapor Fraction on the Quantity q_{cr}	206

CHAPTER EIGHT. ATOMIZING LIQUIDS BY SPRAY NOZZLES

8-1	Methods of Atomizing Liquids by Spray Nozzles	211
8-2	Principal Parameters Determining the Atomizing Process.	212
8-3	Breakup of a Simple Jet	215
8-4	Breakup of a Single Drop.	220
8-5	Mean Drop Diameter in Atomization by Pneumatic Spray Nozzles	224
8-6	Fractional Composition of a Jet Atomized by a Pneumatic Spray Nozzle (Spray Density).	228
8-7	Motion of a Liquid in the Chamber of a Centrifugal Spray Nozzle.	231
8-8	Coefficient of Discharge for a Mechanical Centrifugal Spray Nozzle.	240
8-9	Liquid Atomization by a Mechanical Centrifugal Spray Nozzle.	243

CHAPTER NINE. DROP ENTRAINMENT BY A GAS STREAM AND DROP SEPARATION FROM THE STREAM

9-1	General Character of the Process	246
9-2	Mechanism of Drop Formation on the Surface of a Dynamic Two-Phase Layer.	252
9-3	Motion of Drops Torn Away from the Surface in a Gas Stream	254
9-4	Some Experimental Data on Drop Entrainment by a Gas Stream from a Bubble Column.	256
9-5	Stripping of the Liquid Film	271

CHAPTER TEN. SOME PROBLEMS IN EXPERIMENTAL TECHNIQUE

10-1	Measurement of Liquid-Drop Entrainment	274
10-2	Investigation of the Hydrodynamics of Two-Phase Layers . .	284
	References.	295

INTRODUCTION

Both in nature and engineering, in addition to flows of homogeneous liquids, there also exist two-phase flows--namely, flows of a gas or a liquid carrying suspended solid particles, flows of a "mixture" of a gas and a liquid, or flows of two mutually insoluble liquids.

Flows of the first type are usually called flows of suspensions; the transportation of solids by a gas or a liquid is called pneumatic transport. Flows of the second kind are simply called two-phase flows. The basic difference between mechanisms of motion of these two kinds of two-phase systems is that the solid particles conserve their shape and mass in pneumatic transport (the process of pulverization is an exception) while the discrete elements of the flow of a gas-liquid mixture (bubbles, drops, and films) generally change their shape in motion, and often also their mass, as a result of the coalescence or breakup of separate bubbles and drops.

The hydraulics of gas-liquid systems is a branch of the mechanics of liquids and gases in which the combined flow of these media is examined. The flows studied by the hydraulics of gas-liquid systems always have not only definite external bounding surfaces (channel walls, surfaces of bodies washed by the flow), but also internal interfaces between the flowing media, generally variable in space and time.

Interactions of forces and, in nonisothermal flow, thermal interactions as well arise at interfaces. These interactions fundamentally affect the changes in the fields of flow velocities, pressures, temperatures, thermal and diffusion fluxes transferring from one point

of space to another point separated from the first by an interface. In many cases, sudden changes in the velocity vector and the pressure develop at the phase boundary.

A specific feature of gas-liquid mixtures is also that even when they are composed of incompressible components they behave as a whole; in many respects, like compressible liquids. The latter phenomenon is exhibited in those instances where the phase velocities, and, correspondingly, also the density of the mixture, change in the direction of flow.

The types of combined gas-liquid motion are widely different and include all possible conditions--from the motion of two continuous parallel flows interacting only along one continuous interface to the motion of a stream of foam in which both phases form a complex, fine, and unstable structure.

Thus, the types of motion in two-phase flows are considerably more diversified and their laws substantially more complicated than the types of motion and laws of hydrodynamics in homogeneous media.

In connection with this, the methods of a generalized analysis of experimental data have even greater significance in this case than in the hydraulics of homogeneous flow. In the investigation of the motion of a single bubble (drop), or of flows of a gas and a liquid with a single continuous interface (films, open-channel flow, etc.), a fundamental system of equations can be formulated with all necessary rigor.

However, in the most complex motion, when the flow components are broken up into separate elements and there are a series of regions confined by boundaries, definite difficulties arise in the formulation of the fundamental equations, since in such cases the probability

laws governing multielement systems begin to apply. There are at present no coherent analytical methods for such systems. Here, experiment and the method of similitude have a decisive importance.

In this case, however, it is necessary to have a general method of derivation and analysis of the dimensionless parameters of the process. Such a general method, to which the authors adhere, amounts to the assumption that, as a whole, all the interactions taking place in any two-phase flow, however complex, are described for each of its separate zones by the same fundamental equations as for a system having a single interface. As a result, the criteria of similitude can be derived from these equations for the complex system as a whole; in addition, it is necessary to introduce the equations or parameters determining the sizes of the produced discrete elements, and determining the probability of their dispersion in space.

CHAPTER ONE

FUNDAMENTAL PARAMETERS AND EQUATIONS

1-1. Conditions Uniquely Defining a Hydrodynamic Process in an Isothermal Gas-Liquid System

A physical process may be considered as uniquely defined when the following characteristics of the phenomenon are known:

- (1) geometrical properties of the system in which the examined process takes place;
- (2) physical constants, essential to the process, of the bodies forming the system;
- (3) initial state of the system;
- (4) conditions at the boundary surfaces (external boundaries) of the system during the process.

The geometrical configuration of the space in which the gas-liquid system moves, as well as the initial state of the system (phase distribution, character of its motion, etc.) and the conditions at the boundary surfaces, can vary greatly in different technological applications.

Given the whole set of conditions enumerated above, the remaining gas-liquid characteristics--namely, the pressure drops between the various points in the system, the time average of the distribution of the phase components in space, the character of the fluctuation in the

phase-distribution density, the hydrodynamic conditions for the phase components and for the system as a whole (laminarity, turbulence, etc.), will be uniquely defined.

1-2. Reference Phase Velocities, True and Average Fraction of Gas in the Stream

If we pass some control plane through the flow of the gas-liquid mixture (two-phase flow) perpendicular to the direction of the time-averaged flow-velocity vector, we may write the volumetric flow rate of the phase in question, per unit area of this cross section, as

$$w_i = \frac{V_i}{u} = \frac{1}{u \Delta t} \int_0^{\Delta t} \int_A v_i dA dt; \quad (1-1)$$

where $V [m^3/sec]$ is the volumetric flow rate of the given component of the flow;

$u [m^2]$ is the cross-sectional area;

$\Delta t [sec]$ is a period of time substantially greater than the quantity $\frac{1}{u}$, where $u [sec^{-1}]$ is the frequency of passage of discrete formations of a given component (bubbles, drops) through the cross section in question;

$v [m/sec]$ is the actual velocity of the given component.

Thus, the quantity w_0 (") is the average flow velocity of a phase component of the stream and will be called the reference velocity of the given phase.

The quantity

$$\beta = \frac{w_0}{w_0 + w_1} \quad (1-2)$$

is called the volumetric flow fraction of gas in the two-phase stream. In reality, the flow of one of the components of the gas-liquid system need not, at a given instant of time, fill up the whole cross section of the channel. Generally, part of the channel is occupied by the other phase. Therefore, Expression (1-1) is more correctly written in the form of a sum of integrals:

$$\bar{w}_g = \frac{1}{\Delta t} \int_L \left(\sum_i \int_{\Omega_i} w_i d\Omega \right) dt, \quad (1-3)$$

where i is the number of discrete formations of the phase under consideration in a given section and at a given instant of time.

The ratio

$$\varphi = \frac{1}{\Delta} \sum_i \Omega_i \quad (1-4)$$

is the instantaneous value of that fraction of the section of the stream occupied by the gas phase, i.e., the true fraction of gas in a two-phase layer of thickness Δn , where n is the normal to the surface Ω .

The true average velocity of a given component of the stream is

$$\bar{w} = \frac{1}{\Delta \cdot \Delta t} \int_L \left(\sum_i \int_{\Omega_i} w_i d\Omega \right) dt, \quad (1-5)$$

i.e., the true average velocities and the reference velocities of the phases are related by the functions

$$\bar{w} = \frac{w_g}{\varphi}, \quad (1-6)$$

$$\bar{w} = \frac{w_l}{1-\varphi}. \quad (1-7)$$

The ratio of the total mass flow rate of the phases to the product of the cross-sectional area of the channel and the density of the heavy phase is usually designated as the flow velocity of the two-phase stream:

$$w_0 = \frac{fV' + f'V''}{f''} = w_0' + \frac{f'}{f''} w_0'' \quad (1-8)$$

The ratio of the reference velocity of the gas to the flow velocity of the mixture is always within the region of finite values determined by the condition

$$0 < \frac{w_0''}{w_0} < \frac{f'}{f''} \quad (1-9)$$

Where $\frac{w_0''}{w_0} = 0$, the stream consists of one liquid phase;

where $\frac{w_0''}{w_0} = \frac{f'}{f''}$, the stream consists of a gas phase only.

The average relative velocity of the gas phase is

$$\bar{w}_r = \bar{w} - \bar{w}_0 = \frac{w_0''}{f''} - \frac{w_0''}{1-f''} \quad (1-10)$$

hence

$$\bar{w}_r^2 - (w_0' + w_0'' + \bar{w}_r) + w_0' = 0 \quad (1-11)$$

Solving this equation for \bar{w}_r , and taking into account that when $w_0'' = 0$, $\bar{w}_r = 0$, we obtain:

$$\bar{w}_r = \frac{w_0' + w_0'' + \bar{w}_r}{2} - \sqrt{\left(\frac{w_0' + w_0'' + \bar{w}_r}{2}\right)^2 - \frac{w_0''}{f''}} \quad (1-12)$$

When $w_r'' = 0$, we have:

$$\varphi = \frac{w_0}{w_0 + w_l} = 1.$$

The quantity $w_m = w_0' + w_0''$ is usually designated as the velocity of the mixture.

Thus, at zero relative phase velocity, the true and volumetric flow fractions of gas in the stream are equal.

When the relative gas velocity is positive, the true fraction of gas in the stream is smaller than the flow fraction of gas β .

The inequality of the averaged phase velocities is sometimes called "slip" of the gas flow relative to the liquid flow. As will be shown in the following chapters, this "slip" changes the energy losses in the gas-liquid system, as compared to the case where the relative phase velocity is zero.

1-3. Average Density of the Mixture

The weight of the mixture is

$$G_m = \gamma'V' + \gamma''V''.$$

Introducing the concept of average specific gravity of the mixture, we have:

$$\bar{\gamma}_m = \frac{G_m}{V' + V''}.$$

hence

(1-13)

$$\bar{\gamma}_m = (1 - \bar{\gamma})\gamma' + \bar{\gamma}\gamma''.$$

or

$$\bar{r}_m = r' - (r' - r)\bar{r}.$$

(1-13a)

The relative density of the mixture is

$$\phi = \frac{1}{r} = 1 - \frac{r' - r}{r} \phi.$$

(1-13b)

1-4. Fundamental Dimensionless Parameters of a Two-Phase Flow

Setting aside a more detailed concept of the character of the phase interaction, we may enumerate a series of physical quantities which definitely influence the hydrodynamic process in gas-liquid systems. These values are given in Table 1-1.

Table 1-1 contains nine dimensional variables composed of three primary dimensions (kg, m, and sec). According to the well-known theorem of dimensional analysis, the greatest necessary number of dimensionless groups that can be composed from these quantities is

$$i = 9 - 3 = 6.$$

These groups are given in Table 1-2.

By combining the criteria given in Table 1-2, we may obtain a series of new, more specialized groups, such as the Archimedes criterion

$$\frac{g}{\nu} \cdot \frac{r' - r}{r} = \left(\frac{g}{\nu}\right)^{\frac{1}{2}} \frac{r'}{r} \left(1 - \frac{r'}{r}\right).$$

which characterizes the ratio of the buoyant (Archimedes) force acting on a given element of the stream (such as a gas bubble rising in a motionless liquid) to the drag generated by the viscosity of the medium surrounding this element.

Correspondingly, the group

$$\frac{\rho^2}{\eta} \cdot \frac{r}{r-r'}$$

may be considered to be a measure of the interaction between buoyancy and inertia.

1-5. Fundamental Equations of Hydrodynamics

Even very small liquid drops and gas bubbles which are components of some gas-liquid system contain such a great number of molecules that such static concepts as pressure, temperature, viscosity, etc., may be applied to them. Thus, a gas bubble 1 micron (i.e., 10^{-3} mm) in diameter, at $p = 1$ atm. abs. and $t = 0^\circ$ C, contains $1.4 \cdot 10^7$ molecules. Under normal conditions, gas bubbles about 1 mm in diameter contain about 10^{16} molecules.

On this basis, we may consider that for practical purposes the motion of the medium within any region of a gas-liquid system is determined by the ordinary equations of hydrodynamics -- namely, by the equation of motion and the equation of continuity. As we know, in vector notation these equations have the form:

$$\vec{g} - \text{grad } p + \mu \left(\nabla^2 \vec{w} + \frac{1}{3} \text{grad div } \vec{w} \right) - \rho \left[\frac{\partial \vec{w}}{\partial t} + (\vec{w} \cdot \text{grad}) \vec{w} \right]; \quad (1-14)$$

$$\frac{\partial \rho}{\partial t} + \text{div}(\rho \vec{w}) = 0; \quad (1-15)$$

here ρ is the density of the medium;

μ is the viscosity of the medium;

p is the pressure;

\vec{w} is the true (actual) flow velocity of the medium;

t is the time.

In the case of an incompressible liquid, when $\rho = \text{const}$, the equations of motion and of continuity are simplified and take the following form:

$$\vec{g} - \text{grad } p + \mu \nabla^2 \vec{w} - \rho \left[\frac{\partial \vec{w}}{\partial t} + (\vec{w} \cdot \text{grad}) \vec{w} \right]; \quad (1-16)$$

$$\text{div } \vec{w} = 0. \quad (1-17)$$

The equation for heat transfer within the given phase region, when the flow velocities are small enough to justify disregarding the kinetic energy of the stream as compared to its heat content, has the form:

$$\lambda \nabla^2 t - c_T \left[\frac{\partial t}{\partial t} + (\vec{w} \cdot \text{grad } t) \right]. \quad (1-18)$$

Translator's note: There is a quantity omitted in the original under the arrow in the first line of this equation.

Table 1-1. Physical Quantities Determining the Hydraulic Process in Isothermal Gas-Liquid Systems

Nr	Quantity	Symbol	Dimensions	Character of physical effect
1	Volumetric flow rate of heavy phase per unit cross-sectional area of the stream of the mixture	w_0^I	$\frac{m^3}{m^2 \cdot sec}$	Determines the order of the true velocities of the elements in the heavy phase
2	Volumetric flow rate of light phase per unit cross-sectional area of the stream of the mixture	w_0^II	$\frac{m^3}{m^2 \cdot sec}$	Determines the order of the true velocities of the elements in the light phase
3	Density of the heavy phase	ρ^I	$\frac{kg \cdot sec^2}{m^4}$	Specific gravity of the heavy phase
4	Density of the light phase	ρ^{II}	$\frac{kg \cdot sec^2}{m^4}$	Specific gravity of the light phase
5	Viscosity of the heavy phase	μ^I	$\frac{kg \cdot sec}{m^2}$	Characterizes molecular friction (viscosity) in the elements of the heavy phase
6	Viscosity of the light phase	μ^{II}	$\frac{kg \cdot sec}{m^2}$	Characterizes molecular friction in the elements of the light phase
7	Surface tension at the phase boundary	σ	$\frac{kg \cdot m}{m^2}$	Characterizes the work expended for changing surface of the phase boundary
8	Acceleration created by the gravitational field	g	$\frac{m}{sec^2}$	Characterizes the effect of gravity on the stream
9	Linear dimension of the system (for a given configuration)	l	m	Characterizes the spatial scale of the hydrodynamic processes under consideration

Table 1-2. Dimensionless Groups Determining the Hydrodynamic Process in the Two-Phase Flow

Nr.	Group	Physical significance of group
1	$\frac{w''_0}{w'_0}; \frac{w''_0}{w'_0}; \beta$	Describes the volumetric flow ratio of phases in the ratio.
2	$\frac{w_1}{\nu}$	<p>Describes the hydrodynamic conditions in the the given phase (laminarity, turbulence). Here</p> $Re = \frac{w}{\nu} \left[\frac{m}{sec} \right]$ <p>In order to describe the flow conditions in the two phases the following pairs of quantities must be given, all other conditions being equal:</p> $\frac{w'_0}{\nu'}; \frac{w''_0}{\nu''} \text{ or } \frac{w'_0}{\nu'}; \frac{\nu''}{\nu'} \text{ or } \frac{w''_0}{\nu''}; \frac{\nu''}{\nu'}$ <p>The latter two pairs are equivalent to the first as long as the ratio w''_0/w'_0 or β is given.</p>
3	$\frac{\rho''}{\rho'}$	Describes the ratio of the phase densities and the associated ratio of the inertial and volumetric forces applied to these phases.
4	$\frac{\sigma}{\rho' l^2}$	<p>Describes surface tension and gravity. As follows from the Laplace equation, a physically more accurate notation is</p> $\frac{\sigma}{(\rho'' - \rho') l^2}$
5	$\frac{w^2}{g l}$	<p>Describes the ratio of inertial forces and gravity in the stream. When $\frac{w''^2}{w'^2}$ or β is given, knowing $\frac{w'^2}{g l}$ or $\frac{w''^2}{g l}$ is enough.</p>

Here $\lambda \left[\frac{\text{kcal}}{\text{m} \cdot \text{deg} \cdot \text{hr}} \right]$ is the heat conductivity of the medium;

$c \left[\frac{\text{kcal}}{\text{kg} \cdot \text{deg}} \right]$ is the specific heat;

$t [^{\circ}\text{C}]$ is the temperature.

The quantity $a = \frac{\lambda}{c \gamma}$ is called the thermal diffusivity and describes the time rate of change of the temperature of a given element of the medium, or the temperature gradient along the path the element travels.

1-6. Mechanical Interaction of the Phases at Boundaries

In order to combine the equations of motion written in pairs for each of the phase regions of the gas-liquid system under study, conditions must be given which relate the pressure and velocity fields of the two phases at the interface.

Let us single out, by means of a control surface F , the bounded region V which includes a part of the interface (Fig. 1-1). To the surface F are applied normal stresses σ_n and tangential stresses τ_t . The condition for dynamic equilibrium in the region under study will take the form:

$$\int_V \vec{f} dV + \int_F \vec{\sigma}_n dF + \int_F \vec{\tau}_t dF = M \frac{d\vec{w}_0}{dt}. \quad (1-19)$$

where M is the mass in the volume V ;

$\frac{d\vec{w}_0}{dt}$ is the acceleration of the center of gravity of this volume.

On the other hand

$$\left. \begin{aligned} \oint \vec{v} \cdot d\vec{F} &= \int \vec{v}_1 \cdot d\vec{F}_1 + \int \vec{v}_2 \cdot d\vec{F}_2 \\ \oint \vec{v}' \cdot d\vec{F} &= \int \vec{v}'_1 \cdot d\vec{F}_1 + \int \vec{v}'_2 \cdot d\vec{F}_2 \end{aligned} \right\} \quad (1-20)$$

here, as before, the single prime refers to the liquid phase, and the double prime to the gaseous phase.



Figure 1-1. Derivation of the conditions of phase interaction at the boundary.

When the volume of region V approaches zero as surface F is drawn toward the interface F_b bounded by the region under study, the mass forces and the inertial term of Equation (1-19) vanish.

On the other hand, normal and tangential stresses, being perpendicular to each other, will not balance. Consequently, the condition for dynamic equilibrium at the phase boundary is resolved into two equations:

$$\left. \begin{aligned} \oint \vec{v} \cdot d\vec{F} &= 0; \\ \oint \vec{v}' \cdot d\vec{F} &= 0. \end{aligned} \right\} \quad (1-21)$$

Thus, the forces which the components of the gas-liquid system exert against each other are equal in magnitude and opposite in direction.

If we place a rectangular system of coordinates on the interface in such a way that the plane is tangent to the interface at the given point, and the z axis is normal to the surface, we will have, according to the familiar equations of hydrodynamics:

$$q_0 = q_1 = -p + \frac{2}{3} p \operatorname{div} \vec{w} + 2p \frac{\partial w_z}{\partial y} :$$

$$q_{1,xy} = p \left(\frac{\partial w_x}{\partial y} + \frac{\partial w_y}{\partial x} \right) ; \quad (1-22)$$

$$q_{1,xy} = p \left(\frac{\partial w_x}{\partial y} + \frac{\partial w_y}{\partial x} \right) .$$

When the phases do not slip relative to each other where they are in contact along the interfaces, the projections of the velocity vectors on the xz plane (which is tangent to the interface) are equal:

$$w'_{1x,z} = w'_{2x,z} . \quad (1-23)$$

The velocity components on the phase boundary which are normal to the xz plane are determined by the mass rate of change of phase $\dot{\xi}_n$ and by the specific gravity of the corresponding phase:

$$\left. \begin{aligned} w'_z &= \pm \frac{\dot{\xi}_n}{\gamma} ; \\ w'_z &= \mp \frac{\dot{\xi}_n}{\gamma} . \end{aligned} \right\} \quad (1-24)$$

The mass rate of change of phase is expressed in kg/sec per m^2 of interface. Consequently, in the absence of change of phase ($\dot{\xi}_n = 0$) at the interface, the tangential components of the phase velocity vectors, as well as the vectors themselves, coincide in magnitude as well as in direction. When there is a change of phase, the phase-velocity vectors on the boundary are not equal, owing to the appearance of a flow of material across the interface and owing to the inequality of the specific gravities of the phases.

When a change of phase is present, the inequality of quantities

w_n' and w_n'' results in a change in the momentum of the stream of material G_n as it passes through the interface. As we know, the change in momentum of the per-second flow rate of material causes the appearance of force of reaction exerted against the above-mentioned cross section of the system. In the given instance a force appears which is normal to the interface and is equal to

$$P_s = \frac{G_n}{\tau} (w_n' - w_n'). \quad (1-25)$$

Taking into account (1-24), we obtain:

$$P_s = \frac{G_n^2}{G_n^2} \left(1 - \frac{r}{r}\right). \quad (1-26)$$

The mass rate of change of phase is

$$K_s = \frac{q_s}{r}.$$

where q_s is the density of the heat flux absorbed in the change of phase per m^2 of interface;

$r \left[\frac{\text{kcal}}{\text{kg}} \right]$ is the latent heat of change of phase.

Substituting this value of G_n into (1-26), we obtain:

$$P_s = \frac{q_s^2}{G_n^2} \left(1 - \frac{r}{r}\right). \quad (1-27)$$

Using the latter equation, it is easily shown that the reaction resulting from the change in flow velocity as the stream of material passes through the interface, is very small in ordinary engineering

problems. Thus, for example, with a water evaporation rate corresponding to a heat-flux density on the interface of 1,000,000 kcal/m²·hr and atmospheric pressure we have:

$$r = 539 \text{ kcal/kg}; \quad \gamma'' = 0.58 \text{ kg/m}^3; \quad \gamma' = 953 \text{ kg/m}^3$$

$$P_n = \frac{1}{9.81 \cdot 0.539} \cdot \left(\frac{10^6}{3600 \cdot 539} \right)^2 \left(1 - \frac{0.58}{953} \right) = 0.045 \text{ kg-force/m}^2.$$

At a heat flux density of 100,000 kcal/m²·hr, we have, for the same medium, the quantity $P_n = 0.00045 \text{ kg-force/m}^2$.

1-7. Pressure Jump at the Phase Boundary

The molecules of the liquid at its boundary with a gas, a solid body, or another liquid are in the field of force of both the given liquid and the molecules of the other medium. As a result of this, the force exerted by the surrounding molecules on a molecule of the surface layer is asymmetrical, the consequence being the appearance of a force directed toward the denser medium (Fig. 1-2). The ef-



Figure 1-2. Diagram of the forces acting on a molecule within the interior of the liquid and in the superficial layer.

fective radius of a molecule is very small; the force of molecular interaction is reduced by three orders of magnitude if the distance is changed from one to two effective molecular diameters. In connection with this, the boundary layer has a thickness of the order

of only two molecular diameters, i.e., less than 10^{-7} cm. The molecules on the surface layer have available free energy and, consequently, the change in the interface is accompanied by an energy effect. Since a system is at stable equilibrium when the free energy is minimum,

the free surface of a liquid will be reduced to a minimum. As a consequence of this, a liquid which is not subjected to a unilateral force will take the shape of a sphere.

The work required to increase the interface by one unit area is called surface tension:

$$\sigma = \frac{dW}{dA} \quad (1-28)$$

The curvature of the interface causes the appearance of a pressure jump defined by the Laplace formula:

$$p_2 - p_1 = \sigma \left(\frac{1}{R_1} + \frac{1}{R_2} \right) \quad (1-29)$$

where $\sigma \left[\frac{\text{kg-force} \cdot \text{m}}{\text{m}^2} \right]$ is the surface tension at the phase boundary;
 $R_1, R_2 \left[\text{m} \right]$ are the principal radii of curvature of the interface at a given point.

The radii of curvature are considered positive if they are directed into the first phase. For a sphere, $R_1 = R_2 = R$; consequently, the pressure in a gas bubble exceeds the pressure in the surrounding liquid by the quantity

$$\Delta p = \frac{2\sigma}{R} \quad (1-30)$$

Another important surface tension effect is the fact that saturation pressure also depends on the curvature of the interface. According to the Kelvin formula, the change in saturation pressure, with

reference to the pressure above the plane at a given temperature, is

$$\Delta p = -\frac{r}{r-r'} \left(\frac{1}{R_1} + \frac{1}{R_2} \right). \quad (1-31)$$

1-8. Thermal Interaction of the Phases at Their Boundary

Let us formulate the heat balance of the above-considered volume V , which includes the interface:

$$-\oint \lambda \frac{\partial t}{\partial n} dF + \oint i_1 w_n dF - \int c_1 \frac{\partial t}{\partial \tau} dV; \quad (1-32)$$

here $\left[\frac{\text{kcal}}{\text{m} \cdot \text{degree} \cdot \text{hr}} \right]$ is the heat conductivity of the medium;

i $\left[\frac{\text{kcal}}{\text{kg}} \right]$ is the enthalpy of the medium;

c $\left[\frac{\text{kcal}}{\text{kg} \cdot \text{degree}} \right]$ is the specific heat of the medium;

t $\left[^\circ\text{C} \right]$ is the temperature;

n $\left[\text{m} \right]$ is the external normal to the surface.

Taking into account the direction of the heat-flux vector due to conduction and the direction of the enthalpy-flux vector with respect to the control surface F on both sides of the phase boundary (Fig. 1-1), we may rewrite Equation (1-32) in the following form:

$$\int_V \left(-\lambda' \frac{\partial \theta}{\partial x} + \rho' \gamma' \theta' \right) dF - \int_V \left(-\lambda'' \frac{\partial \theta}{\partial x} + \rho'' \gamma'' \theta'' \right) dF = \int_V c_p \frac{d\theta}{dt} dV. \quad (1-33)$$

When there is a change of phase it follows from the condition of conservation of mass that on the interface

$$\rho' \theta' - \rho'' \theta'' = \rho_s. \quad (1-34)$$

Reducing the volume V to zero by drawing the control surface F toward the interface F_0 , we obtain

$$-\lambda' \left(\frac{\partial \theta}{\partial x} \right)_0 = -\lambda'' \left(\frac{\partial \theta}{\partial x} \right)_0. \quad (1-35)$$

where $r = \frac{1}{\rho_s} = \frac{1}{\rho} \left[\frac{\text{kcal}}{\text{kg}} \right]$ is the latent heat of change of phase.

In the absence of a temperature jump it follows that

$$t'_0 = t''_0. \quad (1-36)$$

1-9. Equation of Averaged One-Dimensional Motion of a Gas-Liquid Mixture in a Circular Tube

Let us consider a motion, averaged over the cross section, of a gas-liquid mixture in a tube whose axis we will take as the x axis (Fig. 1-3).

The resultant of gravity and pressure which are exerted on the volume $dV = \pi R^2 dx$ is equal to the change in momentum of the per-second flow rate of material in section dx :

$$\begin{aligned}
 & \sigma_x [(1-\varphi)\bar{v}' + \varphi\bar{v}'] = R^2 dx - \frac{\partial p}{\partial x} R^2 dx - \tau_w 2\pi R dx = \\
 & = \frac{1}{g} [(G' + dG')(\bar{w}' + d\bar{w}') + \\
 & + (G'' + dG'')(\bar{w}'' + d\bar{w}'') - G'\bar{w}' - G''\bar{w}''].
 \end{aligned}
 \tag{1-37}$$

Here, φ is the instantaneous true fraction of gas in the volume V of mixture;

$\tau_w \left[\frac{\text{kg-force}}{\text{m}^2} \right]$ are the tangential stresses at the tube wall;

$G \left[\frac{\text{kg}}{\text{sec}} \right]$ is the per-second flow rate of the medium;

$g_x \left[\frac{\text{m}}{\text{sec}^2} \right]$ is the projection of the vector g on the x-axis;

$\bar{w} \left[\frac{\text{m}}{\text{sec}} \right]$ is the average velocity of the medium; and

$R \left[\text{m} \right]$ is the radius of the tube.

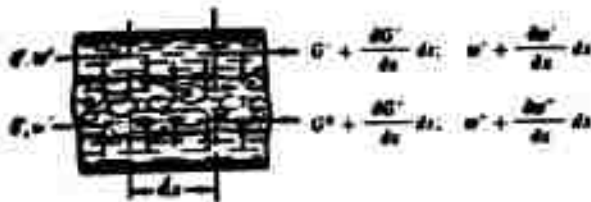


Figure 1-3. Diagram of a two-phase flow in a tube.

The per-second flow rates of the phases are related to the true fraction of gas in the mixture and the average velocities, by the equations:

$$\left. \begin{aligned}
 G' &= (1-\varphi)\bar{w}'\pi R^2; \\
 G'' &= \varphi\bar{w}''\pi R^2.
 \end{aligned} \right\}
 \tag{1-38}$$

The phase velocities averaged throughout the tube cross section are functions of time and the x -coordinate; i.e., from the definition of a total differential,

$$d\bar{w} = \frac{\partial \bar{w}}{\partial t} dt + \frac{\partial \bar{w}}{\partial x} dx. \quad (1-39)$$

Removing the parentheses in the right-hand member of Equation (1-37) and disregarding the quantities of the second order of smallness, we obtain:

$$\begin{aligned} & \varepsilon_s [v' - (v' - v'')v] - \frac{\partial p}{\partial x} - \frac{p_w}{R} = \\ & - \frac{1}{\alpha R^2 g} \left(\sigma' \frac{\partial \bar{w}}{\partial x} + \sigma'' \frac{\partial \bar{w}}{\partial x} + \bar{w}' \frac{\partial \sigma'}{\partial x} + \bar{w}'' \frac{\partial \sigma''}{\partial x} \right). \end{aligned} \quad (1-40)$$

When there is a change in the state of aggregation, the amount of vapor formed is equal to the amount of liquid evaporated, i.e.,

$$-\frac{\partial \sigma'}{\partial x} = \frac{\partial \sigma''}{\partial x} = \frac{\partial \sigma_s}{\partial x}. \quad (1-41)$$

It follows from (1-39) that

$$\frac{\partial \bar{w}}{\partial x} = \frac{\partial \bar{w}}{\partial t} \cdot \frac{dt}{dx} + \frac{\partial \bar{w}}{\partial x} = \frac{1}{v} \cdot \frac{\partial \bar{w}}{\partial t} + \frac{\partial \bar{w}}{\partial x}. \quad (1-42)$$

Substituting into (1-40) the values \bar{g} and $\frac{d\bar{w}}{dx}$ from (1-38) and (1-42), we obtain:

$$\begin{aligned} & \varepsilon_s [v' - (v' - v'')v] - \frac{\partial p}{\partial x} - \frac{p_w}{R} = (1-v)v' \left(\frac{\partial \bar{w}}{\partial t} + \bar{w}' \frac{\partial \sigma'}{\partial x} \right) + \\ & + v'' \left(\frac{\partial \bar{w}}{\partial t} + \bar{w}'' \frac{\partial \sigma''}{\partial x} \right) + \frac{\bar{w}' - \bar{w}''}{\alpha R^2 g} \cdot \frac{\partial \sigma_s}{\partial x}. \end{aligned} \quad (1-43)$$

The continuity equation of the average flow of the gas-liquid mixture takes the form:

$$\frac{\partial}{\partial t} [v' - (v' - v'')v] + \frac{\partial}{\partial x} [(1-v)v'v] + \frac{\partial}{\partial x} (vv''v'') = 0, \quad (1-44)$$

which we can easily prove by formulating the material balance for the volume V .

The total change in the amount of the given phase in the section dx is equal to

$$dQ = g v R^2 dx \left[\frac{\partial}{\partial t} (v'') + \frac{\partial}{\partial x} (v' v'') \right] \quad (1-45)$$

Thus, the hydraulic equation of motion for a stream of gas-liquid mixture in a tube will finally take the form:

$$g, v' - (v' - v'')v] - \frac{\partial p}{\partial x} - \frac{\partial v}{\partial x} = (1-v)v' \left(\frac{\partial v}{\partial t} + v' \frac{\partial v}{\partial x} \right) + \\ + v'' \left(\frac{\partial v}{\partial t} + v' \frac{\partial v}{\partial x} \right) + (v' - v'') \left[\frac{\partial}{\partial t} (v'') + \frac{\partial}{\partial x} (v' v'') \right]. \quad (1-46)$$

The last term of this equation is the Meshcherskiy force of reaction which arises during a change in the state of aggregation of a gas-liquid system whose relative average phase flow velocity is different from zero; i.e., this term is the resultant of the reaction P_{Σ} [see Formula (1-25)] acting on the interfaces included in a unit volume of the mixture.

If the phases can be considered incompressible, i.e., if it is assumed that $\rho' = \text{const}$ and $\rho'' = \text{const}$, then, turning to the reference velocities, we obtain hydraulic equations of motion and continuity for

the mixture in the following form:

$$\begin{aligned} & \rho \left[1 - \left(1 - \frac{\rho'}{\rho} \right) \right] - \frac{\partial \rho}{\partial x} - \frac{\partial \rho}{\partial x} = \\ & - \rho' \left(\frac{\partial u_0}{\partial x} + \frac{u_0}{1-\gamma} \cdot \frac{\partial \gamma}{\partial x} \right) + \rho'' \left(\frac{\partial u_0}{\partial x} + \frac{u_0}{\gamma} \cdot \frac{\partial \gamma}{\partial x} \right) + \\ & + \left(\frac{\rho' u_0}{1-\gamma} - \frac{\rho'' u_0}{\gamma} \right) \frac{\partial \gamma}{\partial x} + \left[\rho' \left(\frac{u_0}{1-\gamma} \right)' - \rho'' \left(\frac{u_0}{\gamma} \right)' \right] \frac{\partial \gamma}{\partial x} + \\ & + \rho' \left(\frac{u_0}{\gamma} - \frac{u_0}{1-\gamma} \right) \left(\frac{\partial \gamma}{\partial x} + \frac{\partial \gamma}{\partial x} \right); \end{aligned} \quad (1-46a)$$

$$\left(1 - \frac{\rho'}{\rho} \right) \frac{\partial \gamma}{\partial x} - \frac{\partial \gamma}{\partial x} - \frac{\rho'}{\rho} \cdot \frac{\partial \gamma}{\partial x} = 0. \quad (1-47)$$

In the absence of a change of phase, $u_0' = u_0'' = 0$, and the equation of continuity (1-47) resolves into two independent equations:

$$\left. \begin{aligned} \frac{\partial \gamma}{\partial x} - \frac{\partial \gamma}{\partial x} &= 0; \\ \frac{\partial \gamma}{\partial x} + \frac{\partial \gamma}{\partial x} &= 0. \end{aligned} \right\} \quad (1-48)$$

In agreement with this, the last term of Equation (1-46) vanishes as well, i.e., the hydraulic equation of motion of the gas-liquid mixture in the absence of evaporation or condensation takes the form:

$$\begin{aligned} & \rho \left[1 - \frac{\rho'}{\rho} \right] - \frac{\partial \rho}{\partial x} - \frac{\partial \rho}{\partial x} = (1-\gamma) \rho' \left(\frac{\partial u_0}{\partial x} + \frac{u_0}{\gamma} \frac{\partial \gamma}{\partial x} \right) + \\ & + \rho'' \left(\frac{\partial u_0}{\partial x} + \frac{u_0}{1-\gamma} \frac{\partial \gamma}{\partial x} \right). \end{aligned} \quad (1-49)$$

For incompressible components, and in the absence of change of phase, we obtain the following system of equations in terms of reference velocities:

$$\begin{aligned} & \rho' \left[1 - \left(1 - \frac{r'}{r} \right) \right] - \frac{\partial p}{\partial x} - \frac{2\tau_w}{R} = \rho' \left(\frac{\partial u_0}{\partial x} + \frac{v_0}{1-\gamma} \frac{\partial u_0}{\partial x} \right) + \\ & + \rho' \left(\frac{\partial u_0}{\partial x} + \frac{v_0}{\gamma} \frac{\partial u_0}{\partial x} \right) + \left(\frac{r' u_0}{1-\gamma} - \frac{r' v_0}{\gamma} \right) \frac{\partial \gamma}{\partial x} + \left[\rho' \left(\frac{v_0}{1-\gamma} \right)^2 - \right. \\ & \left. - \rho' \left(\frac{v_0}{\gamma} \right)^2 \right] \frac{\partial \gamma}{\partial x} \end{aligned} \quad (1-50)$$

$$\left. \begin{aligned} \frac{\partial \gamma}{\partial x} - \frac{\partial u_0}{\partial x} &= 0; \\ \frac{\partial \gamma}{\partial x} + \frac{\partial u_0}{\partial x} &= 0; \\ \frac{\partial u_0}{\partial x} + \frac{\partial v_0}{\partial x} &= 0. \end{aligned} \right\} \quad (1-51)$$

1-10. Heat Balance Equation for the Flow of a Gas-Liquid Mixture in a Tube

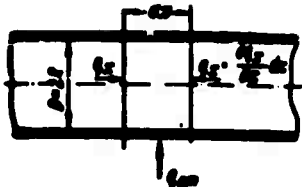


Figure 1-4. Diagram showing heat transfer in an element of a two-phase stream.

Figure 1-4 shows a diagram of the heat fluxes entering an elementary volume of mixture $dV = \pi R^2 dx$. The amount of heat flowing in through the surface of the tube

is

$$dQ_w = q_w 2\pi R dx, \quad (1-52)$$

where $q_w \left[\frac{\text{kcal}}{\text{m}^2 \text{hr}} \right]$ is the heat-flux density relative to the inner surface of the tube.

The change in the heat flux by conduction through the gaseous and liquid phases in the direction of the axis is

$$\begin{aligned} \frac{\partial Q_x}{\partial x} = \frac{\partial}{\partial x} \left[\frac{1}{\Delta t} \int_{\Delta t} \left(\sum_{m'} \int_{m''} -\lambda' \frac{\partial T'}{\partial x} d\Omega \right) dt + \right. \\ \left. + \frac{1}{\Delta t} \int_{\Delta t} \left(\sum_{m'} \int_{m''} -\lambda'' \frac{\partial T''}{\partial x} d\Omega \right) dt \right]; \end{aligned} \quad (1-53)$$

here, m' and m'' are the numbers of discrete phase elements in the given cross section Ω .

Introducing phase temperatures averaged in some way over the cross section, we rewrite (1-53) in the following form:

$$\frac{\partial Q_x}{\partial x} = \frac{\partial}{\partial x} \left[-\lambda' (1-\varphi) \frac{\partial T'}{\partial x} - \lambda'' \varphi \frac{\partial T''}{\partial x} \right] \pi R^2. \quad (1-54)$$

If the quantity \bar{t} in (1-53) and (1-54) stands for the temperature averaged over the fluctuation period, then λ is the sum of the molecular and turbulent heat conductivities. The difference $\frac{\partial Q_w}{\partial x} - \frac{\partial Q_x}{\partial x} dx$ is equal to the sum of the time change in the enthalpy of the volume of mixture dV , and of the enthalpy flux along the x -axis, i.e.,

$$\begin{aligned} \frac{\partial Q_w}{\partial x} - \frac{\partial Q_x}{\partial x} = \pi R^2 \left\{ \frac{\partial}{\partial t} [(1-\varphi) T' \bar{t} + \varphi T'' \bar{t}] + \right. \\ \left. + \frac{\partial}{\partial x} [(1-\varphi) T' \bar{t} \bar{w} + \varphi T'' \bar{t} \bar{w}] \right\}. \end{aligned} \quad (1-55)$$

Substituting into (1-55) the values $\frac{\partial Q_w}{\partial x}$ and $\frac{\partial Q_x}{\partial x}$ from (1-52) and (1-54) we obtain:

$$\begin{aligned} \frac{\partial T}{\partial t} + \lambda' (1-\varphi) \frac{\partial T'}{\partial x} + \lambda'' \varphi \frac{\partial T''}{\partial x} = \frac{\partial}{\partial t} [(1-\varphi) T' \bar{t} + \varphi T'' \bar{t}] + \\ + \left(\lambda' \frac{\partial T'}{\partial x} - \lambda'' \frac{\partial T''}{\partial x} \right) \frac{\partial \bar{t}}{\partial x} + \frac{\partial}{\partial x} [(1-\varphi) T' \bar{t} \bar{w} + \varphi T'' \bar{t} \bar{w}]. \end{aligned} \quad (1-56)$$

In the case of thorough phase mixing, when the temperature throughout the cross section can be considered equalized ($t' = t'' = \bar{t}$). Equation (1-56) takes the form:

$$\begin{aligned} \frac{\partial \bar{t}}{\partial t} + [\lambda'(1-\varphi) + \lambda''\varphi] \frac{\partial \bar{t}}{\partial x} = \frac{\partial}{\partial x} \{ [(1-\varphi)\gamma'c' + \varphi\gamma''c''] \bar{t} \} + \\ + (\lambda' - \lambda'') \frac{\partial \bar{t}}{\partial x} \cdot \frac{\partial \bar{t}}{\partial x} + \frac{\partial}{\partial x} [(c'\gamma'w_0 + c''\gamma''w_0) \bar{t}]. \end{aligned} \quad (1-57)$$

1-11. Method of Dimensional Analysis and Similarity

Equations describing some class of physical processes can always be presented in dimensionless form. This operation can be accomplished either by dividing the equation by one of its terms or by introducing scale quantities. For example, it is possible to derive a dimensionless velocity by dividing w at a given point and at a given instant of time by the average flow velocity in the tube, or by the velocity outside the boundary layer in the case of unbounded flow past a body. We may also choose as a scale a combination of certain quantities which determine the course of the process under study; for example, we may take the quantity $w_0 = \sqrt{\frac{\gamma}{\rho}}$; or the ratio $\frac{w}{w_0}$ as the velocity scale.

By dimensional theory, the highest number of dimensionless groups characterizing a given process is given by the formula

$$j = n - m. \quad (1-58)$$

in which

n is the number of dimensional parameters characterizing the process;

m is the number of primary dimensions.

We have already made use of this method in Section 1-4.

The number of dimensionless parameters in the process is lower than the number of dimensional parameters, while their magnitude does not depend on the system of units chosen. This determines the advantage of switching over to the analysis of equations and experimental data in terms of dimensionless parameters.

Processes in which the domains of corresponding dimensionless parameters are geometrically identical are physically similar. This means that the values of corresponding dimensional parameters at corresponding points of similar systems differ only by a scale factor.

The dimensionless parameters of the process are also called criteria of similarity since in similar systems corresponding criteria of similarity have the same numerical values.

The criteria are divided into two groups: determining and non-determining (determinable) criteria. Criteria composed only of quantities that are among the conditions uniquely defining a process are determining.

Each of the nondetermining criteria is a function of all the determining criteria.

The law of model study formulated by M. V. Kirpichev and A. A. Gukhman follows from this basic proposition of the method of similarity. Processes of the same physical nature are similar if they have similar uniquely defining conditions and if they have corresponding determining criteria that are numerically identical.

By reducing equations of the process to a dimensionless form, we can obtain criteria of various forms, depending on how this operation is carried out. Such criteria are called primary criteria. However, the total number of criteria does not depend on the method by which the equations are reduced to a dimensionless form, but is precisely one unit less than the number of terms in the given equation.

In analyzing the conditions of similarity, it is necessary to define all the determining criteria of the process under consideration. To do this, we have to form such combinations of primary criteria as will provide the greatest possible number of criteria composed only of quantities which are among the uniquely defining conditions. But the total number of criteria (the number of determining criteria plus the number of nondetermining criteria) must remain unchanged.

The number of determining criteria is equal to the difference between the number of independent variables of a given process and the number of primary quantities (dimensions) of which they are composed. If the equations of the process are given, the independent variables entering into a given term of the equation as products or as ratios are considered as single quantities having the resulting dimensions.

In hydraulics as a whole, and in the hydraulics of gas-liquid systems in particular, the method of similarity plays an important part, as it allows us to analyze in a distinct and general form the effect of a great number of factors determining the motion of a stream.

CHAPTER TWO

MOTION OF DISCRETE BUBBLES AND DROPS IN THE ENTRAINING MEDIUM

2-1. Steady Motion of a Small Bubble

The smaller the dimensions of a gas bubble moving in a liquid medium, the stabler is its spherical shape. Conversely, as a bubble's dimensions increase, its shape deviates more and more from the spherical, and mushroom-shaped bubbles are formed with concavities in the rear; there is a general tendency toward flattening of the bubble in the direction of its motion.

Accurate theoretical solutions are available only for spherical bubbles, i.e., very small ones.

In the case of steady motion of a spherical bubble rising in a large volume of liquid, only the drag of the surrounding liquid and buoyancy, which is a function of the difference in density of the gas and the liquid, act on the bubble. Let us write the condition for equilibrium of these forces

$$\left(\frac{\rho_l}{2} w^2 - (\rho' - \rho) V \right) = 0 \quad (2-1)$$

where f is the drag coefficient of the bubble;

w is the velocity of ascent of the bubble;

a is the cross-sectional area of the bubble;

V is the volume of the bubble.

Hence

$$w = \sqrt{\frac{2\gamma(\gamma' - \gamma)V}{\gamma^2 a}} \quad (2-2)$$

For a spherical bubble, it follows from (2-2) that:

$$w = \sqrt{\frac{2\gamma(\gamma' - \gamma)R}{3\gamma}} \quad (2-3)$$

where R is the radius of the bubble.

In the case of a liquid drop settling in a gas jet, the velocity of settling is determined by the same formula, but in the denominator the value γ' is replaced by the value γ'' under the radical sign.

Examining this problem in the light of the general hydrodynamic equations, it is expedient to combine the center of a spherical system of coordinates with the center of gravity of the moving bubble (drop). In such a case, the drop as a whole is considered to be motionless, and the external jet to be moving at a velocity w'' .

The equations of motion and continuity are written separately for the external medium and the medium contained in the bubble, in the form of Equations (1-16) and (1-17). Accordingly, to these equations we add the boundary conditions (1-22), (1-23) and (1-24) (at $\xi_n = 0$) on the phase boundary, and the condition that $w = 0$ at a large distance from the bubble.

The solution obtained by Rybchinskiy and Hadamard, has the form:

$$w = \frac{2(\gamma' - \gamma)R}{3\gamma} \cdot \frac{1 + \frac{\gamma''}{\gamma}}{2 + 3\frac{\gamma''}{\gamma}} \quad (2-4)$$

At $\mu'' \gg \mu'$, the Rybczynski-Hadamard formula changes into the well-known Stokes Law for the motion of small solid spheres in a liquid medium:

$$w = \frac{2(\eta' - \eta'') R^2}{9\eta'} \quad (2-5)$$

At $\mu'' \ll \mu'$ Formula (2-4) gives:

$$w = \frac{(\eta' - \eta'') R^2}{3\eta'} \quad (2-6)$$

As the condition $\mu'' \ll \mu'$ corresponds to the case of a gas moving in a liquid, it appears from the comparison of (2-6) and (2-5) that gas bubbles must rise 1.5 times faster than solid spheres. This is explained by the mobility of the interface between the liquid and the gas phases, as a result of which the velocity of the liquid at the bubble surface is lower than at the surface of a solid particle.

Solutions (2-4) and (2-5) are valid for spherical particles when

$$Re = \frac{2\eta' R}{\nu} < 2.$$

For the range $Re \approx 50$ to 800, a theoretical solution was found by G. Levich. However, the solution is not accurate because of the separation of the boundary layer at the wake of the particle at $Re > 2$. It is only important to mention that in this case the mobility of the interface results in a flow which is different from the flow past a solid sphere, namely, the separation point in the case of a mobile boundary is displaced nearer to the wake of the flow. Therefore

the drag of such a particle is also smaller.



Figure 2-1. Effect of impurities on the velocity of ascent of air bubble in water: (1) theoretical curve according to Levich; (2) ordinary water; (3) distilled water; (4) water twice distilled with permanganate.

However, the experiments and subsequent theoretical investigations of A. I. Prumkin and V. G. Levich showed that a substantial deviation in the motion of gas bubbles or drops of an immiscible liquid within another liquid from the motion of solid particles occurs only when the interacting media are unusually pure. Small impurities strengthen the surface film to a degree where the motion of bubbles or drops, for practical purposes, no longer differs sub-

stantially from the motion of solid particles.

Figure 2-1 shows the results of a series of experiments on the motion of gas bubbles in water which has been subjected to various degrees of distillation.

2-2. Law of Drag for a Sphere with a Motionless Surface

Figure 2-2 shows the relationship between the drag coefficient of a solid sphere and the Reynolds number plotted on logarithmic coordinates. In the region $Re < 2$ laminar flow past the sphere takes place, and Stokes' Law applies:

$$S = 6\pi\eta Rv.$$

(2-7)

to which corresponds the value

$$C_D = \frac{24}{Re}. \quad (2-8)$$

The substitution of (2-8) into (2-3) leads to Formula (2-5). Within the range $1 \cdot 10^3 < Re < 2 \cdot 10^5$, the drag coefficient remains almost constant and equal to approximately 0.4. At $Re > 2 \cdot 10^5$ the drag coefficient decreases sharply, which is caused by a displacement of the separation point of the boundary layer (Fig. 2-3).

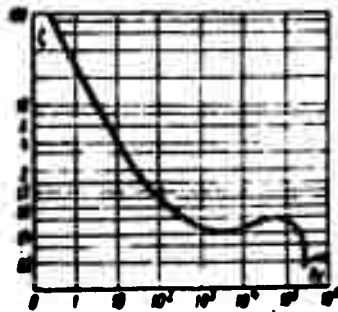


Figure 2-2. Drag coefficient C_D vs. Re number for a sphere with motionless surface.



Figure 2-3. Flow of a liquid past a sphere.

2-3. Free Motion of Gas Bubbles in a Liquid

The following act on a gas or steam bubble floating upwards in a liquid: the buoyancy caused by the pressure gradient in the direction of motion of the bubble; the drag of the liquid layers surrounding the bubble; and surface tension. The latter tends to give the bubble a spherical shape.

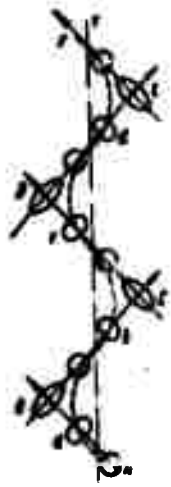


Figure 2-4. Character of the motion of a single bubble in a liquid.

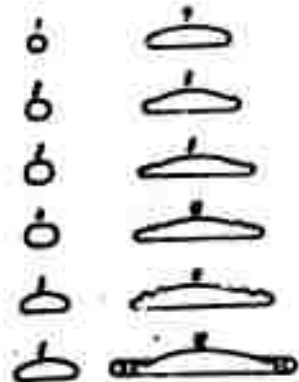


Figure 2-5. Schematic representations of air bubbles of various sizes:

(1) $V = 0.01 \text{ cm}^3$	(7) $V = 1.43 \text{ cm}^3$
(2) $V = 0.95 \text{ "}$	(8) $V = 2.5 \text{ "}$
(3) $V = 0.15 \text{ "}$	(9) $V = 4.0 \text{ "}$
(4) $V = 0.28 \text{ "}$	(10) $V = 13.3 \text{ "}$
(5) $V = 0.5 \text{ "}$	(11) $V = 20. \text{ "}$
(6) $V = 1.0 \text{ "}$	(12) $V > 20.0 \text{ "}$

However, owing to the unequal pressures around the bubble, the latter becomes deformed. In this case, the greater the volume of the bubble, the more its shape will differ from that of a sphere. The smaller the bubble, the greater the surface tension, and the more stable is its shape. Very small bubbles are almost entirely spherical. In large bubbles, the influence of surface tension is small [see Formula (1-30)] as compared to the dynamic effect of the liquid medium, and the bubble assumes flattened, mushroom-like, and extremely unstable shapes. The time change in the shape of such a bubble leads to variations in the velocity of its ascent and to deviations in the trajectory of its motion from the vertical.

Figure 2-4 shows a diagram of the motion of a bubble from Miyagi's observations; Fig. 2-5 shows the diagrams of air bubbles from R. M. Ladyzhenskii's observations; Fig. 2-6 shows graphs of velocity variations

in the ascent of steam bubbles from Shamshev's experiments. These data clearly illustrate the unstable shape and motion of gas bubbles in a liquid.

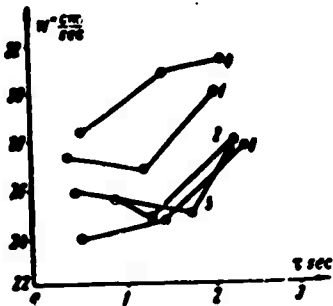


Figure 2-6. Variations in velocity of ascent of a steam bubble in a large volume of water at $p = 1$ atm. abs.

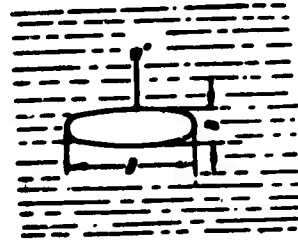


Figure 2-7. Diagram of a flattened spheroid entrained by a stream.

D. A. Frank-Kamenetskiy showed that the relative velocity of a flattened spheroid (Fig. 2-7) does not depend on its size.

The flow work, resulting in a change $d\delta$ in the thickness of the bubble, is accomplished against the surface tension--i.e.,

$$dL = \left(\frac{V}{2\delta} \right) d\delta = -\delta d\delta. \quad (2-9)$$

From the condition that the volume of the spheroid be constant, we have

$$V = 2\delta = \text{const.}$$

$$2\delta + \delta d\delta = 0.$$

On these grounds, replacing in Equation (2-9) the quantity σ by the quantity $-\sigma \sin \theta$, we find that

$$\dot{z} = \frac{2\sigma}{\rho_1 r^2} = \frac{V}{2} \quad (2-10)$$

By substituting into (2-2) the value $\frac{V}{2}$ of a flat spheroid from (2-10), we obtain:

$$w = \sqrt{\frac{4\sigma^2 (\gamma' - \gamma)}{\rho_1^2}} \quad (2-11)$$

It follows from this formula that the average ascent velocity of large flattened bubbles (or the descent velocity of flattened drops) does not depend on their size. Consequently, Formulas (2-10) and (2-11) describe two limiting conditions of motion of bubbles (drops) in an entraining medium--namely, the first formula describes the law of motion for very small bubbles, while the second describes the law of motion for very large bubbles.

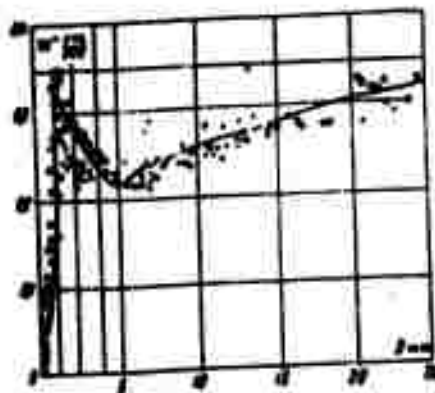


Figure 2-8. Ascent velocity of a single air bubble in water vs. bubble diameter at $p = 1$ atm. abs.

Figure 2-8 gives a series of experimental data on the ascent velocity of gas bubbles in water. In the case of diameters of the order of 2 to 5 mm, the ascent velocity decreases owing to the starting deformation of the bubbles and to the resultant increase in the drag coefficient. By the time a certain stability of the flattened shape is reached, the ascent velocity of the bubble increases somewhat as its diameter (or more exactly its volume) increases and then becomes more or less constant.

2-4. Effect of the Finite Dimensions of the Vessel

Let us examine the ascent of a bubble in a tube whose diameter we will make commensurate with the diameter of the bubble (Fig. 2-9). In this case, the drag of the bubble can be determined by the relative velocity

$$w_r = w'' - w' \quad (2-12)$$

in which w'' is the absolute velocity of the bubble and w' is the average flow velocity of the liquid in the annular space between the bubble and the tube.

During its motion, the bubble vacates a space equal to $\pi R_0^2 dx$ which is then filled up by the liquid flowing into it.

Hence

$$\pi R_0^2 dx = -w' \pi (R_0^2 - R^2) dt \quad (2-13)$$

where R_0 is the radius of the tube and t is the time. Noting that

$$\frac{dx}{dt} = w'', \text{ we obtain:}$$

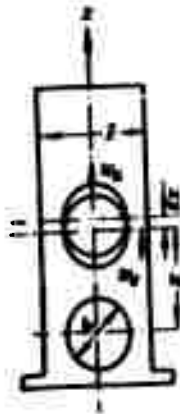
$$w' = w \left[1 - \left(\frac{R}{R_0} \right)^3 \right] \quad (2-14)$$

$$w' = \frac{w}{1 - \left(\frac{R}{R_0} \right)^3} \quad (2-15)$$

Substituting this value into (2-3), we find:

$$w' = w_0 \left[1 - \left(\frac{R}{R_0} \right)^3 \right] \quad (2-16)$$

where w_0 is the ascent velocity in a large volume of liquid ($R_0 \gg R$).



Thus, in the case of motion in a tube, the ascent velocity of the bubble decreases. As will be shown later, experiments disclose a more substantial influence of the quantity $\frac{R}{R_0}$ on w than follows from the elementary calculation given above.

Figure 2-9. Diagram for the problem of bubble motion in a tube.

2-5. Generalization of Experimental Data on the Ascent Velocity of Single Bubbles

Let us consider in general the conditions determining the motion of a bubble in a liquid. The ascent velocity of the bubble depends on the difference in the densities of the liquid and the gas, and on

the drag of the surrounding liquid determined both by the physical properties of this liquid (μ' , γ' , σ) and by the shape and dimensions of the bubble itself. However, as contrasted to flow past solid bodies, the shape of a bubble is not invariable but depends on the conditions of the flow past the bubble, on the interaction of the forces on the surface film of the bubble and in the stream of liquid. In the case of very pure liquids, when flow on the phase boundary is observed, the effect of the viscosity of the gas also becomes noticeable.

Disregarding the latter factor for the time being, we may describe the motion of a liquid flowing past a bubble by the following system of equations:

$$\left. \begin{aligned} \vec{g}(p' - p'') - \text{grad } p' + \rho' \vec{v} \vec{v} &= \rho' \frac{D\vec{v}}{dt}; \\ \text{div } \vec{v} &= 0; \\ p_b - 2\gamma' \left(\frac{\partial x}{\partial y} \right)_b &= p'_b + \sigma \left(\frac{1}{R_1} + \frac{1}{R_2} \right); \\ \sigma_b &= \sigma'_b; \\ F_b(x; y; z) &= 0. \end{aligned} \right\} \quad (2-17)$$

The first two equations of (2-17) are the conventional equations of motion and of continuity of an incompressible fluid. The third equation (2-17) expresses the condition of the equality of the normal stresses on the phase boundary, taking into account the effect of surface tension and disregarding the influence of the viscosity of the gas. In this case, p' is the pressure in the liquid, and p'' is the pressure in the bubble. The last equation of (2-17) is the equation of the interface.

When converted into a dimensionless form, the system (2-17) gives the following primary similarity criteria:

$$\left\{ \frac{r'w^3}{g(r'-r)} : \frac{\Delta p}{\rho'w^3} : \frac{w^3}{v} : \frac{w^3}{l} : \frac{2g}{v} : \frac{2g}{\rho'w^3} \right\}. \quad (2-18)$$

Let us introduce new criteria, consisting of part of the criteria in (2-18):

$$\left. \begin{aligned} \frac{\Delta p}{\rho'w^3} \cdot \frac{v}{\Delta p l} \cdot \frac{\rho'w^3}{g(r'-r)} &= \frac{v}{(r'-r)R} : \\ \left(\frac{w^3}{v} \right)^2 \left[\frac{v}{(r'-r)R} \right]^2 \cdot \frac{g(r'-r)}{\rho'w^3} &= \\ &= \frac{g}{v^2} \left(\frac{v}{r'-r} \right)^2 \left(1 - \frac{r'}{r} \right) = \frac{v^2}{R^2 \sqrt{1-r'}} \end{aligned} \right\} \quad (2-19)$$

Furthermore, we note that the group

$$\frac{\Delta p l}{\rho'w^3} = \frac{\Delta p}{\rho'w^3} \cdot \frac{w^3}{v}.$$

i.e., is not a specific criterion and can be excluded from consideration. Consequently, taking into account (2-19) instead of the system of criteria (2-18), we may write the following equivalent system:

$$\left\{ \frac{w^3 R}{v} : \frac{\Delta p}{\rho'w^3} : \frac{w^3}{R} : \frac{v}{(r'-r)R^2} : \frac{v^2}{R^2 \sqrt{1-r'}} \right\}. \quad (2-20)$$

In this case, on the strength of the penultimate equation of (2-17), the ascent velocity of the bubble w'' is accepted as the characteristic velocity. The free ascent velocity of the bubble will be uniquely defined if the volume of the bubble as well as the physical properties of the gas and the liquid are known. Attention should be given to the fact that the volume of the bubble is always among the conditions which uniquely define a given phenomenon, while the shape of the bubble and its radius are functions of the process.

Since the volume is proportional to the cube of the characteristic linear dimension, we may introduce into (2-20) the equivalent

radius of the bubble:

$$R_{eq} = \sqrt[3]{\frac{3V}{4\pi}}$$

In the system (2-20), the last two criteria consist only of quantities that are among the uniquely defining conditions. Consequently, these criteria also determine the process of the rise of the gas bubble in a liquid. Hence

$$\frac{w^* R_{eq}}{v} = f \left[\frac{\frac{\sigma}{\rho_0} \frac{1}{R_{eq}}}{(1 - \frac{v^*}{v}) R_{eq}^2}; \frac{\sigma}{(1 - \frac{v^*}{v}) R_{eq}^2} \right] \quad (2-21)$$

or

$$\frac{w^* R_{eq}}{v} = f_1 \left[\frac{g R^2}{v^2} \left(1 - \frac{v^*}{v} \right); \frac{\sigma}{(1 - \frac{v^*}{v}) R_{eq}^2} \right] \quad (2-22)$$

The group $\frac{g R^2}{v^2} \left(1 - \frac{v^*}{v} \right)$ is called the Archimedes criterion.

Based on numerous experiments by Peebles and Garber and by other authors, the following specific expressions for the function f can be assumed.

1. The conditions of laminar flow past a bubble which remains spherically shaped at $Re = \frac{2w^* R}{v} < 2$ are

$$w^* = \frac{2(1 - \frac{v^*}{v}) R^2}{9\mu};$$

$$\zeta = 24 Re^{-1}.$$

2. The conditions of motion of bubbles having the shape of flat pulsing spheroids at $2 < Re < 4A^{0.42}$ are:

$$w' = 0.33 \frac{A^{0.25}}{r^{0.25}} R^{1.25}; \quad (2-23)$$

$$\zeta = 18.7 Re^{-0.25}. \quad (2-24)$$

3. The conditions of motion of bubbles having the shape of flat, relatively stable spheroids at $4A^{0.42} < Re < 3A^{0.50}$ are:

$$w' = 1.35 \sqrt{\frac{R^2}{(1'-1')R}}; \quad (2-25)$$

$$\zeta = 0.0275 A^{-1} Re^4. \quad (2-26)$$

4. The conditions of motion of mushroom-shaped bubbles at $Re < 3A^{0.50}$ are:

$$w' = 1.18 \sqrt{\frac{R^2 (1'-1')}{1'}}; \quad (2-27)$$

$$\zeta = 0.82 A^{-0.25} Re. \quad (2-28)$$

In these formulas, $A = \frac{\sigma \rho_1}{\rho_2 V \sqrt{1'-1'}}$ denotes the first of the criteria written in functional notation in (2-21).

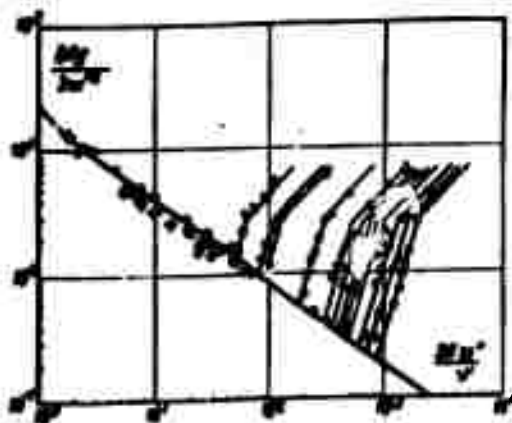


Figure 2-10. Generalized data on ascent velocities of single bubbles. Lines calculated by Formulas (2-5), (2-23), (2-25), and (2-27).

Figure 2-10 shows the results of experiments by Peebles and Garber, plotted on f , Re coordinates. The curves passing through the points were calculated from the above-mentioned formulas. As is evident from the graph, experimental points for various liquids up to a certain Re value fall on the general curve corresponding to the Stokes formula ($Re < 2$) and to Formula (2-24) ($Re > 2$). When the value $Re > 4A^{0.42}$ is reached, the single-valued relationship between f and Re is violated, and the experimental points for each liquid fall on a separate curve corresponding to Formulas (2-26) and (2-28).

2-6. Relative Motion of Single Drops

The relative motion of drops of a liquid in a stream of another liquid in the absence of mass transfer is described by the same system of equations as the motion of single gas bubbles in a liquid. Accordingly the functional relation (2-21) is also valid. A number of experiments on the motion of drops were carried out by N. I. Smirnov and V. L. Ruban. The special feature of these experiments was the fact that in them the ratio of drop diameter to container diameter was varied--i.e., the relationship between w and the parameter $\frac{R}{R_0}$ was determined experimentally. Unfortunately, there are no data in these experiments on surface tension coefficients at the boundary separating the liquids used. Therefore, we can plot only the relationships

$$Re = f\left(Ar; \frac{D}{D_0}\right). \quad (2-29)$$

where

$$Ar = \frac{gD^2}{\nu^2} \left(1 - \frac{\rho}{\rho_1}\right); \quad D = 2R; \quad D_0 = 2R_0.$$

Figure 2-11 shows the relationship between the group $\frac{18 Re}{Ar}$ and $\frac{D}{D_0}$ within the range of the Stokes law of drag ($Re < 2$). Within this range, according to Formula (2-5),

$$\left(\frac{18 Re}{Ar}\right)_{\frac{D}{D_0} \rightarrow 0} = 1.$$

Curve 1 in Fig. 2-11 corresponds to calculation by means of Formula (2-10). As can be seen, most of the experimental points demonstrate that the commensurability of the tube and the drop sizes has a greater influence than follows from the calculation given in Section 2-4. This circumstance can apparently be explained by the fact that the influence of the dimensions of the container is manifested not only by the appearance of a reverse current with the velocity w' of the entraining medium, but also by a retarding effect due to internal friction in the entraining stream.

As a result, there is a certain relationship between the function

$$\frac{Re}{Ar} = f\left(\frac{D}{D_0}\right)$$

and the criteria Ar and

$$\frac{D}{D_0}.$$

Thus far, however, the experimental data are insufficient for a detailed answer to this problem.

The results of experiments by N. I. Smirnov and V. L. Ruban with large drops are shown in Fig. 2-12 in the form of the relation

$$Re = f(Ar).$$

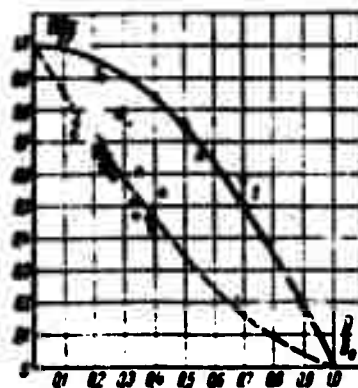


Figure 2-11. $\frac{18 Re}{Ar}$ vs $\frac{D}{D_0}$ from experiments with drops of one liquid in another liquid.

The range of Re values covered by these experiments corresponds, for a solid sphere, to the variation of f approximately from 0.75 to 0.45. As for the experiments under consideration, they can be satisfactorily correlated by the relation

$$Re = 2.6 Ar^{0.5},$$

(2-30)

which corresponds to a value of f of the order of 0.2 in Formula (2-3).

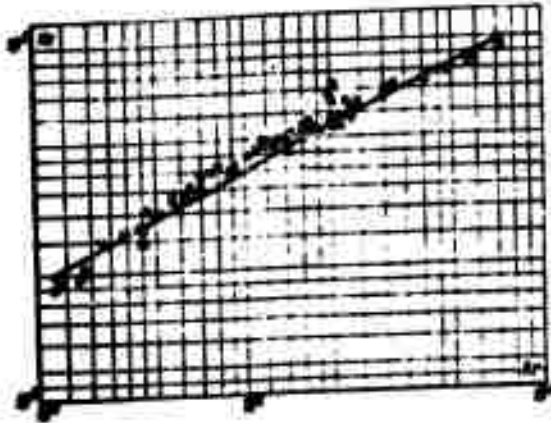


Figure 2-12. Re vs. Ar from experiments with drops of one liquid in another liquid.

Furthermore, the graph in Fig. 2-12 does not indicate any appreciable influence of the ratio $\frac{D}{D_0}$, although the authors of these experiments themselves arrived at the conclusion that they had discovered such an influence.

2-7. Release Diameter of a Gas Bubble Growing on a Solid Wall

In liquid degassing, boiling, and also in a series of heterogeneous chemical reactions, gas or vapor bubbles grow on a solid wall. The shape of a bubble on the wall varies with the wettability of the surface by the given liquid. The more wettable the wall, the smaller the angle of contact θ formed by the solid surface and the tangent to the bubble surface at its point of contact with the wall. The bubble is attached to the wall by a force which is proportional to surface tension σ . The Archimedes force and the dynamic pressure of the flowing liquid tend to sweep away the bubble from the wall.

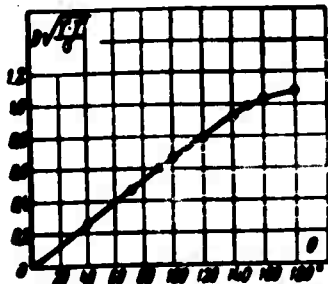


Figure 2-13. Release diameter vs. angle of contact of a bubble on a solid wall.

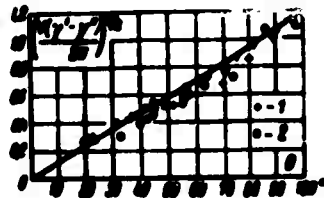


Figure 2-14. Comparison of calculations by Formula (2-31) (solid line) with experimental data. (1) hydrogen; (2) water vapor.

Figure 2-13 shows the results of calculations by V. Fritz determining the bubble diameter at the instant of its release from the wall (release diameter) in a motionless liquid phase. This relationship may be expressed by the interpolation formula

$$D_{\text{release}} = 0.0188 \sqrt{\frac{\sigma}{\gamma - \gamma_0}} \quad (2-31)$$

in which θ^0 is the angle of contact for wetting.

Figure 2-14 compares the results of these calculations with certain experimental data.

S. G. Teletov showed that in a moving liquid the release diameter of the gas bubble decreases as a function of the criterion $\frac{w'^2}{gD}$.

2-8. Formation of a Vapor Bubble on a Heating Surface

When a liquid boils on a heating surface and the heat flux is lower than the critical flux (see Chapter 7), vapor is generated in the form of bubbles at individual points of the heating surface. These points are called vaporization nuclei and are microscopic irregularities of the surface. If the heating surface is sufficiently large, the distribution of active nuclei becomes equally probable in all sections of the heating surface.

The temperature of the saturated vapor in a vapor bubble which is in a state of thermodynamic equilibrium is

$$t_R = t_{R\infty} + \Delta p_s \frac{dt''}{dp} \quad (2-32)$$

in which Δp_s is the effective pressure drop due to surface tension;

$t''_{R=\infty}$ is the saturation temperature above the plane at a pressure equal to the pressure in the liquid at the level of the bubble.

From Formulas (1-30) and (1-31) it follows that

$$\Delta p_s = \Delta p + \Delta p'' = \frac{2\sigma}{R(1-\gamma)} \quad (2-33)$$

The quantity $\frac{dt''}{dp}$ is determined by the well-known thermodynamic formula

$$\frac{dt''}{dp} = \frac{AT''(v'' - v')}{r''T''} \quad (2-34)$$

in which $A = \frac{1}{427}$ kcal/kg-m is the heat equivalent of work.

Hence, the radius of the bubbles formed in the superheated layer of the boiling liquid is determined by the formula

$$R_{min} = \frac{2AT''_0}{r''\Delta t} \quad (2-35)$$

in which Δt is the degree of superheating of the layer relative to the saturation temperature above the plane at the given pressure.

In the absence of microscopic protrusions (or depressions) on a heating surface with a radius of the order of R_{min} , vaporization is hampered and can take place only as the result of density fluctuations in the superheated liquid.

Figure 2-15 shows several frames of a motion-picture film from the work of L. M. Zysina-Molozhen and S. S. Kutadeladze on which the process of bubble boiling was recorded by high-speed exposure.

The first frame shows the instant at which the entire central part of the heating surface (dark stripe in the lower part of the frame) is wetted by the liquid (water).

In the second frame, 0.00475 second later, a small dark cone indicates the spot where a vapor bubble is forming. The linear dimensions in the frame are determined by a scale wire 0.2 mm in diameter, visible as an inclined dark line in the center of the frame.

In the third frame, 0.0095 second later, we see a vapor bubble

which has already taken shape; and finally, in the last (sixth) frame, 0.0285 second later, the vapor bubble is released from the heating surface and the latter is again in contact with the liquid phase at this point.



Figure 2-15. Growth process of a vapor bubble on the heating surface.

Figure 2-16 shows the results of frequency measurements of

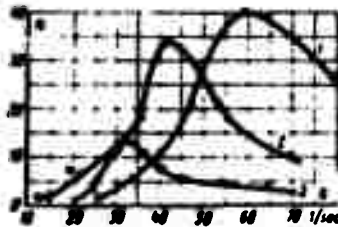


Figure 2-16. Bubble distribution as a function of the frequency of bubble formation (boiling water):

- (1) $\bar{p} = 1$ atm. abs.;
- (2) $\bar{p} = 1.95$ atm. abs.;
- (3) $\bar{p} = 2.77$ atm. abs.

vapor bubble formation in the same experiments. These data clearly illustrate the statistical nature of the process of bubble boiling. The well-defined maxima on the curves $n(u)$ denote the most probable frequency (under the given conditions) of vapor bubble formation. This quantity declines with increase of absolute pressure in the liquid.

2-9. Equation of Motion for a Bubble (Drop) in an Entraining Stream

If there is a pressure gradient in the entraining stream, due not only to the change in level (hydrostatics) but also to frictional losses (such as in flow through a tube), then in such a stream not only the Archimedes force but also the force due to the presence of $\text{grad } p_r$ will act on a bubble or drop.

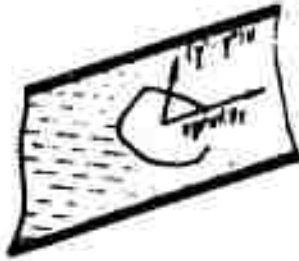


Figure 2-17. Diagram showing the interaction of the Archimedes force and the force proportional to $\text{grad } p_r$.

In the general case, the resultant action of these forces is equal to the vector sum

$$[\vec{g}(\rho' - \rho'') + \text{grad } p_r] V.$$

in which V is the volume of the bubble (drop).

The interaction of these forces is schematically shown in

Fig. 2-17.

The equation for the relative motion of a bubble (drop) in the entraining medium may be written in the following form:

$$\begin{aligned} & \left[\vec{g}_r(\rho' - \rho'') + \frac{dp_r}{dx} \right] V - \xi \frac{\rho'(\vec{w}' - \vec{w}'')^2}{2} Q - \\ & - \psi' V \frac{dw'}{dt} = \rho'' V \frac{dw''}{dt} + \phi(\vec{w}'' - \vec{w}') \rho'' \frac{dV}{dt}; \end{aligned} \quad (2-36)$$

here \vec{w}'' and \vec{w}' are the absolute velocities (relative to the container) of the bubble and of the entraining medium;

t is the time;

Q is the calculated bubble cross section;

ξ is the coefficient of resistance to relative motion of the bubble in the entraining medium, or drag coefficient;

ξ is the coefficient of entrainment of the entraining medium ("bound mass") equal to 0.5 for a sphere;

ϕ is the coefficient of reactivity which is a function of the unequal rate of evaporation (condensation) along the bubble surface.

The first term of this equation describes the force of expulsion of the bubble as a result of the pressure differences on its surface which are functions of the pressure field in the entraining stream. The second term describes the force of resistance to the relative motion of the bubble in the entraining medium. The third term describes the inertia of the bound mass (entrained with the relative motion of the bubble) of the entraining medium. The fourth term describes the inertia of the bubble itself. The fifth term describes the reactive force (Meshcherskiy Force) generated by the change in the mass of the bubble (drop) as a result of the processes of evaporation, condensation, combustion, or diffusion.

For a bubble having the shape of a sphere (i.e., of a rather small bubble), it follows from (2-36) that:

$$\begin{aligned} & R_s(\rho' - \rho'') + \frac{\partial \rho_l}{\partial t} - \frac{3\rho'}{4D} (w' - w)^2 - \\ & - \frac{1}{2} \frac{dw'}{dt} = \rho' \frac{dw'}{dt} + \rho' \frac{2w'}{D} (w' - w) \frac{dD}{dt}. \end{aligned} \quad (2-37)$$

Calculations show that the time of nonsteady motion of bubbles (drops) with a constant mass is very short. Thus, for example, at $\rho'' = 8 \text{ kg/m}^3$, $\rho' = 950 \text{ kg/m}^3$ and $D = 0.2 \text{ mm}$, the time of acceleration of the bubble from zero to 99% of the equilibrium relative velocity is of the order of 10^{-5} second; under the same conditions and $D = 5 \text{ mm}$, this time is of the order of 10^{-3} second.

CHAPTER THREE

DOWNFLOW OF LIQUID FILMS

3-1. Flow Regimes in Thin Films

Comparatively thin, flowing liquid films, washed by a gas or steam, are found in different condensation, absorption and other equipment. Depending on the value of the criterion of kinematic similarity

$$Re = \frac{u \delta}{\nu}, \quad (3-1)$$

where δ is the thickness of the film; three fundamental types of flow regimes can be observed:

- 1) laminar flow of liquid film with a smooth interface
($Re < 30$ to 50);
- 2) laminar flow of liquid film with a rippled interface
(30 to $50 < Re < 100$ to 400);
- 3) turbulent flow of liquid film ($Re > 100$ to 400).

The mass flow rate of liquid per 1 m width of film is

$$G_1 = \rho \delta u \quad (3-2)$$

and consequently,

$$Re = \frac{\rho \cdot \bar{u} \cdot \delta}{\mu}$$

(3-3)

Thus, the Reynolds criterion of the liquid film can be calculated without any direct separate measurement of the thickness and average velocity of the film.

3-2. Equations of Motion for a Film

As a result of the slight thickness of the film, its flow may be considered to be planar, even on curved surfaces (tubes, nozzles). Also, by virtue of the same slight thickness of the film the derivatives of velocity taken across the film are large in comparison with the derivatives along the film, and the pressure change across the film is, for all practical purposes, nil. In this connection, the equations of flow for the film (Fig. 3-1) may be written in the following form:

$$\left. \begin{aligned} \frac{\partial v}{\partial y} &= 0; \\ \rho \left(\frac{\partial v}{\partial t} + v \frac{\partial v}{\partial x} + w \frac{\partial v}{\partial y} \right) &= -\rho \left(\frac{\partial u}{\partial x} + v \frac{\partial u}{\partial x} + w \frac{\partial u}{\partial y} \right); \\ \frac{\partial u}{\partial x} + \frac{\partial v}{\partial y} &= 0. \end{aligned} \right\} \quad (3-4)$$

Thus the equations for the film are analogous to the familiar equations for the boundary layer of an unbounded liquid stream.

At the wall

$$u_x = u_y = 0.$$

At the interface

$$p' = p'' + p_0;$$

$$p' \frac{\partial u_x}{\partial y} = \pm \xi'' \frac{p'' u_x}{\delta};$$



Figure 3-1. Diagram of film flow on a vertical wall.

here ξ'' is the coefficient of friction of the gas against the film surface, whose sign depends

on the direction of the gas flow relative to the direction of the vector \vec{g} .

It follows from the equation of continuity that:

$$u_x' = - \int \frac{\partial u_y}{\partial x} dy. \quad (3-5)$$

The condition of continuity of flow in an elementary volume of the film $dV = \delta \cdot 1 \cdot dx$ gives:

$$u_x' = \frac{d}{dx} \int_0^\delta u_y dy. \quad (3-6)$$

in which δ is the thickness of the film;

u_{ch}' is the rate of change of phase at the film surface.

Assuming that the curvature of the film changes substantially only in the direction of flow--i.e., along the x -axis--we may write that the excess pressure is equal to

$$p' = \gamma x + \frac{\sigma}{R_s} \quad (3-7)$$

The radius of curvature of the film surface is related to its thickness and to the x -coordinate by the well-known function

$$R_s = - \left[1 + \left(\frac{\partial h}{\partial x} \right)^2 \right]^{3/2} \frac{1}{\frac{\partial^2 h}{\partial x^2}}$$

Since $\frac{\partial h}{\partial x} \ll 1$, Equation (3-7) may be rewritten in the following form:

$$p' \approx \gamma x - \sigma \frac{\partial^2 h}{\partial x^2} \quad (3-8)$$

Substituting this value of p' into the equation of motion for the film, we obtain:

$$\begin{aligned} \rho_s (p' - p'') &= \sigma \frac{\partial^2 h}{\partial x^2} - \gamma \frac{\partial^2 h}{\partial y^2} = \\ &= \gamma \left[\frac{\partial^2 h}{\partial t^2} + u_x \frac{\partial^2 h}{\partial x} - \left(\int \frac{\partial^2 h}{\partial x} dy \right) \frac{\partial^2 h}{\partial y} \right] \end{aligned} \quad (3-9)$$

3-3. Laminar Flow of a Film of Constant Thickness on a Vertical Wall

When the motion of a film of constant thickness ($q' = \text{const}$; $\delta = \text{const}$) is slow and steady, the interface remains strictly parallel to the surface of the wall along which the film is flowing. In this case the equation of motion takes the elementary form:

$$\tau' - \tau'' + \rho' \frac{dw'}{dy'} = 0. \quad (3-10)$$

The boundary conditions for this equation are:

$$\left. \begin{array}{l} y=0, \quad w'=0; \\ y=\delta, \quad \rho' \frac{dw'}{dy'} = \pm \zeta' \frac{\tau' \sigma_r'}{2g} \end{array} \right\} \quad (3-11)$$

Integrating (3-10) and taking Conditions (3-11) into account, we obtain:

$$w' = \left(\pm \zeta' \frac{\tau' \sigma_r'}{2g\rho'} + \frac{\tau' - \tau''}{\rho'} \right) y - \frac{\tau' - \tau''}{2\rho'} y^2. \quad (3-12)$$

For downflow of gas, a plus sign must be used in the second term of this equation (the gas carries the liquid film along in the same direction as the force of gravity). For upflow of gas (the gas retards the downflow of the film), a minus sign is used.

The velocity of the liquid on the phase boundary is

$$w'_\delta = \pm \zeta' \frac{\tau' \sigma_r'}{2g\rho'} \delta + \frac{\tau' - \tau''}{2\rho'} \delta^2. \quad (3-13)$$

The relative velocity of the gas is equal to

$$w'_r = w' - w'_\delta. \quad (3-14)$$

The average (flow) velocity of the liquid in the film is

$$\bar{v} = \frac{1}{\delta} \int_0^\delta v dy = \pm C \frac{r_0^2}{2\eta} + \frac{r-r_0}{2\eta} v. \quad (3-15)$$

When the gas flows upward the liquid flow velocity becomes negative (the whole film is carried along upward) at

$$\frac{2C r_0^2}{\eta(r-r_0)} > 1. \quad (3-16)$$

Condition (3-16) determines the "flooding" of the apparatus.

In view of the low flow velocities in a viscous film, we may assume for practical purposes that $w_r'' = w''$ without resorting to the calculation of the quantity w_b' by means of Equation (3-13).

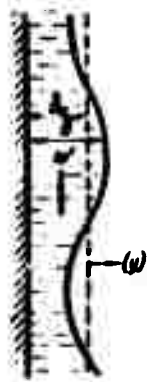
Multiplying both parts of Formula (3-15) by the quantity $r'\delta$, we obtain:

$$Q_1 = \pm C \frac{r_0^2}{\eta} v + \frac{\delta(r-r_0)}{2\eta} v. \quad (3-17)$$

this equation permits us to calculate the thickness of the laminar film from the known liquid flow rate. Particularly for the case of flow in a practically motionless gas,

$$\delta = \sqrt{\frac{2\eta Q_1}{\delta(r-r_0)}}. \quad (3-18)$$

3-4. Wave Flow of Film at $w'' \approx 0$



In the case of a wave regime capillary waves appear on the surface of the film (Fig.3-2). The capillary forces, which then appear as the result of a deformation of the interface, are commensurate with the forces of gravity and viscosity acting in the film. This type of flow was investigated by P. L. Kapitsa, whose solution was

Figure 3-2. Wave-like motion of a defined somewhat more accurately by V. G. Levich and V. K. Bushmanov.

At $w'' \approx 0$, tangential stresses on the free surface of the film are for practical purposes absent, and the velocity profile when the surface is undisturbed has, according to (3-12) and (3-15), the form:

$$u_z = \frac{\bar{w}_z}{1} \left(y - \frac{y^2}{2} \right) \quad (3-19)$$

In wave motion, the average velocity along the cross section is a function of the x -coordinate as well as of time τ . Therefore, we assume for the case under study that:

$$u_z = \frac{\bar{w}_z(x, \tau)}{1} \left(y - \frac{y^2}{2} \right) \quad (3-20)$$

This equation satisfies the boundary conditions (3-11) at $w'' = 0$.

By substituting the value of w_x^i from (3-20) into the equation of motion for the film (3-9), by integrating the obtained equation term by term within the limits of $y = 0$ and $y = \delta$, and by dividing by δ (i.e., by averaging over the thickness of the film), we obtain:

$$\frac{\partial \bar{w}_x}{\partial t} + \frac{\partial}{\partial x} \bar{w}_x \frac{\partial \bar{w}_x}{\partial x} = \frac{\rho}{\rho'} \cdot \frac{\partial^2 \bar{w}_x}{\partial x^2} - \frac{\partial \bar{w}_x}{\partial x} + \frac{1' - 1'}{\rho'}. \quad (3-21)$$

The equation of continuity (3-6) at $w_n^i = 0$ takes the form:

$$\frac{\partial}{\partial t} = - \frac{\partial (\bar{w}_x)}{\partial x} \quad (3-22)$$

Considering waves of small amplitude only we will express the film thickness in the form of a binomial:

$$\delta = \bar{\delta} + \varphi \delta \quad (3-23)$$

where $\bar{\delta}$ is the average thickness of the film;

φ is the coefficient of deviation of the instantaneous value of the thickness from its average value.

Capillary waves originating on the surface of a film flowing downward under the influence of gravity are not damped. Thus, we may consider that all the quantities in Equation (3-21) are functions of the x -coordinate and the phase velocity v , i.e., of the argument $(x - vt)$. Then

$$\left. \begin{aligned} \frac{\partial}{\partial x} - v \frac{\partial}{\partial x} &= -v \frac{\partial}{\partial x} \\ \frac{\partial}{\partial x} - v \frac{\partial}{\partial x} &= -v \frac{\partial}{\partial x} \end{aligned} \right\} \quad (3-24)$$

Introducing these expressions into Equations (3-21) and (3-23), we obtain:

$$\left(\frac{\partial}{\partial x} - v \right) \frac{\partial \bar{w}_x}{\partial x} = \frac{\partial}{\partial x} \frac{\partial \bar{w}_x}{\partial x} - \frac{\partial \bar{w}_x}{\partial x} + \frac{\partial \bar{w}_x}{\partial x} \quad (3-25)$$

$$\frac{\partial}{\partial x} [(v - \bar{w}_x) \bar{w}_x (1 + v)] = 0. \quad (3-26)$$

It follows directly from the latter equation that

$$\bar{w}_x (v - \bar{w}_x) (1 + v) = \text{const } \bar{w}_x (v - w_0). \quad (3-27)$$

where w_0 is the average velocity in a stream of cross section \bar{w} .

It follows from (3-27) that the following relation applies in the wave at the film surface:

$$\bar{w}_x = v - \frac{v - w_0}{1 + v}. \quad (3-28)$$

expanding this expression into a series, we have:

$$\left. \begin{aligned} \bar{w}_x &= w_0 + (v - w_0) (v - v^2 + v^3 \dots) \\ \frac{\partial \bar{w}_x}{\partial x} &= (v - w_0) (1 - 2v + 3v^2 \dots) \frac{\partial v}{\partial x} \end{aligned} \right\} \quad (3-29)$$

Substituting these expressions into (3-25), we obtain an equation for the dimensionless amplitude ψ . At small amplitudes $\psi \ll 1$, which allows us to consider only first approximations for w'_x and $\delta \bar{w}'_x / \delta x$.

The energy loss due to friction in the film, per m^2 of wall surface, is

$$-\frac{dE}{dt} \approx \mu \int_0^{\lambda} \left(\frac{\partial w'_x}{\partial y} \right)^2 dy = 3\mu \int_0^{\lambda} \frac{\bar{w}_x'^2}{\delta} dx. \quad (3-30)$$

Averaging along the wavelength we obtain,

$$\left(\frac{dE}{dt} \right)_\lambda = -\frac{3\mu}{\lambda} \int_0^{\lambda} \frac{\bar{w}_x'^2}{\delta} dx. \quad (3-31)$$

where λ is the wavelength in the given instance.

The average work of gravity per m^2 of wall is

$$L = G'_\lambda. \quad (3-32)$$

In a steady-state process, the condition

$$\left| \frac{dE}{dt} \right| = L.$$

must be satisfied, from which it follows, after transformation, that:

$$\bar{p} = \frac{\sigma' g_1}{g(\bar{r}' - r')} \Phi. \quad (3-33)$$

where

$$\Phi = \frac{1}{\lambda} \int_0^{\lambda} \left(\frac{1 + \frac{\sigma'}{\sigma_0} \psi}{(1 + \psi)^2} \right) dx. \quad (3-34)$$

By V. G. Levich's calculations, as a second approximation,

$$\left. \begin{aligned} \psi &= 0.21 \sin [k(x - vt)]; \\ k &= \left(0.9 \frac{\sigma' g_1}{\gamma \rho} \right)^{1/2}; \\ v &= 2.4 w_0; \\ \Phi &= 0.8. \end{aligned} \right\} \quad (3-35)$$

The measurements of the wave profile, carried out by means of the shadow method by P. L. Kapitsa and S. P. Kapitsa, showed satisfactory agreement of theory and experiment. At the same time, another important circumstance was discovered in the course of the experiments: the wave regime in the film flow is relatively easily transformed into a turbulent regime when external perturbations act on the stream.

3-5. Turbulent Flow of a Film of Constant Thickness on a Vertical Wall

As a first approximation, a turbulent flow may be divided into a laminar sublayer and a turbulent core (Fig. 3-3). The velocity profile in this case is determined by a system of two equations:

$$\left. \begin{aligned} v_{x,y_1} &\approx \mu' \frac{dv}{dy}; \\ v_{x,y} &\approx \mu' x^2 y^2 \left(\frac{dv}{dy} \right)^2 \end{aligned} \right\} \quad (3-36)$$

here y_1 is the calculated thickness of the laminar sublayer;

x is a constant characterizing the structure of the turbulent stream.

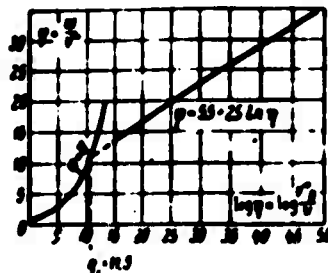


Figure 3-3. Velocity distribution for a two-layer pattern of turbulent flow.

According to available experimental data $x = 0.4$ and $y_1 = 11.6 x \sqrt{\frac{\mu}{\rho}}$. Expressions (3-36) have approximate-equality signs since, in reality, the turbulent fluctuations also penetrate into the laminar sublayer, and since the viscous friction plays a well-known part in the turbulent core in the

vicinity of the sublayer. Besides, the expression given above for the tangential stress which is due to turbulent friction is itself only approximate.

In the film, the tangential stresses in a steady flow balance the effect of gravity and the friction of the gas against the free surface of the liquid, i.e.,

$$\dot{\gamma} = g(\rho' - \rho'')(1-y) \pm \tau' \frac{\dot{\gamma} w^2}{g} \quad (3-37)$$

On a solid wall $y = 0$ and the tangential stresses are

$$\tau_w = g(\rho' - \rho'')(1) \pm \tau' \frac{\dot{\gamma} w^2}{g} \quad (3-38)$$

On the phase boundary $y = \delta$ and the tangential stresses are

$$|\tau_\delta| = \tau' \frac{\dot{\gamma} w^2}{g} \quad (3-39)$$

As a result of the small thickness of the laminar sublayer, tangential stresses in this layer may be considered practically constant and equal to τ_w . For a slowly moving gas ($w_R'' \approx 0$), we have

(a) in the laminar sublayer

$$g \frac{r' - r''}{r'} (1 - y) = \tau' \frac{dw}{dy} \quad (3-40)$$

(b) in the turbulent core

$$g \left(\frac{r' - r''}{r'} \right) (1 - y) = r' y' \left(\frac{dw}{dy} \right)^2 \quad (3-41)$$

Integrating (3-40), we obtain:

$$w'_{y, < \delta} = \frac{\delta}{y} \cdot \frac{y - y_1}{y} \cdot \gamma; \quad (3-42)$$

accordingly, on the boundary between the sublayer and the core.

$$w_i = 11.6 \sqrt{\delta \left(1 - \frac{y_1}{y}\right)^3}. \quad (3-43)$$

Integrating (3-41), we obtain:

$$w'_{y, > \delta} = \frac{1}{2} \sqrt{\delta \left(1 - \frac{y_1}{y}\right)} \times \\ \times \left(2\sqrt{1-y} + \sqrt{2} \ln \frac{\sqrt{1-y} - \sqrt{1}}{\sqrt{1-y} + \sqrt{1}} + C\right). \quad (3-44)$$

The constant of integration is determined by the condition that at $y = y_1$, $w' = w'_1$. Finally, we have:

$$w'_{y, > \delta} = w'_i + \frac{1}{2} \sqrt{\delta \left(1 - \frac{y_1}{y}\right)} \left[2\sqrt{1-y} - 2\sqrt{1-y_1} - \right. \\ \left. + \sqrt{2} \ln \frac{(\sqrt{1-y_1} - \sqrt{1-y})(\sqrt{1-y_1} - \sqrt{1-y_1})}{(\sqrt{1-y_1} + \sqrt{1-y})(\sqrt{1-y_1} + \sqrt{1-y_1})}\right]. \quad (3-45)$$

In the vicinity of the solid wall, where $y \leq \delta$, we may assume that $\sqrt{1 - \frac{y}{\delta}} = 1 - \frac{y}{2\delta}$, and Formula (3-45) takes the form:

$$\begin{aligned}
 v \approx v_1 + \frac{1}{2} \sqrt{s \left(1 - \frac{r_1}{r}\right)^3} \times \\
 \times \left[\frac{2-y}{1} + \ln \frac{r \left(2 - \frac{2y}{s}\right)}{r_1 \left(2 - \frac{2}{s}\right)} \right] \approx v_1 + \\
 + \frac{1}{2} \sqrt{s \left(1 - \frac{r_1}{r}\right)^3} \ln \frac{r}{r_1}.
 \end{aligned}
 \tag{3-46}$$

The last expression is the familiar logarithmic law of velocity distribution in a turbulent stream in the vicinity of a solid wall.

As may be seen from these calculations, although a relatively simple logarithmic velocity profile does not satisfy the boundary conditions on the free surface of the film, it nevertheless does permit calculating the velocities in various cross sections of the film with an error not exceeding 5% in most cases of practical interest.

In this case, the greatest error is made in the immediate vicinity of the free surface of the film. This circumstance is explained by the fact that the most substantial velocity change takes place in the relatively thin layer of the film in the vicinity of the wall when $y \ll \delta$ and Formula (3-46) is sufficiently valid. In the external layers of the turbulent film, however, velocity varies relatively little.

We must also point out that in the external boundary of the film the intensity of the turbulent fluctuations may be damped, not only as a result of the decrease in the quantity dy/dy , but also under the influence of the resistance of the surface layer of molecules, i.e., as a result of the surface tension of the liquid.

The influence of this effect can hardly be substantial since in the vicinity of the film surface the velocity varies negligibly.

Table 3-1. Comparison of velocity profiles in a film freely flowing down a smooth vertical wall, calculated from Formula (3-45) and approximate Formula (3-46).

$\frac{z}{\delta}$		0.00	0.25	0.50	0.75	1
$\frac{z_1}{\delta} = 0.10$	$v = w \sqrt{\frac{z}{z_w}}$ by (3-45)	11.6	13.9	15.7	16.9	18.3
	$v = w \sqrt{\frac{z}{z_w}}$ by (3-46)	11.6	13.9	15.6	16.6	17.3
	$\frac{v-v_1}{v_1} 100\%$	0.0	0.07	-0.06	-1.8	-5.5
$\frac{z_1}{\delta} = 0.01$	$v = w \sqrt{\frac{z}{z_w}}$ by (3-45)	17.3	19.6	21.4	22.6	24.1
	$v = w \sqrt{\frac{z}{z_w}}$ by (3-46)	17.3	19.6	21.4	22.4	23.1
	$\frac{v-v_1}{v_1} 100\%$	0.0	0.0	0.0	-0.9	-4.1

The average velocity in the film is

$$\bar{w} = \frac{1}{\delta} \left(\int_0^{\delta} w dy + \int_{\delta}^{\delta_1} w dy \right).$$

Substituting the value w' from (3-46) into this formula and assuming that $y_1 \ll \delta$, we obtain:

$$\begin{aligned} \bar{w} &\approx \frac{w_1}{\sqrt{z_1}} \left(1 - \frac{z_1}{z} \right) + \\ &+ \frac{1}{z_1} \sqrt{g \delta \left(1 - \frac{z_1}{z} \right)} \left(\ln \frac{z}{z_1} - 1 \right). \end{aligned} \quad (3-47)$$

Multiplying both members of this equation by the ratio $\frac{\delta}{\gamma}$ and introducing the values x and y_1 , we obtain:

$$\begin{aligned} \text{Re} - \frac{G_1'}{g} &\approx \sqrt{\frac{g^2}{\gamma^2} \left(1 - \frac{\gamma'}{\gamma}\right)} \left(11.6 + \right. \\ &\left. + 2.5 \left[\ln \left(\frac{1}{11.6} \sqrt{\frac{g^2}{\gamma^2} \left(1 - \frac{\gamma'}{\gamma}\right)} - 1 \right] \right) \right]. \end{aligned} \quad (3-48)$$

Substituting the value of G_1' into this equation, it is possible to calculate the thickness of the turbulent film at a given liquid flow rate.

3-6. Laminar Flow on a Film when Condensation and Evaporation Occur

In the case of a film freely flowing downward, it follows from Formula (3-12) that

$$w = \frac{\gamma' - \gamma}{\gamma} \left(2y - \frac{\gamma^2}{2} \right). \quad (3-49)$$

When vapor condensation or evaporation occurs at the film surface, the rate of change of phase is not zero. Then, according to (3-6),

$$\frac{d}{dx} \int_0^{\delta} w' dy = w_s. \quad (3-50)$$

Substituting into the latter expression the value of the flow velocity of the film from (3-49), we obtain:

$$\delta \frac{d\delta}{dx} = \frac{r'}{T' - T''} \delta^2 = \frac{r' \Delta t}{\rho \lambda (T' - T'')} \quad (3-51)$$

in which $r \left[\frac{\text{kcal}}{\text{kg}} \right]$ is the latent heat of vaporization;

$\frac{\delta}{\lambda}$ is thermal resistance of the laminar film.

After integration, we obtain:

$$\delta = \sqrt{\delta_0^2 + \frac{r' \Delta t x}{\rho \lambda (T' - T'')}} \quad (3-52)$$

At $\delta_0 = 0$

$$\delta = \sqrt{\frac{r' \Delta t x}{\rho \lambda (T' - T'')}} \quad (3-53)$$

and consequently,

$$q_s = \frac{\lambda}{\delta} = \sqrt{\frac{\rho \lambda (T' - T'')^3}{r' \Delta t x}} \quad (3-53)$$

3-7. Heat Transfer between a Turbulent Film and a Vertical Wall

We may write the following equation for the coefficient of heat transfer from the turbulent stream to the wall:

$$\frac{h}{k} = \frac{1}{2} f(Pr; Re), \quad (3-54)$$

in which $Pr = \frac{c_p \mu}{k}$.

In a substantial range of Prandtl and Reynolds numbers (but at $Pr > 0.6$)

$$f(Pr; Re) \approx Pr^{0.4}. \quad (3-55)$$

Taking into account that

$$Re = \frac{\bar{u}^2}{\nu} = \frac{q_1}{\mu},$$

we may write:

$$\frac{h}{k} \approx \frac{1}{2} \left(\frac{\nu}{\alpha} \right)^{0.4} \frac{q_1}{\mu} \cdot \frac{1}{l}. \quad (3-56)$$

Expressing the tangential stresses on the wall in terms of the dynamic head of the film, we have:

$$\tau_w = \zeta' \frac{\bar{u}^2}{2g}. \quad (3-57)$$

Combining (3-57) and (3-37) at $y = 0$, we obtain for a slowly moving gas (vapor):

$$\frac{\rho}{\rho_0} = \left[\frac{c^2}{2g^2(r-r_0)} \right]^{\frac{1}{2}} \left(\frac{\partial \phi}{\partial r} \right)^{\frac{1}{2}}. \quad (3-58)$$

By substituting this value of $\frac{\rho}{\rho_0}$ into (3-56), we find that

$$\frac{\rho}{\rho_0} \left(\frac{\partial \phi}{\partial r} \right)^{\frac{1}{2}} \approx \left(\frac{c^2}{2g^2} \right)^{\frac{1}{2}} \left(\frac{\partial \phi}{\partial r} \right)^{\frac{1}{2}} \left(\frac{\partial \phi}{\partial r} \right)^{\frac{1}{2}}. \quad (3-59)$$

CHAPTER FOUR

DISCHARGE OF A GAS INTO A LIQUID

4-1. Peculiarity of the Discharge of a Gas into a Liquid

In contrast to so-called submerged jets, where the material in the jet and the material filling the space are capable of molecular mixing, interfaces appear when a gas is discharged into a liquid. In this case, the molecules of the light and heavy components of the system do not mix. Penetration of one phase into the other takes place in the form of separate small jets, bubbles, and drops.

4-2. Dimensions of a Bubble Released from an Orifice

In the case of moderate escape velocities, the light phase flows out from the nozzle orifice in the form of bubbles (drops) successively breaking away. In the general case, the bubble which forms is acted upon by buoyancy and convection currents in the liquid, which tend to sweep the bubble away from the rim of the orifice. The force pressing the bubble against the rim of the orifice is proportional to the surface tension and the perimeter of the orifice.

When the convection currents are weak and the viscosity of the liquid is low, we have:

$$\frac{4}{3}\pi R_0^3(\gamma' - \gamma) = 2\pi R_1 s, \quad (4-1)$$

where R_0 is the radius of the bubble at the instant of its release and R_1 is the radius of the orifice. Hence,

$$R_0 = \sqrt[3]{\frac{3R_1 s}{2(\gamma' - \gamma)}}, \quad (4-2)$$

or, in a dimensionless form,

$$\frac{R_0}{R_1} = 1.14 \sqrt[3]{\frac{\gamma}{(\gamma' - \gamma) R_1^2}}. \quad (4-3)$$

In the general case, the proportionality factor in Formula (4-3) is a function of the criteria which determine the hydrodynamic process in the two-phase system as a whole.

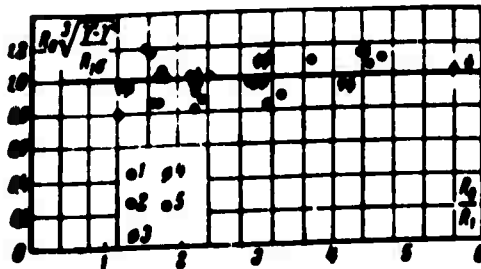


Figure 4-1. Value of $\frac{R_0}{R_1} \sqrt[3]{\frac{\gamma}{(\gamma' - \gamma) R_1^2}}$ from experimental data. Gas: air; liquid medium: (1) ethyl alcohol; (2) benzene; (3) water; (4) nitrobenzene; (5) carbon tetrachloride.

Figure 4-1 shows, on the coordinates of Formula (4-3), the results of the experiments by N. I. Smirnov and S. E. Polyut. As can be seen, this simple formula generally agrees rather well with experimental data, but the coefficient of the radical should be taken approximately as unity. The

empirical formula advanced by the authors mentioned above has the form:

$$\frac{R_2}{R_1} = \left[1.11 - 122 \left(\frac{r}{r' - r} \right)^{0.88} \right] \left(\frac{r}{r' R_1} \right)^{0.22} \quad (4-4)$$

4-3. Velocity of Discharge Through a Rather Large Orifice

Let us consider the discharge of a light component into a heavy one as the successive formation and release of a series of separate bubbles (drops). The diagram for such a discharge that is characteristic of a two-phase system is shown in Fig. 4-2.

If we disregard inertial forces, the work of bubble formation is the sum of the work of changing the free interface and the work of overcoming hydraulic resistance to the displacement of the growing bubble.

The work of formation of the free surface is

$$dL_s = \sigma dF_b \quad (4-5)$$

In the case of a spherically-shaped interface

$$F_b = 4\pi R^2$$

and

$$dL_s = 2\pi R dR. \quad (4-6)$$

The resistance to the displacement of the bubble is

$$S = \zeta \frac{\rho w^3}{2} dR. \quad (4-7)$$

where ζ is the drag coefficient (generally variable);

w is the velocity of the phase boundary relative to the heavy phase.

Hence, the elementary work of the drag is

$$dL_s = \zeta \frac{\rho w^3}{2} dR. \quad (4-8)$$

Comparing (4-6) and (4-8), we find that the ratio of the elementary work of the free surface formation and the work of overcoming the drag of the heavy phase is

$$\frac{dL_s}{dL_s} = \frac{2\pi R}{\zeta \rho w^3 R}. \quad (4-9)$$

Assuming that when convection currents are weak, the relative velocity is equal to the rate of growth of the bubble.

$$w = \frac{dR}{dt}. \quad (4-10)$$

in which τ is the time, we obtain

$$\frac{dL_2}{dL_1} = \frac{\rho_2}{\rho_1 R} \left(\frac{dR}{d\tau} \right)^2. \quad (4-11)$$

The equation of the conservation of mass gives:

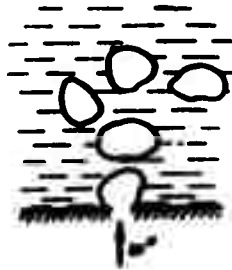
$$4R_1^2 \gamma_1' w_0' d\tau = \gamma' 4\pi R^2 dR, \quad (4-12)$$

in which w_0' is the velocity of discharge, i.e., the flow velocity of the light phase through the nozzle orifice. Hence,

$$\frac{dR}{d\tau} = \frac{w_0'}{4} \left(\frac{R_1}{R} \right)^2. \quad (4-13)$$

Substituting this value of $dR/d\tau$ into (4-11), we have

$$\frac{dL_2}{dL_1} = \frac{22\pi w_0'^2}{(\gamma_1'^2 R_1^2)}; \quad (4-14)$$



as an example of this, for the discharge of air into water at

$$w_0' = 1 \text{ m/sec};$$

$$\gamma' = 1,000 \text{ kg/m}^3;$$

$$\sigma = 7 \cdot 10^{-3} \text{ kg-force/m};$$

$$R_1 = 3 \cdot 10^{-3} \text{ m};$$

Figure 4-2. Diagram showing discrete discharge of the light phase into the heavy phase.

$R \approx R_1$ and when a turbulent flow past the bubble is present
($f \approx 0.4$) we obtain:

$$\frac{dL_s}{dL_1} = \frac{288 \cdot 0.01 \cdot 7 \cdot 10^{-3}}{0.4 \cdot 1^2 \cdot 1000 \cdot 3 \cdot 10^{-3}} = 15.$$

In this connection, as a first approximation for turbulent flow past a bubble, we may consider only the quantity

$$L_s = \int_0^2 dL_s = 4\pi R_1^2 \tau. \quad (4-15)$$

In the case of laminar flow past a bubble ($Re < 2$)

$$\zeta = \frac{24}{Re} > 12. \quad (4-16)$$

as a consequence of which L_s and L_1 become commensurate.

The work of bubble formation is accomplished at the expense of loss in kinetic energy of the light phase flowing into the bubble during the time τ_1 of bubble formation, i.e.,

$$L = \int_0^{\tau_1} \pi R_1^2 \frac{v_1^2}{2} \omega_1 dt. \quad (4-17)$$

Hence,

$$\frac{\bar{u}}{\Delta t} = \int u_i dt. \quad (4-18)$$

The average flow velocity through the orifice is

$$\bar{u}_i = \frac{1}{\Delta t} \int u_i dt. \quad (4-19)$$

and the time of bubble formation is

$$t_1 = \frac{4R_0^2}{3\bar{u}_i}. \quad (4-20)$$

The average flow velocity of the light phase during the time lapse $\Delta t > t_1$ is

$$\bar{u} = \bar{u}_i. \quad (4-21)$$

where

$$t = \frac{t_1}{1 + t_2/t_1}. \quad (4-22)$$

here t_2 is time lapse between the instant one bubble is released and the instant another bubble begins to form.

Let us assume that

$$\frac{dR}{dt} = Cr^2; \quad (4-23)$$

therefore

$$R = \frac{C}{n+1} r^{n+1} \quad (4-24)$$

and

$$w_1' = \frac{6C^2}{R_1^2(n+1)^2} r^{2n+2}. \quad (4-25)$$

Substituting the value of w_1'' from (4-25) into (4-19), we find after calculation that

$$w_1' = 3\bar{w}_1'(n+1) \left(\frac{r}{r_1}\right)^{2n+2}. \quad (4-26)$$

Substituting the values of \underline{L}_e and w_1'' into (4-17) we obtain, after integration,

$$\bar{\sigma} = \epsilon \sqrt{\frac{9}{8} \cdot \frac{9m+7}{(m+1)^2} \cdot \frac{\sigma}{r^2 R_0}} \quad (4-27)$$

Assuming that in the case of weak convection currents the magnitude of R_0 may be determined from Formula (4-2), we have after simple transformations

$$\frac{\bar{\sigma} \sqrt{r}}{\sqrt{\sigma (r^2 - r)}} = 0.47 \epsilon \sqrt{\frac{9m+7}{(m+1)^2}} \sqrt{\frac{\sigma}{(r^2 - r) R_0^2}} \quad (4-28)$$

At a constant rate of growth of the bubble ($m = 0$), we obtain the following expression:

$$\frac{\bar{\sigma} \sqrt{r}}{\sqrt{\sigma (r^2 - r)}} = 1.28 \epsilon \sqrt{\frac{\sigma}{(r^2 - r) R_0^2}} \quad (4-29)$$

4-4. Formation of a Stable Gas Cushion Under the Orifice of a Perforated Plate

One of the problems of practical importance in the hydraulics of two-phase flow is the question of a steady work regime of a horizontal perforated plate through which vapor (gas) bubbles into the

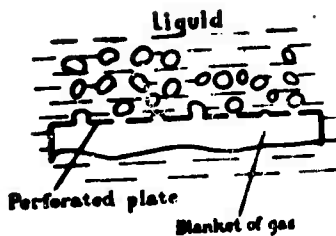


Figure 4-3. Diagram showing the operation of a submerged perforated plate.

liquid layer (Fig. 4-3). In this case, there is a steady supply of gas along with the formation of a continuous gas layer (gas cushion) under the perforated plate.

Evidently, the condition for the steady existence of a stable gas cushion is the requirement that

$$\bar{w} > \bar{w}_c. \quad (4-30)$$

in which \bar{w}_c/m is the minimum flow velocity corresponding to the continuous discharge of bubbles. Corresponding to this condition are $r_2 = 0$ and $\xi = 1$ --i.e., within the range of applicability of Formula (4-29):

$$\frac{\bar{w}_c \sqrt{r_1}}{\sqrt{r_1(r-r_1)}} = -1.25 \sqrt{\frac{r_1}{(r-r_1)R_1}}. \quad (4-31)$$

It follows from the obtained formulas that the velocity of the light phase passing through the orifice depends little on the orifice diameter, relatively little on the surface tension at the phase boundary and on the specific gravity of the heavy phase, and decreases substantially with an increase in the density of the light phase (i.e., in the case of a gas with an increase in pressure).

4-5. Comparison of Theory with Experimental Data

The characteristics of the bubbling (dynamic) liquid layer have steady values only if the layer is thick enough. This is explained

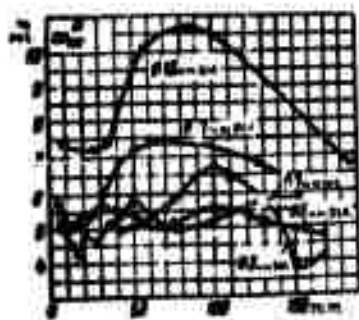


Figure 4-4. \bar{w}''/\bar{m} vs. liquid level from experiments with air and water.

by the fact that the periodic generation of bubbles causes considerable fluctuations in the thin layer, in which case a resonance may develop leading to an abrupt disturbance of the stability of the mixture. The results of measuring quantity \bar{w}''/\bar{m} given in Fig. 4-4, from K. A. Blinov's experiments with small layer

depths show that fluctuations also

take place in layers having a depth of about 100 to 150 mm.

Photographs taken by K. A. Blinov and S. M. Broderzon of the discharge of a gas into a liquid confirm the discrete character of the motion of the light phase (see Fig. 4-5).

Figure 4-6 compares calculations by means of Formula (4-31) with K. A. Blinov's experiments carried out with a layer 100 mm thick. As can be seen, the above-stated theory of gas discharge into a liquid not only reflects the qualitative aspect of this complicated phenomenon well, but also gives sufficiently accurate quantitative results.

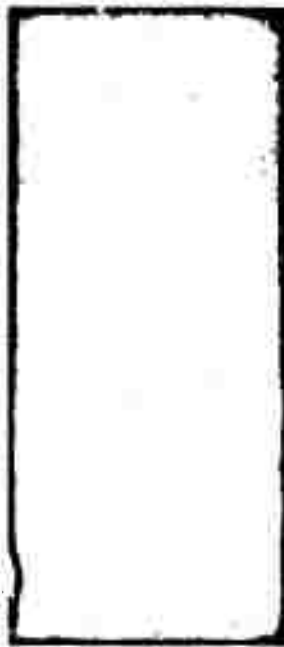


Figure 4-5. Photograph of process of discharge of a gas into a liquid.

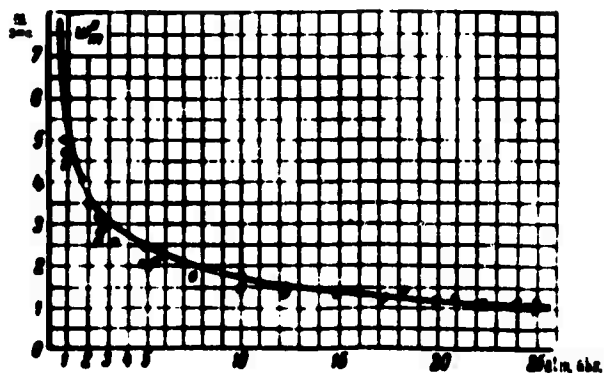


Figure 4-6. Comparison of data computed by means of Formula (4-31) with experimental data.

4-6. Discharge into a Viscous Medium

Substituting the value of \dot{r} from (4-16) into (4-8) and at $\underline{w}''/\underline{r} = \underline{dR}/\underline{dr}$, we obtain

$$dL_s = 6\pi\eta R \frac{dR}{dt} dt \quad (4-32)$$

At $\underline{dR}/\underline{dr} = \text{const}$ ($\underline{m} = 0$) we have [see Formulas (4-13) and (4-26)]:

$$\left. \begin{aligned} R &= \frac{dR}{dt} \tau; \\ \frac{dR}{dt} &= \sqrt{\frac{3}{\pi} \frac{w_i R_i^2}{\tau_i^3}}; \\ w_i &= 3\bar{w}_i \left(\frac{\tau}{\tau_i}\right)^3. \end{aligned} \right\} \quad (4-33)$$

Substituting these expressions into (4-32) and integrating the obtained equation within the limits $\tau = 0, \tau = \tau_1$, we obtain:

$$L_s = 6\pi\eta \left(\frac{dR}{dt}\right)^3 \int_0^{\tau_1} \tau d\tau = \frac{3}{4} \pi \eta \bar{w}_i R_i^2 \tau_1 \quad (4-34)$$

Further, taking into account (4-18) and (4-33), we have:

$$L_0 + L_s = \frac{\pi \eta R_i^2 \bar{w}_i}{2g\tau_i^4} \int_0^{\tau_1} \tau^4 d\tau = \frac{16\pi}{7g} \eta \bar{w}_i R_i^2 \tau_1 \quad (4-35)$$

Solving this equation by substituting into it \underline{L}_0 from (4-15) and \underline{L}_s from (4-34), we find that

$$\bar{w} = \left[\frac{2gR_1^2}{16\gamma R_0^3} + \sqrt{\frac{49g^2 R_1^4}{256\gamma^2 R_0^6} + \frac{14g\gamma}{9\gamma R_0}} \right] \quad (4-36)$$

At $\mu' = 0$, this formula turns into Formula (4-27) (at $m = 0$).

However, the viscosity of the liquid not only influences the discharge velocity \bar{w} but also the size of the release diameter of the bubble. This influence may be approximately taken into account by introducing into Formula (4-1) another term which takes Stokes' viscous friction into consideration. We have:

$$\frac{4}{3} \pi R_0^3 (\gamma' - \gamma) - 2\pi R_0 \gamma + 6\pi \eta R_0 \left(\frac{dR}{dt} \right)_{R=R_0} \quad (4-37)$$

From (4-13) and (4-33) it follows that

$$\left(\frac{dR}{dt} \right)_{R=R_0} = \frac{3}{4} \bar{w}_1 \left(\frac{R_1}{R_0} \right)^2 \quad (4-38)$$

Substituting this expression into (4-37), we obtain the equation

$$\left(\frac{R_2}{R_1} \right)^2 = \frac{3\gamma}{2(\gamma' - \gamma) R_1^2} + \frac{27\eta \bar{w}_1}{8(\gamma' - \gamma) R_1 R_0} \quad (4-39)$$

where

$$\bar{w}_i = \frac{\bar{w}_0}{t}$$

Therefore, in a viscous liquid, other conditions remaining the same, the release diameter of the bubble is greater. The experiments of K. A. Blinov confirmed this conclusion.

Simultaneous solution of Equations (4-36) and (4-39) also leads to the conclusion that an increase in viscosity causes a decrease in the quantity \bar{w}/\underline{m} . However, this circumstance became noticeable in experiments only at a viscosity of more than 10^6 Engler.

4-7. Thickness of a Gas Cushion Under a Horizontal Perforated Plate

The pressure in the gas cushion is the sum of the pressure in the liquid at the level of the perforated plate, the pressure drop in the orifices, and the excess pressure caused in the bubble by surface tension.

$$P_{\text{cushion}} = P + \frac{2\sigma}{R} + \int_{\text{orifice}} \frac{1}{2g} \frac{v^2}{2g} \quad (4-40)$$

The difference in pressures

$$\Delta P = P_{\text{cushion}} - P$$

averaged over the time lapse $t_1 + t_2$, is balanced in a freely submerged

plate by the difference in the hydrostatic pressures at the level of the plate and at the level of the lower surface of the gas blanket.

Hence, the thickness of the gaseous layer is

$$h_{\text{min}} = \frac{\bar{p}_1 - \bar{p}_2}{\gamma - \gamma'} \approx 2 \sqrt{\frac{\sigma}{(\gamma' - \gamma) \rho R_1}} + \frac{\gamma' \bar{p}_1}{2g(\gamma' - \gamma)} \quad (4-41)$$

The minimum thickness of the stable gas layer under the perforated plate is determined by Formula (4-41) when $\bar{w}'' = \bar{w}_m''$.

CHAPTER FIVE

DYNAMIC TWO-PHASE LAYERS

5-1. General Information

We call a liquid layer through which a gas is blown (is bubbling) a dynamic two-phase layer. A two-phase (or, more accurately, a two-component) layer may also be formed by two mutually insoluble liquids of different densities.

Bubbling through a liquid layer is used in widely varied technological processes. These include various types of bubble columns used in chemical technology, the Bessemer process used in metallurgy, the scrubbing of steam in steam boilers, etc.

With the emergence of the gas on the surface of the two-phase dynamic layer, bursting of gas bubble shells, for practical purposes, takes place instantaneously in a pure liquid. Therefore, the stability of such a dynamic two-phase layer is nil in the absence of a flow of the light phase, i.e., the two-phase layer exists only in the course of motion. More accurately, the discontinuance of gas feeding into the liquid layer will lead to the two-phase dynamic layer changing into a single-phase layer within a short time interval. The latter is equal to the sum of the ascent time of the bubbles through the liquid layer, and the very short "life span" of the bubbles on the surface of this layer.

Even a small admixture of surface active substances in the liquid becomes concentrated at the phase boundary; this usually results in a considerable increase in the time required for liquid films to rupture (in a number of cases, finely dispersed solid particles suspended in the liquid produce an analogous effect).

If the surface active substances exhibit structural viscosity, the rupture time of the films may be considerable when external influences are absent. In such cases, when bubbling is slow, a layer of foam accumulates on the surface of the dynamic two-phase layer. Foam is a film-cellular system whose individual bubbles are connected by their separating films into a general framework. The thickness of the foam layer is determined by the average life span of the individual bubbles, and by the rate of growth of the layer from beneath due to the arrival of new bubbles.

At bubbling rates commonly occurring in engineering equipment, the foam on the surface of the two-phase layer is rapidly destroyed by the dynamic effect of the gas and the liquid. Therefore, as a rule, no significant layer of practically motionless foam is observed on the surface of the dynamic two-phase layer. However, an increase in the stability of the gas bubbles in the liquid has great influence on the structure of the two-phase layer itself. In a "foaming" liquid, the bubbles do not aggregate so well: they rise more slowly and after reaching the surface of the layer burst more slowly. In this case, swelling increases sharply, and the density distribution along the top part of the dynamic two-phase layer changes.

The mechanism of the effect of impurities in the liquid on the dynamic two-phase layer has remained almost completely uninvestigated thus far.

The basic regime characteristics of a dynamic two-phase layer are:

- a) conditions ensuring the continuous feeding of the bubbling medium through the orifices of the nozzles or of the perforated plate;
- b) density of the mixture;
- c) stability of the bubbling layer;
- d) hydraulic resistance of the layer.

The first of these questions was examined to a certain extent in the preceding chapter. Some data on the other questions are given below.

5-2. Dimensionless Parameters of a Dynamic Layer

Let us consider the physical factors affecting the bubbling of pure liquids.

For each bounded volume of a given phase, we may write the pertinent equations of motion and continuity, namely:

- a) equations of motion and continuity applying within the elements of the heavy phase:

$$\left. \begin{aligned} \vec{g}\rho' - \text{grad } p' + \rho' \nabla^2 \vec{w}' &= \rho' \frac{D\vec{w}'}{dt}; \\ \text{div } \vec{w}' &= 0; \end{aligned} \right\} \quad (5-1a)$$

- b) equations of motion and continuity applying within the elements of the light phase:

$$\left. \begin{aligned} \vec{g} \rho'' - \text{grad } \rho'' + \rho'' \vec{v}' \cdot \vec{v}'' &= \rho'' \frac{D \vec{v}''}{dt}; \\ \text{div } \vec{v}'' &= 0; \end{aligned} \right\} \quad (5-1b)$$

c) equations of mechanical interaction of the phases at the phase boundary:

$$\left. \begin{aligned} \gamma'_{1,2} &= \gamma'_{1,2}; \\ \sigma'_{1,2} &= \sigma'_{1,2}; \\ \omega'_1 &= \omega'_1. \end{aligned} \right\}$$

At the same time, we have to take into account the pressure jump

$$\Delta p_b = \sigma \left(\frac{1}{R_1} + \frac{1}{R_2} \right),$$

where R_1 and R_2 are the principal radii of curvature at a given point on the boundary.

The totality of the independent variables in these equations, and the conditions for introduction of the light phase into the bubbler, determine the hydrodynamic regime of a pure two-phase layer.

These independent variables are the physical constants of the phases $\gamma', \gamma'', \sigma', \sigma'', \sigma$, the acceleration of gravity g , the characteristic velocity of the heavy phase w'_0 , the characteristic velocity of the light phase w''_0 , and the geometric dimensions of the bubble equipment.

The above-mentioned quantities are combined into dimensionless groups given in Table 1-2.

Thus, if the determinable dimensionless characteristic of the two-phase layer is φ_1 , then for pure liquids in the general case:

$$\varphi_1 = \varphi_1 \left(\frac{\sigma_0}{\sigma_0} : \frac{\sigma_0}{\sigma_0} : \frac{\sigma_0}{\sigma_0} : \frac{\sigma_0}{(\gamma - \gamma')^n} : \frac{\gamma'}{\gamma} : \frac{\gamma'}{\gamma} : \frac{h}{l} \dots \right) \quad (5-2)$$

here, $l, l_1, l_2 \dots$ are geometric characteristics of the bubbler.

These criteria may be combined into certain groups which are more convenient for further analysis.

We have:

$$\left(1 - \frac{\gamma'}{\gamma}\right) \left(\frac{\sigma_0}{\sigma_0}\right)^2 \frac{\sigma_0}{\sigma_0} \left[\frac{\sigma_0}{(\gamma - \gamma')^n}\right]^{\frac{1}{n}} = \frac{\sigma_0 \gamma'}{\sigma_0 \sqrt{\gamma - \gamma'}} \quad (5-3)$$

$$\left(\frac{\sigma_0}{\sigma_0}\right)^{\frac{1}{n}} \left(\frac{\gamma - \gamma'}{\sigma_0}\right)^{\frac{1}{n}} = \sigma_0 \sqrt{\frac{\gamma - \gamma'}{\sigma_0}} \quad (5-4)$$

Criterion (5-3) describes the interaction of buoyancy (the Archimedes force) in the two-phase layer with viscous friction in the heavy phase and surface tension.

Criterion (5-4) describes the relationship between the reference velocity of the light phase and the limit relative velocity of single bubbles; this is disclosed by comparing (5-4) with (2-11).

Consequently, Relation (5-2) is equivalent to the relation

$$\varphi_1 = \varphi_1 \left(\frac{\sigma_0}{\sigma_0} : \sigma_0 \sqrt{\frac{\gamma - \gamma'}{\sigma_0}} : \frac{\sigma_0 \gamma'}{\sigma_0 \sqrt{\gamma - \gamma'}} : \frac{\sigma_0}{(\gamma - \gamma')^n} : \frac{\gamma'}{\gamma} : \frac{\gamma'}{\gamma} : \frac{h}{l} \dots \right) \quad (5-5)$$

The latter expression is convenient because the number of criteria containing the basic linear dimension of the system l , and the phase velocities w_0' and w_0'' , is minimized.

It follows from what was said above on the physical meaning of Criterion (5-4) that the functional Relation (5-5) must be particularly convenient for those regimes in which the light phase moves in the form of discrete bubbles or their associations.

In the second limiting regime for the motion of a two-phase flow, the shells of the individual bubbles are destroyed, the motion of the light phase takes on the character of a jet, and the interaction of the phases is to a considerable extent determined by inertial forces. Naturally, we should take the quantities $w_0'^2$ and $w_0''^2$ as the scales for these inertial forces.

In this case, it is expedient to use a notation of the criteria somewhat different from (5-5), namely:

$$\pi = \left(\frac{g}{w_0'^2} \sqrt{\frac{r}{r_0}} : \frac{g}{w_0''^2} \sqrt{\frac{r}{r_0}} : \frac{g}{w_0'^2} \sqrt{\frac{r}{r_0}} : \frac{g}{w_0''^2} \sqrt{\frac{r}{r_0}} : \frac{r}{r_0} : \frac{r}{r_0} : \frac{r}{r_0} \dots \right) \quad (5-6)$$

The criterion

$$\frac{g r}{w_0'^2} = \frac{g}{w_0'^2} \sqrt{\frac{r-r_0}{r_0}} \sqrt{\frac{r}{r-r_0}} \quad (5-7)$$

describes the relation between the kinetic energy of the light phase, the surface energy on the phase boundary, and the gravitational field.

The physical importance of writing the criteria of the type in (5-6) becomes clear if we consider in greater detail those processes in which the dynamic head of the phase is most important. Such, for example, is the process of discharge examined above in Chapter 4, where the group (5-7) stands out as the basic quantitative criterion of the process. The core pattern of two-phase flow in a round tube, examined below in Chapter 6, is also such a regime.

In the case of a bubbler in a stagnant heavy phase, the criterion $\frac{w_0'}{w_0''}$ drops out of the systems (5-2), (5-5), and (5-6).

The geometric features of such a layer are: the effective cross section φ_1 of the perforated plate or of the nozzles, the average depth h' of the layer of the heavy phase and the diameter D_1 of the nozzle orifices.

The volumetric fraction of the light phase in the layer is related to the velocities by Formula (1-12). At $w_0' = 0$, it follows from (1-12) and (1-13) that:

$$\varphi = \frac{w_0''}{w_0'' + w_0'} \quad (5-8)$$

$$\varphi = \frac{1}{1 + \frac{w_0''}{w_0'}} = 1 - \frac{w_0''}{w_0'' + w_0'} \quad (5-9)$$

The depth of the dynamic layer ("swelling") is

$$h_1 = \frac{h'}{1 - \varphi} \quad (5-10)$$

The average depth of the heavy phase may be determined as the ratio of the volume V' occupied by that phase in the dynamic layer to the cross-sectional area of the bubbler. When there is no loss of the heavy phase through the orifices of the nozzles (or of

the perforated plate), and no bubbling, the quantity h' is equal to the thickness of the layer of the heavy phase.

It appears from the ratios given above that any of the following quantities may be chosen as the determinable dimensionless characteristic of the layer:

$$\tau: \varphi: \frac{v_r}{v_0}: \frac{h_1}{h}.$$

5-3. Structure of a Two-Phase Dynamic Layer

The structure of a two-phase dynamic layer depends on the physical properties of both the fluid surrounding the bubbles and the fluid within the bubbles, on the geometric dimensions of the bubbler, and on the bubbling rate.

The results of one of a series of experiments by S. S. Kutadeladze and V. N. Moskvicheva on water bubbling through a layer of mercury, shown in Fig. 5-1, indicate how complicated the structural changes of the dynamic layer can be.

Curve 1 corresponds to the regime of a discrete (drop-wise) flow

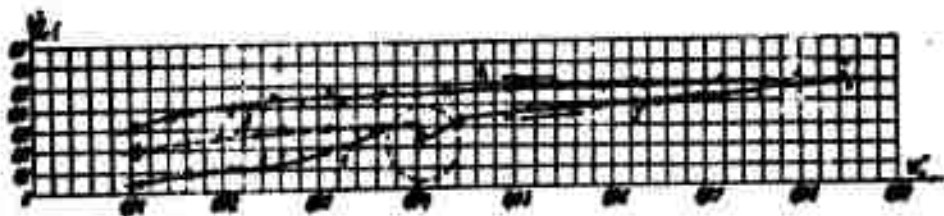


Figure 5-1. Variation in volumetric fraction of light component in a water-mercury mixture as a function of the reference velocity of the water:

$$D_{\text{orifice}} = 5 \text{ mm}; \quad \varphi_1 = 4.5\%; \quad v'/v'' = 13.6; \quad h' = 335 \text{ mm}.$$



Figure 5-2. Function $\varphi(w'')$ for an air-water mixture with small depths of layers.

of water through a layer of mercury. In the vicinity of A there occurs a sharp change in the structure of the layer: the mercury is fragmented into separate (mostly large) drops suspended in the water stream. The relative velocity of the water increases, and the water

fraction in the layer decreases.

A further increase in water flow rate again increases the swelling of the layer along Curve 2.

In the vicinity of B there is another critical change due to high dispersion and entrainment of mercury from the layer by the water stream.

Upon reaching the vicinity of A once the structural change in the layer has occurred, if we begin to decrease the water flow rate,

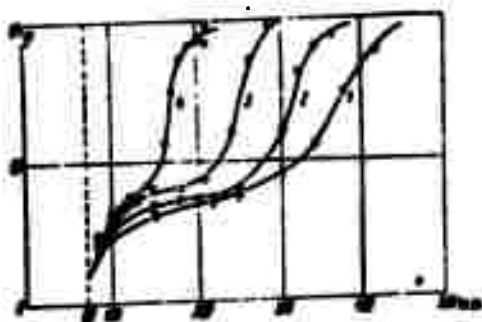


Figure 5-3. Distribution of volumetric fraction of steam as a function of the depth of the layer of the water-steam

- (1) gravimetric level 220 mm;
- (2) gravimetric level 170 mm;
- (3) gravimetric level 120 mm;
- (4) gravimetric level 70 mm.

the layer thickness will no longer decrease along Curve 1, but rather along Curve 3, i.e., the stability of the discrete structure of the mercury in the layer is preserved.

Similarly, after the structural change has occurred in the vicinity of B, if we reduce the water flow rate, the layer thickness decreased along Curve 4.

Structural variations are likewise observed when a gas is bubbled through a liquid, which is indicated by the data of M. Ye. Pozin and Ye. S. Tumarkina (shown in Fig. 5-2) on the variation of

the depth of the layer when water is bubbled through a 20% tri-ethanolamine solution.

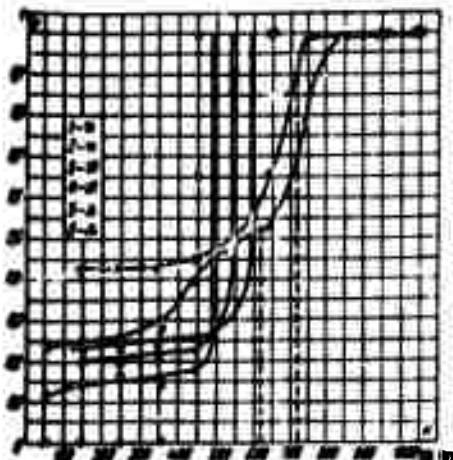


Figure 5-4. Distribution of volumetric density as a function of the depth of the layer of water-mercury mixture. $D_{\text{orifice}} = 5 \text{ mm}$;

- $\varphi_1 = 33\%$; $\frac{\gamma'}{\gamma''} = 13.6$;
 $h' = 404 \text{ mm}$; (1) $w_0'' = 0$;
 (2) $w_0'' = 0.023 \text{ m/sec}$;
 (3) $w_0'' = 0.0325 \text{ m/sec}$;
 (4) $w_0'' = 0.0410 \text{ m/sec}$;
 (5) $w_0'' = 0.0470 \text{ m/sec}$;
 (6) $w_0'' = 0.0660 \text{ m/sec}$.

The density of the mixture also varies as a function of the depth of the layer. Measurements of true density in various cross sections of the two-phase layer were carried out by the authors and their collaborators (Ya. G. Vinokur, Ye. Z. Miropol'skiy, V. N.

Moskvicheva, and others) by the method of gamma-ray examination (see Chapter 10).

The experimental data given in Figs. 5-3, 5-4, and 5-5 show that the character of phase distribution as a function of the depth of the layer is generally the same in both a gas-liquid system and a liquid-liquid system. In

the great bulk of the layer, the density is practically constant. Some density increase is observed in the vicinity of the discharge of the light phase from the dispersing orifices. In the upper part of the layer we note a decrease in the density of the mixture, while

in the vicinity of low w_0'' and correspondingly low values of φ the transition region is small for the bulk of the layer (20 to 30 mm).

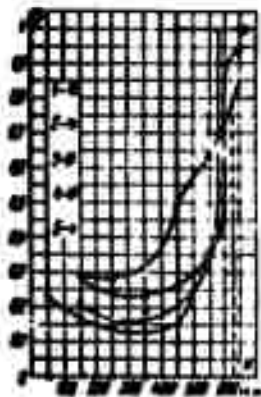


Figure 5-5. Distribution of volume density as a function of the depth of the layer of water- CCl_4 mixture.

$D_{\text{orifice}} = 5 \text{ mm}$; $\varphi_1 = 4.5\%$;

$\frac{r_1}{r} = 1.61$; $h' = 404 \text{ mm}$; (1)

$w_0'' = 0$; (2) $w_0'' = 0.0146 \text{ m/sec}$;

(3) $w_0'' = 0.0223 \text{ m/sec}$; (4)

$w_0'' = 0.0287 \text{ m/sec}$; (5)

$w_0'' = 0.0395 \text{ m/sec}$.

At high reference velocities of the light phase, the transition zone is greatly extended upwards and reaches 400 to 500 mm for a steam-water system with $w_0'' = 1$ to 1.5 m/sec and $\varphi = 0.6$ to 0.7.

Figures 5-6 and 5-7 show a comparison of values of $\bar{\varphi}$ determined by the method of gamma-ray examination in the diametrical plane of the column and by the measurement of the discrepancy between the true and gravimetric levels of the mixture. The first method gives the actual value of φ in the path of the gamma ray. By the second method a certain effective value φ_{eff} is calculated for the entire cross section of the bubbler.

In the region of low values of φ , where accuracy of measurement is not great (particularly by the method of discrepancy in levels), the discrepancies between the measurements given by the two methods are inconsistent. In cases where φ is more significant, this quantity, as given by gamma-ray examination is 10 to 15% more stable than the quantities obtained from the discrepancy in levels. Further ex-

periments by M. A. Styrikovich, Ya. G. Vinokur, L. S. Sterman and B. A. Dement'ev indicated that even in large diameters (200 to 250 mm) columns with local values of ψ in the center of the bubbler

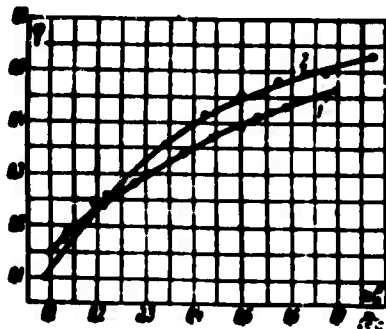


Figure 5-6. Comparison of values of ψ obtained by different methods. Steam-water system, $p = 17$ atm. abs.; (1) from discrepancy of physical and gravimetric level of mixture; (2) gamma-ray examination

are appreciably higher than in the periphery. Therefore, in determining ψ it is necessary to carry out radioscopy in a series of cross sections, averaging them afterward. Such measurements showed that the magnitudes of ψ , obtained by gamma-ray examination and from the discrepancy between the physical and gravimetric levels, coincide with each other.

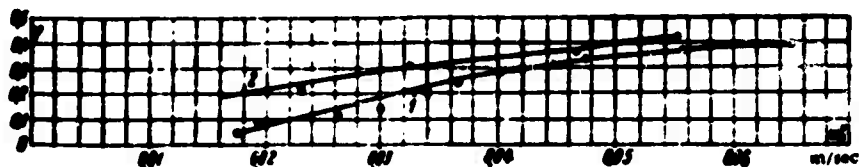


Figure 5-7. Comparison of values of ψ , obtained by different methods. Mercury-water system: (1) from discrepancy between physical and gravimetric level of mixture; (2) gamma-ray examination.

5-4. Effect of Geometric Factors on the Hydrodynamics of the Layer

It was determined above that the fundamental geometric characteristics of a dynamic layer whose heavy phase is stagnant ($w_0' = 0$) are: the diameters D_1 of the orifices dispersing the light phase; their relative cross section ϕ_1 ; and the reference level of the heavy phase. The dimensionless values of D_1 and h' may be formed by multiplying these quantities by $\sqrt{\frac{\gamma' - \gamma''}{\rho}}$.

The extent of the effect of the orifice diameter can be theoretically evaluated for the case of the motion of noninteracting single bubbles of light phase.

In a medium of low viscosity, the relative velocity of these bubbles is determined by Formula (2-25) or (2-27).

In a regime corresponding to Formula (2-25), the relative velocity w_r'' depends on the radius of the bubble R . Substituting R from (4-3) into (2-25), we obtain:

$$w_r'' = 1.28 \sqrt{\frac{\rho''}{(\gamma' - \gamma'') D_1}} \quad (5-11)$$

When the regime corresponds to Formula (2-27), the quantity w_0'' does not depend on R .

Thus, we should expect that orifice size will not strongly affect the hydrodynamic characteristics of a two-phase layer, particularly at sufficiently high ratios $\frac{h'}{D_1}$.

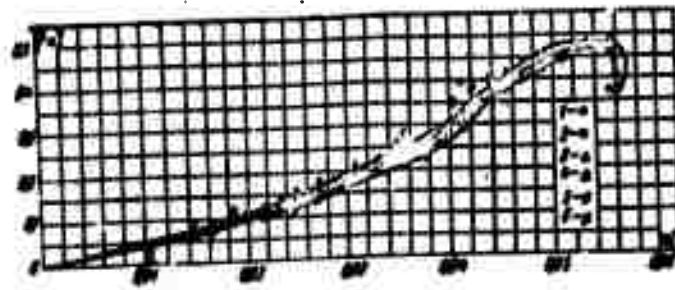


Figure 5-8. Relationship between $\bar{\varphi}$ and w_0'' .
 Mercury-water system, $h' = 425$ mm; plate $\varphi_1 = 33\%$
 (1) series I } $D_0 = 10$ mm; (3) series I } $D_0 = 3$ mm;
 (2) " II } $D_0 = 10$ mm; (4) " II } $D_0 = 3$ mm;
 (5) series I } $D_0 = 5$ mm.
 (6) " II } $D_0 = 5$ mm.

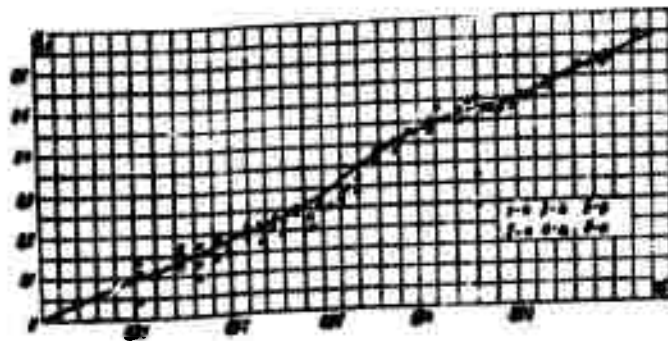


Figure 5-9. $\bar{\varphi}$ vs. w_0'' . Mercury-water system,
 plate $D_0 = 5$ mm; $h' = 155$ mm;
 (1) series I } $\varphi_1 = 44.5\%$ (3) series I } $\varphi_1 = 12.5\%$
 (2) " II } $\varphi_1 = 44.5\%$ (4) " II } $\varphi_1 = 12.5\%$
 (5) series I } $\varphi_1 = 32.3\%$
 " II } $\varphi_1 = 32.3\%$

Neither should the cross section of the dispersing device under these conditions appreciably influence the structure of the layer, since the bubbles fill up the entire bubble cross section very rapidly.

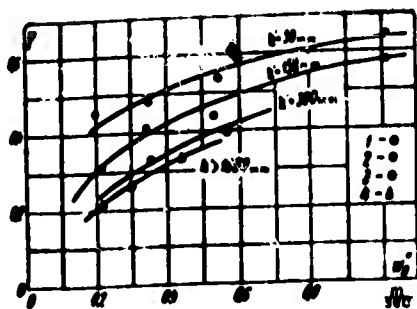


Figure 5-10. Effect of reference heavy-phase level h' on the hydrodynamics of the system. (1,2,3) air-water, $D_1 = 5$ mm, $\varphi_1 = 4.5\%$, $\frac{\gamma'}{\gamma''} \approx 800$; (4) water-steam (experiments by Behringer), $p = 2.4$ atm. abs.

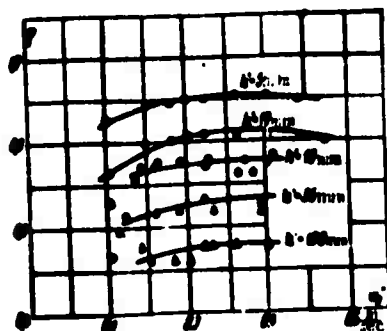


Figure 5-11. Effect of the reference level of the heavy-phase h' on the hydrodynamics of an air-water system. $D_1 = 1.3$ mm; $\varphi_1 = 1.7\%$; $\frac{\gamma'}{\gamma''} \approx 800$.

Certain experimental data given in Figs. 5-8 and 5-9 generally confirm these conclusions.

The reference depth h' of the heavy phase substantially affects the hydrodynamics of the layer at not very great values of $\frac{h'}{D_1}$. The general tendency is that when h' is reduced the relative average velocity w_{Σ}'' of the light phase is also reduced, and the quantity $\bar{\varphi}$ is accordingly increased.

Experimental data of K. A. Blinov and A. L. Rabinovich given in Figs. 5-10 and 5-11 show the character of this relationship for a gas-liquid system. The data of Fig. 5-12 illustrate the same situation for a liquid-liquid system.

As may be seen from Figs. 5-10 through 5-12, the influence of the quantity h' is strongly manifest only in layers of small thickness. If h' is increased, the quantity $\bar{\varphi}$ tends toward some constant value, all other conditions being equal.

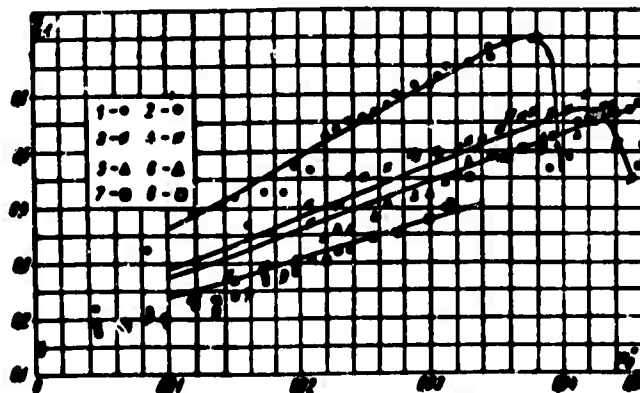


Figure 5-12. Effect of the reference level of the heavy phase on the hydrodynamics of a mercury-water system.

$$D_0 = 10 \text{ mm}; \quad \varphi_1 = 37\% \quad \frac{\gamma'}{\gamma''} = 13.6$$

$$\left. \begin{matrix} (1) \\ (2) \end{matrix} \right\} \text{series I} \left. \begin{matrix} \\ \\ \end{matrix} \right\} h' = 155 \text{ mm}; \quad \left. \begin{matrix} (3) \\ (4) \end{matrix} \right\} \text{series I} \left. \begin{matrix} \\ \\ \end{matrix} \right\} h' = 245 \text{ mm};$$

$$\left. \begin{matrix} (5) \\ (6) \end{matrix} \right\} \text{series I} \left. \begin{matrix} \\ \\ \end{matrix} \right\} h' = 335 \text{ mm}; \quad \left. \begin{matrix} (7) \\ (8) \end{matrix} \right\} \text{series I} \left. \begin{matrix} \\ \\ \end{matrix} \right\} h' = 425 \text{ mm}.$$

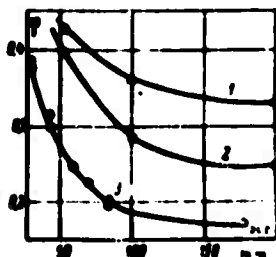


Figure 5-13. Effect of the diameter of the bubbler (tube in which the bubbling takes place) on the hydrodynamics of a water-steam system. (1) $p = 2.5 \text{ atm. abs.}$; $w_0'' = 0.55 \text{ m/sec}$; (2) $p = 4.0 \text{ atm. abs.}$, $w_0'' = 0.42 \text{ m/sec}$; (3) $p = 1.0 \text{ atm. abs.}$, $w_0'' = 0.3 \text{ m/sec}$.

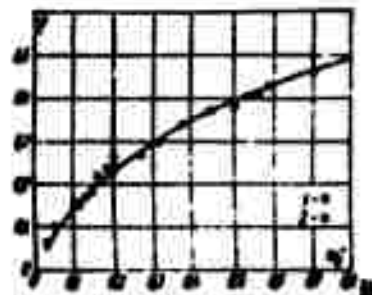


Figure 5-14. Effect of the diameter of the bubbler on the hydrodynamics of a water-steam system. (1) $p = 18 \text{ atm. abs.}$, $D_{\text{bub}} = 82 \text{ mm}$,

$$\frac{\gamma'}{\gamma''} \approx 10 \text{ (experiments by Behringer); (2) } p = 17 \text{ atm. abs.}, \quad D_{\text{bub}} = 238 \text{ mm},$$

$$\frac{\gamma'}{\gamma''} \approx 10 \text{ (experiments by Sterman)}.$$

The influence of the diameter of the bubbler can be visualized by means of the curves in Fig. 5-13, plotted according to the data of B. A. Dement'ev and Behringer. As we can see, as the diameter of

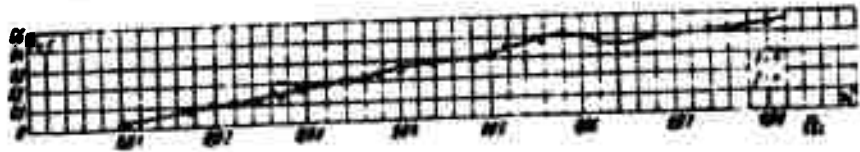


Figure 5-15. \bar{w}_{ef} vs. w''_0 for a mercury-water system. $D_0 = 5$ mm; $\varphi_1 = 33\%$; (1) $h' = 425$ mm, column I. D. 100; (2) $h' = 404$ mm; column 100 x 100.

the bubbler (or more accurately, the group $D_{bub} \sqrt[4]{\frac{\gamma' - \gamma''}{\rho}}$) increases, its influence decreases.

The limited nature of the influence of D_{bub} is also confirmed by comparison of the data of Behringer and L. S. Sterman, shown in Fig. 5-14, for bubblers made of tubes 82 and 238 mm in diameter.

Figure 5-15 shows analogous data for a mercury-water system.

5-5. Experimental Data on the Relationship Between φ and w''_0 in a Gas-Liquid System

The above-mentioned data on the hydrodynamics of a two-phase dynamic layer clearly indicate how complex that process is. We may say that until recently this circumstance was far from being clear to many experimenters.

As a result, we must state that until recently the available experimental material could not be used as a basis for obtaining generalized relations, owing to the insufficiently systematic character of individual investigations and the absence of some of the data necessary for comparing them.

Bubbling of steam through a layer of water is of great practical

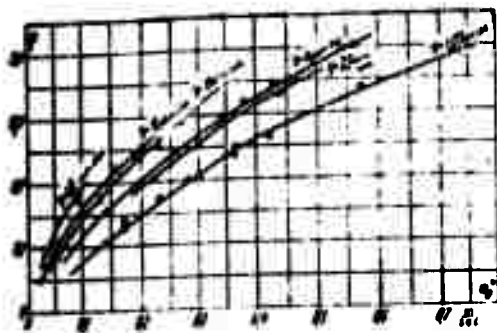


Figure 5-16. ϕ vs. w_0'' for steam bubbling through a thick layer of saturated water. Bubbler diameter 82 mm; $h_{\text{layer}} = 2,500$ mm.

In these experiments, steam was generated by electric heating elements located in the lower part of the tube. Figs. 5-13 and 5-14 compared these experiments with experiments in which the light phase was fed through a perforated plate. As can be seen, when the

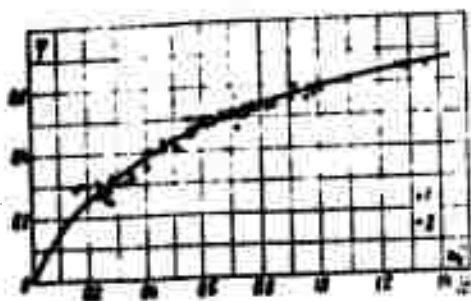


Figure 5-17. Comparison of the data of Fig. 5-16 with data for conditions of hampered circulation of water in a vertical steam-generating tube. (1) Tube $D = 82$ mm, $p = 11$ atm. abs. (experiments by Behringer); (2) tube $D = 76$ mm; $p = 11-12$ atm. abs. (experiments by Mochan).

importance in engineering (conditions of hampered circulation in steam-generating tubes, steam scrubbing by bubbling, mixing equipment, etc.).

Figure 5-16 shows the relationship between ϕ and w_0'' when steam is bubbled through a considerable layer of water (without condensing) from Behringer's experiments.

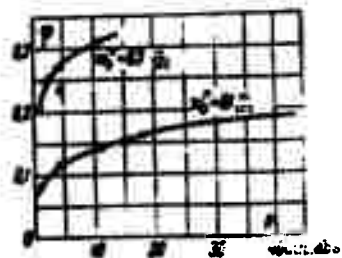


Figure 5-18. Effect of pressure on ϕ for steam bubbling through a layer of saturated water.

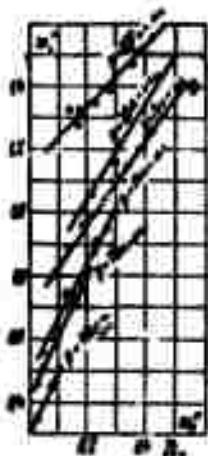


Figure 5-19. w''_r vs. w''_0 and p for steam bubbling through a thick layer of saturated water.

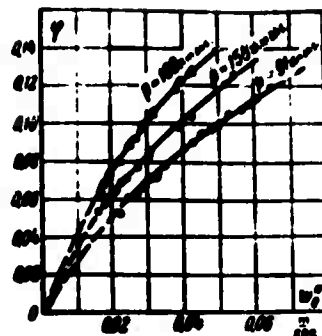


Figure 5-20. Data on steam bubbling through water at high pressures.

ratios $\frac{\gamma'}{\gamma''}$ are the same, all the data are in good agreement.

Figure 5-17 compares Behringer's data with S. I. Mochan's data for conditions of hampered circulation in a vertical steam-generating tube. Here, also, the experimental points agree well.

Figure 5-18 shows the relationship between ψ and the steam pressure from the data in Fig. 5-16. The sharp change in ψ in the low-pressure region gives way to a rather weak relationship in the high-pressure region.

The same data are shown in Fig. 5-19 on w''_r , w''_0 coordinates. The average relative velocity of the steam within the entire range of w''_0 investigated is considerably higher than the free ascent velocities of single bubbles and, for practical purposes, increases linearly as the reference velocity of the steam increases. As pressure increases, w''_r decreases.

Figure 5-20 shows the relationship between ψ and w''_0 for very high-pressure steam from T. Kh. Margulova's experiments. Although these

data do not agree quantitatively with Behringer's data (Margulova's curve for $p = 91$ atm. abs. lies below Behringer's curve for $p = 40$ atm. abs.), the qualitative picture remains the same.

Considering a sufficiently thick dynamic layer of components of low viscosity, we may disregard the criteria $\frac{\sigma \sqrt{r}}{\mu \sqrt{r-r'}} \cdot \frac{r'}{r}$ and $\frac{\sigma}{(r-r')^2}$. In such a case, for a bubbler with a zero flow rate of the heavy phase, we obtain from (5-5):

$$v \approx v_0 \left(\sigma_0 \sqrt{\frac{r-r'}{\sigma}} : \frac{r'}{r} \right) \quad (5-12)$$

Since the quantity v increases with an increase in the velocity of bubbling w_0'' , it follows from (5-16) that v decreases little with

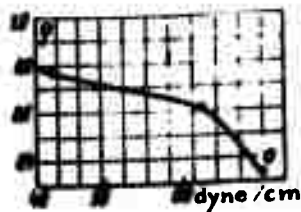


Figure 5-21. v vs. σ .

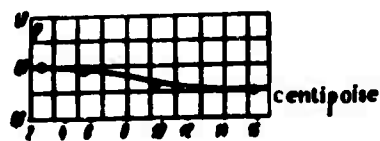


Figure 5-22. v vs. μ' .

an increase in the surface tension σ . The experiments by M. Ye. Pozin and Ye. S. Tumarkina shown in Fig. 5-21, qualitatively confirm this conclusion.

As may be seen from Fig. 5-22, the experiments carried out by the same authors also reveal a weak influence of the viscosity of the heavy phase on v . However, we should keep in mind that in these experiments the quantities σ and μ' were varied by introducing admixtures.

Figure 5-23 gives the results of the processing of Behringer's

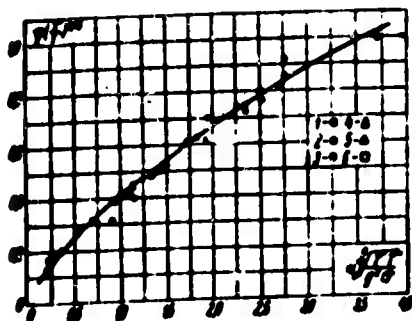


Figure 5-23. Data in Fig. 5-16 on the bubbling of steam through a thick layer of saturated water, plotted on the generalized coordinates of (5-12). (1) $p = 1.07$ atm. abs.; (2) $p = 2.4$ atm. abs.; (3) $p = 4$ atm. abs.; (4) $p = 11$ atm. abs.; (5) $p = 18$ atm. abs.; (6) $p = 40$ atm. abs.

experiments on the coordinates of Relation (5-21).

The experimental points are satisfactorily correlated by a single curve. The above-mentioned experimental data of S. I. Mechan and L. S. Sterman fall on the same curve.

In Fig. 5-24 the results of the experiments of T. Kh. Margulova are plotted on the same system of coordinates.

With a spread not exceeding $\pm 5\%$, all points in the given case also fall around a single curve.

However, as already mentioned above, Margulova's data lie somewhat lower than the equivalent data of other authors.

The data of Fig. 5-23 are represented in Fig. 5-25 on a logarithmic system of coordinates. The straight line drawn through the experimental points fits the equation.

$$r = 0.4 \left(\frac{r}{r_0} \right)^{0.25} \left(\frac{r_0}{r_0 - r} \right)^{0.25}$$

(5-13)

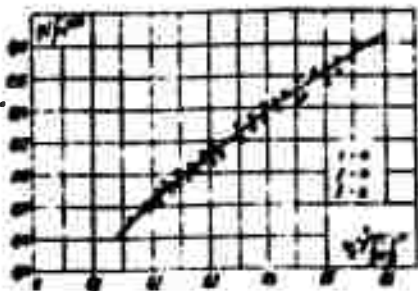


Figure 5-24. Data of Fig. 5-20 on the coordinates of (5-12). (1) $p = 91$ atm. abs.; (2) $p = 150$ atm. abs.; (3) $p = 190$ atm. abs.

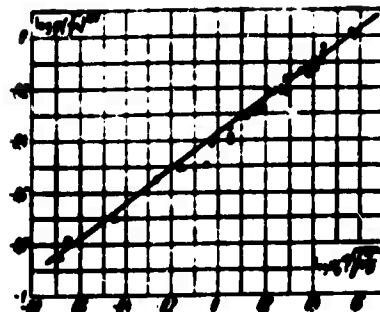


Figure 5-25. Data of Fig. 5-23 in a logarithmic system of coordinates. Slope of the straight line $n = 0.68$.

A formula of this type is used only with values of ψ rather different from unity ($\psi \leq 0.7$), since as

$$\sqrt{\frac{1-\psi}{\psi}} \rightarrow \infty,$$

the value $\psi \rightarrow 1$.

5-6. Effect of Admixtures on the Dynamic Layer in a Gas-Liquid System

Very few investigations have been made into the case of a "foaming" liquid in which the density distribution varies as a function of depth: however, the available data indicate a very great influence of an increased bubble-shell stability on the operation of the dynamic two-phase layer.

In experiments conducted by M. A. Styrikovich and G. G. Bartolomé with a steam-water system at atmospheric pressure, the measurements were carried out with "technically pure" water, as well as with the

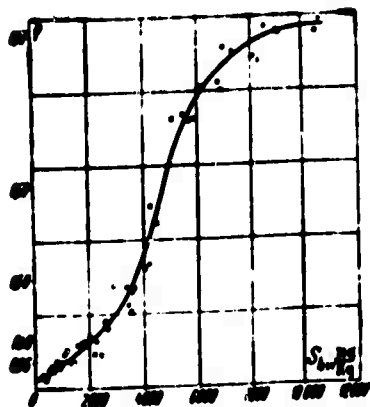


Figure 5-26. Effect of salt fraction in water on the density of the mixture for steam bubbling at atmospheric pressure. $h' = 120$ mm, $w_0'' = 0.32$ m/sec.

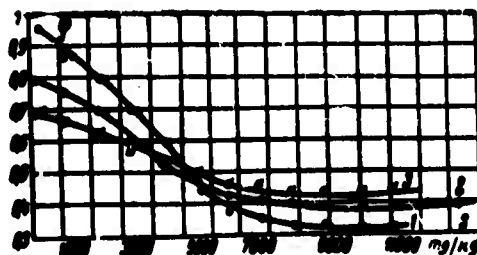


Figure 5-27. Effect of fraction of salt in water on the density of the mixture for steam bubbling at atmospheric pressure. $h' = 120$ mm; (1) $w_0'' = 0.32$ m/sec, $R_S = 1,150$ m³/m³-hour; (2) $w_0'' = 0.64$ m/sec, $R_S = 2,300$ m³/m³-hour; (3) $w_0'' = 0.85$ m/sec, $R_S = 3,060$ m³/m³-hour.

introduction of admixtures to stabilize the bubble shells.

With "technically pure" water, the amount of swelling consis-

tently increased with increase

in the reference steam velocity

(Fig. 5-26). As shell stability

increased, the amount of swelling

increased over the whole range

of the investigated reference

steam velocities (from 0.25 to

0.85 m/sec). These variations

are comparatively small at a high

reference steam velocity and in-

crease considerably at low bubbling

rates. As a result, when shell

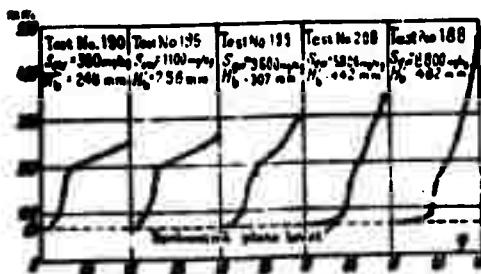


Figure 5-28. Distribution of the local volumetric steam fractions with constant load: column height plotted against the salt fraction in the boiler water.

stability is maximum, swelling increases as the reference steam velocity declines (Fig. 5-27).

With still lower steam flow rates ($w_0'' < 0.1$ m/sec), a stable layer of very light film-cellular foam formed on the surface of the layer, filling the whole space, which in a number of experiments was 700 to 800 mm high.

The pattern of density distribution in the mixture as a function of the depth of the dynamic two-phase layer also varies considerably. When "technically pure" water was used, the portion of the cross section occupied by steam had become stabilized at a distance of 20 to 30 mm above the perforated plate. This ties in well with the notion of the bubble rapidly attaining its equilibrium velocity.

Later on, ψ varied extremely little according to the depth of the layer, and only at the surface was there observed a somewhat ill-defined transition from the two-phase layer to steam.

We should point out that this ill-defined region increased with an increase in w_0'' , and that its depth tied in well with the visually observed region of agitation on the surface of the two-phase layer.

With an increased stability of the films, the pattern was qualitatively similar in the lower part of the bubbling layer. However, the absolute magnitude of ψ was in this case considerably greater, i.e., the relative velocity of the steam was considerably lower, evidently owing to the smaller bubble size (this is precisely what was observed visually). In this region, as with "pure" water also, ψ increased with an increase in w_0'' .

In the upper part of the layer, the bubbles emerging on the surface burst slowly. As a result of this, a layer highly enriched with bubbles, and which only gradually released the water, aggregated

near the surface. In the region of the visible level, on whose surface the agitation was considerably less than with technically pure water, the average fraction of steam was as high as 95 to 98% (Fig. 5-28) and declined almost linearly at deeper levels in the layer.

The developed region of "retarded" bubble motion extended to a great depth (down to 300 mm from the visible surface of the layer) and almost reached the perforated plate when the layer thickness was small.

5-7. Experimental Data on the Relationship Between ψ and w_0'' in a Liquid-Liquid System

The bubbling of a liquid through a liquid was never investigated until recently. A series of systematic data on this matter has been obtained only in the last few years. We will discuss here only some general information on this process.

As we can see by comparing Figs. 5-1 and 5-16 for water bubbling through a stagnant layer of mercury, a considerably more complex relationship between the density of the dynamic layer and the reference velocity of the light phase applies than for steam bubbling through a stagnant layer of water.

However, we must keep in mind that the liquid-gas system has not yet been investigated in sufficient detail either; and, for example, the experiments shown in Fig. 5-2 also reveal that the function $\psi(w_0'')$ is nonmonotonic.

Besides, the admixtures of surface-active substances may affect the liquid-liquid system as well.

Qualitatively, the influence of a number of factors on the hydrodynamics of a two-phase layer is the same for a liquid-liquid system as for a gas-liquid system.

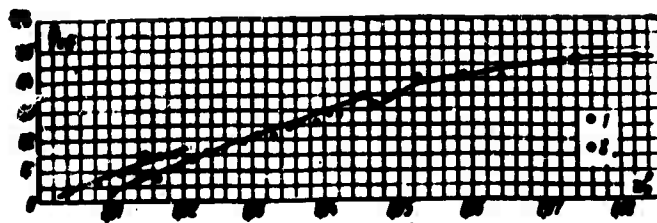


Figure 5-29. \bar{v} vs. w_0'' Plate $D_0 = 5$ mm;
 $\varphi_1 = 24.6\%$; $h' = 335$ mm; (1) $\frac{\gamma'}{\gamma''} = 13.6$;
 (2) $\frac{\gamma'}{\gamma''} = 1.61$.

Comparison of data in Figs. 5-10 to 5-12 shows that in all cases with low reference levels h' of the heavy phase, "swelling" of the layer is greater than at high values of h' .

The influence of the other geometrical factors D_1 and φ_1 is also qualitatively the same in all cases. However, an inconsistency in the values of φ on the generalized coordinates of (5-12) is revealed.

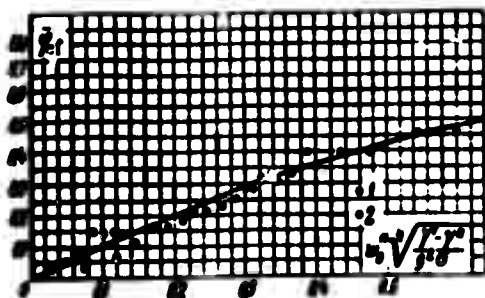


Figure 5-30. \bar{v} vs. $w_0'' \sqrt{\frac{\gamma'}{\gamma''}}$
 Plate $D_0 = 5$ mm; $\varphi_1 = 24.6\%$;
 $h' = 335$ mm; (1) $\frac{\gamma'}{\gamma''} = 13.6$;
 (2) $\frac{\gamma'}{\gamma''} = 1.61$.

Figure 5-29 shows the relations $\varphi(w_0'')$ for a carbon tetrachloride-water system and a mercury-water system with identical absolute geometrical parameters of the layer.

The same data are plotted in Fig. 5-30 on the coordinates of (5-12). The experimental points generally agree, but the curve is

different in character from the corresponding curve for a steam-water mixture shown in Fig. 5-23. These curves coincide only within the range of small values of $w_0'' \sqrt{\frac{1-f}{\alpha}}$ (< 0.15). Within the range of values of $w_0'' \sqrt{\frac{1-f}{\alpha}} > 0.1$, the curve in Fig. 5-30 begins to rise sharply, as compared to the curve in Fig. 5-23.

The available experimental data are thus far still insufficient for a reliable analysis of the causes of that deviation.

5-8. Dynamic Layer with Crossflow of Phases

Figure 5-31 shows a diagram of a gas or vapor being scrubbed by

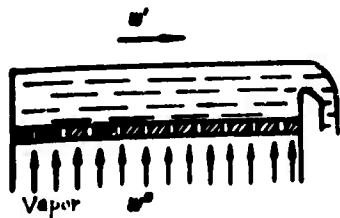


Figure 5-31. Diagram of a gas or vapor scrubbed by bubbling through a stream of liquid.

bubbling through a stream of liquid. The gas is fed under the perforated plate along which a relatively thin layer of liquid flows.

An experimental investigation of such a system was carried out by A. P. Turovskiy by bubbling

air at atmospheric pressure through water.

The depth of the dynamic layer in the given case depends on the geometry of the perforated plate (D_1, α_1), the height of the overflow weir h_{weir} , and the liquid and gas flow rates.

At a given liquid flow rate, the dynamic layer "swells" with an increase in gas flow rate only up to a definite magnitude. Further "swelling" ceases as part of the liquid layer flows over the weir. This phenomenon is reflected in the experimental data shown in Fig. 5-32.

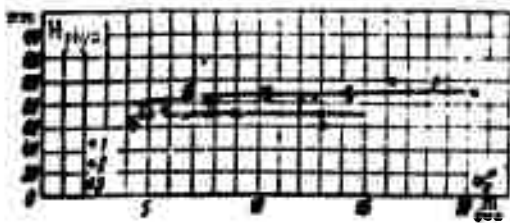


Figure 5-32. Variation in the depth of a two-phase layer as a function of the average air velocity in the orifices of the perforated plate. Weir height $h_{\text{weir}} = 52 \text{ mm}$; liquid flow rate $10.8 \text{ m}^3/\text{m} \cdot \text{hr}$:
 (1) $D_0 = 5 \text{ mm}$; $\varphi_1 = 2.2\%$;
 (2) $D_0 = 5 \text{ mm}$; $\varphi_1 = 4\%$; (3)
 $D_0 = 10 \text{ mm}$; $\varphi_1 = 4.36\%$.

The density of the layer varies continuously with an increase in w_0 (Fig. 5-33). In this case, as in the case of a layer with a stagnant heavy phase, the influence of the geometric factors D_1 and φ_1 is weak.

In very thin layers (5 to 10 mm) at small w_0 , spherical caps of hubbles are formed above each orifice, and, at high gas velocities, craters are formed above the orifices.

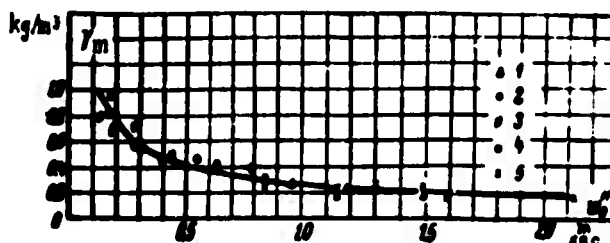


Figure 5-33. Variation in specific gravity of the air-water mixture, as a function of the reference velocity of the air. $h_{\text{weir}} = 52 \text{ mm}$. water flow rate $10.8 \text{ m}^3/\text{m} \cdot \text{hr}$; (1) $D_0 = 5 \text{ mm}$, $\varphi_1 = 17\%$; (2) $D_0 = 10 \text{ mm}$, $\varphi_1 = 4.36\%$;
 (3) $D_0 = 5 \text{ mm}$, $\varphi_1 = 2.2\%$; (4) $D_0 = 5 \text{ mm}$, $\varphi_1 = 4\%$;
 (5) $D_0 = 10 \text{ mm}$, $\varphi_1 = 17\%$.

CHAPTER SIX

TWO-PHASE FLOW IN CIRCULAR TUBES

6-1. General Information

In general, a two-phase flow in tubes is determined by a system of dimensionless parameters already discussed in the previous chapters. The most important parameters are:

- (a) the true relative volumetric fraction of light phase ψ ;
- (b) the volumetric flow fraction of the light phase $\beta = \frac{w_0^i}{w_0^i + w_0^j}$
or the ratio of velocities $\frac{w_0^i}{w_0^j}$;
- (c) the relative density of the phases $\frac{\gamma^i}{\gamma^j}$;
- (d) the criterion $\frac{w^2}{gD}$;
- (e) the criterion $\left(\frac{\gamma^i - \gamma^j}{\gamma^i + \gamma^j} \right)^2$

In a two-phase flow, the total pressure drop along the tube is, as usual, the sum of:

- (a) head losses due to friction and local resistances;
- (b) hydrostatic pressure of the column of mixture;
- (c) energy losses due to acceleration of the flow (either owing to the expansion of the gaseous component or to vaporization in the case of the flow of a vapor-liquid mixture).

In flow in horizontal or inclined tubes, the heavy phase, under the action of gravity, tends to transfer to the lower part of the

tube. This phenomenon causes an asymmetry in the flow of mixture and impairs the heat loss in the upper half of the tube when it is slightly wetted by the liquid phase. In flow in a vertical tube, there may be reverse currents (also due to gravity) in the liquid ring that usually forms near the tube wall. The degree to which these effects appear depends in the first place on the ratio between the kinetic energy of the stream and gravity, i.e., is characterized by the parameter $\frac{W^2}{g_1}$ or other criteria derived from it.

The parameter $\frac{\sigma}{(r-r')\rho}$ and the wettability of the tube walls substantially influence the structure of the mixture (i.e., the dimensions of the discrete phase elements: bubbles, drops, films). This latter influence is very strong.



Figure 6-1. Photographs of the motion of a steam-water mixture in vertical tubes. From left to right are shown tubes with gradually increasing fractions of steam.

When the liquid wets the tube wall, the gas tends to move in the center of the stream, and the great bulk of the liquid component concentrates around the tube walls. In this case, at small values of β , the gas moves in the form of separate bubbles, small at the beginning

and later larger as the relative gas flow rate increases. At low pressures, the so-called "slug" motion in this case arises when huge gas bubbles, which at times occupy the entire cross section of the tube and may be from several tens of centimeters up to meters long, burst in the liquid stream. Each such "slug" is followed by a series of relatively small bubbles.

At the same time the bulk of the liquid is pressed more and more strongly against the tube walls, and finally a continuous stream of a true gas-liquid emulsion is formed in the center of the tube, which, as observed through a glass wall, often seems to occupy the whole cross section of the tube.

Further increase in gas flow rate leads to the disappearance of the emulsion and to a central motion of the gas jet with a portion of the liquid component dispersed in it. A considerable portion of the liquid in this case moves along the tube wall in the form of a well-defined annular film.

In the case of a liquid that does not wet the tube walls (such as mercury in a steel or glass tube), the pattern of motion is reversed--i.e., gas bubbles break up between the tube wall and the liquid stream, finally forming a more-or-less well-defined tubular layer of gas in whose center moves the strongly pulsating liquid jet.

A further increase in relative gas flow rate results in a complete dispersion of the liquid phase. At a considerable relative density of the gas $\frac{\gamma''}{\gamma}$, and with little surface tension (which is the case, for example, with the motion of a vapor-water mixture at high pressure), the main type of flow of the mixture is an emulsion regime.

As we already mentioned, in the case of the motion of a gas-liquid mixture in a horizontal or slightly inclined tube with small

fractions of gas, we observe a well-defined asymmetry in the flow velocities affecting the distribution of the components along the cross section of the stream. The liquid component, under the influence of gravity, concentrates mainly in the lower part of the tube. As a result of this, wetting of the upper part of the tube is impaired and sometimes even becomes periodical.

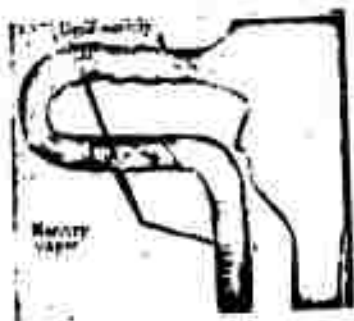


Figure 6-2. Photograph of the motion of a vapor-mercury mixture in a tube. Dark spots: liquid mercury; light spots: mercury vapor.



Figure 6-3. Various forms of motion of a gas-liquid mixture in tubes. The flow rates of the mixtures are the same; (1) vertical tube; (2) horizontal tube; (3-6) motion in a horizontal tube at various velocities of the mixture.

Figures 6-1, 6-2, and 6-3 show photographs of various flow regimes for a gas-liquid mixture, from data obtained at the TsKTI [Central Scientific Research Institute for Boilers and Turbines] and ENIN [Institute of Power Engineering (Im. G. M. Krzhizhanovskiy)] by V. V. Pomerantsev, S. N. Syrkin, A. N. Lozhkin, S. I. Kosterin, and L. Yu. Krasyakova. A characteristic feature of these flow regimes is the mobility of the interface, in most cases accompanied by wave formation.

6-2. Flow Regimes in a Gas-Liquid Mixture in Straight Tubes

As has already been shown above, the flow regimes of a gas-liquid mixture in tubes vary greatly and depend basically on the flow velocity, the volumetric fraction of gas in the stream, and the relative density of the phases. In this section, we shall examine in more detail the flow regimes observed in mixtures whose liquid phases wet the tube wall. This investigation is based on observations of the flow of air-water and steam-water mixtures, i.e., systems in which the liquid component has low viscosity.

At moderate velocities of the mixture, the effect of gravity is very pronounced, and the flow regime depends appreciably on the slope of the tube axis with reference to the horizontal plane. In this case, even small deviations of the tube from the vertical upset the axial symmetry of the phase distribution in the cross section of the tube.

At small flow velocities in horizontal or slightly inclined tubes, the flow may become completely stratified. But at very high velocities of the mixture, the phase distribution in the cross section approaches axial-symmetric distribution, even in horizontal tubes.

Let us first consider flow regimes in vertical tubes at high values of $\frac{\gamma'}{\gamma''}$ (such as an air-water mixture at $p \approx 1$ atm. abs.).

In vertical tubes, with a low velocity of the gas-water mixture and reduced gas content, the bubbles are relatively small--from one to several millimeters in diameter--and are almost uniformly distributed in the whole cross section of the tube. Such a regime is

called emulsion flow.

With an increase in the fraction of gas, the bubbles begin to coalesce and finally occupy the whole central part of the cross section of the tube, sometimes attaining a length of 1 m or more. Such a long bubble is separated from the tube wall by a thin layer of water and its head has the shape of an ellipsoid, while the rear part is almost flatly truncated, giving it a resemblance to an artillery projectile. Because of this, such a flow regime in the mixture is usually called a "slug" regime.

A further increase in the fraction of gas results in an increase in the length of the "slug" and the water seals between the "slugs" become thinner and thinner, until finally the individual "slugs" coalesce into a continuous column of gas ("core") surrounded by a water ring ("core" flow regime). The thickness of the water ring depends on the quantity of water flowing through the tube per unit of time, as well as on gas flow rate. At a high reference gas velocity, the gas stream sweeps a considerable portion of the water from the wall and entrains it in the form of separate drops. Sometimes only a very small part of the water remains on the wall, moving on it at a velocity considerably lower than the average gas velocity.

At atmospheric pressure ($\frac{\gamma'}{\gamma''} \approx 800$) a core flow regime was observed only at very high reference gas velocities (15-20 m/sec) and at a relatively low water flow rate. The slug regime is the main type of regime for air-air [sic] and steam-water mixtures, and embraces a wide variety of flows.

At high gas densities, flow regimes have been investigated only in steam-water mixtures. With increasing pressure in the steam-water mixture, the range of the emulsion flow regime increases considerably

and the range of slug flow regime decreases correspondingly. At a pressure of 30 atm. abs. ($\frac{\gamma'}{\gamma''} \approx 60$), the typical slug regime is almost absent, and at a higher fraction of steam (more than 80% by volume) we observe only a mixed slug-emulsion regime. In this case, the tube is filled with numerous small steam bubbles through which break the remainder of the heads of separate large bubbles ("slugs"), accompanied by the bulk of the small bubbles.

At a pressure of the order of 100 atm. abs. ($\frac{\gamma'}{\gamma''} = 13$), the slug regime disappears completely, and with an increase in the steam fraction, the emulsion regime apparently turns directly into a core regime (at a very high fraction of steam--above 95% by volume, i.e., about 60% by weight at this pressure). In this case we observe a flow regime characterized by the presence of a thin water film on the tube surface, and by the entrainment of a considerable part of the water by the central steam jet.

For steeply inclined tubes whose axis forms an angle of more than 30 to 40° with the horizontal plane, flow regimes have been investigated very little, but apparently they are very similar to the flow regimes in vertical tubes, differing mainly by a certain asymmetry resulting from the fact that the bubbles are squeezed against the upper generatrix of the tube. Besides, as has been established by measurement of the absorption of gamma radiation, the relative velocity of steam (gas) in inclined tubes is higher than in horizontal and vertical tubes ($v_{\text{incl}} < v_{\text{vert}} < v_{\text{horiz}}$).

In slightly inclined or horizontal tubes asymmetry occurs particularly at very low velocities of the mixture. Nonuniformity in the distribution of steam and liquid in the cross section of the tube is characteristic of all flow regimes for a gas-liquid mixture in

horizontal tubes. At low flow velocities, this nonuniform distribution of steam and liquid in the cross section of the tube may go so far as to separate the two phases completely (the so-called stratified or trough flow).

In spite of the fact that in horizontal tubes the buoyant force causing the bubbles to rise is perpendicular to the direction of the main motion of the stream, in almost all regimes the relative velocity of steam is high, i.e., the average velocity of steam appreciably exceeds the average velocity of water.

The only exception is the stratified flow regime with a very low fraction of steam, when the steam, occupying a small part of the cross section in the upper part of the tube, wets a considerable part of the tube perimeter. Therefore, the hydraulic diameter of a steam jet is considerably smaller than in the case of water jets, and the velocity of the steam jet is correspondingly reduced and may (particularly at high pressures, when the densities of steam and water are not very different) even be less than the average velocity of the water.

When the velocity of the mixture in horizontal tubes is increased, stratified flow turns into a slug flow with a well-defined asymmetry (the liquid ring is thicker in the lower part of the tube). With a further increase in the velocity of the mixture and with moderate gas fractions, the "slugs" begin to break up and the flow approaches an emulsion regime, also characterized by a considerable nonuniformity in the phase distribution according to the depth of the cross section.

When the gas fraction is large, there is an increase in the range of mixture velocities at which a stratified regime is observed, and at very high values of β (> 0.9 to 0.95) when there is an increase in the mixture velocity, the stratified flow turns directly into a core flow.

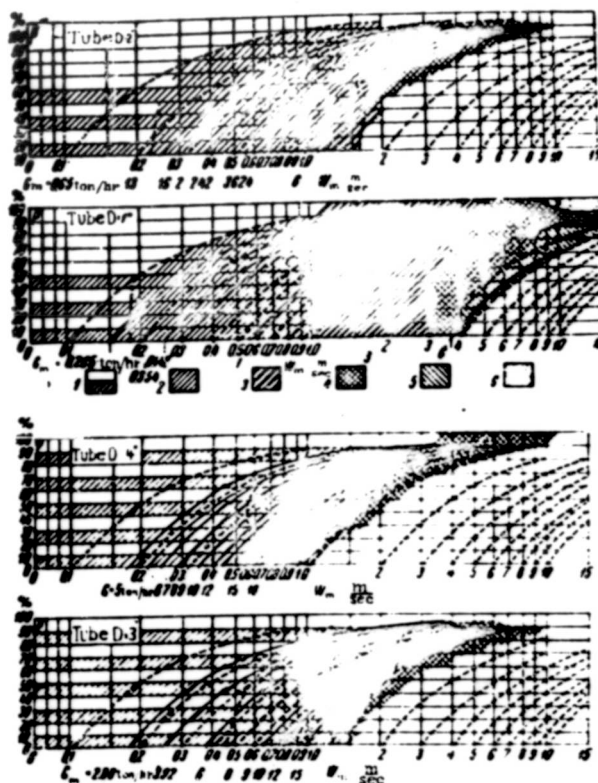


Figure 6-4. Flow regimes in an air-water mixture at atmospheric pressure in horizontal round tubes. (1) Divided flow; (2) smooth plug flow; (3) plug flow with foaming behind bubble; (4) plug flow with foaming along the entire boundary; (5) steady flow in form of emulsion; (6) annular flow.

This is well marked in Fig. 6-4, which shows the influence of the velocity of the mixture ($w_m = w_0' + w_0''$) and of β on the flow regime, as visually observed at the ENIN [Institute of Power Engineering (Im. G. M. Krzhizhanovskiy)] (Kosterin, Teletov). The increase in the tube diameter results in a change in the values of w_m at which transition from stratified flow to slug flow is observed (at low β , $w_{m,cr} \approx 0.2$ m/sec for a tube of $D = 26$ mm, and almost 1 m/sec for a tube of $D = 100$ mm).

No direct observations of flow regimes in horizontal tubes have been made at increased pressures, and under such conditions we can visualize the flow regimes only through data obtained from investigations on the heat transfer from tube walls to steam-water mixtures. Such experiments were carried out at pressures of 1 atm. abs. ($\frac{\gamma'}{\gamma''} \approx 1,650$) and up to 220 atm. abs. ($\frac{\gamma'}{\gamma''} \approx 2$) in steam-water mixtures.

It has been established that at low pressures (close to 1 atm. abs.) sudden variations in the rate of heat transfer were observed in the vicinity of a slug regime, with periods equal to the period of passage of the "slugs"; at the same time fluctuations in pressure drop were also observed. At higher pressures (20 to 220 atm. abs.) no periodic fluctuations of the wall temperature were noticed. We may therefore assume that in horizontal tubes a pressure rise in the steam-water mixture will lead to the disappearance of the "slug" regime. With an increase in mixture velocity at high pressures, stratified regime turns directly into emulsion regime, and afterward into a core regime. This is also confirmed by the character of salt deposits on the surface of the heated tubes.

Quantitative data on the distribution of both phases in the cross section of the tube at the various flow regimes in a gas-liquid mixture are meager, and such data cover, as a rule, only air-water mixtures at room temperature and atmospheric pressure.

Figure 6-5 shows the distribution of both phases according to the depth of the cross section of the tube, as obtained by A. A. Armand by means of a special device consisting of a knife which can be shifted up and down and which cuts the stream into two parts directed into two different separators. Thus, it was possible to measure the fraction of air and water both in the upper and in the lower part of the tube cross section.

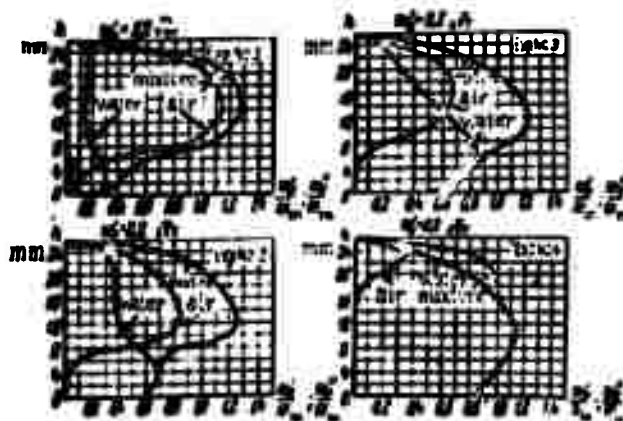


Figure 6-5. Phase distribution in the flow of an air-water mixture at atmospheric pressure in a horizontal tube of $D = 26$ mm. Experiment No. 1: $G' = 4,200$ kg/hr, $q'' = 22.2$ kg/hr; experiment No. 2: $G' = 4,200$ kg/hr, $q'' = 6.0$ kg/hr; experiment No. 3: $G' = 4,200$ kg/hr, $q'' = 4.56$ kg/hr; experiment No. 4: $G' = 4,200$ kg/hr, $q'' = 0.33$ kg/hr.

In Fig. 6-5, the height from the lower generatrix of a tube with an inside diameter of 26 mm is laid off on the ordinate, and the ratios of the local values of the velocity of the air-water mixture and of the reference velocities of the air and of the water to the average mixture velocity are laid off on the abscissa. All three $\sqrt{\text{sic}}$ graphs were obtained at a constant and rather high water flow rate $w_0' = 2.2$ m/sec, but with different volumetric air flow fractions of β .

As may be seen from the graphs in Fig. 6-5, at a small value of ($\beta = 6.2\%$) all the air moves in the very upper part of the tube and the profile of the velocity field differs relatively little from the case of motion of pure water in a tube.

If the volumetric air fraction increases up to $\beta = 7.5\%$, the long air bubbles ("slugs") occupy a considerable part of the cross section of the tube, and only in the lowest part of the cross section does almost pure water flow. At $\beta = 81.5\%$ the distribution of air and water over the height of the cross section is comparatively uniform. With such high fractions of gas and sizable velocities of the mixture (in the experiment with $\beta = 81.5\%$, the velocity of the mixture was more than 10 m/sec), the motion of the gas-liquid mixture approaches axially symmetric motion, and the flow regime in horizontal tubes differs little from the regime existing in vertical tubes.

Figure 6-6 shows variation in the dynamic and total head of the stream over the cross section of a horizontal tube, obtained in experiments carried out by L. Yu. Kras'yakova by means of a velocity tube that can move up and down the tube cross section. The experiments were carried out at low reference velocities of the water ($w_0' = 0.1$ m/sec) and with very high fractions

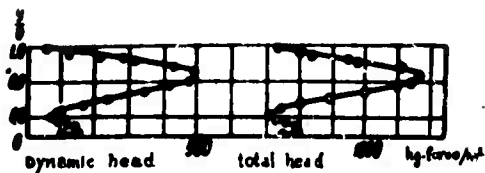


Figure 6-6. Field of dynamic heads in a horizontal tube. Air-water mixture: $p = 1$ atm. abs.; $w_0^I = 0.2$ m/sec; $w_0^{II} = 27.4$ m/sec.

of air ($\beta = 99.4$ to 99.8%), i.e., with a pure core regime.

As may be seen from the graphs, even at relatively high reference velocities of air the stream still remains considerably asymmetric. The lower part of the water ring is considerably thicker, and there is in this zone a well-defined second velocity head maximum.

The stream becomes almost axially symmetric only at very high reference air velocities ($w_0^{II} = 46$ m/sec), and there is little thickening of the water ring at the lower generatrix.

Since in these experiments concentration of gas and water was not measured simultaneously in the whole cross section of the tube it is not possible to convert the fields of dynamic heads into velocity fields directly.

6-3. Symmetrical Laminar Flow of a Liquid Layer

The number of different types of flows in a two-phase stream which at the present time may be systematically analyzed is extremely limited. At the same time, the flows being computed are very schematic and not very close to the corresponding forms of actual streams. Nevertheless, their theoretical analysis has great value for gaining knowledge since it affords a sufficiently accurate explanation of physical laws underlying the influence of different stream

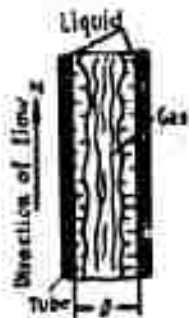


Figure 6-7. Diagram of core motion of a mixture.

parameters on the stream's fundamental hydraulic characteristics.

In this connection, an investigation of the flow of a mixture with a symmetrical liquid film is extremely useful, although such a flow takes place, in reality, only at very high fractions of gas in the mixture. The first studies along these lines were carried out simultaneously

and independently by A. A. Armand and S. S. Kutateladze. A model for the "slug" flow of a mixture was investigated by V. A. Schwab (Shvab) and N. N. Konstantinov.

Let us consider a mixture of a gas with a very viscous liquid at gas flow velocities so high that all the liquid is concentrated around the tube walls in the form of a symmetrical film (Fig. 6-7). As a result of high viscosity, the film flows in a laminar fashion, and as a result of the high velocity of the gas, frictional resistance is much greater than the force of gravity.

Under the indicated conditions, the ordinary parabolic law of velocity distribution applies to the liquid film:

$$v = -\frac{1}{4\eta} \frac{dp_f}{dx} (R_0^2 - R^2). \quad (6-1)$$

where $\frac{dp_f}{dx}$ [kg-force/m²m] is pressure loss due to friction;
 R_0 , R [m] are the inside radius of the tube and the radius of interest.

The average flow velocity of the liquid in the film is

$$\bar{w} = \frac{2}{R_0^2(1-\eta)} \int_{R_0\sqrt{\eta}}^{R_0} wR dR. \quad (6-2)$$

It is assumed here that all of the liquid component of the mixture is concentrated in the film and, consequently,

$$\eta = \left(\frac{R}{R_0}\right)^2. \quad (6-3)$$

in which R_b is the radius of the film at the boundary with the gas jet.

Substituting the value of w from (6-1) into (6-2), and noting that

$$(1-\eta)\bar{w} = w_0, \quad (6-4)$$

we obtain:

$$-\frac{dw_0}{dx} = \frac{32\eta w_0}{D^2(1-\eta)^2}, \quad (6-5)$$

where $D = 2R_0$ is the inside diameter of the tube.

At $\eta = 0$ we obtain the familiar formula for a homogeneous stream:

$$-\left(\frac{dw_0}{dx}\right)_0 = \frac{32}{D^2} w_0. \quad (6-6)$$

hence,

$$\frac{\Delta p}{\Delta p_{f,0}} = \frac{1}{(1-\varphi)^2}. \quad (6-7)$$

or

$$\varphi = 1 - \sqrt{\frac{\Delta p_{f,0}}{\Delta p}}. \quad (6-8)$$

The pressure over the cross section of the mixture is constant. Therefore, considering the flow of the gas jet inside the liquid ring as analogous to flow in an ordinary tube, we may write:

$$-\frac{\Delta p}{dx} = \zeta'' \frac{\rho_g \dot{w}_g^2}{2gD\sqrt{\varphi}}. \quad (6-9)$$

in which ζ'' is the coefficient of friction of the gas against the film.

On the other hand, the relative velocity of the gas is

$$w_r = \frac{w_g}{\varphi} - w_l. \quad (6-10)$$

Substituting here the value of the velocity of the liquid on the film surface w_b^l , as calculated according to Formula (6-1) at $R = R_0 \sqrt{\varphi}$, we obtain:

$$w_r = \frac{w_g}{\varphi} + \frac{\Delta p_f}{dx} \cdot \frac{D}{16\mu} (1-\varphi).$$

or, taking into account (6-5):

$$\alpha_1^2 = \frac{\alpha_0^2}{\eta} - \frac{\alpha_0^2}{1-\eta}. \quad (6-11)$$

By combining Formulas (6-6) and (6-9), we have:

$$\frac{\Delta p_1}{\Delta p_{1,0}} = \zeta' \frac{1 \cdot \alpha_1^2 D}{4 \alpha_0^2 \alpha_1 \sqrt{\eta}}.$$

or, taking into account that the friction coefficient when a homogeneous laminar stream flows in a tube is

$$\zeta = \frac{64}{Re}, \quad (6-12)$$

where, in the given instance,

$$Re' = \frac{\alpha_1^2 D}{\eta}, \quad (6-13)$$

we obtain:

$$\frac{\Delta p_1}{\Delta p_{1,0}} = \frac{\zeta \eta}{4 \alpha_1 \sqrt{\eta}} \left(\frac{\alpha_1^2}{\alpha_0^2} \right)^2. \quad (6-14)$$

this formula is of general significance since it is valid for laminar as well as for turbulent flow of phases.

Substituting into (6-14) the value of $\frac{w}{r}$ from (6-11) and f_0 from (6-12), we have:

$$\frac{\Delta p_1}{\Delta p_{1,0}} = \frac{C_T Re'}{64 r^2 v^2} \left(\frac{u_0}{u_0'} - \frac{2v}{1-v} \right)^2. \quad (6-15)$$

Further, combining Formulas (6-7) and (6-15), we find that

$$\frac{v}{1-v} \left(v^{\frac{1}{2}} \sqrt{\frac{64}{C_T}} + 2 \sqrt{Re' \frac{r}{r'}} \right) = \frac{u_0}{u_0'} \sqrt{Re' \frac{r}{r'}}. \quad (6-16)$$

In the case of a turbulent flow in a gas jet, which also takes place under actual conditions, $f'' \ll 1$. The quantity $v^{\frac{1}{2}}$ is close to unity even at comparatively small v . The maximum value of Re' in laminar flow is approximately 2,000. Hence, it is not difficult to compute that, at low and medium pressures,

$$v^{\frac{1}{2}} \sqrt{\frac{64}{C_T}} > 2 \sqrt{Re' \frac{r}{r'}}.$$

For these conditions, with sufficient accuracy

$$\frac{\Delta p_1}{\Delta p_{1,0}} = \frac{C' \gamma' Re'}{48 \gamma' \eta^2} \left(\frac{u_0'}{u_0} \right)^3 \quad (6-17)$$

$$\frac{u_0'}{u_0} = \frac{u_0'}{1-\gamma} \sqrt{\frac{C' \gamma' Re'}{48 \gamma'}} \quad (6-18)$$

Table 6-1. Calculations of the Characteristics of a Two-Phase Stream with a Symmetrical Laminar Liquid Layer at

$$\frac{u_0'}{u_0} > \frac{2\gamma}{1-\gamma}$$

γ	0	0.16	0.29	0.46	0.58	0.74	0.80	0.90	0.95	0.97	0.98	0.99	0.995
$\frac{\Delta p_1}{\Delta p_{1,0}}$	1	1.42	2.00	3.44	5.68	14.8	25	100	400	1.10 ³	5.10 ³	1.10 ⁴	4.10 ⁴
$\frac{u_0'}{u_0} \sqrt{\frac{C' Re' \gamma'}{48 \gamma'}}$	0	0.12	0.30	0.70	1.27	2.64	3.80	6.80	18.3	32	49	99	200

Thus, under the indicated conditions, γ and

$$\frac{\Delta p_1}{\Delta p_{1,0}}$$

are single-valued functions of the group

$$C' Re' \frac{\gamma'}{\gamma} \left(\frac{u_0'}{u_0} \right)^3,$$

which is a specific combination of criteria describing the relation-

ship between the kinetic energies of the phases, their friction at the boundary, and the viscous friction within the liquid phase film.

Formula (6-10) also shows the relationship between the effect of the criteria $\frac{\rho}{\rho_1} \sqrt{\frac{r}{r_1}}$ and $\frac{r}{r_1}$ on such hydraulic characteristics of a two-phase flow as ψ and $\frac{\Delta p_f}{\Delta p_{f,0}}$.

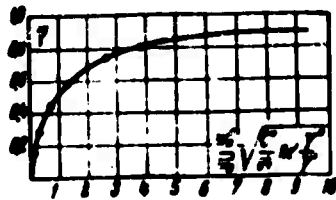


Figure 6-8. ψ vs. $\frac{\rho}{\rho_1} \sqrt{\frac{r}{r_1}}$

from theoretical calculation.

As may be seen, the independent influence of the relative density of the phases $\frac{\rho}{\rho_1}$ becomes apparent only at rather high values of this criterion. The mechanism of this effect is due to the fact that under these conditions the relative velocity of the phases begins to be substantially different from the reference velocity. At sufficiently low

$\frac{r}{r_1}$, the densities of the phases for practical purposes influence the hydrodynamics of the two-phase flow only through the relationship

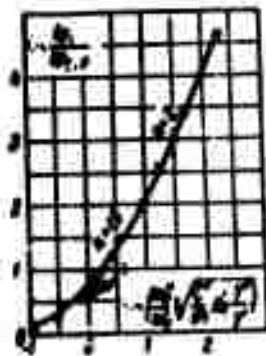


Figure 6-9. $\log \frac{\rho}{\rho_1}$ vs. $\frac{r}{r_1}$ from theoretical calculation.

between the kinetic energies of the phases and through other criteria into which r' and r'' enter separately or jointly, but in combination with a third quantity (such as $\frac{\rho}{(\rho' - \rho'')^2}$).

Table 6-1 shows the results of calculations by Formulas (6-7) and (6-18).

The data of this table are plotted in the Figs. 6-8 and 6-9. As may be seen, pressure losses increase very rapidly with an increase in the relative flow fraction of gas in the mixture. The true relative fraction of gas in the mixture increases with an increase in the flow fraction of gas very sharply at the beginning, and later very slowly.

Within the region $0 < \frac{w_0}{w_0} \sqrt{C' Re' \frac{Y'}{Y}} < 8$ the loss of head is proportional, on the average, to approximately the 1.3 power of this group.

When $\frac{w_0}{w_0} \sqrt{C' Re' \frac{Y'}{Y}} > 8$, the quantity ψ approaches unity, and

$$\frac{\Delta h}{\Delta h_0} \approx \frac{C' Re' Y'}{64 Y} \left(\frac{w_0}{w_0} \right)^2. \quad (6-19)$$

6-4. The Re' and Re'' Numbers as Characteristics of the Phase-Flow Regime in an Annular Liquid Film

The equivalent hydraulic diameter of a liquid ring wetting the wall unilaterally is

$$D_{e1} = D(1-\psi); \quad (6-20)$$

accordingly, the Reynolds number of such a ring

$$Re' = \frac{\bar{u} D_{e1}}{\nu} = \frac{u_0 D}{\nu}. \quad (6-21)$$

Therefore, the flow regime of the liquid phase may be determined by the same limits of $Re = Re'$ as for the flow of a homogeneous liquid.

For the gas jet

$$Re'' = \frac{\bar{u} \cdot D \sqrt{\gamma}}{\nu} = \frac{u_g D}{\nu_g} \quad (6-22)$$

Since the quantity ψ approaches unity even at low values of $\frac{w_0}{w_T}$, the flow regime of the gas stream may be rather accurately described by the parameter.

$$Re'' = \frac{u_g D}{\nu_g} \quad (6-22a)$$

6-5. Experimental Data on Head Losses in a Two-Phase Flow with a Laminar Layer of Liquid

Let us examine the experimental data obtained by Martinelli, Bolter, Taylor, Thomson, and Morrison. These experiments were conducted in a glass tube, $D = 25.4$ mm.

The component characteristics of the investigated mixtures are given in Table 6-2.

Data on the range of changes in criteria for each series of experiments are given in Table 6-3.

It is apparent that, for practical purposes, only the quantity $\frac{\gamma''}{\gamma}$ remains constant in these experiments. All other criteria vary

Table 6-2. Characteristics of the Investigated Media

Liquid	Gas	p, atm.abs.	t° C	$\gamma', \text{kg/m}^3$	$\mu' \cdot 10^4$ kg-sec/m ²	$\sigma \cdot 10^3$ kg/m
Water	Air	1.28	15.6	1000	1.03	7.5
Water + Nekal	"	1.26	26.6	1000	0.80	3.12
Kerosene	"	1.26	25.6	830	1.91	2.86
Diesel oil	"	1.26	26.6	867	4.56	2.74
Mixture No. 1	"	1.26	28.4	901	38.5	2.91
Mixture No. 2	"	1.26	29.5	913	113.5	3.00
Petroleum "B"	"	1.26	29.5	912	245	3.11

within an exceedingly wide range. On the basis of these criteria, we may evaluate to what extent each criterion affects the law of resistance.

Figure 6-10 shows the dependence of quantity $\zeta = \frac{\Delta p}{\rho v^2}$ on the criteria $\frac{v_0}{v}$ and Re' at a practically constant value of the criterion

$Fr = \frac{v_0^2}{gD}$. The loss of head is found to be strongly dependent on the ratio of the reference velocities of the phases, as well as on the Re' number of the liquid.

In Fig. 6-11 the same data are presented in the form of a relationship between $\frac{\Delta p}{\rho v^2} Re'$ and the group $\frac{v_0}{v} \sqrt{Re' \frac{v}{v_0}}$. In good agreement with the above-stated theory, all the experimental points fall along a single line.

In Fig. 6-12, data from the whole series of experiments are plotted on the same coordinates.

Table 6-3. Experimental Data

Liquid	$Re' = \frac{W_0 D}{\nu}$	$Fr = \frac{W_0^2}{gD}$	$\frac{W_0}{W_0'}$ min.	$\frac{W_0}{W_0'}$ max.	$Re'' = \frac{W_0 D}{\nu''}$ max.
Petroleum "B" $\gamma'' / \gamma' = 1.43 \cdot 10^{-3}$ $\mu'' / \mu' = 0.075$	4.8 9.6 19 28 47 57	0.01 0.04 0.15 0.33 0.96 1.4	12.6 6.2 0 0 0 9.7	790 345 128 76 15 9.7	70 000 63 000 45 000 40 000 14 000 10 000
Mixture No. 2 (Diesel oil + petroleum) $\gamma'' / \gamma' = 1.43 \cdot 10^{-3}$ $\mu'' / \mu' = 0.162$	10 21 41 60 123 164 204 306	0.0096 0.04 0.16 0.33 1.4 2.5 3.84 8.7	51 39 3.5 2.4 1.2 9.6 0.8 0.6	846 345 165 112 43 18 4.7 0.6	75 000 62 000 60 000 59 000 46 000 45 000 14 000 1 700
Mixture No. 1 (Diesel oil + petroleum) $\gamma'' / \gamma' = 1.44 \cdot 10^{-3}$ $\mu'' / \mu' = 0.505$	32 64 160 256 334 640 860 1280	0.01 0.04 0.25 0.64 1.44 4.0 9.0 16.0	5.8 5.8 2.4 1.47 0 0 0 0	870 470 174 109 57 25 7.4 2.8	79 000 85 000 79 000 79 000 62 000 45 000 20 000 10 000
Water $\gamma'' / \gamma' = 1.3 \cdot 10^{-3}$ $\mu'' / \mu' = 17.9$	1080	0.008	557	970	81 000
Kerosene $\gamma'' / \gamma' = 1.57 \cdot 10^{-3}$ $\mu'' / \mu' = 9.6$	1210	0.047	39	438	86 000
Diesel oil $\gamma'' / \gamma' = 1.5 \cdot 10^{-3}$ $\mu'' / \mu' = 4.0$	940 1880	0.16 0.64	62 10	259 130	95 000 95 000

As can be seen, when $\frac{w_0}{w_1} \sqrt{Re' \frac{L}{r}} < 40$ the experimental points clearly begin to group according to the Froude numbers. Evidently, flow asymmetry and wave formation at the interface become substantial in this area. In the same figure, the dotted line indicates the

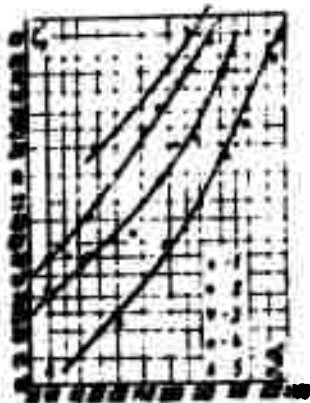


Figure 6-10. Given drag coefficient, f'_0 vs. $\frac{w''_0}{w'_0}$

from experiments with laminar flow of a liquid layer: (1) Petroleum "B" (Re = 9.6, Fr = 0.04); (2) Mixture No. 1 (Re = 64, Fr = 0.04); (3) Water (Re = 1080, Fr = 0.01); (4) Mixture No. 2 (Re = 21, Fr = 0.04); (5) Kerosene (Re = 1210, Fr = 0.05)

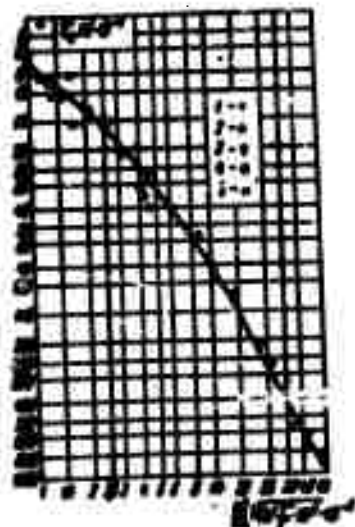


Figure 6-11. Group $\frac{w_0}{w_1} \sqrt{Re' \frac{L}{r}}$ vs. Re'

(1) Petroleum "B" (Re = 9.6, Fr = 0.04); (2) Mixture No. 1 (Re = 1080, Fr = 0.01); (4) Mixture No. 2 (Re = 21, Fr = 0.04); (5) Kerosene (Re = 1210, Fr = 0.05)

theoretical curve in which $f' = \text{const}$; it is calculated according to Table 6-1 by making the theoretical value of the group $\frac{w_0}{w_1} \sqrt{Re' \frac{L}{r}}$ identical with the value of the group $\frac{w_0}{w_1} \sqrt{Re'}$ when $\frac{w_0}{w_1} = 400$. Evidently, the experimental points in the region of diminishing values of the variables fall above the calculated line. This circumstance indicates that the friction coefficient between the gas and the liquid is not constant, but diminishes with an increase

in the gas flow velocity. Besides, at small $\frac{\rho_g}{\rho_l} \sqrt{\frac{g}{\gamma}}$, when flow asymmetry and wave formation become substantial, the coefficient of friction also becomes a function of the Froude number.

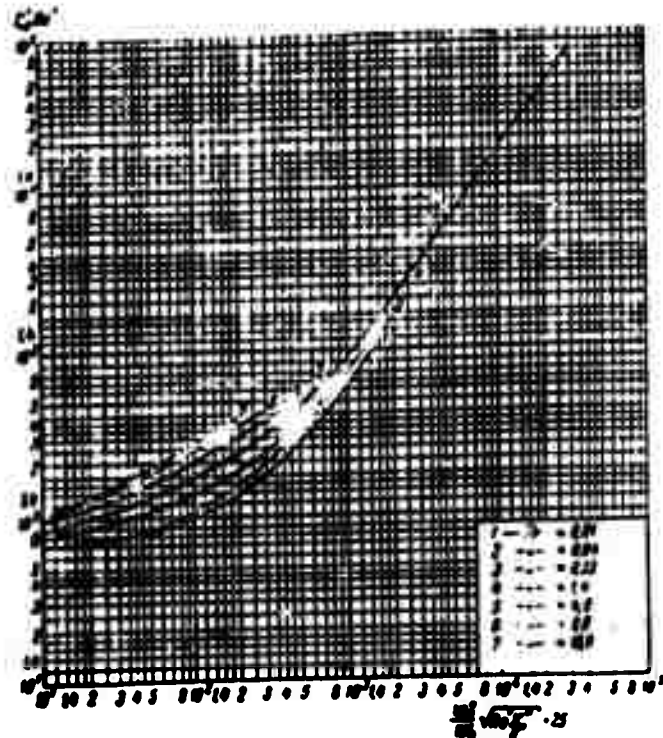


Figure 8-12. Effect of the Froude criterion on resistance for laminar flow of the liquid layer. (1) $Fr = 0.01$; (2) $Fr = 0.04$; (3) $Fr = 0.1$; (4) $Fr = 0.33$; (5) $Fr = 1.0$; (6) $Fr = 9.0$; (7) $Fr = 10$.

As has been determined in the preceding chapters, any determinable criterion for a two-phase flow in a general case is a function of a series of parameters--namely,

$$\gamma = \gamma \left(\frac{\rho_1}{\rho_2}; \frac{\rho_2}{\rho_1}; \frac{r_1}{r_2}; Re'; \frac{\rho_1}{\rho_2}; \frac{1}{(\gamma' - \gamma) \rho}; \frac{h}{r} \dots \right). \quad (6-23)$$

The described experiments, as well as S. I. Kosterin's experiments, confirm the fact that the influence of criteria $\frac{\rho''}{\rho'}$ and $\frac{1}{(\gamma' - \gamma) \rho}$ on the hydraulic characteristics of a two-phase stream flowing in a tube can be disregarded.

In the particular problem under consideration, theory leads to a specific combination of the parameters $\frac{w_0''}{w_0'}$, Re' , and $\frac{\gamma''}{\gamma'}$. Consequently, deviations from the theoretical line must actually be functions of the Froude number and, to a certain degree, of the ratio $\frac{\gamma''}{\gamma'}$ (since these deviations are a measure of the additional dynamic effect on the interface). As has been found in preceding chapters, generally speaking, these parameters enter the functional expression as the product $Fr \frac{\gamma'}{(\gamma' - \gamma'')}$.

Figure 6-13 shows that the influence of the Froude number is generally small. Namely, even in the area of its greatest influence on the process, a 1,500-fold change in Fr alters the ratio $\frac{\Delta p_f}{\Delta p_{f,0}}$ by a factor of 2.7 only. Based on the above-mentioned data, at

$\frac{w_0''}{w_0'} \sqrt{Re' \frac{\gamma''}{\gamma'}} > 40$, we may recommend the working formula

$$\frac{\Delta p_f}{\Delta p_{f,0}} = 1 + 0.1 \left(\frac{\rho_1}{\rho_2} \sqrt{Re' \frac{r_1}{r_2}} \right)^{1.5}. \quad (6-24)$$

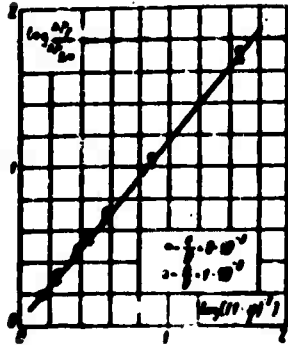


Figure 6-13. $\log \frac{\Delta p_f}{\Delta p_{f,0}}$
as a function of $\log (1-\phi)^{-2}$
theoretically computed for
turbulent flow of a liquid
film.

Evidently, the experimental exponent is very close to the theoretical value (see Fig. 6-9). The unity in the right member of Formula (6-24) is introduced in order to carry the calculation to $w_0'' = 0$.

$$\text{At } \frac{w_0''}{w_0'} \sqrt{\text{Re}' \frac{\gamma''}{\gamma'}} < 40, \text{ it is}$$

possible to make use of the mean curves drawn through the experimental points shown in Fig. 6-13.

6-6. Symmetrical Turbulent Flow of a Liquid Layer

The velocity profile in a turbulent film flow can be expressed with sufficient accuracy for our purposes by the expression

$$v = 2.5v^* \ln \left(1 + \frac{y}{\delta} \right); \quad (6-25)$$

here, v^* is so-called dynamic velocity:

$$v^* = \sqrt{\frac{g \delta^3}{\gamma'} \left(-\frac{d\phi}{dx} \right)};$$

y is the distance from the tube wall;

δ is the scale factor.

For tubes with granular roughness we can assume, if the quadratic law of resistance applies, that

$$\delta = \frac{y}{2}.$$

where e is the height of the protrusions.

For smooth tubes we can assume

$$\delta = 11.6 \frac{y}{\sqrt{e}}.$$

Let us assume, as has already essentially been done in the preceding paragraphs, that

$$-\frac{\Phi_1}{\Delta} = \zeta \frac{w_0^2}{2D}. \quad (6-26)$$

in which ζ' is the conditional (referred to w_0) drag coefficient of two-phase flow.

Calculating the value of w_0 from Formula (6-2) by substituting into it the value of w' from (6-25) and disregarding in the obtained solution the terms of the order of $\frac{e}{30}$, we arrive at the equation*

$$\frac{1}{V\zeta} = \frac{1.25}{V_2} \left[(1-\varphi) \ln \left[1 + 15(1-\sqrt{\varphi}) \frac{D}{\delta} \right] + \frac{1-\varphi}{2} + \sqrt{\varphi} \right]. \quad (6-27)$$

*In turbulent film flow, the central gas jet usually contains liquid drops; as a result, the average velocity of liquid flow

Taking into consideration that

$$-\left(\frac{d\varphi}{dx}\right)_0 = \zeta \frac{v_0^3}{2gD} \quad (6-28)$$

where f_0 is the drag coefficient at $\varphi = 0$, we obtain:

$$\frac{d\varphi}{d\varphi_0} = \frac{\zeta}{\zeta_0} = -\frac{1.25}{\zeta_0} \left\{ (1-\varphi) \ln \left[1 + 15 \left(1 - \sqrt{\varphi} \right) \frac{D}{\delta} \right] + \frac{\varphi-3}{2} + \sqrt{\varphi} \right\}^{-1} \quad (6-29)$$

The results of calculations by this formula are given in table 6-4.

In the film is

$$\bar{x} = \frac{2 \left(1 - \frac{v_0^3}{v_0^3} \right)}{R_0(1-\varphi)} \int_{R_0}^R w R dR.$$

where \bar{x} is the weight fraction of liquid in the gas. Accordingly, Formula (6-9) is more correctly written in the following form

$$-\frac{d\varphi}{dx} = \zeta \frac{v'(1+x)v_0^3}{2gDv_0^3}.$$

In subsequent formulas, when we take into account the fraction of liquid entrained by the gas stream, we should replace the quantity $\sqrt{f_0'}$ by the following quantity

$$\frac{\sqrt{\zeta_0}}{1 - \frac{v_0^3}{v_0^3}}.$$

and replace f'' by the quantity $f'' (1 + \bar{x})$.

Table 6-4. Results of Calculations by Formula (6-29)

	$\frac{\Delta P_f}{\Delta P_{f,0}}$			
	$\frac{e}{D} = 8 \cdot 10^{-3}$	$\frac{e}{D} = 4 \cdot 10^{-3}$	$\frac{e}{D} = 2 \cdot 10^{-3}$	$\frac{e}{D} = 1 \cdot 10^{-3}$
0	1	1	1	1
0.16	1.53	1.52	1.51	1.50
0.25	2.01	1.98	1.96	1.94
0.36	2.95	2.88	2.85	2.80
0.41	3.58	3.46	3.40	3.33
0.49	5.11	4.94	4.83	4.71
0.64	11.8	11.3	10.8	10.4
0.81	57.3	52.7	49.3	46.4
1	∞	∞	∞	∞

From these calculations it follows that the dependence of $\frac{\Delta P_f}{\Delta P_{f,0}}$ (or the inverse dependence) in turbulent flow is hardly influenced by the relative roughness of the tube.*

In Fig. 6-13 the relationship between $\frac{\Delta P_f}{\Delta P_{f,0}}$ and ψ from the data on Table 6-4 is shown. The equation for the logarithmic straight line shown on the graph is

$$\frac{\Delta P_f}{\Delta P_{f,0}} = \frac{1}{(1-\psi)^{2.3}}. \quad (6-30)$$

It is interesting to note that this relationship is very close to Formula (6-7) which describes the corresponding relationship for a stream exhibiting laminar flow of the liquid phase. Consequently, the function

*As is known, roughness, in the case of laminar flow, does not influence the hydraulic characteristics of a stream flowing in a tube.

$$\frac{\Delta p}{\Delta p_0} = f(\eta) \quad (6-31)$$

is only slightly sensitive to the flow regime of the stream.

For a smooth tube the solution remains the same as for a rough tube; but the following quantity should be substituted for $30 \frac{D}{\epsilon}$ in the formulas

$$11.6 \frac{Dv}{\nu} = 4.05 Re \sqrt{\epsilon} \quad (6-32)$$

Thus, the hydrodynamic regime of a two-phase flow in a smooth pipe also depends on the effective Reynolds number of the liquid phase defined by Formula (6-21). The influence of the viscous sub-layer on the flow of the liquid phase in the immediate vicinity of the smooth surface is a physical factor governing the appearance of the Re' number as a determining parameter of the two-phase flow.

The relative velocity of the gas jet, calculated from Formula (6-10) for the distribution of velocities in a liquid ring according to (6-25), is

$$w_r = \frac{w_0}{\eta} - 2.5 w_0 \ln \left[1 + \frac{Re}{\eta} (1 - \sqrt{\eta}) \right] \quad (6-33)$$

Introducing this value into Formula (6-14) and noticing that

$$w = w_0 \sqrt{\frac{\epsilon}{D}} \quad (6-34)$$

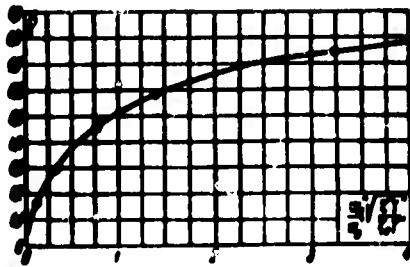


Figure 6-14. ψ as a function of $\frac{\dot{m}_1}{\dot{m}_0} \sqrt{\frac{\epsilon}{\epsilon_0} \frac{r}{r_0}}$ from theoretical calculations.

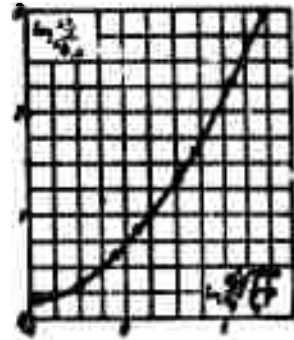


Figure 6-15. $\log \frac{\dot{m}_n}{\dot{m}_m}$ vs. $\log \frac{\dot{m}_1}{\dot{m}_0} \sqrt{\frac{\epsilon}{\epsilon_0} \frac{r}{r_0}}$.

we obtain for rough tubes:

$$\frac{\dot{m}_1}{\dot{m}_0} = \frac{\epsilon_0 r_0}{\epsilon r} \left[\frac{\dot{m}_1}{\dot{m}_0} - 2.5 \sqrt{\frac{\epsilon}{\epsilon_0}} \ln \left[1 + 15 \frac{D}{r} (1 - \sqrt{\epsilon}) \right] \right]^2. \quad (6-35)$$

Combining this expression with (6-30) and solving the obtained equation for $\frac{\dot{m}_0}{\dot{m}_1}$, we obtain:

$$\frac{\dot{m}_1}{\dot{m}_0} \sqrt{\frac{r}{r_0}} = \frac{\sqrt{\frac{\epsilon}{\epsilon_0}}}{(1 - \epsilon)^{1/4}} \times \left[\epsilon^{1/4} + 0.88 \sqrt{\frac{\epsilon r}{r_0}} \ln \left[1 + 15 \frac{D}{r} (1 - \sqrt{\epsilon}) \right] \right]. \quad (6-36)$$

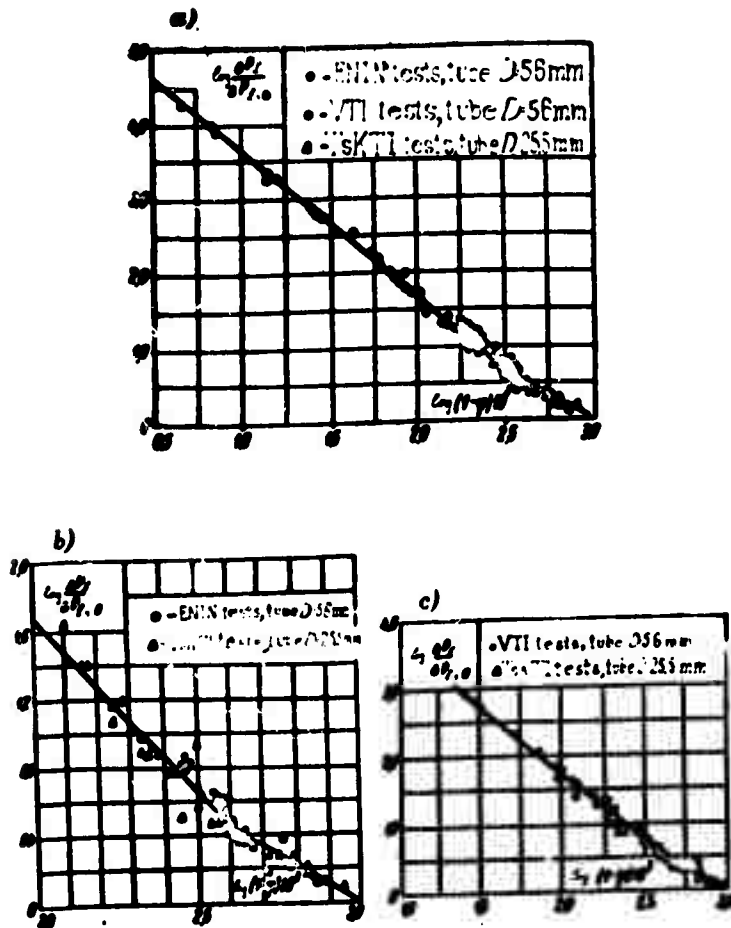


Figure 6-16. Variation in the ratio between resistance to flow of the vapor-water mixture and resistance to flow of the same mass flow rate of water, depending on the sine of the relative fractional of the cross section occupied by the liquid: (a) at a pressure of 32 to 35 atm. abs., (b) at a pressure of 60 to 64 atm. abs., (c) at a pressure of 90 to 110 atm. abs.

The structure of this formula, in relation to the influence of the criteria $\frac{v}{v_r} \sqrt{\frac{r}{r_r}}$ and $\frac{v}{v_r}$ on ψ , is analogous to the structure of Formula (6-16). The independent influence of $\frac{v}{v_r}$ begins to develop only at sufficiently great values of this criterion--i.e., only at

sufficiently high pressures in the gas-liquid mixtures.

In Figs. 6-14 and 6-15 the dependences of ψ and $\frac{\Delta p_f}{\Delta p_{f,0}}$ on the group $\frac{w_0''}{w_1''} \sqrt{\frac{\xi_0''}{\xi_0} \frac{\gamma''}{\gamma}}$ are plotted. They are calculated from (6-36) and (6-30) for such ratios $\frac{\gamma''}{\gamma}$ at which the second term in the brace may be disregarded.

Evidently, also, in turbulent flow of the liquid film, an abrupt increase in ψ is observed in the region of small $\frac{w_0''}{w_1''}$. In the region of values of $\frac{w_0''}{w_1''} \sqrt{\frac{\xi_0''}{\xi_0} \frac{\gamma''}{\gamma}}$ from 1 to 10, the quantity $\frac{\Delta p_f}{\Delta p_{f,0}}$ is proportional to a power of the order of 1.4 of this criterion, while the exponent increases with an increase in the argument.

In Fig. 6-16 the results of a considerable number of tests with steam-water mixtures are shown plotted on the system of coordinates of (6-31) by A. A. Armand. It is found that this function is clearly single-valued; at $\psi < 0.5$, the exponent in the formula of the type in (6-30) is ~ 1.2 ; while at $\psi > 0.5$ such an exponent is described satisfactorily by the formula

$$n = 1.9 + 2.5 \frac{\psi}{\gamma}. \quad (6-37)$$

Thus, the theoretical solution for the turbulent motion of a stream of mixture with an annular layer also generally leads to conclusions well supported by experimental data. This case emphasizes once again the fruitfulness of theoretical analysis, even of extremely abstract models of the studied physical phenomenon, and permits, at least qualitatively, clarification of the nature of the basic

interrelationships characterizing a given phenomenon. As has been pointed out before, in reference to flow in smooth tubes, the substitution into (6-29) of the quantity $11.6 \frac{\nu'}{\nu}$ for $\frac{\nu}{\nu_0}$ produces the Re' number as the determining criterion in the formula for turbulent flow of a liquid layer as well. However, in turbulent flow, the influence of this criterion develops substantially only in the region of small Re' numbers (of the order of 3,000 to 15,000). At large values of Re' , the influence of this criterion upon the values ΔP_f and $\frac{\Delta P_f}{\Delta P_{f,0}}$ is slightly perceptible. In Fig. 6-17 are given experimental data illustrating what was said above.

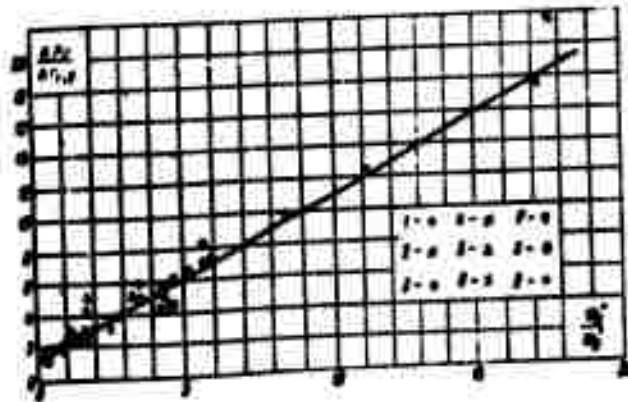


Figure 6-17. Dependence of the resistance of a two-phase flow in a smooth tube on the ratio $\frac{w_0''}{w_0}$ and on the Re criterion of a liquid.

Water: $\frac{\nu''}{\nu} = 1.3 \cdot 10^{-3}$; (1) $Re = 5,120$; (2)

$Re = 21,000$; (3) $Re = 32,400$; (4) $Re = 43,250$;
(5) $Re = 64,300$; (6) $Re = 90,500$;

Kerosene: $\frac{\nu''}{\nu} = 1.0 \cdot 10^{-3}$; (7) $Re = 18,100$; (8)

$Re = 30,200$; (9) $Re = 42,300$.

6-7. Certain Peculiarities of the Emulsion Flow Regime of a Gas-Liquid Mixture

As has been pointed out already, core regime arises in a stream with a sufficiently high fraction of gas. At average and small values of β and at large $\frac{\gamma''}{\gamma}$ the emulsion regime is characteristic of the flow of a gas-liquid mixture. As has been described in Section 6-2, when this regime occurs the gas is moving in the form of single bubbles of different sizes--filling up, more or less evenly, the entire volume of the entraining stream. However, in contrast to slug regimes, the dimensions of most of the bubbles are more or less the same, and are small in relation to the tube diameter.

Let us assume that the relative motion of these bubbles is determined by Formula (2-11). In this case ψ can be calculated from Formula (1-12) by substituting into it the values of w_r'' from (2-11). We obtain:

$$\psi = \frac{1}{2} \left[1 + \frac{1}{2} \sqrt{\frac{C_D}{C_D(r-r')}} \right] - \sqrt{\frac{1}{2} \left[1 + \frac{1}{2} \sqrt{\frac{C_D}{C_D(r-r')}} \right] - \frac{1}{2} \sqrt{\frac{C_D}{C_D(r-r')}}}} \quad (6-38)$$

here, C_D is the drag coefficient of a bubble in the shape of a flattened spheroid. In the given case, C_D is a certain effective value of the indicated coefficient, and depends to a certain degree on the totality of parameters determining the flow of the mixture in

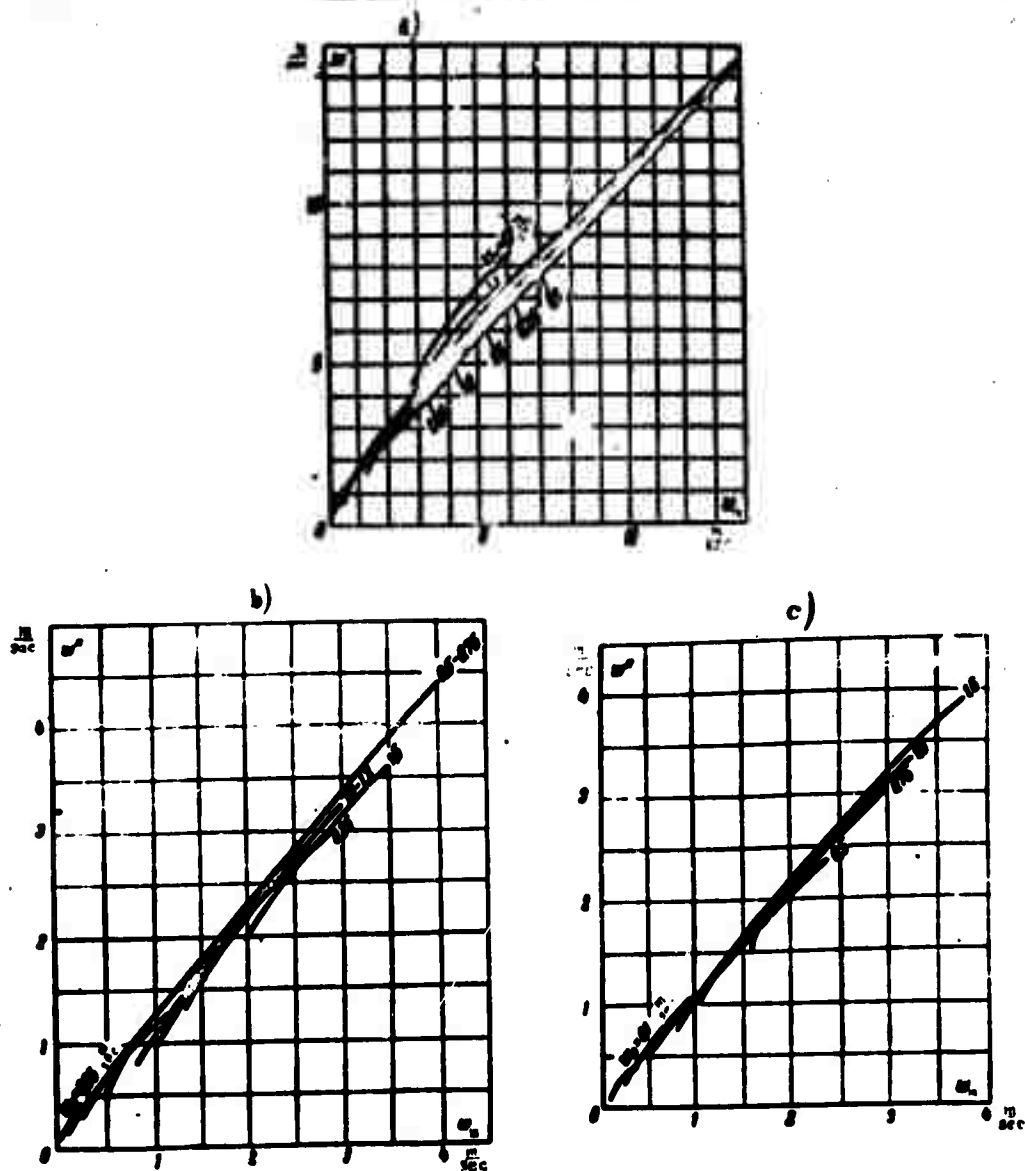


Figure 6-18. Average absolute velocity of steam vs. reference velocity of a steam-water mixture, according to averaged data for vertical tubes. Circulation velocity is the parameter: (a) $p = 11$ atm. abs.; (b) $p = 111$ atm. abs.; (c) $p = 181$ atm. abs.

Formula (6-38) shows that in the case of emulsion flow the value of ψ depends on a unique combination of the Froude and Weber criteria:

$$\psi = \sqrt{\frac{r^2}{\sigma(g-r)}} = \sqrt{\frac{\sigma}{\rho}} \sqrt{\frac{g-r}{r}} \cdot \frac{r}{r-r}. \quad (6-39)$$

for the flow fraction β of gas in the mixture and for the effective drag coefficient f of the bubbles.

Further, substituting into (1-11) the value $\frac{w}{r}$ from (2-11), we find that

$$\frac{\sigma}{\sigma_0} = 1 + \frac{1-f}{\alpha_m} \sqrt{\frac{\sigma_0(g-r)}{\sigma_0^2}}. \quad (6-40)$$

Introducing into (6-40) the value of ψ from (6-38), we obtain:

$$\frac{\sigma}{\sigma_0} = \frac{1}{2} \left[1 + \frac{1}{\alpha_m} \sqrt{\frac{\sigma_0(g-r)}{\sigma_0^2}} \right] + \sqrt{\frac{1}{4} \left[1 + \frac{1}{\alpha_m} \sqrt{\frac{\sigma_0(g-r)}{\sigma_0^2}} \right]^2 - \frac{1}{\alpha_m} \sqrt{\frac{\sigma_0(g-r)}{\sigma_0^2}}}. \quad (6-40a)$$

At large values of $\frac{w}{r}$, the quantity $\frac{1}{\alpha_m} \sqrt{\frac{\sigma_0(g-r)}{\sigma_0^2}}$ is substantially less than unity, i.e., under these conditions the absolute velocity of the gas phase in the emulsion flow of the mixture is almost a single-valued function of the group (6-39).

G. Ye. Kholodovskiy pointed out that, within a wide range of values of the flow parameters of a gas-liquid mixture, the quantity

w'' is almost a single-valued function of w_m .

In Fig. 6-18 are shown some experimental data illustrating the above treatment of this problem by us. At the same time, these data confirm the fact that within a given range of the values of β and $\frac{\gamma'}{\gamma}$, the quantity w_m has the most substantial influence on the absolute velocity of the gas.

6-8. Head Losses Due to Friction in a Quasi-Homogeneous Mixture

Let us examine the flow of a quasihomogeneous mixture. The relative velocity of the phases equals zero, and the formula for the pressure losses due to friction can be written analogically to the corresponding working formula for homogeneous stream:

$$-\frac{dw}{dx} = K \frac{\rho_m w^2}{2gD} \quad (6-41)$$

in which ψ is a certain function of the criteria (6-23).

$$\text{At } w_r'' = 0$$

$$\left. \begin{aligned} \psi &= \frac{w_0^2}{w_0^2 + w_1^2} : w_m = \frac{w_0^2}{\psi} = \frac{w_0^2}{1 - \psi} = w_0^2 + w_1^2 \\ L &= \frac{1 \cdot w_0^2 + 1 \cdot w_1^2}{w_0^2 + w_1^2} = \frac{1 \cdot w_0^2}{w_0^2} \end{aligned} \right\} \quad (6-42)$$

Substituting these values of w_m and γ_m into (6-41), we obtain the formula

$$-\frac{dw}{dx} = K \frac{\rho_m w^2}{2gD} \left[1 + \left(1 - \frac{\gamma}{\gamma'} \right) \frac{w_0^2}{w_m^2} \right] \quad (6-43)$$

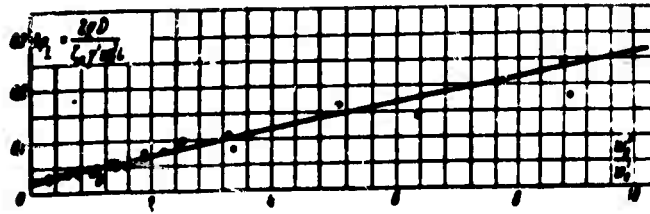


Figure 6-19. $\Delta p_f = \frac{2gD}{C_f u_m^2 L}$ vs. $\frac{w_0''}{w_0'}$ from experiments with a steam-water mixture at $p = 62$ atm. abs.

Comparison of the theoretical calculations and experimental data presented in the foregoing paragraphs shows that the pertinent relationships between the basic hydraulic characteristics of the stream are relatively insensitive to the flow regime of the mixture. This permits anticipating that the coefficient ψ in Formula (6-43) is of the order of unity. In fact, the experimental data presented in Fig. 6-19 confirm this significant conclusion. This fact permits the use of (6-43) as a convenient working formula.

6-9. Head Losses Due to Acceleration of the Mixture

Head loss due to acceleration is equal to the difference between the momenta of the per-second flow rate of the gas-liquid mixture in two given cross sections:

$$\Delta p_{acc} = \left[\frac{\dot{w}_0^2}{g} \cdot \frac{\psi + (1-\psi) \frac{\dot{w}_0^2}{\dot{w}_0'^2}}{\psi - 1} \right]_2 - \left[\frac{\dot{w}_0^2}{g} \cdot \frac{\psi + (1-\psi) \frac{\dot{w}_0^2}{\dot{w}_0'^2}}{\psi - 1} \right]_1. \quad (6-44)$$

Usually, this loss is substantial only in steam-generating tubes, and there only at a comparatively low pressure and for a large heat flux when, in a short section of tube, the steam fraction in the mixture increases sharply.

When we refer to the boiling point, and the relative velocity of steam is disregarded, it follows from (6-44) that:

$$\Delta p_{acc} = \frac{\gamma}{g} \left(1 - \frac{\gamma''}{\gamma}\right) w_{rel}^2 \quad (6-45)$$

At low and medium pressures ($\frac{\gamma''}{\gamma} < 0.05$), the relative velocity of steam reduces losses calculated from Formula (6-45) by approximately 50%. At $\frac{\gamma''}{\gamma} > 0.1$, calculations by this formula become sufficiently accurate. However, the quantity Δp_{acc} itself is usually much less than Δp_f in this case.

6-10. Head Losses in Vertical and Inclined Tubes. For Design Purposes

In vertical and inclined tubes, the pressure drop per unit of tube length is determined by the sum

$$\Delta p = \Delta p_f + \Delta p_{acc} + \gamma_m \cos \alpha, \quad (6-46)$$

where α is the inclination angle of the tube axis from the vertical.

In this case, as a consequence of the disturbance in the symmetry of the stream, the density of the mixture proper γ_m appears

also as a certain, generally rather weak, function of α .

Extensive investigations of the motion of gas-liquid and vapor-liquid mixtures in vertical tubes have been carried out at the TsKTI [Central Scientific Research Institute for Boilers and Turbines], the VTI [All-Union Heat Engineering Institute (im. F. Dzerzhinskiy)], the ENIN [Institute of Power Engineering (im. G. M. Krzhizhanovskiy)], and other organizations. On the basis of these data, design graphs were plotted at the TsKTI in order to calculate the approximate magnitude of ψ . The approximate nature of this quantity is due to the fact that frictional losses were calculated by processing the experimental data by means of Formula (6-43).

In Figs. 6-20 to 6-25 are presented nomograms permitting determination of ψ for design purposes.

In these nomograms

$$\psi = \frac{0.5}{\gamma} \sqrt{\frac{r}{\gamma}}; F = \frac{0.5}{\gamma} \sqrt{\frac{r}{D(r-\gamma)}}.$$

For the steam-water mixture, the pressure p in the tube, rather than the ratio $\frac{\gamma''}{\gamma}$, has been plotted.

Nomogram I is intended for vertical tubes. When the tube is inclined 5° from the vertical, the same value of ψ is used as for vertical tubes. Nomograms II to VI are used for designing tubes inclined by more than 5° from the vertical.

By means of the formulas and graphs given above, the designs can be carried out for two-phase flows in individual tubes as well as in circulation loops. The latter have a series of essential features,

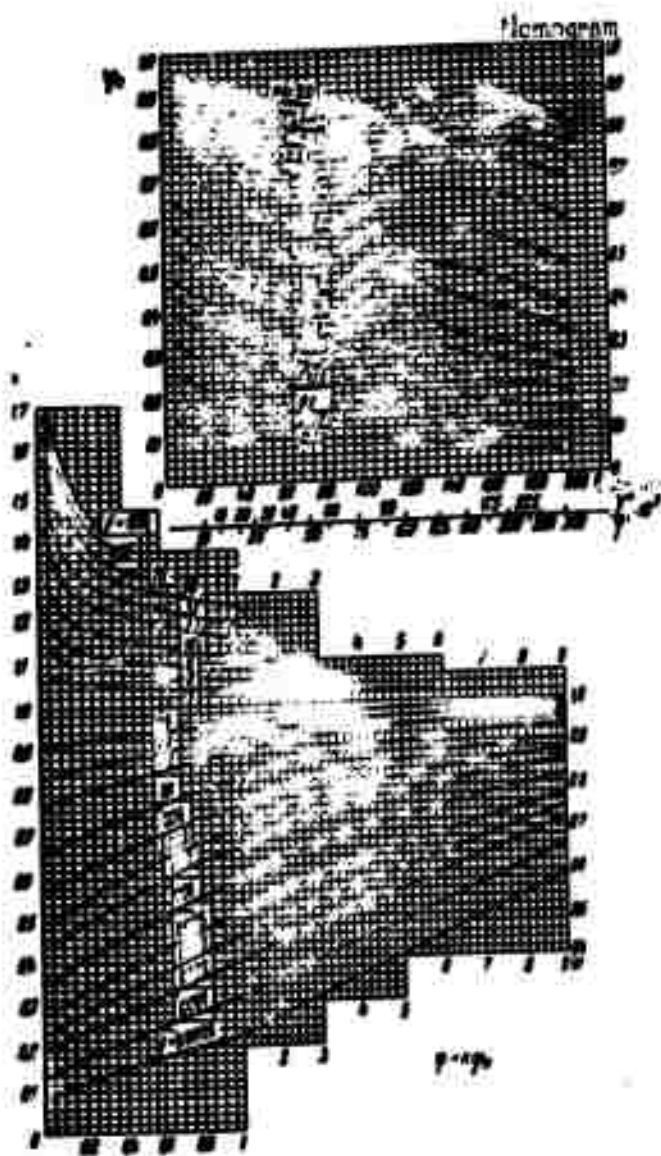


Figure 6-20. Nomogram I.

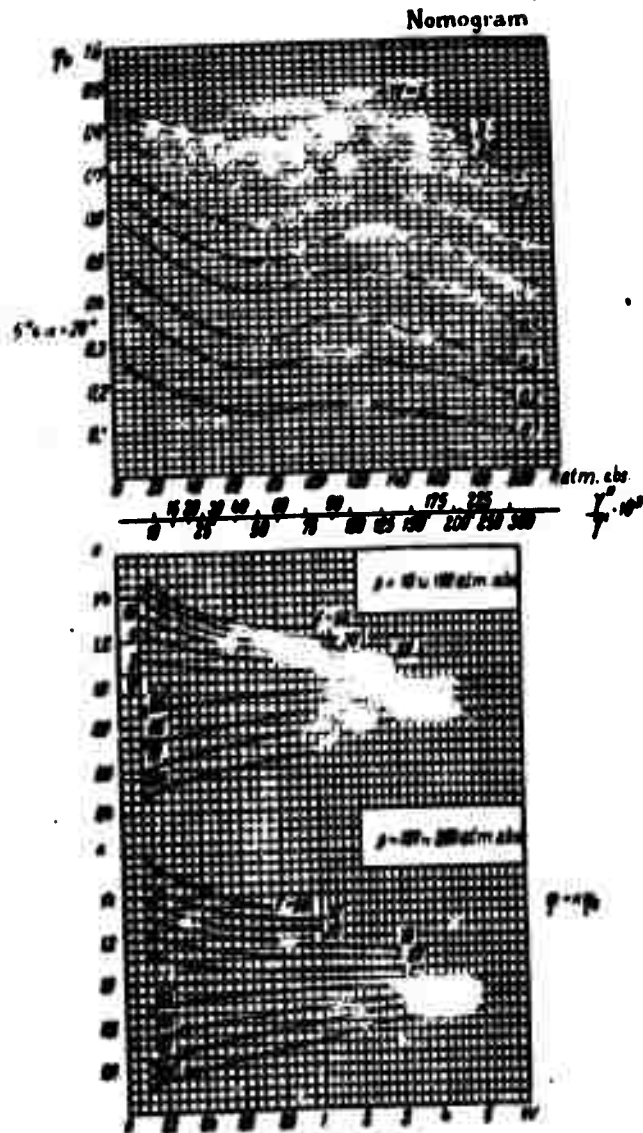


Figure 6-21. Nomogram II.

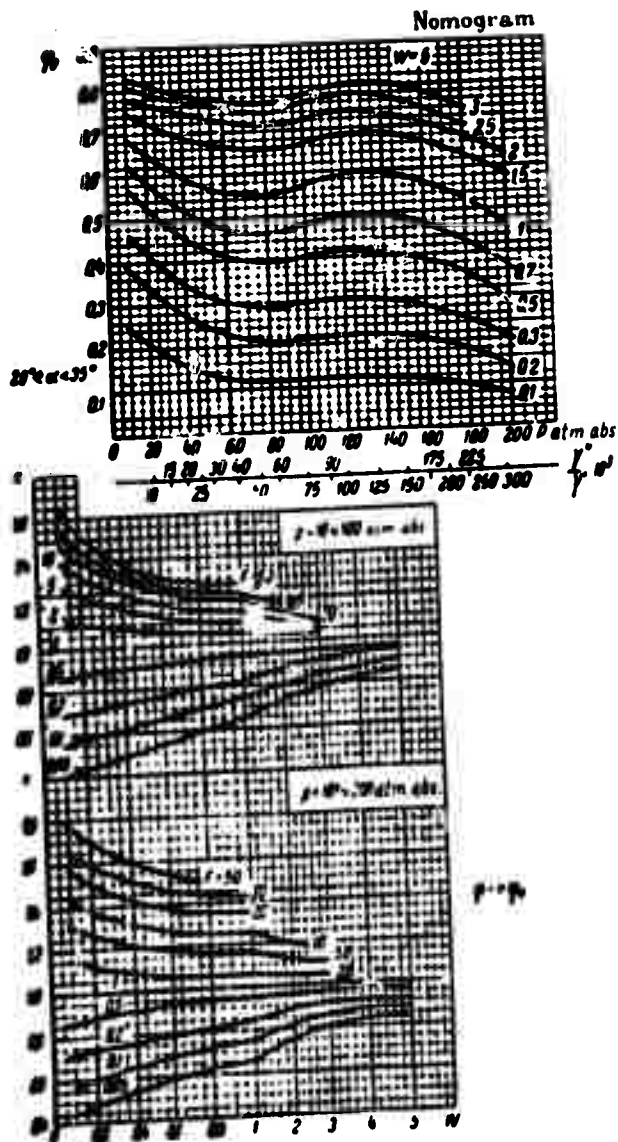


Figure C-22. Nomogram III.

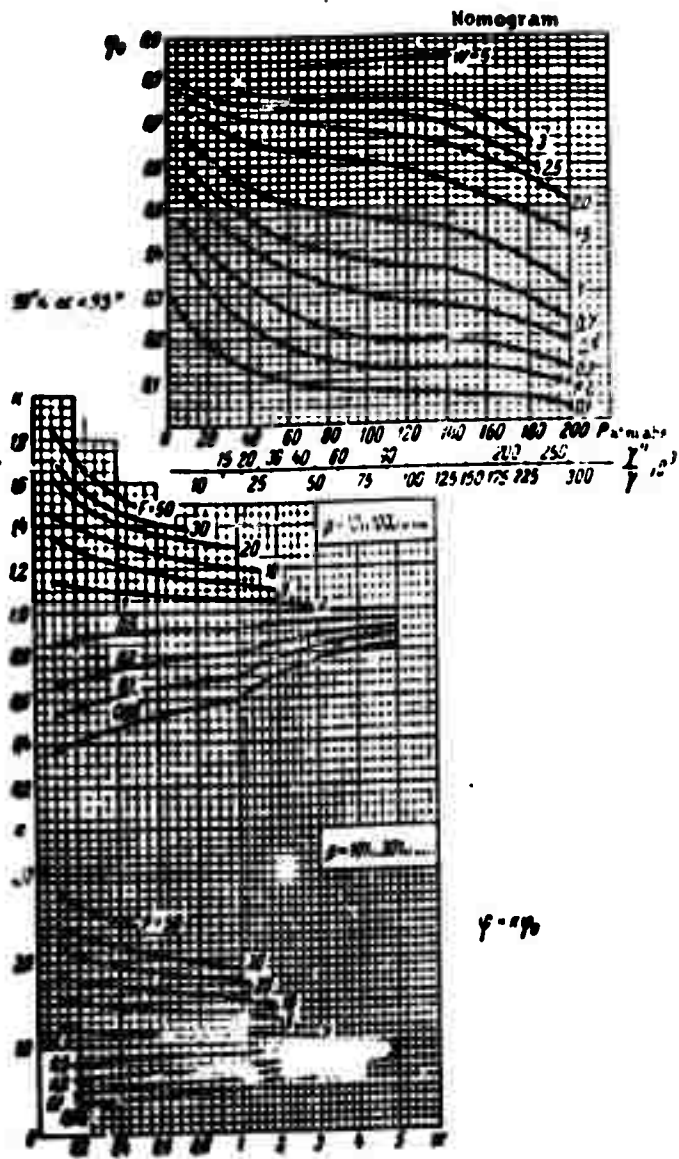


Figure 6-24. Nomogram V.

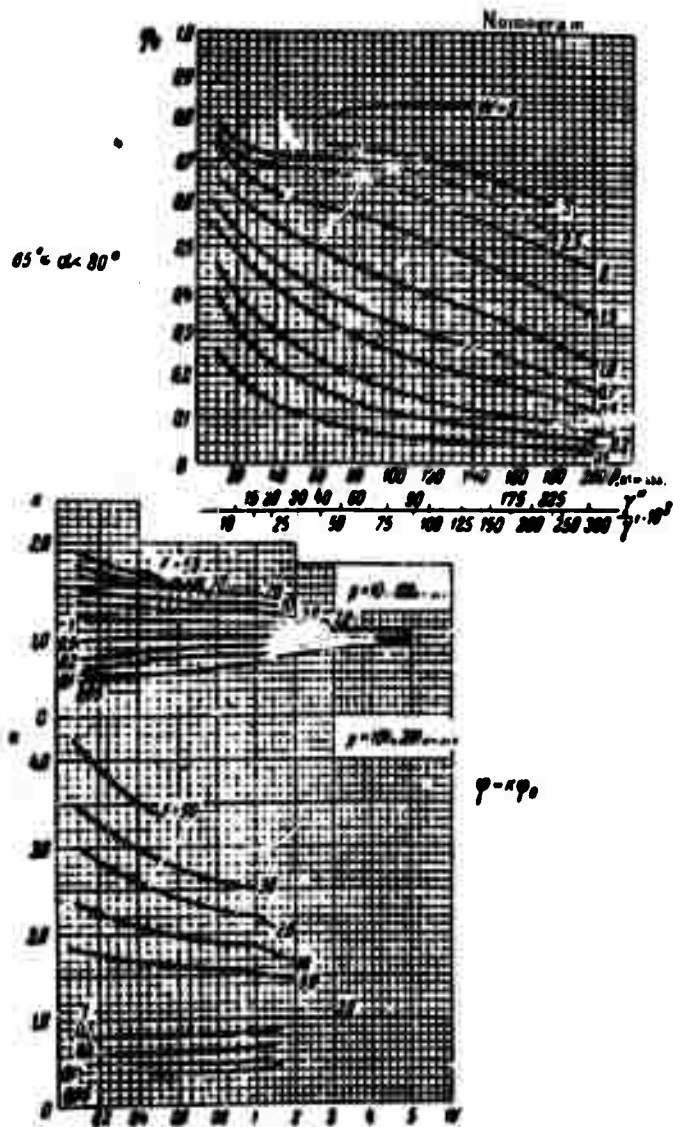


Figure C-25. Nomogram VI.

which are discussed in great detail in the design specifications for circulation in steam boilers.

6-11. Local Drags

The motion of a gas-liquid mixture in a conduit with various bends, constrictions, etc. (local resistances), as well as in collectors, has not been thoroughly studied so far. Some data have been obtained at the TsKTI by S. I. Mochan and I. O. Zamaziy. I. O. Zamaziy conducted experiments with an air-water mixture flowing through a sharp-edged orifice. As a result of these experiments it was ascertained that in practice the orifice drag coefficient can be determined analogously to the resistance of a tube, by means of the formula

$$\zeta = \zeta \left[1 + \left(1 - \frac{r}{r_0} \right) \frac{w_0}{w} \right]; \quad (6-47)$$

here the overall resistance is referred to the head, calculated from the velocity of circulation, i.e.,

$$\Delta p = \zeta \frac{\rho w^2}{2}. \quad (6-48)$$

Figure 6-26 gives the results of experiments by S. I. Mochan determining the overall drag coefficient for the discharge of an air-water mixture from the tube. The great bulk of the experimental points, on the average, is also described by a formula of the same type

as (6-47), namely:

$$C_{disch} = 1.2 \left[1 + \left(1 - \frac{v}{V} \right) \frac{v_0}{v} \right]. \quad (6-49)$$

The experimental points falling outside the line pertain to such small velocities that, for them, the absolute value of Δp_{disch} is negligibly small.

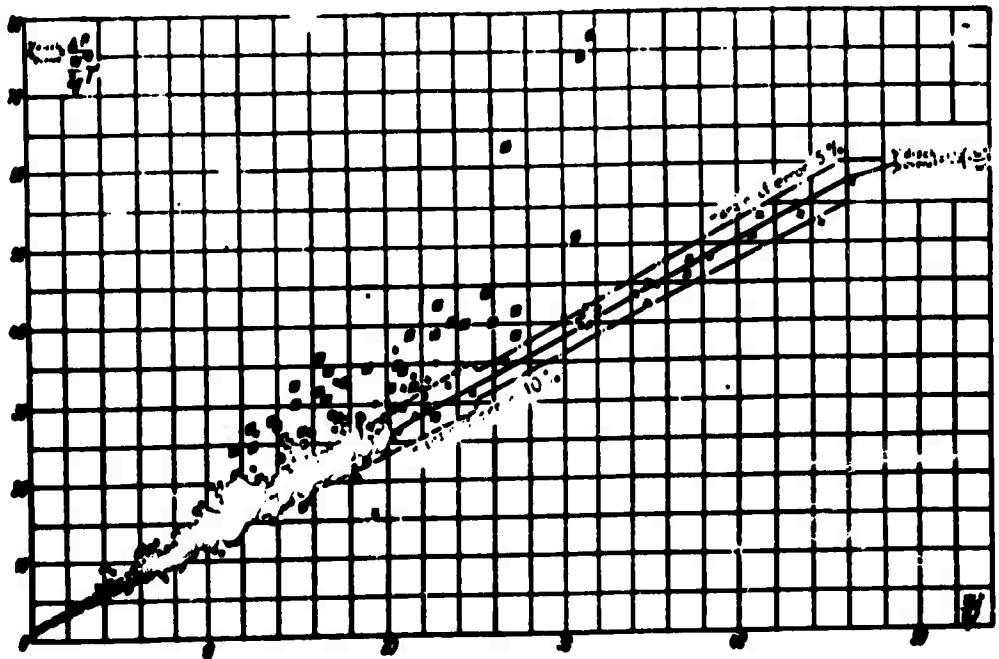


Figure 6-26. Dependence of the overall drag coefficient for discharge on the flow fraction of air and the velocity of water.

The flow pattern associated with the drag which develops when a mixture enters a tube is much more complex. In this case, the perturbing effect of the entrance is felt along a considerable length

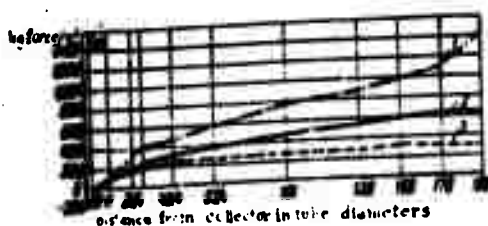


Figure 6-27. Excess pressure drop in the tube section behind the collector caused by the perturbations of the two-phase flow at the entrance of the tube.

Air-water mixture: $p \approx 1 \text{ atm.}$

$$\text{abs.; } \frac{w_0^2}{w_0} = 10; (1) \frac{w_0^2}{D} = 16.2 \text{ m/sec}^2; (2) \frac{w_0^2}{D} = 7.6 \text{ m/sec}^2; (3) \frac{w_0^2}{D} = 4.3 \text{ m/sec}^2.$$

of the pipe (up to 60 to 100 diameters); i.e., the increasing complexity of the hydrodynamics of the two-phase stream is manifested along the length of the input section of the pipe, in addition to the pressure loss due to the last drag itself.

The above-described pattern is clearly revealed by the experimental data given in Fig. 6-27.

At the present time, this problem is still explored very little.

For the time being, S. I. Mochan's design graphs given in Fig. 6-28

can be recommended for tentative estimates. In this graph, the approximate velocity head, as the abscissa, is determined from the formula

$$A = \frac{2}{3} r \left[1 + \frac{2}{3} \left(1 - \frac{r}{r} \right) \right]. \quad (6-50)$$

Figure 6-29 gives graphs for determining the ratio $\frac{h_p}{h_{p,r}}$, where $h_{p,r}$ is the velocity head, and includes the relative velocity according to the formula

$$A_{p,r} = \left(\frac{w_0^2}{2g} + \frac{w_0^2}{2g(1-\phi)} \right) \left(\frac{1}{1-\phi} \right) \quad (6-50a)$$

Experimental drag-coefficient data for a 75° bend for different lengths of tube sections joined behind the bend, are given in

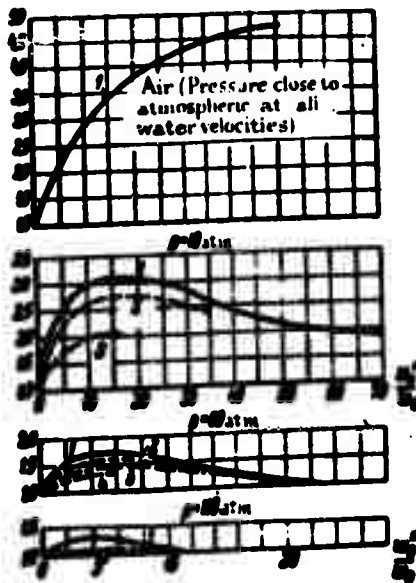


Figure 6-29. Graphs for determining the ratio $\frac{h_p}{h_{p,r}}$

h_p : from Formula (6-50);

$h_{p,r}$: velocity head, accounting for the relative velocity from Formula (6-50a)

- (1) $\frac{w_0^2}{2g} = 1 \text{ m/sec}^2$; (2) 5 m/sec^2 ; (3) 20 m/sec^2 ; (4) 50 m/sec^2 .

Fig. 6-30. Analysis of experimental data suggests that we may assume drag coefficients of bends followed by vertical or inclined pipe sections to be six to seven times higher than the drag coefficients of identical bends under single-phase flow; when the bend is followed by a horizontal pipe section, the suggested drag coefficients are equal to the single-phase flow drag coefficient.

Thus, experiments reveal that local resistances have a greater effect in two-phase flow than in homogeneous flow. This circumstance is explained by the substantial influence of local resistance on phase distribution along the cross section of the stream and, hence, also on the

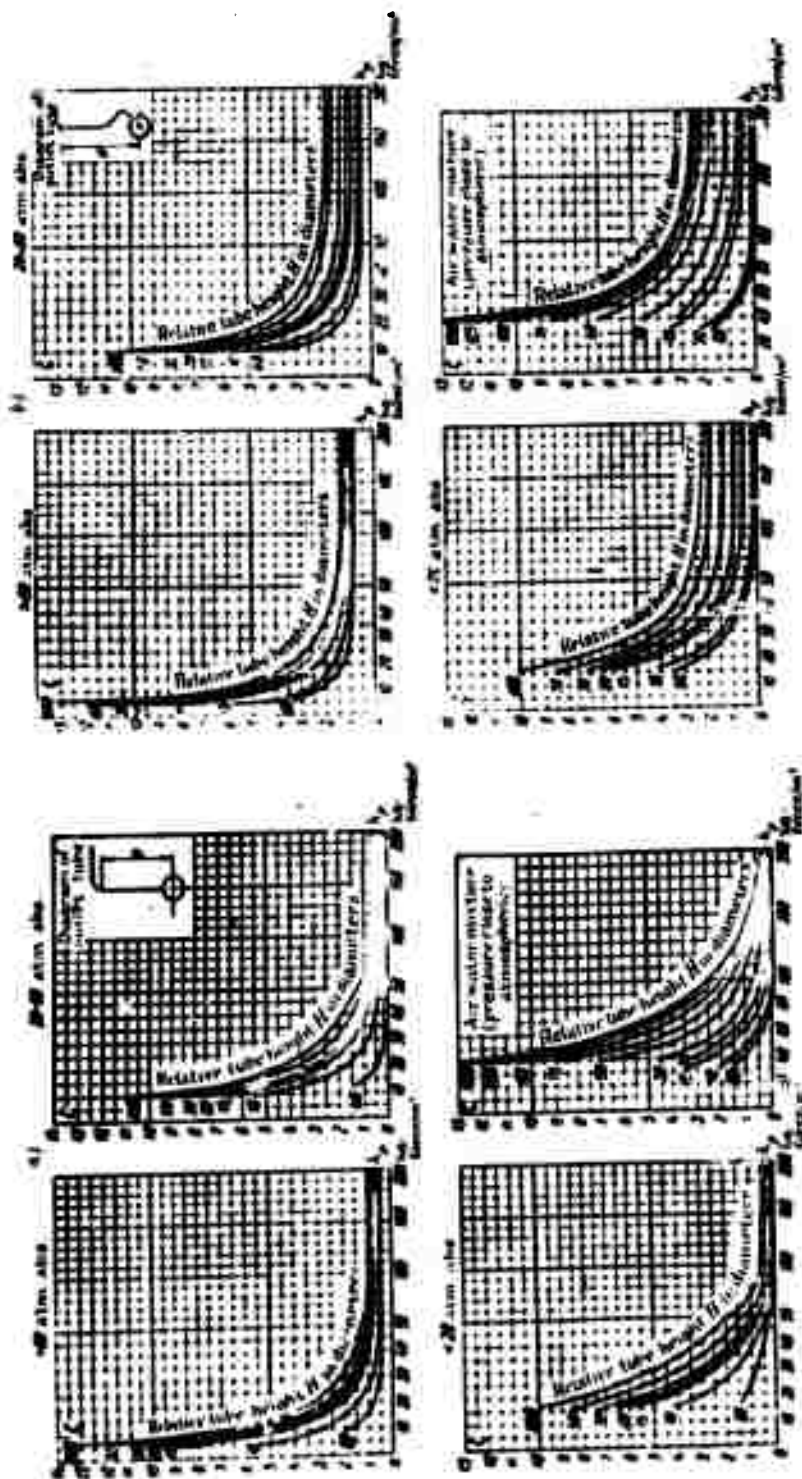


Figure 6-2. Design graphs for determining the drain coefficient at entry into the tube from collector: a - for straight outlet tubes; b - for outlet tubes with elbows.

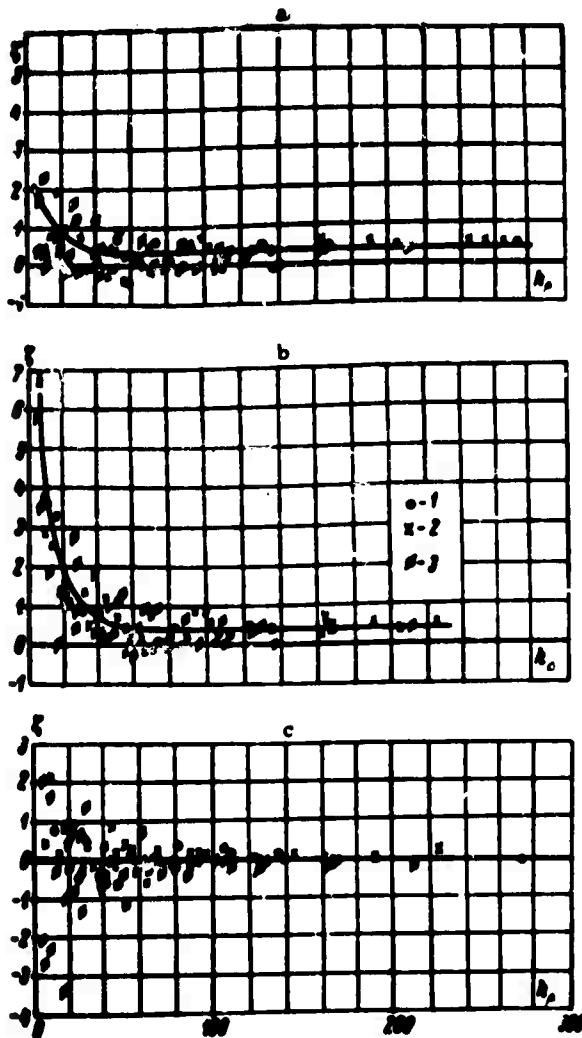


Figure 1-30. Experimental data on drag coefficient of a 75° bend with different lengths of inclined tube section joined behind the bend: (a) length of section following bend: 25 diameters (b) same: 59 diameters; (c) additional drag coefficient of a section of $L = 50$ diameters, 109 diameters away from a 75° bend. (1) $p = 10$ atm. abs.; (2) $p = 30$ and 60 atm. abs. (3) $p > 60$ atm. abs.

hydrodynamic regime of the mixture along a considerable length of the tube following the local resistance.

The phase distribution along the cross section exerts a strong influence on size of the cross-sectional fraction φ occupied by the gas. Therefore, in the sections of the tube located beyond the local resistance, a considerable change (increase) in the specific gravity γ_m of the mixture is observed. If these sections are vertical, or inclined substantially from the horizontal, then to the change in head loss due to friction is added the change in the weight of the column of mixture, the latter circumstance usually turning out to be far more significant than the change in frictional loss.

6-12. Formation of Vortexes during Free Discharge into a Tube

In Fig. 6-31 a diagram is shown of the free discharge of a liquid into a tube. Under certain conditions, a vortex forms above the tube inlet. When the cone of the vortex reaches the inlet orifice both the liquid and the gas bubbles drawn in with the stream from the vortex will enter the tube. Usually an intake of gas or steam into the down tube is undesirable.

The formation and development of a vortex generally depends on the same fundamental criteria as those for the two-phase flows examined earlier.

That height (h_{cr}) of the liquid layer above the down tube at which the top of the vortex cone reaches the inlet orifice may be selected as the parameter to be determined.

When there is a stationary gas layer above the liquid layer, friction at the phase boundary may be disregarded. Moreover, since

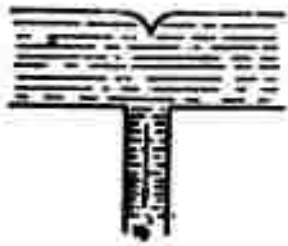


Figure 6-31. Diagram of free discharge of liquid into a tube.

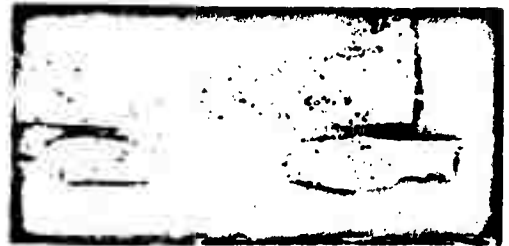


Figure 6-32. Vortex when the liquid approach is symmetrical.

only the formation of a vortex with a continuous boundary separating the liquid and the gas is studied, the influence of surface tension is likewise immaterial.

The force of gravity, acting on the liquid stream forming a vortex, is proportional to the difference in the densities of the phases, and the equation of motion can be written in the following form:

$$\vec{g}(\rho' - \rho) - \text{grad } p + \rho' \vec{v}^2 \vec{e}' = \rho' \frac{D\vec{v}'}{dt}. \quad (6-51)$$

Among the conditions uniquely defining the solution of this problem are:

- (a) the diameter D of the discharge orifice and the geometric configuration of liquid approach;
- (b) the velocity w_0' of liquid discharge through the down pipe; and
- (c) the physical constants entering Equation (6-51).

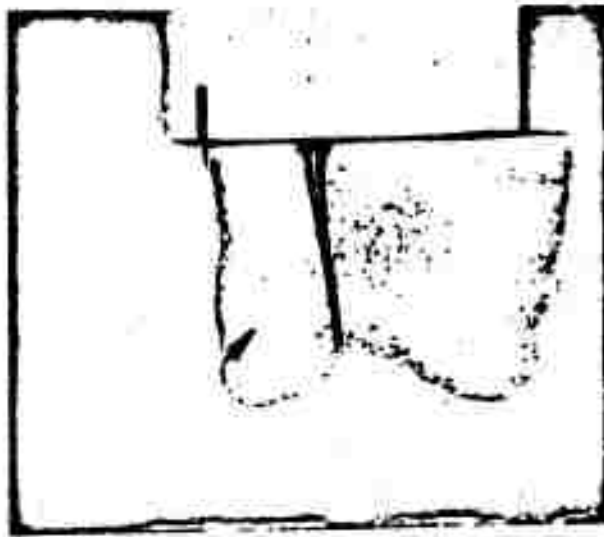


Figure 6-33. Vortex when the liquid approach is asymmetrical.

Under these conditions it follows from Equation (6-51), that at a given configuration of the liquid approach to the tube

$$\frac{h_r}{D} = f\left(\frac{u_0^2 r'}{g D (r' - r)}; \frac{g D}{u_0^2} \cdot \frac{r' - r}{r'}\right). \quad (6-52)$$

In a turbulent liquid flow, the influence of molecular viscosity can be disregarded.

Figures 6-32 and 6-33 show photographs, obtained by O. M. Baldina and Ts. M. Baytina, of the vortex above the down tube in a symmetrical liquid approach and in a unilateral approach, and with a baffle plate in front of the tube.

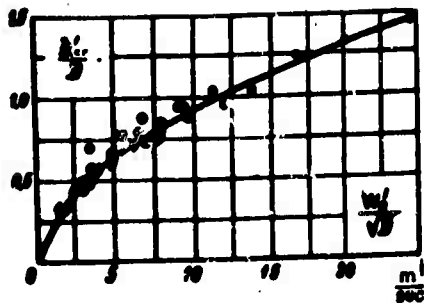


Figure 6-34. Dependence of $\frac{h'}{D}$ on $\frac{w'}{D}$ and D in a symmetrical free discharge.

Figure 6-34 shows experimental data by the same authors for the symmetrical approach of liquid to the down tube. A curve, drawn through these points, is described by the formula

$$\frac{h'}{D} = 0.25 \left(w' \sqrt{\frac{r'}{D(r' - r)}} \right)^{0.5} \quad (6-5)$$

CHAPTER SEVEN

HYDRODYNAMIC THEORY OF CRITICAL CHANGES IN HEAT
TRANSFER DURING BOILING ON HEATING SURFACES

7-1. Two Fundamental Regimes of Boiling

The process of vaporization in a liquid mass is called boiling. Two types of boiling on a heating surface are known: nucleate boiling and film boiling. In nucleate boiling, bubbles of vapor form at different points on the heating surfaces (at vaporization nuclei). At the same time, most of the heating surface is wetted with liquid mixing with released vapor bubbles. As a consequence of this, the rate of heat transfer to the liquid is extremely high. In film boiling, vapor forms a layer separating the heating surface from the liquid mass. Large bubbles are released from the surface of this layer as they go into the mass of the liquid phase.

Because of low thermal conductivity of the vapor layer, the rate of heat transfer in film boiling is many times less than in nucleate boiling. The appearance of one or the other type of boiling is determined by the magnitude of the density of heat flux from the heating surface.

The conditions for transition from one regime (type) of boiling to the other, and the ranges of these regimes, are clearly revealed when we plot the dependence of the heat-transfer coefficient on the

heat-flux density or on the difference between the temperature of the heating surface and the saturation temperature.

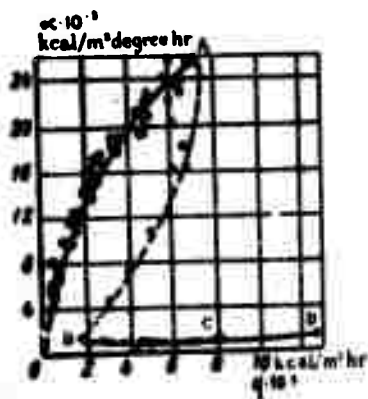


Figure 7-1. Heat-transfer coefficient vs. heat-flux density, boiling of a large volume of water ($p = 1$ atm. abs.).

Figure 7-1 shows a typical relationship between the heat-transfer coefficient and the heat-flux density q at a heating surface submerged in a large volume of boiling liquid. The abruptly rising left-hand segment of the curve expresses the law of heat transfer for nucleate boiling. The lower curve expresses the law of heat transfer for film boiling. Line AB corresponds to the transition regime.

Regardless of the process of heat transfer in the boiling liquid (electric heating, radiation, etc.), as a gradually increasing heat flux reaches point A nucleate boiling is suddenly converted into film boiling (line AC). At the same time, heat transfer decreases $1/20$ to $1/30$ of its original value and, correspondingly, the temperature of the heating surface rises sharply.

With further increase in the heat flux, a stabilization of film boiling takes place.

Figure 7-2 shows photographs of metal tubes destroyed because of a sudden decline in heat transfer at those points where a layer of vapor forms as a regime of film boiling sets in, while Fig. 7-3 shows photographs of a red-hot heating surface enveloped in a dense layer of steam, as film boiling of the water takes place.

Return to nucleate boiling occurs at a heat flux considerably smaller than that at which the regime of nucleate boiling changes to a film-boiling regime. In Fig. 7-1, point B corresponds to this reverse transition.

Thus, the thermal and hydrodynamic phenomena associated with the transition from one regime of boiling to the other undergo a certain hysteresis. We must speak of two critical heat-flux densities: first, that at which transition from the nucleate to the film regime takes place, and second, that at which the vapor layer is destroyed.

In the region of heat-flux densities lying between points A and B either regime of boiling may exist, or the two may even coexist on the very same heating surface over a long period of time.

In a number of cases, when heat flux builds up slowly, it is possible to prolong the critical conditions, maintaining nucleate boiling and its correspondingly high rate of heat transfer up to values of q exceeding the normal critical values by a factor of 1.5 to 2.

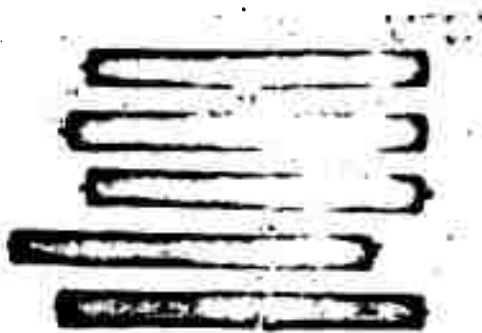


Figure 7-1. Destruction of metal tubes at points where film boiling occurred.



Figure 7-2. Photograph of a red-hot heating surface, film boiling of water under steady conditions.

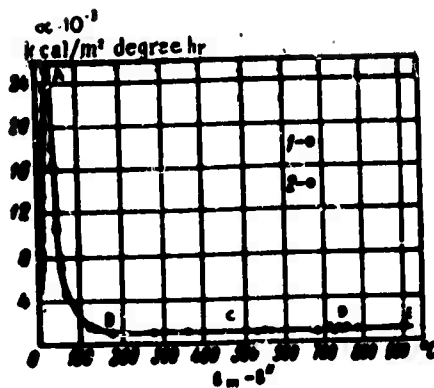


Fig. 7-4. α vs. Δt for boiling water at $p = 1$ atm. abs. (1) electric heating; (2) steam heating.

When the temperature of the heating surface t_w is independently assigned (as when the heating surface is steam-heated), the transition from nucleate to film boiling proceeds somewhat differently. As the maximum heat transfer is reached [point A in Fig. 7-1 and in Fig. 7-4 where the data have been re-

processed in the form of the relation $\alpha = f(\Delta t)$, a further increase in Δt will begin to lower the coefficient of heat transfer gradually, while simultaneously lowering the heat-flux density. Point D corresponds to the establishment of film boiling. With a further increase in the heating-surface temperature, the rate of heat transfer changes slowly.

7-2. The Hydrodynamic Nature of Critical Changes in the Liquid Boiling Mechanism

As explained above there are two fundamental regimes of boiling: nucleate boiling, where steam is generated in the form of discrete bubbles at some points along the heating surface; and film boiling, where the heating surface is separated from the liquid mass by a continuous layer of vapor.

The transition from one regime of boiling to the other has all the features of a critical phenomenon and is accompanied by a rad-

ical change in the hydrodynamic and thermal conditions of the process of heating-surface cooling.

The examined problem is also complicated by the fact that in the boiling mechanism not one but two critical changes take place: first, formation of a continuous film of vapor on the heating surface, and, second, the disintegration of the vapor film and restoration of the regime of nucleate boiling.

At the same time, the heat-flux density during the first critical change is substantially greater than during the second.

Although, with values of q about 0.6 to 0.8 $q_{cr,1}$, the heat-transfer coefficient for nucleate boiling increases substantially with an increase in heat-flux density, in the near-critical region the value of α remains constant. This phenomenon can be explained by the fact that when the regime is nearly critical, the vapor saturation of the two-phase boundary layer at the heating surface is so great that a further increase in the rate of vaporization will increase turbulence in the liquid phase on the one hand and, on the other, will promote expulsion of the liquid phase from the boundary region.

Within a certain range of values of q these two opposite processes to some extent compensate for each other, as a result of which the heat-transfer coefficient remains more or less constant. Finally, however, the stability of the liquid films which cut through the two-phase boundary layer will be completely upset, and the liquid phase will become separated from the heating surface by a continuous layer of vapor.

Thus, a film-boiling regime results from breakdown of the stable two-phase boundary layer which exists in the nucleate boiling regime

prior to this change.

In exactly the same manner, the two-phase boundary layer, which consists of a vapor film on the heating surface and of a liquid mass surrounding it, can exist only as long as the kinetic energy of the vapor flowing in this film is sufficient to keep in suspension the masses of liquid which strive, because of the effect of gravity, to break down the vapor layer at the heating surface.

The hydrodynamic theory of critical changes in the mechanism of boiling on a heating surface was developed by S. S. Kutateladze, and explains well the most essential points of this process.

7-3. Derivation of a Formula for the First Critical Heat-Flux Density for Natural Convection of a Boiling Liquid (First Critical Change in the Regime of Boiling)

The hydrodynamic regime of a two-phase boundary layer can be described by the equations for the motion and the mechanical interaction of the flows in the two phases; i.e., by Equations (1-16) and (1-17), written for a liquid and a vapor; and Equations (1-21), (1-23) and (1-29). Consequently, the system of equations in (5-1) will also fully describe the hydrodynamics of a boiling boundary layer.

Analyzing this system for basic equations, we assume that:

(1) in the near-critical regime, the liquid and vapor are agitated to such an extent by the process of intensive vaporization that molecular friction can be disregarded;

(2) the liquid-phase velocity is substantially lower than the average vapor velocity near the heating surface because of the frictional effect of the heating surface.

With these assumptions, the fundamental system of equations, written in terms of averaged values, takes the form:

$$\left. \begin{aligned} \bar{\rho}' - \text{grad } \bar{p}' + \bar{T} - \rho' \frac{\partial \bar{u}'}{\partial t}; \\ \text{div } \bar{u}' = 0; \\ \bar{g}(\bar{u}' - \bar{r}) - \text{grad } \bar{p}' + \bar{T} - \rho' \frac{\partial \bar{u}'}{\partial t}; \\ \text{div } \bar{u}' = 0; \\ \rho'(\bar{u}'_i \bar{u}'_k) - \rho'(\bar{u}'_i \bar{u}'_k); \\ \bar{u}'_i - \bar{u}'_i = 0; \end{aligned} \right\} \quad (7-1)$$

here \bar{T} stands for turbulent friction, analogous to the term expressing molecular friction;

\bar{u}'_i, \bar{u}'_k are fluctuating velocity components.

The examination of the conditions affecting distribution of vaporization nuclei in the given case may be dispensed with since, in a near-critical regime, the number of active nuclei is so great that the liquid films cutting through the two-phase boundary layer may disintegrate at any point on the heating surface between any neighboring active nuclei. The system of equations in (7-1) gives the following primary criteria for similarity:

$$\left\{ \frac{\bar{u}'^2}{\bar{g}}; \frac{\bar{g} \bar{u}'^2}{\bar{r} \bar{u}'^2}; \frac{\bar{u}'^2}{l}; \frac{\bar{g} \bar{u}'^2}{\bar{r} \bar{u}'^2}; \frac{\bar{u}'^2 \bar{r}}{\bar{g}(\bar{r}' - \bar{r})}; \frac{\bar{u}'^2}{l}; \frac{\bar{g} \bar{u}'^2}{\bar{r} \bar{u}'^2} \right\}. \quad (7-2)$$

Substituting

$$\frac{\bar{g} \bar{u}'^2}{\bar{r} \bar{u}'^2} \cdot \frac{\bar{r}}{\bar{g} \bar{r}(\bar{r}' - \bar{r})} = \frac{\bar{r}}{(\bar{r}' - \bar{r}) l}.$$

we obtain a system of criteria equivalent to (7-2):

$$\left(\frac{w}{u} : \frac{w^2}{u^2 - v^2} : \frac{v}{u - v} : \frac{w^2}{u^2} : \frac{v}{u} : \frac{w}{u} : \frac{v}{u} \right). \quad (7-3)$$

These are the same criteria obtained above for an inviscid dynamic layer. Such a coincidence is by no means accidental; the boiling boundary layer differs from the dynamic layer examined in Chapter 5 only in the mode of light-phase generation. Under conditions of free convection of the liquid, the velocity of its motion and the pressure drops are determined only by the vaporization process--i.e., these quantities are not among the conditions uniquely defining a system. Neither is the time factor among the conditions uniquely defining the solution of this problem, since it is not the duration of the transition from one regime of boiling to the other that is being studied, but rather the heat-flux density at which this transition occurs spontaneously. In such an event, the criteria containing the quantities w , Δp , and τ are non-determining.

The velocity of motion of one of the phases is related to the heat-flux density by Equation (1-35). Writing the latter in the form

$$q = \tau w. \quad (7-4)$$

we get the criterion

$$\frac{q}{\tau w}. \quad (7-5)$$

local values of heat flux densities at phase boundaries are related to the average density of the heat flux through the heating surface by the expression

$$\bar{q} = \frac{1}{F_{\Sigma}} \int_0^{\Delta t} \left(\int_{\Sigma} q_n dF \right) dt. \quad (7-6)$$

where F is the area of the heating surface;

F_{Σ} is the total area of the interfaces in the examined region.

The time interval over which this averaging is performed is selected so that the following condition be fulfilled:

$$\Delta t \gg \frac{1}{u},$$

where u is the frequency of vapor bubble formation. The true vapor velocities are related to the heat-flux density on the heating surface by the equation

$$\bar{q} \Delta t = \gamma \int_0^{\Delta t} \left(\int_{\Sigma} u_n dF \right) dt + \int_0^{\Delta t} \left(\int_{\Sigma} q_{2,n} dF \right) dt. \quad (7-7)$$

where F is a control surface passing through the liquid at a certain distance from the heating surface and equivalent to the latter;

u_n is the component, normal to the surface F , of the vapor velocity vector;

$q_{2,n}$ is heat flux through the ion control surface due to heat conduction averaged convection currents in the liquid phase.

Hence, the averaged velocity of the vapor in the given cross section is

$$\bar{u}_v = \frac{1}{\Delta t} \int_0^{\Delta t} \left(\int_{\Sigma} u_n dF \right) dt = \frac{\bar{q}}{\gamma} \left(1 - \frac{\bar{q}_{2,n}}{\bar{q}} \right). \quad (7-8)$$

In similar systems, the heat-flux fields are similar, i.e.,

$$\frac{\bar{q}}{q} = \text{const.}$$

and, consequently,

$$\bar{w} \sim \frac{q}{\eta}.$$

The quantity $\frac{q}{\eta}$ will be called velocity of vaporization and represents the volumetric flow rate of vapor per unit area of heating surface.

On substitution of the averaged value of the steam velocity (which is proportional to the rate of vaporization) for the actual velocity in the similarity criteria, similarity is assured by the equality of the averaged criteria and by the similarity of the hydrodynamic conditions in the vicinity of the heating surface as a consequence of the equiprobability of distribution of the vaporizing nuclei over the heating surface.

Hereafter, we will omit the bar above the quantity q in the averaged criterion (7-5).

The magnitude of the critical heat-flux density in free convection, according to (7-3), is determined only by the physical characteristics of the liquid and the linear dimensions of the system, i.e., the group

$$\frac{q_{cr}}{\eta^2 w_{cr}} \sqrt{\frac{w_{cr}^2 l}{g(\eta' - \eta)}} = \frac{q_{cr}}{\eta \sqrt{g l^3 (\eta' - \eta)}} \quad (7-9)$$

is the determinable criterion, which is a single-valued function of the determining criterion

$$\frac{\dot{q}_{cr}}{(r-r')^{n_1}} \quad (7-10)$$

With a sufficiently large heating surface, when instability is equally probable on any part of the two-phase boundary layer, the magnitude of \dot{q}_{cr} need not depend on the linear dimension \underline{l} of the system.

A very large horizontal disk, with its heating surface turned up, provides an ideal model fully satisfying this condition.

In such a case, the functional relation between Criteria (7-9) and (7-10) should be such that the quantities entering into them will cancel each other out. The following combination of criteria corresponds to this condition

$$\frac{\dot{q}_{cr,1}}{\sqrt{g(r-r')}} \sqrt{\frac{(r-r')^{n_1}}{g}} = \frac{\dot{q}_{cr,1}}{g \sqrt{(r-r')}} \quad (7-11)$$

here, $\dot{q}_{cr,1}$ is the unknown critical heat-flux density at which nucleate boiling is converted into film boiling.

Since no determining criterion remains in System (7-3) after this operation, then for natural convection and a process independent of the dimensions of the heating surface the solution of the system

of equations under study for the first critical heat-flux density will take the form

$$\frac{q_{cr,1}}{\sqrt{g r^*} \sqrt{V \cdot (r^* - r)}} = k_1 = \text{const.} \quad (7-12)$$

Formula (7-12) shows that the transition in two-phase boundary layer takes place at a specific ratio of the kinetic energy of the stream of vapor to the force of gravity.

In reality, the following quantity is the scale of the kinetic energy of the vapor stream at the heating surface

$$\left(\frac{q}{r^*}\right)^2 \frac{r^*}{g}.$$

The following quantity is the scale of the force of gravity acting on elements of the fluid between the bubbles resting on the heating surface:

$$(r^* - r) \sqrt{\frac{g}{r^* - r}}.$$

The square root of the ratio of these quantities gives us Criterion (7-11). Thus this criterion, because of its physical nature, is

identical to Criterion (5-7).

If we take into account the influence of the viscosity of the liquid phase then, retaining the viscosity term in the equation for the motion of the liquid phase and reasoning as above, we will arrive at the conclusion that with natural convection of the liquid and the nondependence of the process on the dimensions of the heating surface, a relationship having the nature of a criterion must exist in the following form:

$$k = f \left[\frac{\nu}{g} \left(\frac{r - r_0}{r} \right)^3 \right]. \quad (7-13)$$

With small values for the group in the right member of this formula, when the influence of viscosity on the value of q_{cr} can be disregarded, we have a limiting case expressed by Formula (7-12).

In Table 7-1 average values of group k_1 are given from data obtained in a series of experiments.

Some discrepancies in the absolute values from different experiments can be explained by certain differences in the experimental methods and in the condition of the heating surface as well as by the effect of the viscosity of the liquid.

Figure 7-5 shows the relationship between the first critical heat-flux density and pressure, for boiling water, calculated from Formula (7-12) with $k_1 = 0.10$. On the same graph are plotted the results of Ye. A. Kazakova's experiments with disks.

In this graph the maximum critical heat-flux density is clearly within the range of pressures of the order of 70 to 100 atm. abs. Since the critical pressure for water is 225 atm. abs., the maximum

Table 7-1

$$\text{Values of Group } A_1 = \frac{q_{\text{sat}}}{\sqrt{g \cdot \rho \cdot \Delta \rho \cdot (1 - \gamma)}}.$$

Calculated from Experience by Various Authors

Boiling liquid	Heating surface	Method of heating	Limits of variation of saturation pressure,	k_1	Author
Water	Nichrome, wire	By electricity	1-115	0.17	Kazakova
"	Graphite, smooth disks	"	1-30	0.15	Kutateladze
"	Graphite, rough disks	"	1-24	0.19	"
"	Chromel, wire	"	1-8	0.17	Farber and Seorah
"	Nickel, wire	"	1-8	0.15	"
"	Chrome-plated copper tube	Condensing steam	0.1-1	0.14	Braunlich
"	Nickel-plated copper tube	"	0.15-1	0.13	Akin and McAdams
Benzene	Chrome-plated copper, disk	External electric heating	1-41	0.16	Cicchelli and Bonilla
Alcohol	"	"	1-51	0.16	"
Propane	"	"	19-33	0.17	"
Pentane	"	"	2-29	0.19	"
Heptane	"	"	1-15	0.18	"

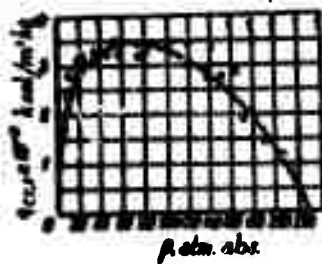


Figure 7-5. Relationship between the first critical heat-flux density and pressure, boiling water. The curve computed from formula, at $k_1 = 0.14$; the points from Ye. A. Kazakova's experiments with disks.

q_{cr} in the given case corresponds to a pressure of the order of (0.3 to 0.4) p_{cr} . In the vacuum range and in the range of near-critical pressures, the critical heat-flux density in the boiling liquid vanishes.

Figure 7-6 shows the relation (7-13) as plotted by V. M. Borishanskii from data of experiments with various liquids.



Figure 7-6. Relation (7-13) from experimental data.

From these data, one can assume that

$$A_1 = 0.13 + 4 \frac{\sqrt{p}}{p^{0.1}} \left(\frac{p - p_{cr}}{p_{cr}} \right)^{0.2} \quad (7-14)$$

7-4. Effect of the Condition of the Heating Surface and
of the Method of Heating on the Quantity q_{cr}

In some experiments a rougher heating-surface increased the critical heat-flux density; this apparently is associated with a greater stability of the liquid films when they adhere to a rough surface.

The orientation of the heating surface is also important in relation to the direction of the gravity vector--namely, for a horizontally-positioned disk the value q_{cr} is less than for the same disk placed on edge. This is explained by the fact that on the lower part of the horizontal disk large vapor bubbles accumulate, facilitating the formation of a continuous vapor layer.

During boiling in a horizontal tube, heated from within by the condensing steam, the values of the first critical heat-flux density also prove to be markedly lower than during boiling in tubes heated by an electric current. Thus, in experiments by Akin and McAdams $q_{cr,1}$ proved to be equal to $600,000 \text{ kcal/m}^2 \text{ hr}$ for water boiling at atmospheric pressure in a copper tube of $D = 13 \text{ mm}$, while for a horizontal plate and electrically heated cylinders, the corresponding $q_{cr,1}$ is more than $1,000,000 \text{ kcal/m}^2 \text{ hr}$.

This substantial deviation is associated not only with some binding of the vapor bubbles in the lower part of the tube, but also with a substantial non-uniformity of the heat flux around the circumference of the horizontal tube when vapor condenses in it. This non-uniformity is explained by a flooding of the lower part of the tube with condensate as a result of which local heat-flux densities in the upper half of the

tube can attain and even exceed the true critical densities at a relatively low average heat-flux density.

These circumstances were investigated experimentally in some detail by M. A. Styrikovich and G. M. Polyakov. In particular, this investigation confirmed the conclusion arrived at theoretically that a horizontal plate with its heating surface turned upward should be used as a standard for comparison.

7-5. Transition From the Film-Boiling Regime to the Bubble-Boiling Regime (Second Critical Change in the Boiling Regime)

Figure 7-7 shows a diagram of film boiling in a liquid on a horizontal cylindrical heating-surface placed in a large volume of boiling liquid. Figure 7-8 shows a photograph of film boiling.

With heat-flux densities substantially higher than the second critical heat-flux density $q_{cr,2}$, the flow of the layer is stable and the phase boundary appears well-defined.

As the heat flux decreases, the boundary separating liquid from vapor begins to pulsate. At heat-flux densities close to $q_{cr,2}$, the vapor layer takes on an irregular shape and oscillates vigorously. It is evident that the stability of this layer substantially decreases.

The second critical change (end of film boiling) is expressed by the ultimate disintegration of the vapor layer and the establishment on the heating surface of a pattern characteristic of normal nucleate boiling.

The hydrodynamic situation above the vapor layer (i.e., in the



Figure 7-7. Diagram of film boiling in a liquid.

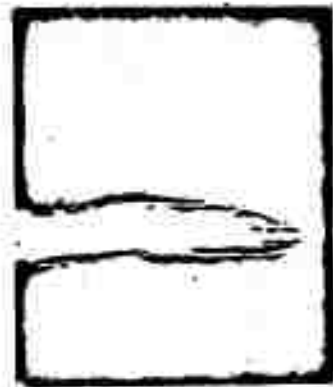


Figure 7-3. Photograph of film boiling.

area filled with the mixture of bubbles swept away from this layer and the liquid bulk) is determined by the system of equations given in Section 7-3.

By adding the equation of the motion of vapor in a continuous layer, we obtain a system of equations describing the motion of the two-phase boundary layer in film boiling.

If we assume that at the instant of the critical change, owing to the pulsations originating in the vapor layer, the inertial forces in the latter are substantially greater than the forces of molecular friction, then the equation of motion of an uninterrupted layer of vapor will have the same form as in the system of Equations (7-1); i.e., this system is also applicable to the instant of the second critical change in the mechanism of boiling. At the same time, the last equation of the System (7-1) is applicable, but only as a fair approximation, and in the present case indicates that the

liquid flow velocity at the boundary of the vapor film is small compared to the average vapor velocity.

At moderate pressures ($\gamma' \gg \gamma''$) and with natural convection in the liquid, the introduction of such simplification of the problem appears to be entirely permissible when the liquid motion is fully controlled by the motion of the vapor.

Consequently, the integral of this system of equations with respect to the second critical heat-flux density, under conditions of natural convection of the liquid and nondependence of the process on the dimensions of the heating surface, also has a form identical to the Formula (7-12). Besides this, owing to the difference in the original structure of the two-phase boundary layer, the value of the constant k_2 will differ from the value of k_1 . Thus, inasmuch as the quantities k_1 and k_2 are constant, between the first and the second critical heat-flux densities in the given liquid a constant ratio applies, determined by the condition

$$\frac{q_{cr,2}}{q_{cr,1}} = \frac{k_2}{k_1} = \text{const.} \quad (7-15)$$

In film boiling, the interface (and consequently also the free energy of the two-phase boundary layer), are smaller than in nucleate boiling. Therefore, if the rate of vaporization is sufficient for uniform feeding of an existing vapor layer, the latter is more stable than the two-phase boundary layer in nucleate boiling.

The result of this is the experimentally revealed fact that film boiling once developed, may continue at heat-flux densities smaller than $q_{cr,1}$. Thus, $q_{cr,1}$, $q_{cr,2}$, and the constant in Formula

(7-15), is less than unity.

In Fig. 7-9, data of experiments by V. M. Borishanskiy and S. S. Kutateladze on the boiling of iso-octane are plotted in the coordinates ($q_{cr,2}$, p); in these experiments, both the first and the second critical heat-flux densities were measured on the same heating surface. These experiments cover values of $\frac{p}{p_{cr}}$ up to 0.6; i.e., both the region where the critical heat-flux density increases with pressure, and the region where it decreases at critical pressure is approached.

By comparing the two curves, it can be established that the constancy of the ratio $\frac{q_{cr,2}}{q_{cr,1}}$ demanded by the theory is generally preserved within the whole range of pressures investigated.

According to existing experimental data, the constant in Formula (7-15), for conditions of natural convection in the liquid, is of the order of 0.17 to 0.22.

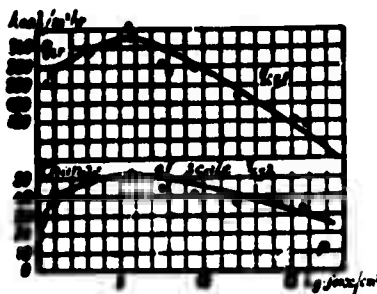


Figure 7-9. Effect of pressure on $q_{cr,1}$ and $q_{cr,2}$ in free convection, from experiments with iso-octane.

7-6. Effect of a Subcooled Liquid (i.e., Below Saturation Temperature) on the Critical Heat-Flux Density

Let us isolate, by means of an arbitrary bounded control surface F , a region (of volume V) of the vapor-liquid mixture.

Inside this isolated region let discrete volumes of vapor and liquid be arbitrarily distributed, and let their number, their distribution, and the quantity of material bounded in the volumes change with time.

The quantity of heat brought into the examined region is the sum of the change in the heat content of the vapor and of the liquid which have passed through surface F , and of the heat which has flowed into the examined volume by conduction. Thus, the heat balance over volume V of the vapor-liquid mixture during the time interval $\Delta t \gg \frac{1}{u}$, where u is the frequency of passage of vapor bubbles through the surface F , can be written in the form of the following integral equation:

$$\begin{aligned} & \int_V \left(\int_V i' \omega' dF \right) dt + \int_V \left(\int_V c' i' \omega' dF \right) dt + \\ & + \int_V \left(\int_V \lambda \frac{\partial t'}{\partial n} dF \right) dt - \int_V \left(\int_V \frac{\partial}{\partial t} [(1-\tau) c' i' t' + \tau i' t'] dV \right) dt \end{aligned} \quad (7-16)$$

here $i'' = \underline{i} + \underline{c''}$, is the heat content of the vapor;

t' is the temperature of the liquid;

$\frac{\partial t'}{\partial n}$ is the temperature gradient;

$\frac{t'}{n}$ is the temperature gradient;
 w_n^l, w_n^v respectively are the components, normal to the surface,
 of the instantaneous velocities for the two phases;
 ϕ is the instantaneous volumetric fraction of vapor in
 Region V .

Given steady-state conditions and a heat transfer by conduction,
 negligible as compared to the transfer by convection, Equation (7-16)
 takes the form:

$$\int_V \left(\int_S t' w_n^l dF \right) dt = - \int_V \left(\int_S t' w_n^v dF \right) dt. \quad (7-17)$$

When the temperature of the liquid phase in the examined region
 is less than saturation temperature ($t' > t''$), the heat content of
 the liquid stream passing through this region increases due to heat
 transfer from the vapor; i.e., the second term of Equation (7-17) is,
 in this case, positive. Correspondingly, the first term of this
 equation becomes negative.

The physical constants of vapor, and time, are essentially
 positive, and therefore the quantity $\int_S w_n^v dF$ is negative; i.e., in
 this case the quantity of flowing vapor decreases due to condensa-
 tion in Region V .

At $t' < t''$, the reverse effect occurs; i.e., an increase in the
 quantity of vapor takes place as it passes through the region of
 superheated liquid.

When vapor bubbles (swept away from the heating surface in nu-
 cleate boiling, or from the vapor layer in film boiling) rise, liquid

flows in to fill the volume left by the bubbles. As a consequence of the resulting internal circulation in the liquid, part of it shifts from the core of the stream toward the boiling boundary layer.

If the liquid is fed from the core of the stream which is below the saturation temperature, then in the region of the boiling boundary layer, a process of vapor condensation takes place, affecting the structure of this layer.

It may be assumed that the peculiarities brought into the structure of the boiling boundary layer by intrusion of cold masses of liquid from the core of the stream are determined by the change in fraction of vapor in this region due to vapor condensation.

In that case, the corresponding determining criterion can be obtained from the balance equation (7-16), written over the region where the examined process takes place. This equation gives the following criteria of similarity:

$$\left[\frac{\rho' u'}{\rho'' u''}; \frac{\lambda'}{\rho' u' l}; \frac{u'}{l} \right]. \quad (7-18)$$

In well-developed turbulent flow $\lambda \sim \rho u l$, and the second criterion can also be omitted from the analysis. The criterion $\frac{u'}{l}$ is retained in the fundamental system of criteris (7-3).

Thus, Equation (7-16) introduces only one additional criterion $\frac{\rho' u'}{\rho'' u''}$ to the system (7-3). In addition, quantity Δt should stand for the degrees of subcooling of the liquid below the boiling point; i.e., into this criterion should be introduced the quantity $\theta = t'' - t'$, where t' is the mean temperature in the core of the liquid flow.

In the examined case we extend the system of equations (7-1)

to the region of two-phase flow beyond the immediate vicinity of the heating surface. In such an area the ascent velocity of the vapor and the velocity of the entrained liquid can be high enough to exclude the possibility of the vanishing of w_b . With such a more general formulation of the problem, the last equation of System (7-1) gives the simplex $\frac{w}{w_b}$. As a result, the final system of the criteria of similarity reduces to the form:

$$\left\{ \frac{w^2}{g(t-t')^3}, \frac{t}{(t-t')^2}, \frac{t}{t_0}, \frac{t'}{t}, \frac{w}{g}, \frac{w'}{t}, \frac{g t_0}{t^2} \right\} \quad (7-19)$$

where, under conditions of natural convection, the last three of these criteria are nondetermining.

By introducing into the first of these criteria the heat-flux density according to (7-4), and considering only the process independent of the linear dimension of the system, we arrive at the criterional relation:

$$\frac{q_w}{\sqrt{g t'} \sqrt{t(t-t')}} = \Phi \left(\frac{t}{t_0}, \frac{t'}{t} \right). \quad (7-20)$$

Taking into consideration that with $\Phi = 0$ the condition (7-12) applies, we can give Relation (7-20) the following form:

$$\frac{q_w}{\sqrt{g t'} \sqrt{t(t-t')}} = h \left[1 + f \left(\frac{t}{t_0}, \frac{t'}{t} \right) \right]. \quad (7-21)$$

We can visualize more specifically the form of the function f by proceeding from the following considerations.

In order for a vapor film to form in a liquid, the great bulk of which is subcooled (at a temperature below saturation), it is necessary to transfer through the heating surface a quantity of heat not less than that required for giving rise to the critical rate of vaporization in the saturated liquid and for preheating up to saturation temperature the liquid mass drawn into the boundary region from the cold core of the flow.

The quantity of liquid drawn into the boundary region from the core, when the latter is not subcooled, is

$$Q = \gamma' \frac{q_w}{\rho'} (1 - \alpha) \quad (7-22)$$

where α is the coefficient of recirculation of the saturated liquid in the boundary region.

This refers to that part of the liquid which fills the volume left by swept-away bubbles, and which does not come from the subcooled core, but is displaced from adjacent points in the boundary region as other bubbles are formed.

Assuming that when the degree of subcooling of the liquid is small the quantity Q' remains unchanged, we can write:

$$q_{cr, \theta} = q_{cr, 0} \left[1 + (1 - \alpha) \frac{\theta}{T_s} \right]$$

(7-23)

here $q_{cr, \theta}$ is critical heat-flux density in the liquid whose core is subcooled;

$q_{cr, 0}$ is the same in a liquid fully at the saturation temperature, other conditions being equal.

From the latter formula it follows that:

(1) q_{cr} increases with an increase in the subcooling of the liquid (below saturation temperature). This increase in the critical heat-flux density is determined by the additional heat which must be spent for preheating the cold masses of liquid brought into the boundary layer by circulation. As a first approximation, q_{cr} is a linear function of θ to the extent to which the coefficient of recirculation is constant at a given pressure;

(2) the relative effect of the subcooling of the liquid on the critical heat-flux density decreases with an increase in pressure. This circumstance is explained by the fact that an increase in pressure increases the density γ'' of the vapor, and decreases, correspondingly, the number and dimensions of the bubbles swept away from the surface of the vapor film. In its turn, the decrease in the volume of the vapor bubbles lessens the quantity of cold liquid drawn into circulation in the vicinity of the heating surface, and consequently the amount of heat required for preheating this liquid to saturation temperature lessens;

(3) the proportionality factor in the group $\frac{\rho' \gamma' \theta}{\rho \gamma}$ is less than unity.

7-7. Some Experimental Data on the Effect of a Subcooled (Below Saturation Temperature) Liquid on the First Critical Heat-Flux Density

In deriving Formula (7-23), it was assumed that the coefficient of recirculation did not depend on the liquid temperature. In this case, according to (7-21), the quantity $(1 - \bar{n})$ is a function only of the relative density of vapor $\frac{\gamma''}{\gamma'}$.

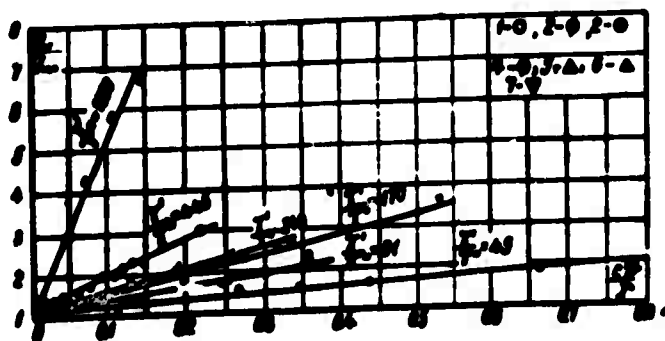


Figure 7-10. Relative change in q_{cr} during boiling in the subcooled liquid with natural convection.
 Alcohol: (1) $p = 1$ atm. abs.; (2) $p = 2$ atm. abs.;
 (3) $p = 5$ atm. abs.; (4) $p = 10$ atm. abs.;
 Water: (5) $p = 1$ atm. abs. (6) $p = 5$ atm. abs.;
 Iso-octane: (7) $p = 1$ atm. abs.

Introducing this dependence into (7-23), we obtain:

$$\frac{q_{cr,0}}{q_{cr,1}} = 1 + f_1 \left(\frac{\gamma'}{\gamma} \right)^{\frac{c_1}{r}}. \quad (7-24)$$

In Fig. 7-10 the experimental data on $q_{cr,1}$ for alcohol, water, and iso-octane with natural convection are plotted on the coordinates of Formula (7-24).

The quantity $\frac{\gamma'}{\gamma}$ is taken as a parameter. From these data it may be seen quite clearly that:

(1) as a first approximation, the linear relationship between q_{cr} and $\frac{c_1}{r}$ quite clearly stands up:

(2) the effect of the group $\frac{c_1}{r}$ decreases with an increase in the relative density of the vapor, or, which is the same, with a decrease in the relative density of the liquid $\frac{\gamma'}{\gamma}$.

Thus, experiment has confirmed these theoretical deductions, which are by no means evident at a glance.

The experimental data given in Fig. 7-10 are described by the formula

$$\frac{q_{cr,0}}{q_{cr,1}} = 1 + 0.085 \left(\frac{\gamma'}{\gamma} \right)^{\frac{c_1}{r}}. \quad (7-25)$$

The derivation of Formula (7-23) is not tied to any consideration of the magnitude of $q_{cr,0}$, i.e., to the presence or absence of a forced flow of the liquid. Therefore, the fundamental conclusions on the character of this relationship are of general value.

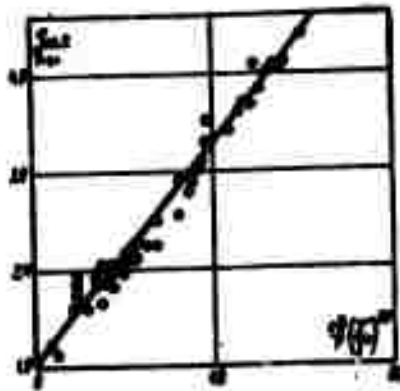


Figure 7-11. Effect of subcooling on the critical heat-flux density $q_{cr, 1}$ for water flow in annular spaces ($p < 22$ atm. abs.).

Figure 7-11 shows V. S. Chirkin's experimental data on the system of coordinates of (7-25). These experiments were conducted in annular spaces by heating the inner core. The pressures varied from 1 to 22 atm. abs. ($\frac{v}{v_s} > 80$), the water flow velocities from 0.5 to 14 m/sec., the degree of subcooling ΔT from 5 to 80° C, the diameter of the heated core from 1 to 10 mm, and the width of the annular space δ from 0.5 to 4.4 mm. The following formula corresponds to a straight line drawn through the experimental points:

$$\frac{q_{cr, \delta}}{q_{cr, 0}} = 1 + 0.067 \left(\frac{\delta}{r} \right)^{0.8} \frac{v}{v_s}. \quad (7-26)$$

The data of S. S. Kutateladze shown in Fig. 7-12 indicate that with extensive subcooling the relationship between q_{cr} and δ is nonlinear.

7-8. Effect of Flow Velocity, Channel Dimensions,
and Vapor Fraction on the Quantity q_{cr}

From (7-3) it follows that the critical heat flux at zero fraction of vapor ($c' \delta / r = 0, w''/w' = 0$) is a function of flow velocity through the dimensionless parameter w'^2/gl . The effect of viscosity is taken into account in conformity with (7-13). In the case of the flow of a vapor-liquid mixture, w''/w' and γ'/γ are added to the number of the determining parameters.

Thus, in a general form, we may write

$$N_{cr} = f \left[w' \sqrt{\frac{r-r_0}{\rho}}, \frac{\mu}{r}, \frac{r_0}{r}, \frac{\gamma'}{\gamma} \left(\frac{r-r_0}{r} \right)^{1/2}, \sqrt{\frac{r-r_0}{r}} \right]. \quad (7-27)$$

Here $\Delta \frac{1}{r} = (\frac{1}{r_{flow}} - \frac{1}{r_0})/r$ is the relative difference between the heat content of the flow and that of the saturated liquid.

With $\bar{t} = t''$, the quantity $\Delta \frac{1}{r}$ is numerically equal to the mass fraction of vapor in the mixture, i.e., it is the mass analog of parameter β . With $\bar{t} < t''$, $\Delta \frac{1}{r} = -c' \delta / r$ can also be considered a "negative fraction of vapor." This modified version of the criterion $K = r/c \Delta t$ was used in such a form by M. A. Styrikovich, Z. L. Miropol'skiy, M. Ye. Shitsman, V. Ye. Doroshchuck and some other investigators.

Under forced flow, in order to produce a continuous vapor film, it is necessary to accelerate the liquid forced out of the layer adjoining the wall to the velocity of the core. In connection with

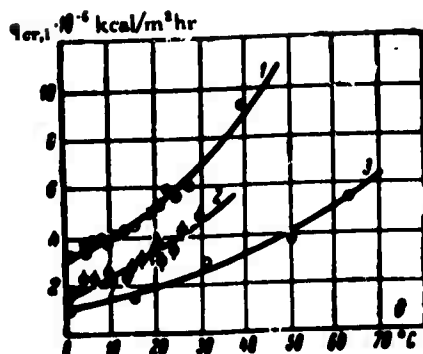


Figure 7-12. $q_{cr,1}$ vs. t for water flow in a wide annular space. ($p \approx 1$ atm. abs.): (1) $w \sim 4$ mm/sec.; (2) $w \sim 1$ m/sec.; (3) natural convection in a large volume.

this, the higher the liquid flow velocity, the larger the work required to form the vapor film. The quantity q_{cr} increases accordingly

In Fig. 7-13 the results of experiments with channels having wide slits ($\delta > 3$ mm) are plotted on generalized coordinates. As may be seen, quite different data are in agreement. The results of a short series of experiments by McAdams conform qualitatively to the findings of Soviet investi-

gators, but their absolute values are lower.

According to V. S. Chirkin, in slit channels with $\delta < 3$ mm, the quantity q_{cr} decreases approximately in proportion to the 0.7th power of δ .

The average line drawn through the points in Fig. 7-13 is described by the formula

$$A_0 = 0.085 w^{0.75} \left(\frac{r' - r}{\delta^2} \right)^{0.125}. \quad (7-28)$$

The action of the fraction of vapor in the stream on q_{cr} has a dual character. At unchanging mass velocity and rather small mass fractions of vapor in the stream, increase in the stream's size gives

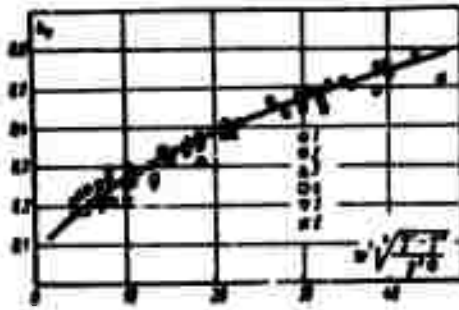


Figure 7-13. $q_{cr} = \frac{q_{cr,0}}{\sqrt{\rho_1 \sqrt{1-\gamma}}}$
vs. $\sqrt{\frac{1-\gamma}{\rho}}$ for flow in

a slit channel. The inner core is heated. Experiments of Kutateladze, $\theta = 0$; (1) $p = 1$ atm. abs.; experiments of Averin and Kruzhilin, $\theta = 0$; (2) $p = 1$ atm. abs.; (3) $p = 3$ atm. abs.; (4) $p = 5$ atm. abs.; (5) $p = 9$ atm. abs.; experiments of Chirkin and Yukin, $\theta > 0$; (6) $p > 22$ atm. abs.

an increase in the velocity of the mixture, which leads to an increase in q_{cr} . This increase is especially noticeable at moderate pressures $\gamma' \gg \gamma''$ when an already small mass fraction of vapor greatly increases the specific volume of the mixture. With a further increase in the fraction of vapor a decrease in the fraction of water of the stream begins to show.

In this region the flow now consists of vapor entraining drops of liquid, and the preservation of the two-phase boundary layer depends on the rate of collection of liquid drops on the wall.

Since the rate of this spraying decreases with a decrease in the fraction of water in the mixture, the specific heat flux at which deterioration of heat transfer begins also decreases abruptly as the fraction of vapor increases. However, the change in the rate of heat transfer in this region of vapor fractions should not be considered as a critical change associated with the upsetting of the stability of the two-phase boundary layer. The laws governing this heat-transfer deterioration have not been studied sufficiently as yet; nevertheless, it can already be affirmed at present that they differ greatly from those which apply in a large volume or in a forced flow

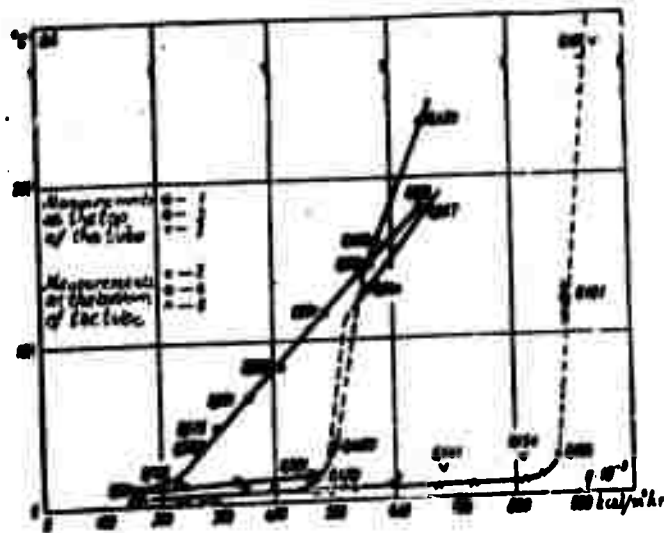


Figure 7-14. Temperature difference (Δt) between wall and stream vs. specific heat flux (q). Obtained by M. Ye. Shitsman and Z. Ya. Miropol'skiy in a stainless-steel tube 21.5 mm in diameter heated directly by an electric current. The points are labeled with reference to relative enthalpies $\frac{1}{2} = \frac{1'}{r} = \frac{x}{x_{in}}$. (1,2) $p = 181.8$ kg-force/cm²; $x_{in} = 0.363$; $\frac{v_0}{x} = 890$ kg-force/m² sec; (3,4) $p = 183.0$ kg-force/cm²; $x_{in} = 0.545$; $\frac{v_0}{x} = 875$ kg-force/m² sec; (5,6) $p = 182$ kg-force/cm²; $x_{in} = 0.074$; $\frac{v_0}{x} = 869$ kg-force/m² sec.

of a stream with a small fraction of vapor.

Even at comparatively moderate flow velocities of the steam-water mixture, the deterioration of the heat transfer loses its critical character. Upon reaching a definite thermal load, the wall temperature increases rapidly but not by jumps (Fig. 7-14). In this region one can no longer speak even of a definite value of p_{cr} , but one can only fix that magnitude of the heat flux at which an increase in the wall temperature is some specific magnitude, for instance, 50°C.

The examined region has a particular significance at increased pressures ($\frac{p}{p_{cr}} > 0.5$), even when an abrupt deterioration of heat

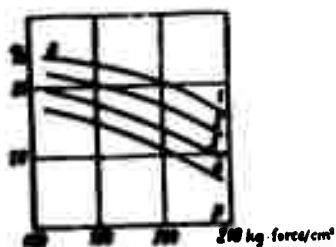


Figure 7-15. Dependence of the critical mass fraction of vapor x_{cr} on pressure and on specific heat flux at reference mass velocity of the vapor $w'' = 140 \text{ kg-force/m}^2\text{sec}$;

- (1) $q = 300,000 \text{ kcal/m}^2 \text{ hr}$;
- (2) $q = 400,000 \text{ kcal/m}^2 \text{ hr}$;
- (3) $q = 500,000 \text{ kcal/m}^2 \text{ hr}$;
- (4) $q = 600,000 \text{ kcal/m}^2 \text{ hr}$.

transfer conditions is observed in sharply reduced heat fluxes ($q \ll q_{cr}$) and vapor fractions $x \ll 1$; this can be seen in Fig. 7-15.

As the experiments of M. A. Styrikovich and co-workers have shown in the field of near-critical pressure, the phenomenon of a critical change in heat transfer during boiling in tubes acquires an extremely singular character, different from the phenomena described above. Investigation of these specific thermal processes is beyond the scope of this book.

CHAPTER EIGHT

ATOMIZING LIQUIDS BY SPRAY NOZZLES

8-1. Methods of Atomizing Liquids by Spray Nozzles

The atomization of liquid is widely utilized in the most diverse branches of modern engineering: liquid fuel is burned in an atomized form in different kinds of combustion systems; hot gases are cooled by means of an atomized liquid in various equipment used in the chemical, fuel, and other industries; vapor-gas mixtures are obtained by means of atomization, etc.

In most cases, the rate at which the pertinent processes takes place is determined by the rate of evaporation of the liquid, and by the diffusion exchange between the medium and the surface of the drop. In connection with this, ability to obtain atomization with proper drop size, knowledge of the fractional composition of the drop-size range, and the spray-density distribution throughout the cross section of the jet--all these are of first rank practical importance.

At the present time two types of atomizers (spray nozzles) are used: mechanical and pneumatic. In the mechanical spray nozzles, the liquid is fed under high pressure (up to several tens of atmospheres) and is discharged into a gaseous medium usually having a low flow velocity. In the pneumatic spray nozzles, the initial liquid velocity is not high and atomization takes place in the gas

stream which entrains the jet.

Pneumatic spray nozzles are generally divided into two types: the high-head nozzles (as high as 3 to 4 atm.) with relatively low specific gas discharge rates (0.3 to 1.0 kg. of gas per kg of liquid), and the low-head nozzles (less than 0.1 atm.) with a relatively high specific gas discharge rate (4 to 10 kg of gas per kg of liquid).

The process of atomization (breakup) of the liquid is determined by the interaction of the liquid with the surrounding gas. Here a most crucial role is played by the shape and the angle of twist of the liquid jet, depending on the configuration of the flux in front of and behind the extrusion orifice of the spray nozzle.

8-2. Principal Parameters Determining the Atomizing Process

Atomization of a liquid jet being discharged from a given orifice into gas-filled space is the result of the interaction of the liquid stream and the gaseous environment. This interaction is extremely complex since not only does the jet itself break up but also the independent primary drops.

The starting conditions for the stream under examination are the conditions for its discharge from the spray nozzle. These conditions are determined by the geometric configuration of the chamber, the spray-nozzle orifice, and the discharge velocity of the jet.

In the most general sense, the process under consideration--as any flow in a gas-liquid system--is described by the equations of motion of the phases and by the conditions for their interaction at the boundaries. Here, because of considerable velocities of the liquid jet, gravitational forces (as compared with inertia) can be

in comparison with inertia.

Moreover, in the region where the breakup process takes place, the liquid-phase flow sets up extremely strong turbulent perturbations in the surrounding gas. In connection with this, the forces of molecular friction in the gas phase can also be disregarded.

Taking into consideration what was said above, we can write the fundamental system of equations in the following form:

$$\left. \begin{aligned} -\text{grad } p' + \rho' \nabla^2 \vec{u} &= \rho' \frac{D\vec{u}}{dt}; \\ \text{div } \vec{u} &= 0; \\ -\text{grad } p' &= \rho' \frac{D\vec{u}}{dt}; \\ \text{div } \vec{u} &= 0; \\ \rho' \left(\frac{\partial u_i}{\partial x_i} + \frac{\partial u_i}{\partial x_i} \right)_b &= -\rho' (\overline{u_i u_i})_b; \\ \rho' - 2\rho' \left(\frac{\partial u_i}{\partial x_i} \right)_b &= \rho' - \rho' (\overline{u_i u_i})_b + \rho' \left(\frac{1}{R_1} + \frac{1}{R_2} \right); \\ \vec{u}_b &= \vec{u}_b; \end{aligned} \right\} \quad (8-1)$$

here, v_i and v_k are the fluctuating velocity components.

These equations give the following primary similarity criteria.

$$\left\{ \frac{\Delta p}{\rho' u^2}; \frac{u'}{u}; \frac{\Delta p}{\rho' u^2}; \frac{u' u'^2}{\rho' u^2}; \frac{\Delta p}{\rho' u^2}; \frac{u'}{u} \right\}. \quad (8-2)$$

Considering that

$$\frac{\Delta p}{\rho' u^2} \cdot \frac{u' u'^2}{\Delta p} = \frac{u' u'^2}{\rho' u^2}$$

and

$$\frac{L_p}{\rho \cdot v^2} = \frac{L_p}{\rho \cdot v^2} \cdot \frac{v'}{v'}$$

we can write a system of criteria, strictly equivalent to (8-2), but containing one less criterion:

$$\left\{ \frac{L_p}{\rho \cdot v^2} : \frac{v'}{v} : \frac{L_p}{\rho \cdot v^2} : \frac{L_p}{\rho \cdot v^2} : \frac{v'}{v} \right\}. \quad (8-3)$$

Among the conditions which uniquely define the examined process are the geometric dimensions of the spray nozzle, flow velocities of the phases, and the physical constants in the equations of (8-1). Let us form, as usual, combinations from the criteria in (8-3), so as to isolate the maximum number of groups composed only of quantities that are among the conditions uniquely defining the problem. We have:

$$\left. \begin{aligned} \frac{L_p}{\rho \cdot v^2} \cdot \frac{v'}{v} \cdot \frac{L_p}{\rho \cdot v^2} &= \frac{L_p}{\rho \cdot v^2} \\ \frac{L_p}{\rho \cdot v^2} \cdot \frac{v'}{v} \left(\frac{v'}{v} \right) &= \frac{v'}{v} \end{aligned} \right\}. \quad (8-4)$$

Consequently, the following system is equivalent to system (8-3):

$$\left\{ \frac{L_p}{\rho \cdot v^2} : \frac{v'}{v} : \frac{L_p}{\rho \cdot v^2} : \frac{L_p}{\rho \cdot v^2} : \frac{v'}{v} \right\} \quad (8-5)$$

four of these criteria are determining.

Evidently, the higher the rate of the breakup process, the greater the dynamic interaction between the jet and the gas. This interaction depends on their relative velocity. Therefore, it is expedient to introduce the relative velocity of the gas into the criteria in (8-5) instead of its absolute velocity:

$$\frac{v}{v_0} = \frac{v}{v_0}.$$

Taking this circumstance into account, we can write that any determinable criterion for the atomization process in geometrically similar spray nozzles is a certain function of the following determining dimensionless parameters:

$$\left[\frac{v}{v_0}, \frac{p}{\rho v^2}, \frac{\rho}{\rho_0}, \frac{\sigma}{\rho v^2} \right]. \quad (8-6)$$

8-3. Breakup of a Simple Jet

A liquid jet discharged into space begins to oscillate, interacts with the surrounding gas, and breaks up into drops.

In Fig. 8-1 are shown photographs of the discharge of the liquid jet into a gas with different densities. As may be seen, the greater the gas density, the more complete is the disruption of the jet.

Figure 8-2 shows the results of one of the experiments by V. I. Blinov and Ye. L. Feinberg (Feynberg) determining the shape of a jet

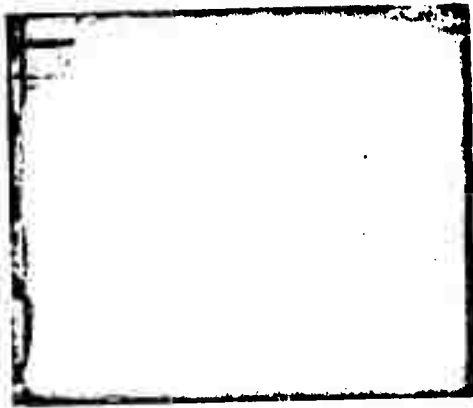


Fig. 8-1. Photographs of a jet of liquid fuel discharging into air at various pressures. $D_{\text{nozzle}} = 0.5 \text{ mm}$; pressure in front of nozzle; 18.6 atm. abs.; liquid viscosity: 0.13 poise; opposing pressure: (1) 0.021 atm. abs.; (2) 1 atm. abs.; (3) 1.4 atm. abs.; (4) 7.8 atm. abs.; (5) 14.5 atm. abs.

discharged from an elliptical orifice. The distance from the plane of the discharge orifice is plotted as the abscissa and the thickness of the jet as the ordinate. As may be seen, the jet has an extremely pronounced wave character. The waves originate at the exit of the nozzle, and are gradually damped as they move away from the orifice. Once these waves have been completely damped, unstable waves begin to develop whose amplitude continually increases along the jet and finally causes it to break up into drops. The charac-

ter of the oscillation of the jet depends essentially on the flow velocity (all other conditions being equal). There exists a velocity at which the stability of the jet is greatest with respect to the extent of its solid portion.

Figure 8.3 shows the results of some experiments demonstrating how the length of the solid portion of the water jet discharged into the atmosphere changes with the head at the nozzle exit.

As yet there are no complete solutions of the problem dealing with the breakup of the jet. However, a quite far-reaching elaboration of it has been accomplished in the works of Rayleigh, Weber, Petrov, Kalinina, and others. This theory is based on the concept that the jet breaks up as a result of an upsetting of the equilibrium

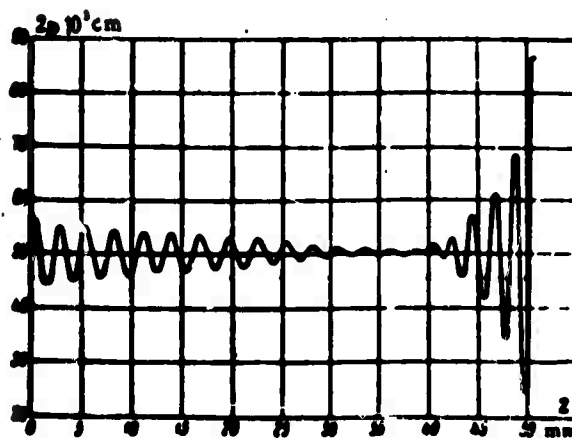


Figure 8-2. Shape of a jet discharged from an elliptical orifice.

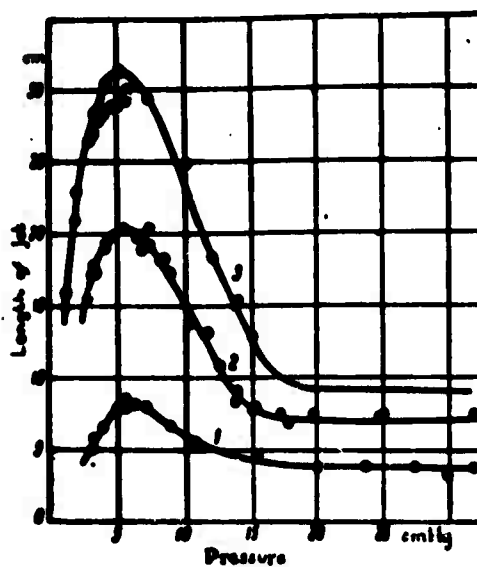


Figure 8-3. Length of the solid portion of a water jet discharged into the atmosphere vs. head at the nozzle exit. (1) Orifice $d = 0.68$ mm; (2) $d = 1.08$ mm; (3) $d = 1.28$ mm.

of the free surface of liquid under the effect of surface tension. The insignificant initial perturbations lead to the formation of waves with spontaneously increasing amplitude, this process being sped up by additional perturbations due to the relative motion of the liquid and the gas.

The equations of motion and continuity for the jet can be written in terms of the corresponding fluctuating components of velocity and pressure in a cylindrical system of coordinates:

$$\left. \begin{aligned} p' \frac{\partial u}{\partial t} &= -\frac{\partial p'}{\partial r} + p' \left(\frac{\partial u}{\partial r^2} + \frac{\partial u}{\partial z^2} + \frac{1}{R} \cdot \frac{\partial u}{\partial R} \right); \\ p' \frac{\partial v}{\partial t} &= -\frac{\partial p'}{\partial z} + p' \left(\frac{\partial v}{\partial r^2} + \frac{\partial v}{\partial z^2} + \frac{1}{R} \cdot \frac{\partial v}{\partial R} - \frac{v}{R^2} \right); \\ \frac{\partial u}{\partial r} + \frac{\partial v}{\partial z} + \frac{v}{R} &= 0; \end{aligned} \right\} \quad (8-7)$$

here \underline{v} , \underline{u} are the fluctuating velocities in the radial and axial directions;

p' is the fluctuating pressure in the jet.

The boundary conditions are written according to (8-1), but in a simpler form. In particular, the tangential stresses on the jet surface are assumed to equal zero. We have:

$$\left. \begin{aligned} \frac{\partial u}{\partial r} &= 0; \\ p' \left(\frac{\partial u}{\partial r} + \frac{\partial v}{\partial z} \right)_b &= 0; \\ p' + 2p' \left(\frac{\partial v}{\partial z} \right)_b &= -\sigma + \sigma_0. \end{aligned} \right\} \quad (8-8)$$

where p' is the fluctuating pressure in the gas;

p_s' is the fluctuating pressure caused by the forces of surface tension.

A particular solution of this system of equations for the time changes in the amplitude of oscillations has the form:

$$b = F\left(\frac{R}{R_0}; \left(\frac{t}{R_0}\right)^q\right).$$

where q is the increment of oscillations in the jet, determined approximately by the equation

$$q^2 + q \frac{2\gamma}{\rho' R_0^3} = \frac{\sigma}{2\rho' R_0^3} (1 - q)^2 + \frac{\rho' \omega^2}{2\rho' R_0^3} f_0(t); \quad (8-9)$$

here R_0 is the mean radius of the jet;

$k = \frac{2\pi R}{\lambda}$ is the wave number (λ is the wavelength of the oscillations).

For oscillations leading to the breakup of the jet, $q > 0$. Then, the most rapidly increasing oscillation is of decisive importance.

Examining Equation (8-9), written for this oscillation, one is convinced that it gives two determining criteria corresponding to the first two criteria of the system (8-6). Moreover, Equation (8-9) gives nondetermining criteria containing the increment and the wave number of the oscillation which leads to the breakup of the jet.

8-4. Breakup of a Single Drop

The behavior of a single drop entrained by a gas stream depends on the relationship between the dynamic effect which the stream has on the drop and the "strength" of the drop, which depends on the surface tension and the viscosity of the liquid. The interaction of the liquid and gas is generally described by the system of equations (8-1). This system leads to four determining criteria in (8-6). For a single drop entrained by a stream, the velocity \underline{w} drops out of the conditions which uniquely define the process, and accordingly the last two criteria of the system (8-6) cease to be determining.

Breakup of a drop of a given diameter begins at a specific velocity of the entraining stream. This velocity, which may be denoted as \underline{w}_{cr} , is a function of conditions which uniquely define the drop breakup process. Among the latter are only the drop diameter and the physical constants in the first two criteria of the system (8-6). Hence, it can be assumed:

$$\frac{\rho \underline{w}_{cr}^3 D_0}{\sigma} = f\left(\frac{\mu^2}{\sigma D_0}\right). \quad (8-10)$$

where \underline{D}_0 is the initial drop diameter.

For low-viscosity liquids, when the breakup process does not for all practical purposes depend on μ , it follows from (8-10) that:

$$\frac{\rho \underline{w}_{cr}^3 D_0}{\sigma} = \text{const.} \quad (8-11)$$

$$w_{cr} = \text{const} \sqrt{\frac{\sigma}{\rho D_0}} \quad (8-12)$$

As M. S. Volynskiy's experiments have shown, one must distinguish two critical velocities of the entraining flow-- $w_{cr,1}$, at which only single drops of diameter D_0 begin to break up, and $w_{cr,2}$, at which all drops of the given diameter break up.

According to these experiments, the interval where the drops become unstable is determined by the inequality

$$14 > \frac{w_{cr,2}}{w_{cr,1}} > 10.7. \quad (8-13)$$

Figure 8-4 gives curves showing the stability of water and gasoline drops in an air stream at atmospheric pressure.

At velocities close to $w_{cr,1}$ the drop splits up into two almost equal parts, and a number of minute droplets are also formed. At velocities of the order of $w_{cr,2}$ and higher, the drop breaks up (is atomized) into a greater number of droplets whose diameters are unequal and considerably less than D_0 .

Figures 8-5 and 8-6 show photographs of the drop-splitting process obtained by M. S. Volynskiy. Figure 8-7 shows photographs of the drop-atomization process obtained by Lane. Apparently, at velocities $w > w_{cr}$, a flying drop is drastically distorted into a

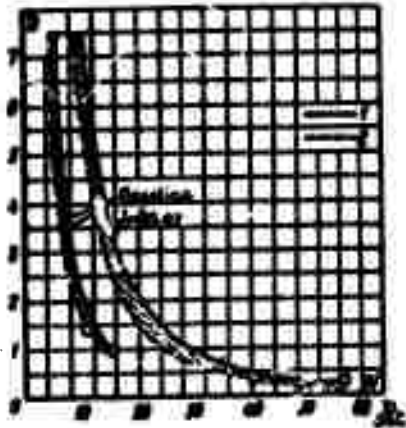


Figure 8-4. The curves of the stability of water and gasoline drops in an air stream of atmospheric pressure. (1) upper limit of stability; (2) lower limit of stability.



Figure 8-5. Splitting drop.
Castor oil: $D_0 = 3.8$ mm;
 $v = 28$ m/sec.



Figure 8-6. Splitting drop.
Castor Oil: $D_0 = 3.8$ mm;
 $v = 35$ m/sec.; nearby, a drop
in a phase corresponding to
the regime when there is no
splitting.



Figure 8-7. Photographs of the drop atomization process.

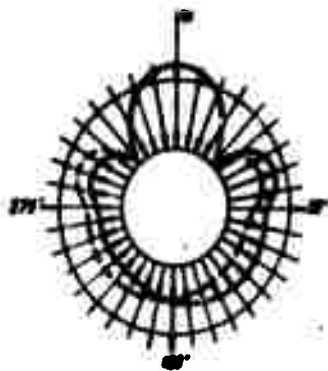


Figure 8-8. Pressure distribution (rosette) in flow past a sphere.

body with a thin shell which when ruptured will give rise to a range of small and minute droplets. The character of the gas flow past the drop is the cause of this distortion.

During flow past an originally spherical drop, the change in flow velocities across the boundary layer and in the separation region (Fig. 8-8) causes distortion of the drop and the subsequent development of a pressure-distribution rosette. At the first stage of this process, the drops flatten out in the direction of the flow, i.e., assume the shape of a round flat disk, the plane of which is perpendicular to the direction of the velocity vector. Later on, distortion becomes more pronounced, having the nature of a burst and leading to atomization of the original drop.

8-5. Mean Drop Diameter in Atomization by Pneumatic Spray Nozzles

As has been pointed out above, the basic characteristics of the nature of atomization are the fractional composition of the drops and the spray density distribution throughout the cross section of the atomized jet. The mean drop diameter is somewhat of an over-all characteristic indicating to some extent the nature of liquid atomization by a given spray nozzle.

There are several methods for determining the mean drop diameter. The mean diameter, determined from the property of weight, is:

$$D = \frac{\sum d_i^3}{\sum d_i^2} \quad (8-14)$$

where Q_i is the total weight of the drops of diameter D_i .

At the present time, there is a considerable amount of experimental research on different spray nozzles.

In order to ascertain the basic laws governing liquid atomization by pneumatic sprayers, let us examine the results of a very thorough and methodical study carried out by L. A. Vitman, B. D. Katsnel'son, and M. M. Efros, under I. I. Paleyev's direction.

Figure 8-9 shows the relationship between the relative mean drop diameter $\frac{D}{D_0}$ (where D_0 is the diameter of the spray-nozzle orifice) and the first group of (8-5), from data for one of the spray nozzles. In these experiments, the air velocity changed within the range from

43 to 121 m/sec., and the liquid velocity within 0.55 to 2.3 m/sec. No influence of the relative flow rate of the phases $\frac{w'}{w''}$ was revealed in these experiments. As may be seen from the graph shown, the experimental points fall properly on a logarithmic straight line with a slope $\underline{n} = -0.45$. At the same time the distance of the drops from the spray-nozzle orifice has no noticeably appreciable influence on the mean drop diameter.

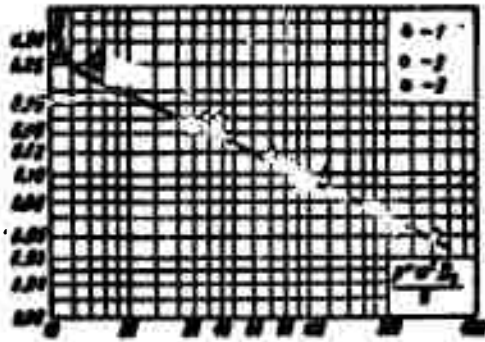


Figure 8-9. $\frac{\bar{D}}{D_0}$ vs. $\frac{\rho w''^2 D_0}{\sigma w'}$ from experiments with pneumatic spray nozzles.

(1) $\underline{n}_1 \approx 6 \cdot 10^{-4}$; (2) $\underline{n}_1 \approx 8 \cdot 10^{-4}$; (3) $\underline{n}_1 \approx 5 \cdot 10^{-5}$; where $\underline{n}_1 = \frac{\underline{n}}{12} = \frac{\underline{n}}{\rho \sigma D_0}$.

The proportionality factor in the relation

$$\frac{\bar{D}}{D_0} = A \left(\frac{\rho w''^2 D_0}{\sigma w'} \right)^{\underline{n}} \quad (8-15)$$

proved to be different for various liquids. It follows from (8-6)--since the experiments reveal no influence of the parameter $\frac{w'}{w''}$ and, consequently, none of parameter $\frac{\rho w''^2 D_0}{\sigma w'^2}$ --that this difference is determined only by the viscosity of the liquid and is characterized by the second criterion of (8-6).

Figure 8-10 shows the relationship

$$\frac{\bar{D}}{D_0} \left(\frac{\rho w''^2 D_0}{\sigma w'} \right)^{\underline{n}} = f \left(\frac{\mu^2}{\rho \sigma D_0} \right) \quad (8-16)$$

plotted from experiments with the same spray nozzle. The viscosity of the atomized liquids varied in these experiments from

$0.067 \cdot 10^{-3}$ to $54.5 \cdot 10^{-3} \text{ kg} \cdot \text{sec}/\text{m}^2$.

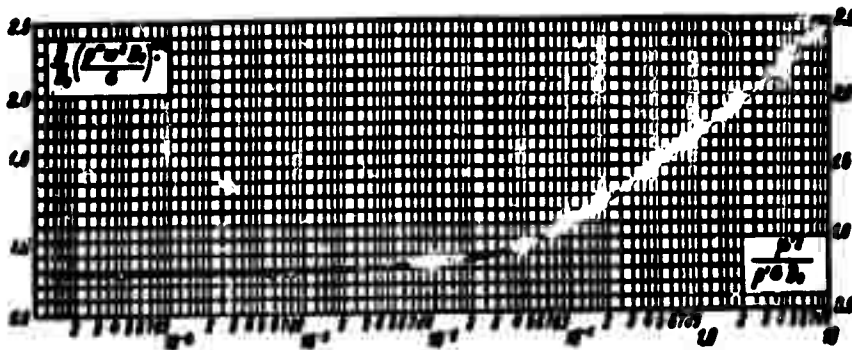


Figure 8-10. Generalized relationship

between $\frac{D}{D_0} \left(\frac{\rho_w^2 D_0}{\sigma} \right)^{0.45}$ and $\left(\frac{\mu^2}{\rho \sigma D_0} \right)$.

From the data shown, it may be seen that the effect of viscosity on the drop size is only substantial when

$$\frac{\mu^2}{\rho \sigma D_0} > 0.1. \quad (8-17)$$

Experiments with a number of other spray nozzles (three of which are shown in Fig. 8-11) have confirmed the indicated laws. The working formulas proposed by L. A. Vitman, B. D. Katsnel'son, and M. M. Efros have the form:

$$\text{at } \frac{\mu^2}{\rho \sigma D_0} > 0.5$$

$$\frac{D}{D_0} \left(\frac{\rho_w^2 D_0}{\sigma} \right)^{0.45} = A_0 + 0.94 \left(\frac{\mu^2}{\rho \sigma D_0} \right)^{0.25}; \quad (8-18)$$

at $\frac{p^*}{p^* D_0} < 0.5$,

$$\frac{\bar{D}}{D_0} \left(\frac{p^* D_0}{p^*} \right)^{0.65} = A_0 + 1.24 \left(\frac{p^*}{p^* D_0} \right)^{0.65}.$$

(8-19)

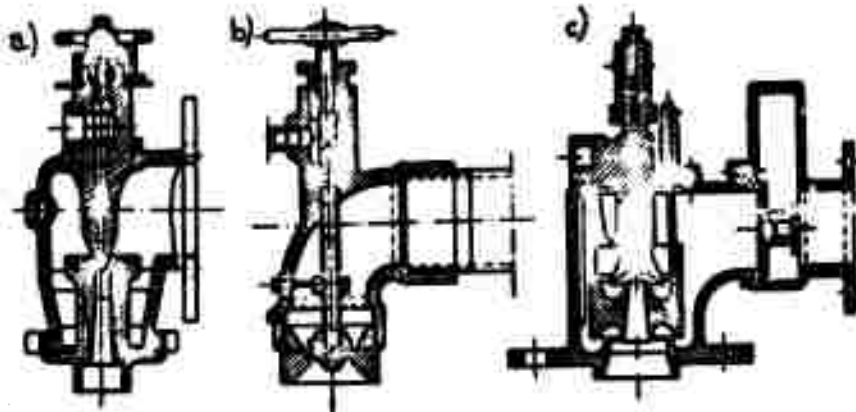


Figure 8-11. Sectional view of spray nozzles:
(a) STS-FDM-1; (b) STS-FOB-2; (c) STS-FDB-1

The quantity A_0 depends on the design of the spray nozzle (Table 8-1).

Table 8-1

Type of Spray Nozzle	A_0	m	Angle of cone
STS-FDB-1	1.20	2.3	28°
STS-FOB-2	0.90	2.8	$30-47^\circ$ *
STS-FDM-1 (Kel'man's)	0.78	2.6 to 3.0	22°
Glushakov's	0.75	2.3	25°
Two-step	0.61	2.8	29°

*Depending on the size of nozzle orifice and insert.

Thus, the fineness of liquid atomization by pneumatic sprayers is approximately inversely proportional to the square root of the kinetic energy of the gas.

The relative velocity of the gas-liquid stream for the case when primary and secondary air are fed to the spray nozzle is calculated by means of the formula

$$w = \sqrt{\frac{w_{10}^2 G_1 + w_{20}^2 G_2}{G_1 + G_2}}. \quad (8-20)$$

w_{10} is the initial relative velocity between the primary air and the liquid jet;

w_{20} is the relative velocity of the gas liquid stream encountering the secondary air;

G_1 is the mass flow rate of primary air;

G_2 is the mass flow rate of the secondary air.

8-6. Fractional Composition of a Jet Atomized by a Pneumatic Spray Nozzle (Spray Density)

The process of liquid breakup still continues after a continuous jet has broken up into single drops by the mechanism described in Section 8-4. The resultant appearance of a complex breakup mechanism in a jet dissolving into a number of drops has a probabilistic character. In fact, the experimental curves of fractional distribution have precisely such a shape. In connection with this, for fractional (drop size) distribution of an atomized liquid, one can adopt the formula

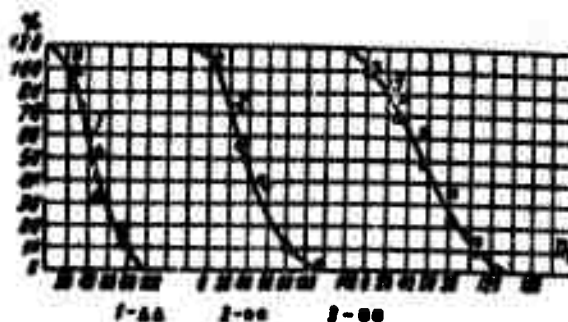


Figure 8-12. Drop-size distribution at various flow rates.
 (1) $w = 120$ m/sec ; (2) $w = 94$ m/sec; (3) $w = 60$ m/sec.

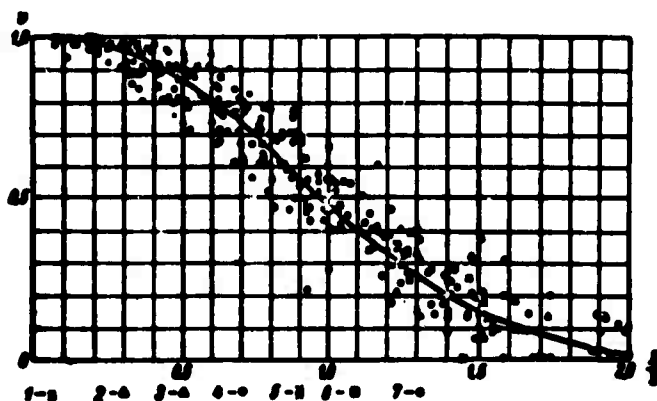


Figure 8-13. Character of drop distribution by fractions when atomized by pneumatic spray nozzles.
 1.15° Engler; (2) 1.3° E.; (3) 3° E.; (4) 7° E.; (5) 13° E.;
 (6) 31.5° E.; (7) 59° E.

$$v = \exp \left\{ - \left[3 \left(1 + \frac{1}{m} \right) \frac{D_1}{D} \right]^m \right\} \quad (8-21)$$

where v is the fraction of liquid consisting of drops of diameter

greater than D_1 ;

m is a parameter characterizing drop distribution.

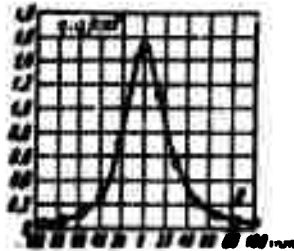


Figure 8-14. Spray density throughout the cross section of a sheet from one of the pneumatic spray nozzles. q [gm/cm²] is the spray density; R is the distance to the axis of the sheet.

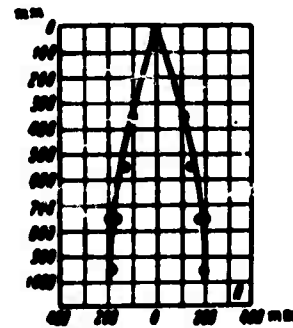


Figure 8-15. The shape of the sheet for the STS-FOB-2 spray nozzle. x is the distance from the orifice; R is the distance from the axis.

Results of experiments by Vitman, Katsnel'son, and Efros, shown in Fig. 8-15, demonstrate that the experimental points for a given type of spray nozzle are satisfactorily correlated by the relation

$$\sigma \cdot \left(\frac{D_1}{D} \right).$$

(8-22)

Values of parameter m for the spray nozzles examined above are shown in Table 8-1.

A typical spray density distribution for pneumatic spray nozzles is shown in Fig. 8-14. Here, by spray density is understood the flow rate of liquid through a unit of jet cross section.

The shape of the atomized jet characteristic of noncentrifugal spray nozzles is shown in Fig. 8-15.

8-7. Motion of a Liquid in the Chamber of a Centrifugal Spray Nozzle

The conditions necessary for jet atomization in mechanical spray nozzles are created by suitable organization of the liquid flow in the chamber preceding the spray nozzle orifice.

The theory of the motion of a liquid in the chamber of a centrifugal spray nozzle was developed by G. N. Abramovich.

A diagram of a centrifugal spray nozzle is given in Fig. 8-16. The liquid is fed into the chamber of the spray nozzle tangentially, as a consequence of which the stream acquires a twisted motion. The nozzle orifice is situated in the front wall of the spray nozzle. When the twisted jet is discharged from the spray nozzle, the effect of centripetal forces from the rigid walls ceases, and the jet breaks down due to non-steady-state oscillations. The drops are thereby scattered in a pattern of rectilinear streams, tangent to the cylindrical surfaces coaxial with the spray nozzle orifice. (Fig. 8-17).

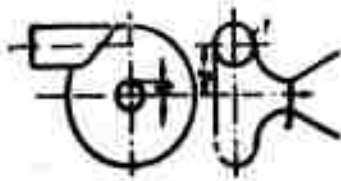


Figure 8-16. Diagram of centrifugal spray nozzle.



Figure 8-17. Sprayer exit orifice cross section.

The angle α , between the lines of atomization and the spray-nozzle axis, is determined by the ratio of the tangential velocity w_t' to the translational velocity w_n' in the exit cross section of the nozzle orifice:

$$\alpha = \tan^{-1} \frac{w_t'}{w_n'} \quad (8-23)$$

If the effect of friction is disregarded, the momentum of a liquid particle moving relative to the sprayer axis, will be constant. Hence,

$$w_n' R' = w_t' R' \quad (8-24)$$

where w_{in}' is the velocity of the liquid entering the spray nozzle;

R' is the radial distance from the spray-nozzle axis to the liquid particle in the entrance orifice of the spray nozzle;

w_t' is the tangential component of the liquid velocity in the spray-nozzle exit orifice;

\underline{R} is the radial distance from the spray nozzle axis to the liquid particle in the exit orifice.

Disregarding the difference in the entrance and exit orifice levels in comparison with the head, on the basis of the Bernoulli equation we can write:

$$\frac{p_{in}}{\gamma} + \frac{w_{in}^2}{2g} = \frac{p}{\gamma} + \frac{w_t'^2}{2g} + \frac{w_n'^2}{2g} = \text{const}; \quad (8-25)$$

hence, taking into account (8-24), we have:

$$\frac{p}{\gamma} = H - \frac{w_n'^2}{2g} - \frac{w_n'^2}{2g} \left(\frac{R'}{R} \right)^2. \quad (8-26)$$

where \underline{H} is the total head:

$$H = \frac{p_{in}}{\gamma} + \frac{w_{in}^2}{2g}.$$

From (8-26) it may be seen that at the spray-nozzle axis ($\underline{R} = 0$) the flow velocity must go to infinity and the pressure must go to minus infinity. Such a state is physically impossible and hence there must be a mechanism maintaining a certain pressure at the spray-nozzle axis. This pressure cannot be noticeably below the pressure in the gas since the axial area of the stream is in contact with the gaseous medium outside the spray nozzle.

Hence, it follows that the central part of the spray nozzle cannot be filled with liquid and that a gaseous vortex with a pressure equal to the gas pressure outside the spray nozzle will develop in that central portion. The liquid is discharged from the spray nozzle through an annular cross section of area

$$S = \pi(R_0^2 - R_v^2). \quad (8-27)$$

where R_0 is the radius of the spray-nozzle orifice;

R_v is the radius of the gas vortex.

The filled fraction of the nozzle (coefficient of the effective nozzle cross section) is

$$\eta = 1 - \left(\frac{R_v}{R_0}\right)^2. \quad (8-28)$$

Let us examine an elementary annular plane $2\pi R \, dR$ in the nozzle-exit cross section. The change in pressure along the nozzle radius is proportional to the centrifugal force, i.e.,

$$\frac{dp}{dR} = \frac{r\omega^2}{gR}. \quad (8-29)$$

From (8-24) it follows:

$$R = \frac{w_{t,0}^2 R_0^2}{2g}, \quad (8-30)$$

where $w_{t,0}$ is the tangential velocity at the surface of the gas vortex.

Differentiating (8-30), substituting the obtained value of dR into (8-29), and integrating, we get:

$$\frac{p}{\gamma} = -\frac{w^2}{2g} + C. \quad (8-31)$$

In the gas vortex, the excess pressure is equal to zero, i.e.,

$$-\frac{w^2}{2g} + C = 0; \quad (8-32)$$

hence

$$\frac{p}{\gamma} = \frac{w^2}{2g} - \frac{w_0^2}{2g}.$$

Combining (8-32) and (8-26), we find that

$$\frac{w_0^2}{2g} = H - \frac{w^2}{2g}, \quad (8-33)$$

i.e., the translational velocity at the exit of the spray nozzle is

a constant quantity

The volumetric liquid flow rate through the spray nozzle is

$$V = w'_0 \pi R_{1n}^2 \quad (8-34)$$

where $w'_0 = \frac{w'}{n}$ is reference velocity of the liquid discharge from the nozzle orifice.

On the other hand,

$$V = w'_n \pi R_{1n}^2 n \quad (8-35)$$

where R_{1n} is the radius of the orifices through which the liquid is fed to the spray nozzle; and
 n is the number of these orifices.

Combining (8-34) and (8-35), and taking into consideration (8-24), we can write that

$$\left. \begin{aligned} w'_n &= w'_0 \left(\frac{R_0}{R_{1n}} \right)^2 \\ w'_0 &= w'_n \left(\frac{R_{1n}}{R_0} \right)^2 \end{aligned} \right\} \quad (8-36)$$

G. N. Abramovich assumes as an approximation that $R' = R_{ch} - R_{1n}$, where R_{ch} is the radius of the vortex chamber.

The tangential velocity near the chamber wall is

$$w_{t,0} = w_0 \frac{(R_1 - R_m) R_0}{a R_m^2} \quad (8-37)$$

On the boundary of the air vortex

$$w_{t,0} = w_0 \frac{(R_1 - R_m) R_0^2}{R_m^2 R_0} \quad (8-38)$$

hence, taking into account (8-28), we get:

$$w_{t,0} = w_0 \frac{(R_1 - R_m) R_0}{a R_m^2} \cdot \frac{1}{\sqrt{1-\gamma}} \quad (8-39)$$

Substituting the value of $w_{t,0}$ from (8-39) into (8-33) and solving the obtained equation for the total head H , we find

$$H = \frac{w_0^2}{2g} \left(\frac{1}{\gamma} + \frac{A^2}{1-\gamma} \right) \quad (8-40)$$

where

A is the geometric characteristic of the spray nozzle:

$$A = \frac{(R_1 - R_m) R_0}{a R_m^2} \quad (8-41)$$

Hence,

$$u_0 = i\sqrt{2gH}. \quad (8-41)$$

where

$$i = \frac{1}{\sqrt{\frac{1}{\varphi} + \frac{A}{1-\varphi}}} \quad (8-42)$$

is the spray-nozzle coefficient of discharge.

In order to establish the relationship between φ and A , which are the fundamental geometric characteristics of the mechanical centrifugal spray nozzle, O. N. Abramovich introduces the condition for maximum rate of discharge of the liquid through the spray nozzle

$$\frac{d}{d\varphi} = 0; \quad (8-43)$$

with this condition

$$\left. \begin{aligned} A &= \frac{1-\varphi}{\sqrt{\frac{\varphi}{2}}} \\ 1-\varphi &= \sqrt{\frac{\varphi}{2}} \end{aligned} \right\} \quad (8-44)$$

The volumetric rate of discharge of the liquid through the spray nozzle, according to (8-34) and (8-41), is

$$V = K R_0 \sqrt{2gH}. \quad (8-45)$$

Figure 8-18 gives the relationship of the coefficient of effective cross section of the spray nozzle orifice and the geometric characteristic \underline{A} , calculated by using the first formula of (8-44).
Introducing into (8-23) the value of \underline{w}_t , referred to the average radius,

$$R_{av} = \frac{R_0 + R_1}{2}. \quad (8-46)$$

i.e., the quantity

$$\underline{w}_{av} = \frac{\underline{w}_t R_0}{R_{av}}. \quad (8-47)$$

we get:

$$\tan \alpha = \frac{(1-\eta) \sqrt{s}}{(1+\frac{1}{1-\eta}) \frac{1}{r}}. \quad (8-48)$$

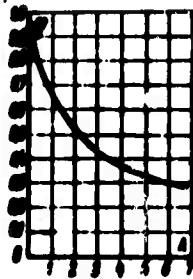


Figure 8-18. Coefficient of effective cross section vs. the geometric characteristic of the spray nozzle.

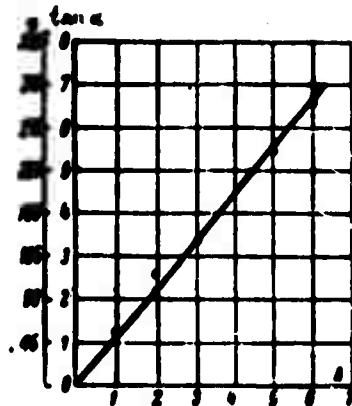


Figure 8-19. $\tan \alpha$ and α vs. A .

Figure 8-19 shows the dependences of $\tan \alpha$ and α on A , calculated from Formula (8-43).

Experimental checking has demonstrated that G. N. Abramovich's theory describes correctly the basic liquid flow characteristics in a centrifugal mechanical spray nozzle. However, this theory does not take into account the viscosity effect on liquid flow in the spray nozzle and says nothing about the atomization process. These problems can be solved by experiments based on the general theoretical propositions developed at the beginning of this chapter.

8-6. Coefficient of Discharge for a Mechanical Centrifugal Spray Nozzle

In a general case, the quantity ξ , entering into Formula (8-45), is a function of the geometric parameters of the spray nozzle and of

the criterion of hydrodynamic similarity:

$$Re' = \frac{\rho_0 D_0}{\nu} \quad (8-49)$$

where $D_0 = 2R_0$ is the diameter of the spray-nozzle orifice.

We will discuss below the basic results obtained in the experi-

mental work of A. G. Blokh and Ye. S. Kichkina. The experiments were conducted with nine spray nozzles designed as in Fig. 8-20. The vortex-chamber diameter $D_{ch} = 2R_{ch}$ varied from 3 to 9 mm, the vortex-chamber height h_{ch} from 2 to 6 mm, the diameter ($D_{in} = 2R_{in}$) of the tangential grooves varied from 0.36 to 1.58 mm, and their number from 1 to 2; the diameter D_0 of the nozzle-exit orifice varied from 0.36 to 1.58 mm, and the geometric characteristic $A =$

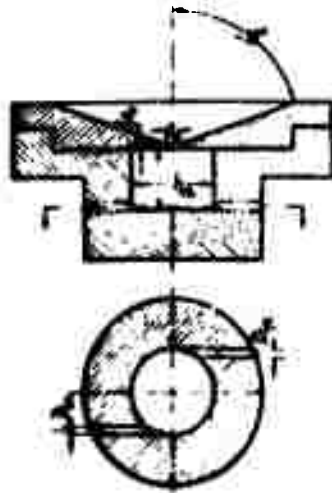


Figure 8-20. Diagram of experimental centrifugal spray nozzle.

$= \frac{(D_{ch} - D_{in}) D_0}{n D_{in}^2}$ varied from 1.72 to 9.51. The experiments were conducted with water, solutions of glycerin and glycerin soap, gas oil, and kerosene.

Results of these experiments relating to the coefficient of discharge of the spray nozzle are shown in Fig. 8-21. It turns out that it may be assumed with sufficient accuracy that

$$\xi = \xi\left(A; \frac{D_h}{D_0}; Re'\right). \quad (8-50)$$

In the region $Re' < 1.6 \cdot 10^4$

$$\xi = \varphi \sqrt{\frac{\nu}{2-\nu}} \cdot 13 \frac{\sqrt{\frac{D_h}{D_0}}}{\sqrt{Re'}}. \quad (8-51)$$

where φ is taken as a function of A from the curve in Fig. 8-18.

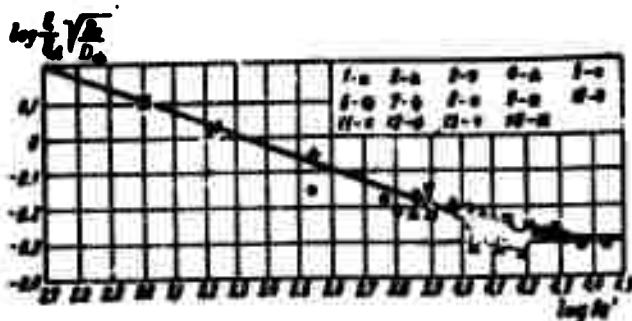


Figure 8-21. Relation (8-50) from experiments with mechanical spray nozzles, ξ_A from Formula (8-42).

Water: (1) $A = 2.62$; (2) 3.74 ; (3) 4.4 ; (4) 1.72 ; (5) 2.12 ;
 (6) 2.35 ; (7) 2.9 ; (8) 3.87 ; (9) 9.1 ; (10) glycerin,
 $\mu = 2.1 \cdot 10^{-4}$ kg-force \cdot sec/ m^2 ; (11) glycerin,
 $\mu = 29.6 \cdot 10^{-4}$ kg-force \cdot sec/ m^2 ; (12) gas oil,
 $\mu = 7.84 \cdot 10^{-4}$ kg-force \cdot sec/ m^2 ; (13) kerosene,
 $\mu = 3.08 \cdot 10^{-4}$ kg-force \cdot sec/ m^2 ; (14) water,
 $\mu = 1 \cdot 10^{-4}$ kg-force \cdot sec/ m^2 .

At $Re' > 1.6 \cdot 10^4$, the coefficient of discharge, for practical purposes, depends neither on viscosity nor, apparently, on $\frac{D_{ch}}{D_0}$.

8-9. Liquid Atomization by a Mechanical Centrifugal Spray Nozzle

The gas vortex in the centrifugal spray nozzle and the rotational motion of the jet being discharged cause the jet to acquire the shape of a hollow rotational body. In connection with this, for the centrifugal spray nozzles a spray density distribution is typical in which the central region of the sheet (the atomized jet) is filled with a small quantity of liquid, and at some distance from the axis the spray density reaches its maximum. The presence of a certain

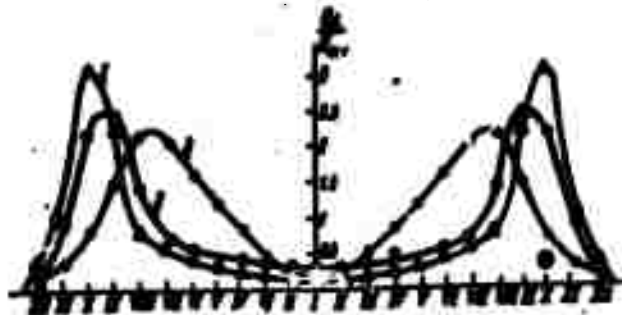


Figure 8-22. Relative spray density distribution during low-viscosity liquid (water) atomization by a mechanical spray nozzle. ($A = 5.58$) (1) $p = 10$ atm. abs.; (2) $p = 29$ atm. abs.; (3) $p = 5$ atm. abs.

Annular zone number	I	II	III	IV	V	VI	VII	VIII	IX	X	XI	XII
Boundary zone diameters, mm	16	48	80	112	144	176	208	240	272	304	336	368

quantity of liquid in the central zone is explained by the fact that individual drops are carried away from the main jet because of

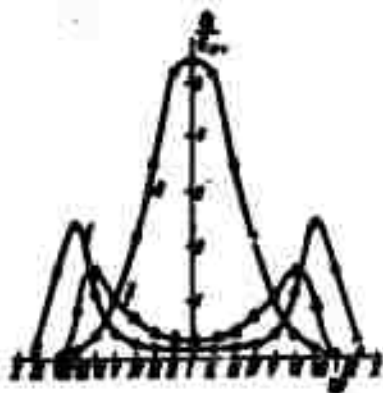


Figure 8-23. Effect of viscosity on the relative spray density in atomization by mechanical spray nozzles. ($A = 4.4$).

- (1) water ($p = 8.5$ atm. abs.;
 $\mu' = 1 \cdot 10^{-4}$ kg-force·sec/m²;
 $\sigma = 7.3 \cdot 10^{-3}$ kg-force/m);
- (2) kerosene ($p = 9.5$ atm. abs.; $\mu' = 3.08 \cdot 10^{-4}$ kg-force·sec/m²;
 $\sigma = 2.8 \cdot 10^{-3}$ kg-force/m);
- (3) gas oil ($p = 6.0$ atm. abs.;
 $\mu' = 7.84 \cdot 10^{-4}$ kg-force·sec/m²;
 $\sigma = 3.6 \cdot 10^{-3}$ kg-force/m).

turbulent fluctuations.

Figures 8-22 and 8-23 show the distribution curves for relative spray density $\frac{q}{q_{av}}$ from experiments by A. G. Blokh and Ye. S. Kichkina. Here q_1 [kg/m²sec] is the local spray density; q_{av} [kg/m²sec] is the average spray density.

These graphs indicate that the structure of the sheet varies depending on the viscosity, the rate of liquid discharge, and the nozzle-orifice diameter. For not-too-viscous liquids, the angle of spray remains constant, for practical purposes, when the rate of liquid discharge varies, and only the character of the spray density distribution curve changes.

In viscous liquids, the rate of discharge affects the angle of spray. Moreover, in this case, the influence of frictional forces increases, and a maximum spray density builds up in the center of the sheet.

Blokh and Kichkina give the following empirical formula for determining the average drop diameter in the sheet projected from the centrifugal spray nozzle;

$$\frac{D}{D_0} = 47.8A^{-0.4} \left(\frac{r'D_0}{r^2} \right)^{0.1} \left(\frac{v}{v_0 D_0} \right)^{0.7} \quad (8-52)$$

The fractional composition of the sheet can be determined according to Formula (8-21), wherein, for the above-mentioned spray nozzles, $\underline{m} = 2$ to 2.5.

Formula (8-52) is applicable for practically all low-viscosity liquids.

According to these same data, the angle of spray at $Re' > 3.5 \cdot 10^3$ and $\frac{\mu'^2}{\rho D_0} > 3 \cdot 10^{-5}$ is determined by the formula

$$\tan \alpha = (\tan \alpha_A) 3.05 \cdot 10^{-1} \left(\frac{D_0}{D_A} \right)^{0.4} \cdot \left(\frac{v'D_0}{r^2} \right)^{0.25} \quad (8-53)$$

where $\tan \alpha_A$ is obtained from Formula (8-48) or Fig. 8-19.

At $Re' < 3.5 \cdot 10^3$ and $\frac{\mu'^2}{\rho D_0} > 3 \cdot 10^{-4}$, $\tan \alpha$ proves to depend also on the Re' number. For this region, the following relationship has been obtained in experiments with a spray nozzle of $A = 4.4$

$$\tan \alpha = (\tan \alpha_A) 1.88 \cdot 10^{-1} \left(\frac{r^2}{r'D_0} \right)^{0.25} \left(\frac{v'D_0}{r^2} \right)^{0.25} \quad (8-54)$$

CHAPTER NINE

DROP ENTRAINMENT BY A GAS STREAM AND DROP SEPARATION FROM THE STREAM

9-1. General Character of the Process

When interacting with a liquid, a gas stream can partially entrain this liquid in the form of drops. The resulting two-phase system is to a greater or lesser extent unstable. Thus, in a moving gas stream containing drops, a partial separation (and under certain conditions, also, a practically total separation) of drops from the stream on the walls of the channels usually takes place.

Both of these processes, drop entrainment and separation of the liquid in drop form, are of great importance for a number of fields (steam power plants, chemical engineering, food industry, etc.). In a number of practical applications, it is necessary to atomize a liquid into small drops; such processes were examined in the preceding chapter. In other cases, it is often necessary to minimize liquid drop entrainment by gas or steam.

In most engineering equipment (steam boilers, evaporators, tubblers, fractionating columns), formation of liquid drops of various sizes and their entrainment by a gas stream, as well as partial separation of drops from a gas stream, will take place in the unit itself. Special equipment (separators), situated outside the main

unit, is also used for separating drops from an entraining stream.

Rational planning of all these processes requires a knowledge of the basic laws governing both the formation and entrainment of liquid drops by a gas stream and the process of drop separation from this stream.

Drop entrainment can proceed under various conditions of the interaction of a gas stream with a liquid. Drops entrained when a gas bubbles through a liquid layer and drops torn away from a free liquid surface by a gas stream are the two main cases. Of lesser importance in the process of drop formation is the tearing away, or the break-up of drops when a liquid jet, or single drops impinge against a liquid surface or the walls of equipment. In the latter case, not only the gas and liquid streams but also solid bodies will interact with these streams. Such an interaction plays an important part in the processes of liquid-drop separation from a stream.

When a gas bubbles through a liquid layer, the burst of the shells of the bubbles coming to the surface, and the simultaneous formation of droplets, give rise to a considerable decrease in the total interface area, since the total surface of the bubbles which have collapsed usually is many times greater than the surface of the newly-formed drops. Therefore, drop formation during bubbling can be due not only to the kinetic energy of the gas, but also to the surface energy released when bubbles burst.

At a moderate rate of bubbling (at small reference gas velocities) and with a considerable thickness of the liquid layer through which bubbles rise, as is characteristic of much engineering equipment, the kinetic energy of the vapor approaching the surface is relatively

small, and the surface energy of the bubble shells plays a basic role in the over-all energy balance. In fact, the average velocity of a gas rising in the dynamic two-phase layer under the usual conditions of high-pressure steam boilers--100 to 120 atm. abs.--does not exceed 0.7 m/sec. In low-pressure evaporators ($p \approx 1$ atm. abs.), this quantity is as high as 2 to 3 m/sec.

The kinetic energy of a bubble is

$$E_k = \frac{V \cdot \rho \cdot v^2}{2} \quad (9-1)$$

The surface energy of a bubble is

$$E_s = F \cdot \sigma \quad (9-2)$$

If we assume, as a rough estimate, that the mean bubble diameter is $\underline{D} = 3$ mm in the first case, and $\underline{D} = 5$ mm in the second, we get: for high pressure boilers ($\sigma \approx 1.2 \cdot 10^{-3}$ kg-force/m²)

$$E_k \approx 2 \cdot 10^{-4} \text{ kg-force}, E_s \approx 5 \cdot 10^{-4} \text{ kg-force}$$

for vaporizers ($\sigma \approx 6 \cdot 10^{-3}$ kg-force/m²)

$$E_k \approx 1.5 \cdot 10^{-4} \text{ kg-force}, E_s \approx 70 \cdot 10^{-4} \text{ kg-force}$$

Thus, under these conditions, the total kinetic energy of the light phase is less than the released surface energy.

This situation could not change substantially if the inequality

of the velocities of individual bubbles were taken into account, since with the usual depth of the bubbling two-phase layer (of the order of 100 to 200 mm), and with a perforated plate, bubble distribution throughout the whole surface becomes rather uniform.

Only with very small thicknesses of the bubbling layer, and with a comparatively large diameter of orifices in the perforated plate, can the vapor bubble velocity at the surface approach its velocity in the orifices of the plate, i.e., become substantial. In this case, or with a very considerable increase in the reference velocity of the gas, the kinetic energy of the gas stream can prove to be greater than the released surface energy.

Up to now, there have been no reliable data on the quantity and especially, the fractional composition of drops tearing away from the surface of the bubbling layers. Therefore, it is impossible to calculate the total surface of the bubbles and to estimate the efficiency of the break-up process. Nevertheless, we can affirm that only a small part of the released energy goes into forming the drops. Here the relative roles played by kinetic and surface energies may not even correspond to the relations given above if the degrees of their utilization will differ. Anyway, with increasing gas reference velocity the drop generation is determined to an ever-greater degree by the kinetic energy of the gas stream. At sufficiently great values of w_0 this process approaches, in its character, the atomization of a liquid by gas jets.

After their formation, the drops move with fairly considerable initial velocity which can cause them to rise in a practically motionless gas to a great height. For example, K. A. Blinov observed that

drops were ejected in atmospheric air to more than 2 m above the bubbling layer of water. However, such a height is reached only by individual drops that have the greatest velocity, and a nearly vertical direction of flight at the instant of their break off; and the bulk of the drops is ejected to a considerably lesser height (Fig. 9-1). At low gas densities (air at atmospheric pressure, for example), the height of ascent (the "ejection") of relatively large



Figure 9-1. Part graph of trajectories of ejected drops due to the collapsing of air bubbles on the water layer surface

drops is determined, for practical purposes, only by the direction of the initial velocity vector. At high gas densities, as for very small drops, resistance of the medium begins to play a noticeable role. Thus, for example, for drops 0.2 mm in diameter flying up vertically at an initial velocity of 2 m/sec. in motionless steam, the height of ascent decreases from 100 mm at $p = 1$ atm. abs.

($\gamma'' = 0.6 \text{ kg/m}^3$), to 10 mm at $p = 110 \text{ atm. abs.}$ ($\gamma'' = 60 \text{ kg/m}^3$).

For practical purposes, gas may be considered motionless at very small values of w_0'' only. At considerable gas velocities we must take into account the effect of the gas velocity proper on the height of drop ascent.

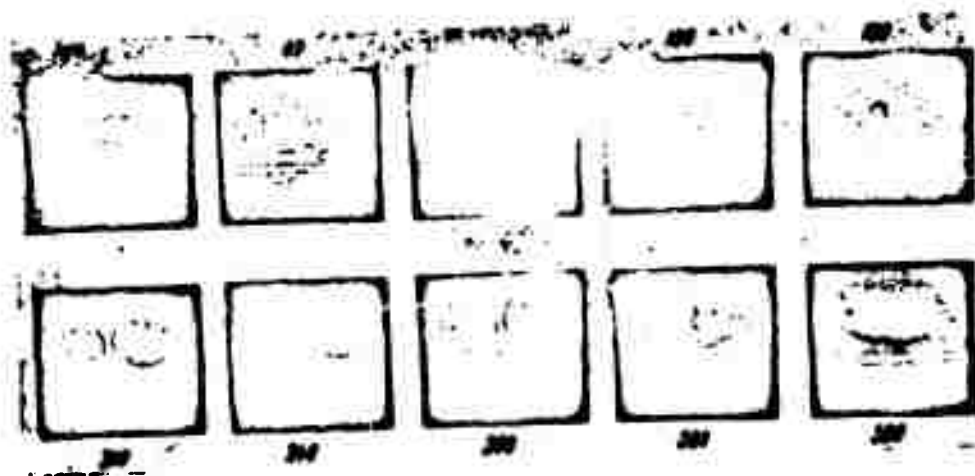


Figure 9-1. Sequence of frames showing the fall of a drop onto the liquid surface and the formation of a new drop.

The presence of a definite gas velocity increases the total height of ascent of all the drops. This circumstance takes on substantial importance when the quantity w_0'' becomes comparable with the velocity of settling of the drop (see Chapter 1).

When $w_0'' > w_{sett}$, independently of the direction of the initial velocity vector, the height of ascent becomes unlimited; i.e., the drop will be carried off with the gas stream. The drops, rising to a limited height, fall back if this height is less than the height of the stable column. Here new drops may be formed (Fig. 9-1). Upon

reaching the top of the column, the drops are entrained in the gas outlet pipes or, in some instances, partially separate on the ceiling surface.

In those cases where the drops which are carried along to the top of the equipment are partially separated in the gas outlet installations, this process should be examined separately, together with the process of drop separation from the stream in special separators.

Separators usually work on the principle of drop precipitation on a wetted surface with a subsequent run-off of the forming liquid film. Spray* separators are extremely diversified, both in their design and in fundamental layout.

9-2. Mechanism of Drop Formation on the Surface of a Dynamic Two-Phase Layer

As has been indicated above, at moderate rates of bubbling a fundamental role in drop formation is played by the burst of the bubble shells on the surface of the dynamic two-phase layer. A high-speed motion picture photograph shows that as a bubble rises to the surface the liquid raised by it runs off from the formed spherical cap, and the liquid film gradually becomes thinner. Finally, at the highest point of the spherical cap, an opening is formed; the forces of surface tension become unbalanced and the opening widens faster (Fig. 9-3).

When the interface is clean, the film is usually drawn into the bulk of the liquid, and the cavity on the surface is filled with

*The term "spray" here and further on refers to the drop-wise entrainment of any liquid by a gas stream. Not only a gas or vapor, but also some other liquid that is relatively lighter than the liquid entrained, may act as the entraining medium.

liquid rushing toward its center. As a result, an annular wave is formed, which, on closing, causes a column of liquid to splash upward; one or more drops may break off once more from this column (Fig. 9-4). In other cases, the collapse of the shell is accompanied by the appearance on its surface of a series of ruptures, with film fragments separating from the liquid mass and coagulating into separate drops. The last form of collapse is especially characteristic of an impure interface when the bubble shell, prior to its rupture, succeeds in attaining a small thickness along the entire surface of its spherical cap, and not just at its peak. At the same time, a considerable number of minute "transportable" drops are formed which are easily entrained even at low upward velocities of vapor.

The pattern described above was observed in the collapse of single bubbles. In the case of a high rate of bubbling, interaction develops between adjacent collapsing bubbles. This interaction can lead to considerably higher rates of drop formation, due both to the interference of the generated waves and to an easier break-up of the simultaneously bursting films of adjacent bubbles.

As the rate of bubbling increases, the kinetic energy of the gas

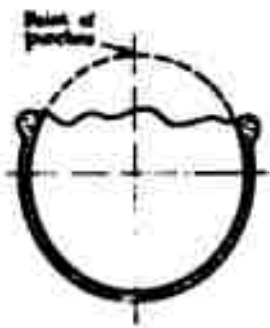


Figure 9-3. Diagram showing collapse of a free bubble.



Figure 9-4. Separation of a series of droplets from the periphery of an annular wave.

begins to play an ever-greater part, and at very high w_0'' , the drop formation process begins to approach the process whereby a liquid breaks up in a rapid stream of gas. In this case, formation of large drops entrained by the gas stream out of the two-phase layer increases radically. Finally, the increase in the rate of bubbling leads to a complete washing out of the two-phase layer and to the entrainment of the entire heavy phase.

9-3. Motion of Drops Torn Away from the Surface in a Gas Stream

Liquid drops torn away from the surface of the bubbling layer can be of widely different sizes--from fairly large, 1 to 2 mm in diameter to extremely small, of the order of several microns. The initial velocity of the drops, especially that of small drops, also varies, within considerable limits, sometimes reaching magnitudes exceeding by many times the velocity of their free fall, i.e., their "settling" velocity.

At the initial stage of their trajectory, the drops may rise with a velocity considerably exceeding the upward velocity of the gas. In such a case, the drop motion is noticeably slowed down by the drag of the medium. This slowing down is especially pronounced for small drops, and at high gas density.

As the upward velocity decreases, the drag of the medium decreases rapidly, and at $w_{ud}' \leq w_0''$ it becomes negative; i.e., the gas stream begins to entrain the drop upwards.

If the gas velocity w_0'' exceeds the settling velocity of the drop, the drop will be carried upwards by the gas to an unlimited height

(completely transportable drops). If $w_{\text{set}} > w_0''$, the drop, having lost its initial energy, begins to fall with a velocity equal to $w_{\text{set}} - w_0''$. The maximum height to which such drops rise depends on the vertical component of the initial velocity of the drops w'_{initial} , on the settling velocity w'_{set} , and on the upward velocity of the vapor w_0'' .

When $w_{\text{set}} \gg w_0''$ (large drops at low upward velocity of the gas), the height of ascent of the drop depends only slightly on w_0'' (region of nearly complete ejection). On the other hand, when the quantities w_{set} and w_0'' come closer, the height of ascent will be determined almost entirely by the value of w_0'' (region of transportation).

The probability of a collision and agglomeration of drops is low because of their extremely small concentration by volume in the gas stream. The probability that the drops will break up in the stream is also slight since the drops are small and the velocities of the gas low. Consequently, for all practical purposes, the influence of both these factors may be neglected (with the exception, perhaps, of the case--rarely encountered in engineering equipment--where the moisture content of the stream is high, or the case where such apparatuses operate at nearly critical pressures).

In a saturated vapor-liquid system, the evaporation of small drops within the vapor stream may play a certain role in connection with the increased curvature of their surface. This evaporation leads to the supercooling of the vapor which, in its turn, slows the process of evaporation. On the other hand, the supercooled vapor begins to condense on the largest drops in the gas stream, or on the liquid films covering the walls of the equipment. Thus, the polydisperse system of drops in a vapor stream is thermodynamically unstable, and, provided it remains undisturbed for a sufficient length of time, all the drops

must collect on the surface of least curvature--the walls of the bubbler.

In large-sized equipment, condensation on the walls can be substantial only for the zone near the walls. In the rest of the stream, condensation will take place on the large drops; these drops will increase up to a size where ($w_{set} > w_0''$), and then begins to fall. As a result, provided the gas remains in the liquid for a sufficient length of time, even in an unlimited cross section of the apparatus, the gas stream should become completely free of drops. In practice, this process occurs slowly, and at the usual length of time the gas stays in the column (0.3 to 1 sec at 1 atm. abs. and up to 30 sec at 180 atm. abs.), its role is evidently not great. This was verified by experiments by A. A. Andreyevskiy and Ya. G. Vinokur, who brought the time of stay as high as 25 to 30 sec at 1 atm. abs. (i.e., 30 to 60 times the usual length of time). At the same time, it was not only impossible to obtain nearly complete condensation, but the usual character of the laws governing the process of drop entrainment did not vary at all.

9-4. Some Experimental Data on Drop Entrainment by a Gas Stream from a Bubble Column

A rather large amount of experimental data on drop entrainment by a gas stream is available. However, only the data obtained in recent years by use of the newest methods of measurement (by means of radioactive isotopes, in the first place) are reliable in the most interesting range of small coefficients of entrainment: 10^{-4} to 10^{-6} .

The coefficient of entrainment is expressed as follows:

$$\epsilon = \frac{W_d}{G}$$

(9-3)

where $\sum G_d$ is the total weight of drops and G is the weight of gas.

For a vapor-liquid system

$$\epsilon = 1 - x,$$

where x is the fraction of liquid in the vapor.

Such low entrainment coefficients are of great importance, particularly in modern steam power installations where it is necessary to obtain steam containing no more than $1 \cdot 10^{-7}$ of non-volatile impurities from water containing a considerable fraction of salts.

Requirements are still higher in nuclear electric power plants, where, in evaporating radioactive wastes, it is necessary to ensure that the fraction of salts in the vapor is not more than 10^{-8} of the fraction of salts in the boiling water, and in homogeneous boiler reactors--even less. In order to obtain these degrees of vapor purification one must resort to scrubbing the vapor with condensate. However, values of ϵ of the order of 10^{-6} and even 10^{-7} can also be obtained by purely hydrodynamic means. The data on gas-liquid systems are fewer, and as a rule the data are reliable only in a region of relatively high entrainment coefficients ϵ (of the order of 10^{-2} to 10^{-3}).

At present the most detailed investigation has been made of a one-dimensional flow diagram of 2 vertical columns of constant cross section above a liquid layer through which vapor is bubbled. In this case, the process is described both by quantities determining the hydrodynamics of the two-phase layer and by quantities determining the performance of the vapor space of the column. Of the latter

quantities only the geometrical ones--the height H_{col} of the vapor space of the column, and its diameter D_{col} --are not among the quantities characterizing the performance of the two-phase layer. Moreover, the quantity μ is important for the processes taking place in the vapor space.

When the ratio of the column diameter D_{col} to its height H_{col} is great enough, the influence of the side walls can be neglected, and accordingly D_{col} can be eliminated from the number of the important quantities.

The height of the vapor space in the column can be considered as a design quantity (for example, from the perforated-plate level to the column top). Nevertheless, it is more rational to reckon the height of the vapor-gas space from the actual surface of the dynamic two-phase layer -- i.e., to allow for a decrease in the height of the vapor space due to swelling.

The assumption of the actual height of the vapor space H_{col}'' as a fundamental quantity makes it easier to bring out the influence of the change in the parameters of the bubbling layer as a generator of drop spray, and of the vapor space as the separator of this spray.

Complete separation of the functions of these two parts of the bubbler would require measuring the quantity of liquid torn away from the surface, an extremely difficult measurement to accomplish. Nevertheless, some idea of the part played by the separator space can be visualized by reference to data from experiments by Bartolomey, conducted with various heights of the vapor space.

From the data shown in Fig. 9-5, it is apparent that an increase in H_{col}'' from 280 to 700 mm decreased the entrainment coefficient from 0.16 to 0.00074; i.e., to less than 1/200 of its initial value.

Thus, under normal conditions the bulk of the liquid torn away from the bubbled layer surface falls back on this layer, and only a very small part of the drops reach the top of the vapor space.

F-TS-9814 V

parated in the vapor-collecting equipment and returned to the column. In such cases, the column is tested, strictly speaking, together with the auxiliary separator, whose features affect the over-all result of the investigation. Therefore, it is more accurate to conduct experiments with a vapor-collecting equipment design in which all the spray reaching the top of the column would be drawn off with vapor.

Investigation of the fractional composition of the drops rising to one height or another, depending on the velocity of the light-phase stream, are of particular value for evaluating roles played by individual factors in the over-all drop entrainment.

Basically, such investigations have been conducted only for an air-water system at a pressure close to 1 atm. abs. As the data from these investigations indicate, at small w_0'' , as a rule, large drops are ejected to a comparatively low height, and only with a considerable increase in the velocity of the light phase does the height to which large drops are ejected increase. Thus, according to K. A. Blinov's data, the maximum height of ejection amounts to only 300 mm at $w_0'' = 0.24$ m/sec, attains 500 mm at $w_0'' = 0.4$ m/sec, and reaches 700 mm at $w_0'' = 0.55$ m/sec.

Therefore, even with an extremely small height of the vapor space (200 mm), but at low gas velocities ($w_0'' = 0.1$ m/sec.), it is mostly the smallest drops transportable by the stream which are entrained; as gas velocity increases, so does the role of ejection, and even at $w_0'' = 0.3$ m/sec a considerable fraction of the entrainment consists of drops whose settling velocity is greater than the upward velocity of the stream.

The fraction of transported drops in the total weight of all the entrained spray is shown in Fig. 9-5 from data by G. M. Yusova.

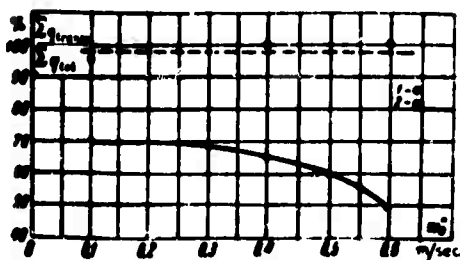


Figure 9-6. Fraction of transported drops ($w_{\text{set}} \leq w''$) in the total entrained mass. Air-water system; $t \approx 20^\circ$; $p \approx 1$ atm. abs.; (1) $H_{\text{col}}'' = 400$ mm; (2) $H_{\text{col}}'' = 200$ mm.

Despite the scarcity of experimental material, it may be seen that at $H_{\text{col}}'' = 200$ mm half of the drops are entrained by their ejection, starting from $w_0'' = 0.60$ m/sec. At the same time, at $H_{\text{col}}'' = 400$ mm, the decisive predominance of transported drops (95 to 98%) is also maintained at $w_0'' = 0.6$ m/sec, particularly if it is taken into account that the maximum upward velocity

of the gas somewhat exceeds the mean velocity (the points falling outside the line at $H_{\text{col}}'' = 400$ mm are the result of the presence of only single large drops in some tests and, thus of considerable deviation in computing their fraction in the over-all entrainment). Thus, at small velocities and moderate heights, the total entrainment is basically determined by the presence of minute spray particles capable of being transported by the gas stream.

With an increase in w_0'' , the number of large drops and the height of their ejection both rapidly increase; accordingly, in this region one should expect a rapid increase in entrainment with an increase in the load, and a sharp decrease in the entrainment with an increase in H_{col}'' . However, even at high gas velocities, the influence of the height of the column is probably significant only up to certain values of $H_{\text{col}}'' > H_{\text{max}}^{\text{eject}}$, entrainment need not depend on H_{col}'' .

It should be noted that only single drops are ejected to the maximum height. Therefore, the role played by the transported drops now becomes dominant at heights considerably less than H_{\max}^{eject} .

According to K. A. Blinov's data the transport of water drops by air at atmospheric pressure accounts for the overwhelming part of the entrainment at $H_{\text{col}}'' = 500$ to 800 mm, even at $w_0'' = 1$ m/sec, when the maximum height of drop ejection exceeds 1000 mm.

Experimental data on the over-all coefficients of drop entrainment are most complete for the steam-water system. For this system, the relationship between the entrainment coefficient and the load on the vaporization surface R_s [$\text{m}^3/\text{m}^2 \text{ hr.}$], or steam velocity w_0'' [m/sec.], has been studied for an extremely wide range of entrainment coefficients--from $\sim 2 \cdot 10^{-6}$ to $\sim 1 \cdot 10^{-1}$.

Regardless of the existence of some discrepancies in the data of individual research workers, one can affirm that in the region of small w_0'' the entrainment coefficient increases very slowly with load, especially at great heights of the vapor space.

Thus, according to M. A. Styrikovich, G. Ye Kholodovskiy, and Ya. G. Vinokur (Fig. 9-7), at atmospheric pressure and with a change in w_0'' from 0.02 to 0.1 m/sec and $H_{\text{col}}'' \geq 500$ mm, $\alpha \sim w_0''^{0.6}$.

With a further increase in w_0'' , the entrainment coefficient increases in proportion to w_0'' , reaching approximately 0.005% at $w_0'' = 1$ m/sec.

These data are also confirmed by recent studies at TsKTI [Central Scientific Research Institute for Boilers and Turbines] (Yu. V. Zenkevich and A. A. Andreyevskiy), the experimental points of which are plotted in the same figure (Fig. 9-7).

With a further increase in w_0'' , the experimental coefficient

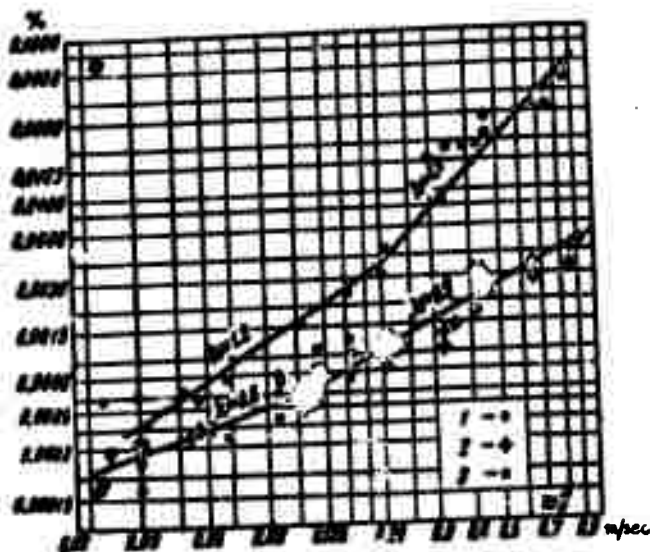


Figure 9-7. Entrainment coefficient vs. reference vapor velocity (tracer $\text{Na}_2\text{HP}^{32}\text{O}_4$) at atmospheric pressure. (1) Height of vapor space referred to gravimetric level $H = 420$ mm; (2) $H = 550$ to 1050 mm; (3) $H > 550$ mm (Experiments at TsKTI).

begins to increase considerably faster, approximately proportionally to $w_0''^3$.

At lesser heights of the vapor space ($H_{\text{col}}'' = 300$ to 400 mm), the entrainment coefficient depends more strongly on w_0'' :

for values of $\omega = 0.0004$ to 0.004% , $\omega \sim (w_0'')^{1.2}$;

for the range $\omega = 0.004$ to 0.04% , $\omega \sim (w_0'')^{1.2}$.

With a further increase in vapor velocity the exponent increases as much as 3 to 4-fold, while at entrainment coefficients $\omega = 0.2\%$, it increases 6 to 8-fold and above.

Analogous relationships are also obtained at higher vapor pressures. The relationship $\omega = f(R_s)$ is shown in Fig. 9-8 for pressures of 17, 91, and 110 atm. abs., according to L. S. Sterman's data at $H_{\text{col}}'' = 500$ to 600 mm.

The relationship $\mu \sim w_0^3$ applies at constant values of H_{col}'' in the μ range between 0.003 to 0.004 and 0.04 to 0.1%. At large μ (from 0.05 to 0.1% to as high as 0.5 to 0.7%) the entrainment coefficient increases proportionally to the 6.5 to 7th power of the velocity of the steam.

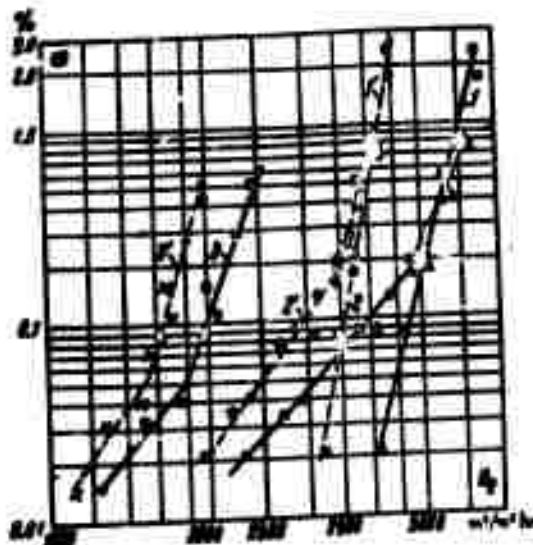


Figure 9-8. Comparison of data obtained at 17, 36, and 91 atm. abs., and $h_{space} = 460$ to 480 mm. 1 and 1' : $p = 17$ atm. abs.; 2 and 2' : $p = 36$ atm. abs.; 3 and 3' : $p = 91$ atm. abs. Dotted line: swelling disregarded; solid line: swelling taken into account.

Analogous data for a pressure of 185 atm. abs. at $H_{col} = 800$ mm, reveal a region of very slight dependence of the entrainment coefficient on the load ($w \sim w_0^{1.2}$)--the same dependence as at 1 atm. abs.

All data indicated above were obtained at a considerable thickness of the bubbling layer ($h_{lay} = 150$ to 250 mm). Therefore, for the identical true vapor-space height H_{col}'' , the geometric characteristics of the perforated plate (D, ψ_1) have no noticeable effect on the quantity of spray entrained by vapor (gas).

The influence of the bubbling-layer thickness h_{lay} itself is,

of course, also negligible at a constant true height of the vapor space.

On the other hand, at small values of $h_{lay} = 5$ to 50 mm, which are characteristic of bubble columns in the chemical industry, the influence of the change in h_{lay} and of the design parameters of the perforated plate (ϕ_1, D) on the entrainment is rather considerable.

The effect of the true height of the vapor space (H_{col}'') (other conditions being comparable) has not been thoroughly studied.

According to M. A. Styrikovich and Bartolomey (Figs. 9-5 and 9-9) at 1 atm. abs., as H_{col}'' increases at $w_0'' = \text{const}$, a rapid decrease in the entrainment coefficient is noticeable, which, in the range $H_{col}'' = 250$ to 500 mm, can be expressed approximately by the relationship $\epsilon \sim (H_{col}'')^{-6}$. At $H > 550$ mm the influence of the height weakens markedly, and its increase over 700 mm will slightly affect the entrainment coefficient. This relationship, revealed at $w_0'' = 0.65$ m/sec, is preserved qualitatively also at other values of w_0'' .

According to V. A. Kolokol'tsev's experiments ($p = 1.3$ atm. abs.), a much weaker relationship between ϵ and H_{col}'' is revealed ($\epsilon \sim H_{col}''^{-2}$), but this also becomes very weak at $H > 500$ mm. A qualitatively analogous relationship was obtained by K. A. Blinov at a pressure of 9 atm. abs. in a column large in diameter (500 mm) at small steam velocities. According to T. Kh. Margulova, this relationship has an analogous character also at high pressures (100 to 185 atm. abs.). According to L. S. Sterman, at pressures of 17 to 110 atm. abs., within the height range from 450 to 800 mm, the relationship between entrainment and height takes the form

$$\epsilon \sim (H_{col}'')^{-2.5}.$$

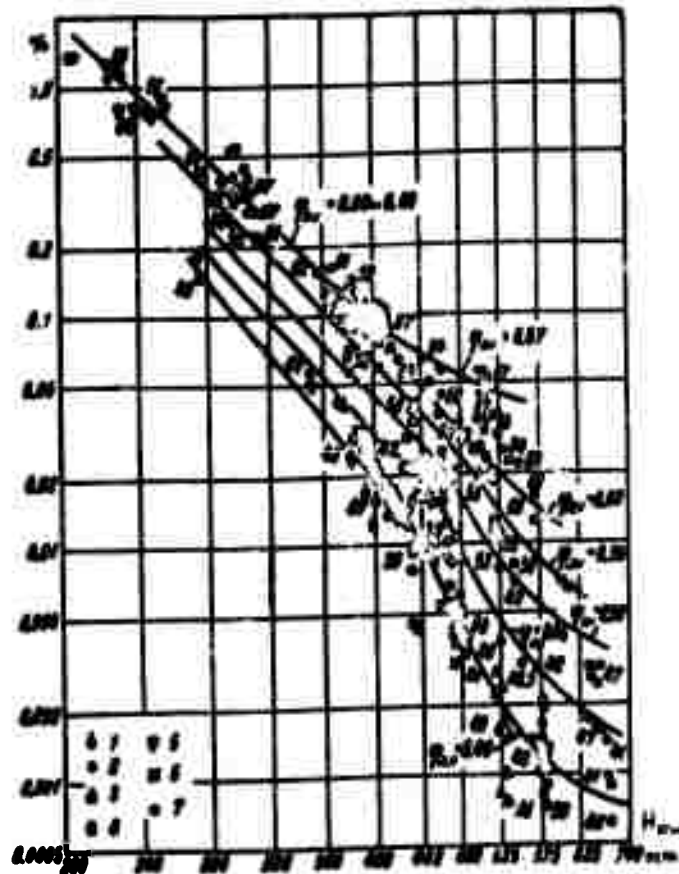


Figure 9-9. Salt entrainment coefficient vs. true height of vapor space for various volumetric fractions of steam and at a constant load, $R_g = 2300 \text{ m}^3/\text{m}^2 \text{ hr}$; $h_{\text{gray}} = 120 \text{ mm}$; (1) 360 mm; (2) 400 mm; (3) 510 mm; (4) 560 mm; (5) 610 mm; (6) 660 mm; (7) 760 mm. Values of v_{av} at the points are indicated in percentages.

This relationship applies in that range of changes in the entrainment coefficient where the latter increases approximately at the cube of vapor velocity.

It can be stated that on the whole, in the area of high entrainment coefficients, the influence of height is apparently somewhat

stronger than at small ω when the entrainment occurs basically by means of transport.

The increased effect of height is also noticeable at small diameters of the column, probably in connection with moisture separation on the walls.

Of great practical interest is the dependence of the entrainment coefficient on the physical parameters of the liquid and of the gas, i.e., on pressure (boiling point) in the case of a water-steam system. In practice, the most significant relationship is that between pressure and the equivalent velocity of the vapor; i.e., that velocity at which the entrainment coefficient remains constant at all pressures

$$\omega_{eq} = f(p).$$

This relationship can be single-valued only in that region of change in the variables where the relationship between the entrainment coefficients and the vapor velocity bears an identical character for all pressures.

Thus for the region of medium entrainment coefficients ($\omega = 0.2$ to 0.1%), for which $\omega \sim w_0''^3$, the relationship between $w_{0,eq}''$ and the pressure can be represented by Curve a in Fig. 9-10, assuming w_{eq} at 1 atm. abs. to be unity.

At smaller entrainment coefficients--i.e., in the region described by the empirical equation $\omega \sim w_0''$ --the relationship between $w_{0,eq}''$ and pressure will be expressed less strongly (Curve b). In the region of high entrainment coefficients where $\omega \sim w_0''^{-(6 \text{ to } 8)}$, the relationship

between $w_{0,eq}''$ and pressure is still weaker (Curve 2).

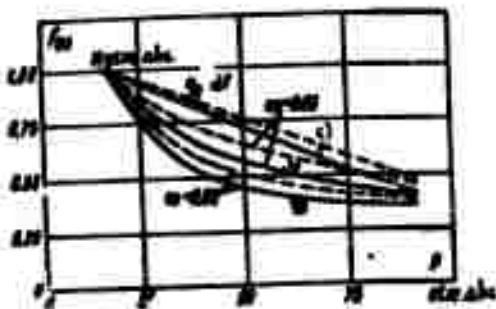


Figure 9-10. Coefficient $f(p)$ calculated by loads, swelling taken into account. Solid line: $h_{space} = 460$ to 480 mm; dashed line: $h_{space} = 842$ to 865 mm.

As is apparent from what has been said above, the basic relationships established are essentially qualitative even for the most highly studied water-steam system. Quantitative discrepancies between individual investigations are quite considerable in a number of cases. This is explained both by the complexity of the phenomenon and the dependence of the entrainment coefficient on many parameters, as well as by the fact that only recently have methods of measurement been developed which are sufficiently sensitive for determining very low values of this coefficient.

An important role is played also by the fact that reliable measurement of the actual height of the vapor space (taking into account the swelling of the layer) became possible, especially at high pressures, only in recent years.

Very substantial discrepancies can also occur due to changes in the strength characteristics of the bubble shells, associated with the presence in the water of impurities of one kind or another. This

factor especially affects the regions of small entrainment coefficients when the great bulk of the entrainment consists of minute transported drops--products of the collapse of bubble shells. Unfortunately, at this time, there exists no reliable criterion for evaluating the influence of surface-active impurities, which, even when present in very small concentrations in the liquid, can exert a very great influence on the structure of the bubble shells.

In engineering equipment built from common grades of steel, the presence of finely dispersed slime in the water of one of the layers also exerts a considerable influence.

The influence of these impurities on the character of the "swelling" of the dynamic two-phase layer has already been mentioned in Chapter 5.

The influence of the salt content on the entrainment of spray by vapor is not great in the region of moderate salt content, but it increases strongly in a certain range of concentration changes in the same range where the conditions of operation of the bubbling layer of water vary sharply.

The effect of this factor is well illustrated in Fig. 9-9, which shows the dependence of the entrainment coefficient on the vapor-space height and on the mean vapor fraction $\bar{\varphi}$ in the two-phase layer at a constant vapor velocity. The change in the average fraction of vapor which, for a given column design, vapor velocity, and pressure, depends only on the properties of the water, characterizes most objectively the state of the layer.

In Fig. 9-9 the values $\bar{\varphi} = 0.4$ correspond to that region of small fractions ($S_{bw}^* < 1000 \text{ mg/kg}$) where a change in the concentration

*Boiling water.

of the solution noticeably affects neither the layer swelling nor the entrainment of spray. On the other hand, the greatest values of $\bar{\varphi}$, which at a given vapor velocity ($w_0'' = 0.64$ m/sec) are equal to $\bar{\varphi} = 0.67$, correspond to that region of high fractions of salt ($s_{\text{dw}} > 10,000$ mg/kg) where further increase in the concentration of the solution, for all practical purposes, affects neither the layer swelling nor the entrainment of spray with vapor.

As is apparent in Fig. 9-9, the entrainment coefficient at maximum fractions of salt ($> 10,000$) is many times greater than the values of α at small concentrations ($< 1,000$). The difference is especially great in the region of large vapor-space heights ($H_{\text{true}} = 500$ to 700 mm) where the bulk of the entrainment is due to the presence of minute drops transported by vapor.

In the region of small heights -- where the bulk of the entrainment consists of larger drops which cannot be entrained by the upward velocity of the vapor, but reach the top of the column due to their initial velocity ("ejection") -- the role of the salt content is considerably weaker.

Actually the region $H_{\text{true}} = 500$ to 700 mm, the entrainment ratio at $\bar{\varphi} = 0.4$ and at $\bar{\varphi} = 0.67$ reaches 20 to 25 and even higher, while for the height $H_{\text{true}} = 300$ mm it only amounts to about 4. Even the latter figure is sufficiently great, however, and consequently the entrainment due to drop ejection also increases quite considerably with increased "foaming" of the water, although not quite so much as the entrainment associated with the transport of minute drops.

It should be noted that in experiments with a variable fraction of salts in water it is very difficult to obtain a reliable reproducibility of the results. The smallest changes in concentration of impurities, especially organic ones, sharply distort the dependence of

entrainment and swelling on the fraction of salt, particularly in the range of small values of the latter. The dependence on $\bar{\varphi}$ is considerably more stable; apparently this quantity well characterizes precisely those properties of the solution which are important for the drop entrainment process.

Unfortunately, very few investigations of entrainment have been made up to the present time with a reliable determination of $\bar{\varphi}$. Under conditions of a "foaming" liquid, this requires that radioscopy be carried out over the whole cross section of the layer -- since, with $\bar{\varphi}$ changing continuously over the cross section in these cases, other methods of measuring $\bar{\varphi}$ do not give reliable results.

9-5. Stripping of the Liquid Film

Separation of liquid drops from the gas stream can be due to turbulent fluctuations and to centrifugal forces.

The so-called linear separator is the most simplified separator, being based entirely on the transfer of drops by turbulent fluctuations and their precipitation on the wetted wall. In its simplest form, this separator is a long straight tube in which the gas flow entraining liquid drops is moving. As a result of turbulent fluctuations in the gas stream, single drops travel in a radial direction. After reaching the wall of the tube wetted by the given liquid, the drops settle on it and form a continuous liquid film. Further separation takes place on the surface of the moving liquid film.

Liquid films form on the effective surfaces (baffles, cyclone walls, etc.) of other types of separators as well.

The process of separation continues until the gas stream begins

to tear the liquid away from the film surface; i.e., until the process of secondary wetting of the gas stream arises.

Examining conditions under which drops are torn away by the gas stream from a free liquid surface, it is easy to prove that the character of the interacting forces under these conditions does not differ from the process of structural change in the two-phase boundary layer.

In this connection, Yu. V. Labinskiy noticed that S. S. Kutateladze's formula (7-13) is also applicable in the given case if we replace the vaporization velocity $\frac{q}{r\gamma}$ by the velocity w , analogous to (4-28).*

As concerns linear tubular separators on the basis of L. K. Ramzin's experiments, it can be assumed that the critical gas velocity (at which secondary wetting begins) is determined by the formula

$$\bar{w}_{cr} \approx 2.1 \sqrt{\frac{\sigma}{\rho_l(\rho_l - \rho_g)}} \sqrt[3]{\frac{\gamma}{r}}. \quad (9-4)$$

Conversion of critical loads of a given type of separator to various pressures may be carried out by means of the formula

$$\frac{R_{a,cr,1}}{R_{a,cr,2}} \approx \sqrt{\frac{\sigma_1 \rho_{l1} (\rho_{l1} - \rho_{g1})}{\sigma_2 \rho_{l2} (\rho_{l2} - \rho_{g2})}} \sqrt[3]{\frac{\gamma_1}{\gamma_2}}. \quad (9-5)$$

See also Criterion (5-7).

Yu. V. Labinskiy has shown on the basis of experimental data, the applicability of Formula (9-5) to the design of a number of separation devices.

CHAPTER TEN

SOME PROBLEMS IN EXPERIMENTAL TECHNIQUE

10-1. Measurement of Liquid-Drop Entrainment

Measurement of liquid-drop entrainment by a gas (vapor) can be conducted by various methods. However, for this a test sample from the stream with a subsequent determination of the fraction of liquid in the sample is almost always required. Therefore, it is necessary to examine separately both the problem of obtaining a representative sample and that of determining the respective fractions of liquid and gas in the sample.

In obtaining a representative sample accurately characterizing the mean ratio of gas and liquid in the stream, very great difficulties are encountered in any two-phase system. In selecting a sample directly from the column, it is necessary, as is well known, to fix the axis of the sampling tube in the direction of flow and to maintain at the tube entrance a velocity equal to the flow velocity. Moreover, in locating the sampling tube in an ascending flow there is always the danger that the drops collecting on the inside surface of the sampling tube will drip back into the stream. With a low upward velocity, this is very difficult to avoid.

It is still more difficult to set up an accurate sampling from

outlet tubes, since, when a gas (vapor) containing drops of liquid moves in tubes, these drops collect rapidly on the inside surface of the tubes, and the test sample from the core of the stream will provide a fraction of liquid that is too low.

The most accurate results are obtained in test sampling by means of a small tube placed at the opening of the sampling tube (Fig. 10-1), where drops have not yet been able to collect on the walls. Results are less accurate if special devices are placed in the tube which strip the film away from the walls and the test

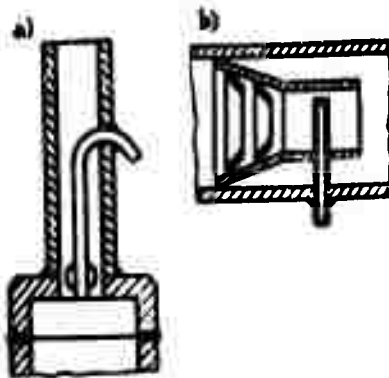


Figure 10-1. Diagram of a spray-sampling device: (a) test sampling at entrance of vapor outlet tube; (b) device with a TsKTI mixer.

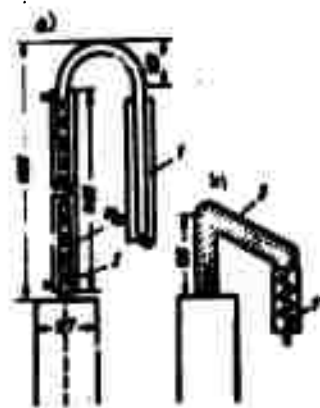


Figure 10-2. Diagram of vapor outlet of test column in experiments by Andreyevskiy and Zenkevich: (1) condensers; (2) steam jacket; (3) heat insulation.

sample is taken directly behind these devices. In this case one has to take into account the errors associated with the pronounced non-homogeneous distribution of the drops throughout the cross section of the flow, and the fact that the velocity of these drops differs greatly from the velocity of the vapor stream.

Coefficient of salt entrainment from boiler water $\times 10^4$

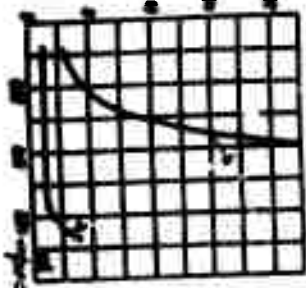


Figure 10-3. Comparison of data obtained in devices shown in Figure 10-2.

Similar errors also arise when all the vapor containing drops escapes along the outlet up-tube with low velocities.

Figure 10-2 shows two alternatives for vapor withdrawal from the column, which were used in experiments by Andreyevskiy and Zenkevich, while Fig. 10-3 shows the results obtained in these experiments.

As is apparent from Fig.

10-3 (Curve a), when one uses a very long up-tube of considerable diameter ($d_{in} = 18$ mm), the entrainment coefficient is many times lower than for a short uptake section of small diameter ($d_{in} = 8$ mm, Curve b), since the great bulk of the spray carried out of the column separates on the tube walls and dribbles back into the column. Only when the velocity in the outlet tube reaches approximately 11 m/sec (w_0 in column = 0.22 m/sec) does the entrainment begin to increase considerably due to re-entrainment by the gas stream of part of the spray separated on the wall of the vapor tube.

It is possible to avoid errors associated with test sampling of the two-phase flow if, prior to sampling, the entire stream is converted into a single-phase state. During studies of the liquid entrainment by vapor, condensing (at atmospheric pressure) at temperatures higher than room temperature, this state is easily attained because the entire stream is cooled to a temperature below the normal boiling point. It is also possible to convert the two-phase system

into a single-phase one by evaporation of the liquid phase and by sampling from the vapor-gas mixture. The disadvantage of both methods is the necessity to remove or add a considerable quantity of heat; this, in high-capacity apparatuses, requires the installation of large heat exchangers. Prevention of drop separation on the walls of the devices for test sampling or gas withdrawal from the apparatus is essential. When we work with vapors which condense above room temperatures, the drops are swept away by the stream of condensate, and it is only necessary to prevent them from dribbling back into the apparatus. For this, the stream withdrawn from the apparatus should be aimed down so that the drops can be entrained by the stream; Fig. 10-4 serves as an example of such a device, showing a column used in experiments by M. A. Styrikovich, Ya. G. Vinokur, and G. G. Bartolomey.

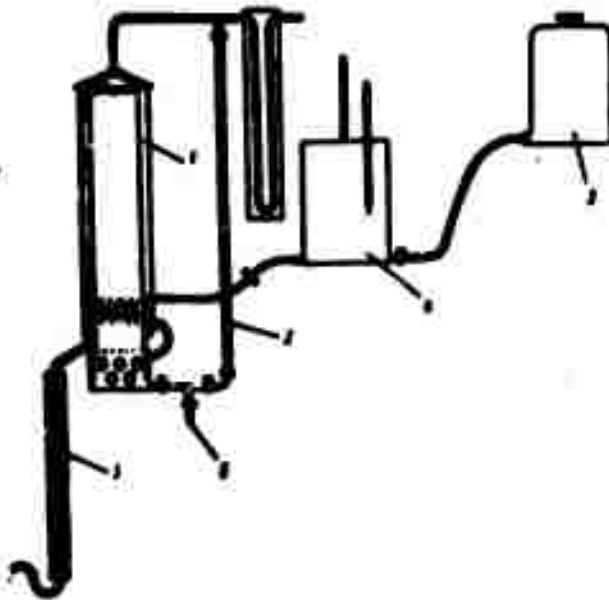


Figure 10-4. Diagram of experimental column with vapor heading downward: (1) separator column; (2) water gauge; (3) condensate cooler; (4) auxiliary feed tank with electrical heating; (5) water storage tank; (6) water sampler.

It may be seen from Fig. 10-4 that the flow, after having reached the top, heads downward along the side channels, and the drops separated on the surface of the top also dribble into the side channels.

Preventing the drops from collecting along the path is considerably more difficult when the gas used will not condense under ordinary conditions. In this case, great numbers of drops collecting on the walls of the conduit can accumulate, and only in the case of a very long experiment will a state of equilibrium be attained.

The errors associated with drops collecting on the conduit walls are particularly great whenever the quantity of liquid entrained by the gas is measured by the fraction in the stream of some substance dissolved in the liquid. In these cases, partial evaporation of the liquid drops settled on the conduit walls and the collecting along the conduit of very great quantities of the substance acting as a tracer of the entrainment may occur.

Considerable time can be saved in the experiment by thoroughly "flushing down" the downtake conduit.

Actual measurement of the fraction of liquid in drop form in the gas flow leaving the apparatus can be conducted by various methods. When the fraction of liquid is considerable, this amount can be determined by measuring the heat content of the mixture. In experiments with liquid-vapor systems of the same liquid we may condense the vapor, measure the discharge of the condensate, its temperature, and the amount of heat liberated per hour --and hence to determine the heat content and thereby also the liquid fraction in the mixture. This method is useful only for very high liquid fractions,

when the heat content of the mixture is substantially below the heat content of the dry vapor.

With low fractions of liquid the method of preheating a wet vapor prior to its superheating is more accurate, since in this case it is sufficient to superheat the vapor by a few degrees; thus, a larger fraction of the total heat supply will be expended for vaporizing the spray. In a well-organized calorimetric measurement of the flow, when the error in the heat balance over the calorimeter is reduced to approximately 2% of the supplied heat, it is possible by this means to measure a liquid fraction of the order of 0.2% with relative precision (10% error) in a water-steam system, for example, at 1 atm. abs. However, this requires that the measurements be carefully conducted (superheat must be maintained on a level not exceeding 2°C, temperature must be measured with a precision of up to hundredths of a degree, flow rate up to fractions of 1 per cent, etc.) and may be achieved only if the vapor flow rate through the calorimeter is so considerable that its heat losses are relatively small.

Formerly, a method of throttling the vapor sample down to a pressure of 1 atm. abs. was often used, suitable for steam at initial pressures up to 100 atm. abs. (at $\leq 4\%$) and even up to 120 atm. abs. (at $\leq 1\%$). With greater liquid fractions and pressures, and when throttling down to 1 atm. abs. is used, the vapor does not become superheated. The method of throttling is very simple, but heat losses to the surroundings--and the difficulties in preventing them by compensatory heating, due to sharp temperature variations along the path of the vapor--make this method unsuitable in practice for any precise measurement of less than 0.2 to 0.3% liquid water in steam.

When working with liquid--permanent-gas systems (the liquid of which is, for practical purposes, non volatile in the gas) we can directly measure the amount of entrained liquid after its separation from the flow. At high entrainment coefficients, this separation can be conducted mechanically, but with small liquid fractions in the stream the errors associated with incomplete collection of the drops in separators become too great. A good separation can be achieved by scrubbing the gas with a layer of a liquid which is a solvent for the entrained liquid, or by passing the flow through a packing which will actively absorb the entrained liquid. However, these methods are very cumbersome.

Indirect methods have received widest application at small entrainment coefficients (hundredths and thousandths of one per cent). Such methods consist in dissolving tracers of various types in the liquid and subsequently determining their concentrations in the samples of gas-liquid mixture. In such a case, the entrainment coefficient is determined as the ratio of the tracer concentration in the gas-liquid mixture to the tracer concentration in the liquid. Salts that are soluble in the liquid and are easily determined chemically--for example, NaCl for water--were formerly used as tracers.

The method now most frequently used involves introduction of radioisotope-containing salts into liquids, and measurement of the entrainment coefficient as a ratio of the specific activities of the gas-liquid sample and of the liquid sample. This method, proposed in 1949 by M. A. Styrikovich, permits the measurement of very small entrainment coefficients while avoiding large salt concentrations in the liquid, which would change physico-chemical properties of the

salts.

Application of these methods repeatedly raised definite objections in connection with the possibility of unequal concentrations of the salt solution in the bulk of the liquid and in the entrained drops--especially in the minute drops obtained as a result of the collapse of bubble shells.

This can definitely take place in organic substances with pronounced surface activity. However, as far as salts are concerned (i.e., fairly active substances), considerable nonuniformity in concentration is highly unlikely. This may be confirmed by Shtump-er's old experiments in which samples of foam and the bulk of the water were taken simultaneously. These experiments revealed a sharp difference in the oxidizability of the two samples and, for practical purposes, an absolute identity in their salt content.

No difference was revealed in the extent of drop entrainment by the liquid as determined from the heat content of the wet vapor (by throttling) or from the coefficient of salt loss; or in L. S. Sterman's experiments if the comparison was made in the range of entrainment coefficients which can be measured accurately enough by throttling.

Experiments by a number of investigators revealed discrepancies between the results of calorimetric determination of the liquid fraction in the vapor and of its measurement in terms of the coefficient of salt loss. This discrepancy was recorded only at low entrainment coefficients where calorimetric determinations are unreliable.

Undoubtedly, there were discrepancies only in those cases where the tracer substance could transfer into the high-pressure vapor, due

to the tracer solubility in the vapor, to an extent commensurate with the drop entrainment coefficient. Therefore, in experiments with high-pressure steam it is preferable to use substances whose coefficient of distribution between steam and water (the ratio of solubility in steam to solubility in water) is known to be much less than the coefficient of mechanical entrainment under the experimental conditions. Most suitable in such cases are sodium sulfate or phosphate, whose distribution coefficient even at $p = 190$ atm. excess --i.e., at almost $0.8 p_{cr}$ --still remains below 10^{-5} .

When using the indirect method for measuring the entrainment coefficient, we must ensure that a reliable measurement is made of the tracer concentration in the liquid through which the gas (vapor) bubble, and that this concentration remains constant in the entire bubbling layer.

Therefore, it is desirable to avoid introducing additional pure liquid, and to prevent dripping of condensate from the walls, into the zone of vapor (gas) separation from the liquid.

If the wet vapor were to remain in the column for a very long period of time (small vapor velocities and great column heights), it would be possible largely to prevent the fine liquid drops on the wall of the vessel from evaporating and condensing on the larger drops.

Evaporation of fine drops due to the increased curvature of the drop surfaces is retarded by supercooling the vapor stream which occurs in the vicinity of these drops. Supercooled vapor condenses on the surfaces of low curvature (the column walls and the surface of large drops). However, when the wet vapor remains in the vapor space of the apparatus for long periods of time, a unit of volume will contain very few small drops and, for practical purposes, there

will be no large drops. Therefore, distillation will proceed very slowly and apparently cannot noticeably affect the total fraction of salt in the vapor.

In the range of small entrainment coefficients the chemical methods for determining entrainment tracer concentration in the condensate sample are not as a rule sufficiently sensitive.

The measurement accuracy can be raised by means of some method of sample concentration; however, such methods are very cumbersome: they require a great deal of time and great quantities of condensate (hundreds of liters).

The use of radioactive isotopes as tracers is incomparably more convenient, since the exceptional sensitivity of this method permits determination of extremely low entrainment coefficients (10^{-5} to 10^{-6} and below) without using methods of sample enrichment. The exceptional selectivity of this method is also very important, permitting avoidance of errors, due to accidental contamination of the sample, that arise easily when other methods are used.

The use of radioactive isotopes also greatly facilitates the correction of errors connected with absorption of the tracer by the conduit walls, vessel walls, etc. A very effective method in this case involves the addition of a nonradioactive sample of the same salt in quantities many times exceeding the anticipated fraction of tracer in the sample.

The technique of applying the radioactive-isotope tracer method has been described frequently in the literature; consequently only certain features are mentioned here in applying the tracer method to the given problem.

10-2. Investigation of the Hydrodynamics of Two-Phase Layers

The main purpose of the investigation has usually been to determine the dependence of the specific gravity (γ_m) of the mixture and of the level swelling (which is uniquely related to it) on the gravimetric level, on the flow rate of the light phase, and on the properties of both substances.

Until recently, these studies were conducted by measuring the two quantities: the gravimetric level h_{grav} and the true level of the mixture h_m .

The measurement of the gravimetric level can be accomplished comparatively easily by means of a water gauge or some differential manometer of one type or another. Depending on the position of the pressure taps (Fig. 10-5), the measurement may yield either the total weight of mixture above the level of the perforated plate (a), or the average weight of the column of mixture between the two taps (b). In the latter case, by using a series of differential manometers, the variation of γ_m with height can also be measured, but only in the range of height segments which are definitely within the bounds of the dynamic two-phase layer.

Another method may be the use of a movable pressure tap, which permits plotting a curve of pressure distribution from top to bottom. When a movable tube is inserted from the top (insertion from the bottom is generally very difficult), the pressure measurement can be conducted by blowing a certain amount of gas into the two-phase layer (Fig. 10-6). In this case, the gas flow rate is reduced

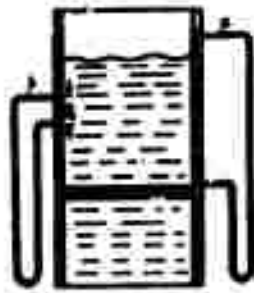


Figure 10-5. Diagram showing pressure tap positions.

At low pressures, visual determination of the layer height is often used; at high pressures and temperatures this is also possible, but the design of sight glasses for visual observation becomes more complex.

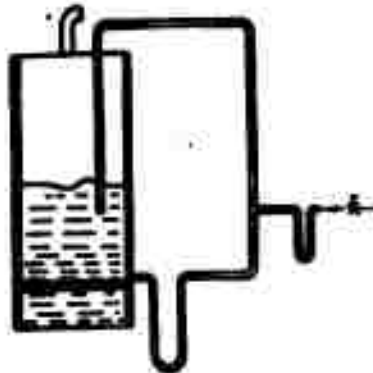


Figure 10-6. Diagram of pressure measurement when a certain amount of gas is blown into the two-phase layer.

to such a small quantity that the pressure losses can be neglected along the gas conduit from the point where pressure is measured to the point where gas is injected into the two-phase layer.

Measurement of the true mixture level is more complicated. At low pressures, visual determination of the layer height is often used; at high pressures and temperatures this is also possible, but the design of sight glasses for visual observation becomes more complex.

In the case of a free level, visual observation is not accurate enough, even by use of objective methods of reading (photographs or motion pictures), especially at considerable light-phase reference velocities.

With an increase in v_g the disturbances on the surface of the two-phase layer increase so that only in relative terms can we speak of a "plane" separating the vapor-phase layer.

Overflow was used in a series of investigations; i.e., the height of the two-phase layer was limited.

ed by means of the continuous overflow of a small quantity of the liquid through an overflow tube (Fig. 10-7), compensated for by a continuous feeding of the corresponding quantity of liquid into the bubble column from the outside.

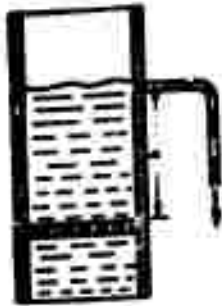


Figure 10-7. Diagram of liquid overflow.

This method leads to certain inaccuracies as well, due to variations in the level, since in this case the overflow-tube orifice is alternately flooded and exposed. The liquid flow rate through the overflow tube then varies from maximum to zero.

If the liquid level were so regulated as to ensure a minimum steady overflow, then the level of the overflow tube would correspond approximately to the level of the deepest troughs between the waves. When the feed is adjusted to give the minimum average overflow, then the level of the overflow tube will correspond approximately to the level of the highest crests of the waves.

The best picture is provided by direct measurement of γ_m by γ - or β -ray radioscopy of the column, the density of the medium being determined from the amount of radiation absorbed in the column.

A device (Fig. 10-8) used for this purpose consists of two lead cylinders placed on both sides of the object to undergo radioscopy. Inside of these cylinders are, respectively, the source and detector of radiation. The cylinders have openings, small in diameter (5 to 15 mm), for passage of a beam of rays located strictly

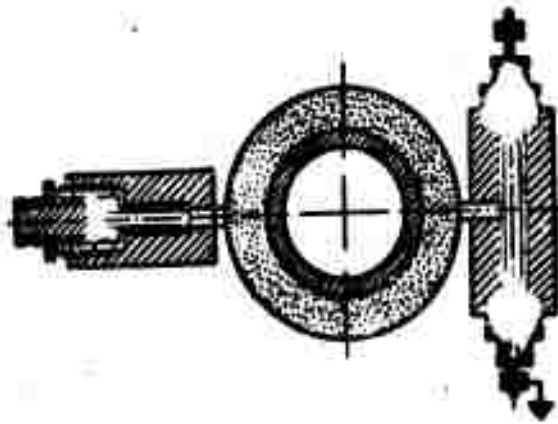


Figure 10-8. Diagram showing arrangement of γ -ray emitter and counter for radio-scropy.

on one axis. A Geiger-Müller tube is generally used as the detector of radiation, and is connected with a counting device or an oscillograph circuit for counting the number of pulses.

It is possible by such a method to measure densities averaged over time and beam length throughout the entire volume of the dynamic two-phase layer. Consequently, it is possible to measure not only the distribution of γ_m along the depth of the layer but also, for example, to measure the change in γ_m along the steam-boiler drum, to control the steady performance of the perforated plate, etc.

If we select a sufficiently high intensity of the radiation source and, instead of the Geiger-Müller tube use a device giving not the record of the number of readings but, directly, the intensity of transmitted radiation (number of γ -quanta per unit time), then we can record also the variation of γ_m with time. It should be taken into account, however, that in this case only the variation of the average intensity along the cross section and according to beam length will be measured. Moreover, it is necessary to account for the fluctuations of the source itself.

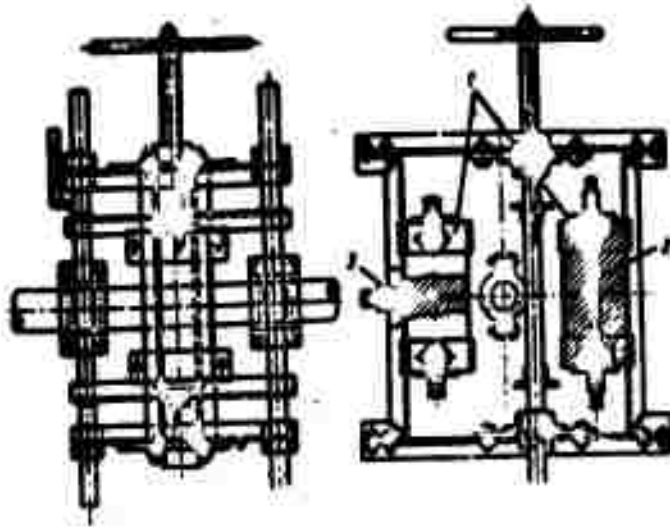


Figure 10-9. Drawing of device for γ -ray radiography of tube. (1) lead casings; (2) counter; (3) ampule with radioactive preparation.

When measuring the distribution of γ_m along the cross section normal to the axis of the ray, we must shift the source and the detector in two directions. At the same time it is very important to maintain the coaxial position of the openings in both protective cylinders. To do this, sufficient accuracy of the shifting mechanism and rigidity of its construction are required.

Figure 10-9 shows a drawing of the installation, and Fig. 10-10 shows an over-all view of it. The movement of the installation is completely automatic and is controlled from a panel (Fig. 10-11). The height to which the frame carrying the source and the detector is raised is recorded through contact assemblies by means of signaling devices.

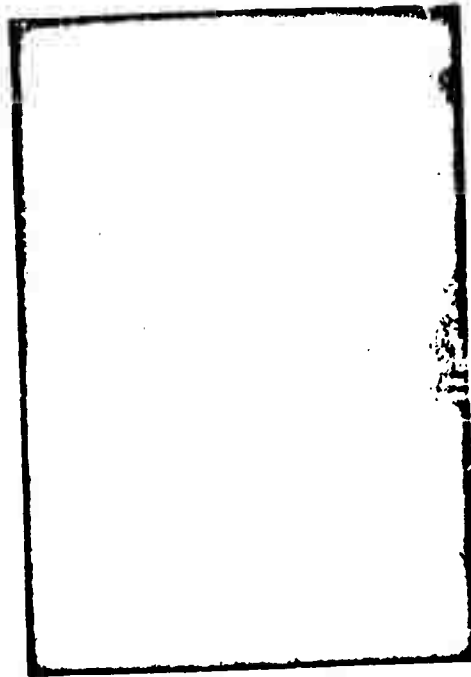


Figure 10-10. Over-all view of the installation.

The network for the control panel and the signaling system is shown in Fig. 10-1, and the hookup of the instruments is shown in Fig. 10-1.

Generally, the pressure drop with change in flow rate of the light phase is measured with a Pitot tube on a U-tube manometer, but in addition, pressure can be recorded by an oscillograph circuit. A manometer with a mechanical transducer designed to relay pressure pulses to an oscillograph can be used as pickup.

Bending of the manometer spring gauge changes the (mechanical) resistance of the device. This resistance is registered on an ID-strain gauge whose output is connected to the measuring oscillograph circuit (the regulating device). Before recording oscillograms, the

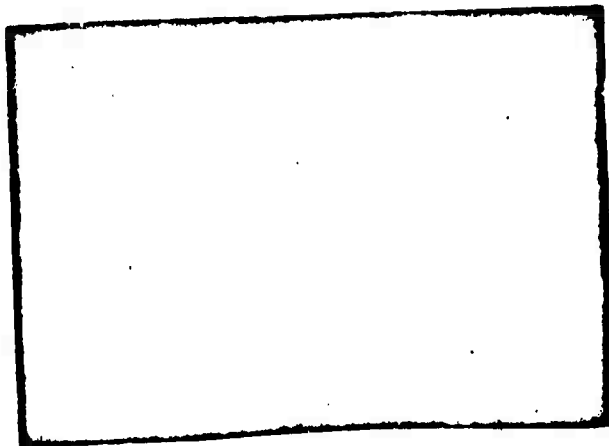


Figure 10-11. Control panel.

Counting rate of γ -tube is determined.

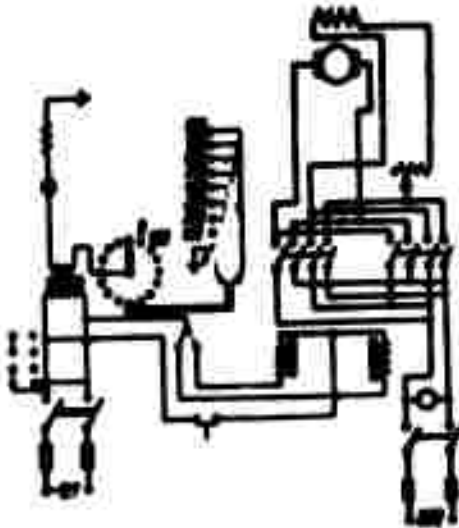


Figure 10-12. Circuit diagram of control panel and the signaling devices.

When measuring with counters, it is necessary to consider a series of factors influencing the results of the measurements, and to introduce corrections. Here are several of the most important corrections: (a) error due to fluctuation of the number of pulses in a given time interval; (b) error in the pulse count due to resolving time; (c) background correction; and (d) reproducibility of counter. Work with counters is described in greater detail in the literature.

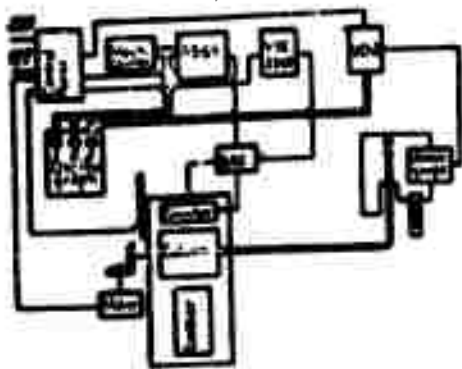


Figure 10-13. Schematic hookup of instruments.

Here we will merely dwell on the fact that the background during measurements, which is the sum of the natural and the specimen backgrounds, should be minimized as far as possible. The magnitude of the specimen background should be brought close to the magnitude of the natural background; this can be achieved by a device specially designed to reduce the scattering of γ -rays as they leave the main

conduit and as they are transmitted to the counter.

Prior to conducting measurements for determining the density of the two-phase layer, it is necessary to determine the γ -ray absorption coefficients of the components of the two-phase stream under study.

The γ -ray (Co^{60}) absorption coefficients for water, mercury, and carbon tetrachloride have the following values:

$$\mu \text{ of mercury} = 0.84 \text{ cm}^{-1}; \quad \mu \text{ of water} = 0.06 \text{ cm}^{-1};$$

$$\mu \text{ of CCl}_4 = 0.095 \text{ cm}^{-1}.$$

When the beam is transmitted through a column filled with light phase, the number of counts per minute recorded by the counter will be determined by the formula

$$n' - n_0 = C e^{-\mu x}; \quad (10-1)$$

here n' is the number of counts per minute as the beam is transmitted through the light phase;

n_b is the count in background unit;

μ is the γ -ray absorption coefficient of the light phase;

x is the thickness of the irradiated layer;

C is some constant taking into account the radiation intensity, the efficiency of the counter, cross-sectional area of the outlet channel in the counter casing, and the distance between the emitter and the counter.

When a beam is transmitted through a column filled with heavy phase,

$$n' - n_b = Ce^{-\mu x}. \quad (10-2)$$

Where n' is the number of counts per minute as the beam is transmitted through the heavy phase;

n_b is the background of counter;

μ is the γ -ray absorption coefficient of the heavy phase.

When the beam is transmitted through the mixture,

$$n_m - n_b = Ce^{-\mu_m x}; \quad (10-3)$$

here, n_m is the number of counts per minute as the beam is transmitted through the mixture;

$n_{b,m}$ is the background of counter;

μ_m is the γ -ray absorption coefficient of the mixture.

The magnitude of μ_m can be determined from the formula

$$p_n = p''q + p'(1-q). \quad (10-4)$$

Let us divide Equation (10-3) by Equation (10-2):

(10-5)

$$\frac{a_n - a_{n-1}}{a' - a'_1} = e^{-x(p_n - p')}; \quad p_n - p' = q(p'' - p');$$

$$\frac{a_n - a_{n-1}}{a' - a'_1} = e^{-xq(p'' - p')}; \quad q = \frac{\frac{1}{x} \ln \frac{a' - a'_1}{a_n - a_{n-1}}}{p'' - p'}.$$

In dividing Equation (10-3) by Equation (10-1) we get:

(10-6)

$$q-1 = \frac{\frac{1}{x} \ln \frac{a' - a'_1}{a_n - a_{n-1}}}{p'' - p'}.$$

Radioactive isotopes are used as a source of γ -ray radiation; most often the radioactive isotope of cobalt, Co^{60} , is used, which has a long half-life (~ 5 years) and produces hard γ -radiation, adequate even when a bubbler with thick metal walls (steel walls up to 100 mm and more) is used.

In bubblers of small cross section, or when tests are conducted in the range of low mixture densities, it is desirable to change to isotopes which give a radiation with a high attenuation factor -- soft γ -radiation or even β -radiation of high intensity. With small bounding-wall thickness, this does not present any difficulties. With considerable wall thickness, the use of weakly penetrating radiation is also possible if at the points of

measurement the wall has a conduit of small diameter (1 to 2 mm) separated from the cavity (which is under high pressure) by a thin layer of metal.

The thickness of this layer, when the channel diameter is small, can be decreased to as low as 0.05 to 0.1 mm, even at high steam pressures (100 to 200 atm. abs.). At very high fractions of gas (measurements in the range of a system of "drops in gas"), one should consider the error introduced by the liquid layer trickling down the wall. In a number of cases this error can be reduced by covering the wall with a hydrophobic film. It is also possible to conduct "control" experiments, in which both the gas in the space and the layer of liquid on the wall would remain, but in which the drops in the stream would be eliminated.

REFERENCES

1. Abramovich, G. N., Prikladnaya gazovaya dinamika [Applied Gas Dynamics], Gostekhnizdat, 1953.
2. Aglintsev, K. K., Dozimetriya ioniziruyushchikh izlucheniya [Dosimetry of Ionizing Radiations], Gostekhnizdat, 1950.
3. Aksel'rod, L. S. and Dil'man, V. V., Udel'nyy ves gazo-zhidkostnoy emul'sii pri barbotazhe [Specific Gravity of a Gas-Liquid Emulsion during Bubbling], "Khimicheskaya promyshlennost" [Chemical Industry] Nr 1, 1954.
4. Aksel'rod, L. S. and Dil'man, V. V., Rabota setchatykh barboterov pri malykh skorostyakh gaza [Performance of Mesh Bubblers at Low Gas Velocities], "Kislород" [Oxygen] Nr 5, 1952.
5. Armand, A. A., Soprotivleniye pri dvizhenii dvukhfaznoy sistemy po gorizontальnym trubam [Resistance to Motion of a Two-Phase System in Horizontal Tubes], Izv. VTI [Bulletin of the Thermo-Technical Institute] Nr 1, 1946.
6. Armand, A. A. and Treshchev, G. G., Issledovaniye soprotivleniya pri dvizhenii paro-vodyanoy smesi v obogrevayemoy kotel'noy trube pri vysokom davlenii [Study of the Resistance to Motion of Steam-Water Mixture in a Heated Boiler Tube Under High Pressure], Izv. VTI, Nr 4, 1947.
7. Armand, A. A., and Nevstruyeva, Ye. I., Issledovaniye mekhanizma dvizheniya dvukhfaznoy smesi v vertikal'noy trube [Study of the Mechanism of Motion of a Two-Phase Mixture in a Vertical Tube], Izv. VTI, Nr 2, 1950.

8. Bagotskaya, I. A., Skorost' padeniya kapel' rtuti v вязкой среде
 [Fall Velocity of Mercury Drops in a Viscous Medium], ZhFKh
 [Journal of Physical Chemistry] Vol XXIV, Nr 1, 1950.
9. Blinov, V. I. and Feynberg, Ye. L., O pul'satsii strui i razryve
 yeye na kapli [Jet Oscillation and Break Down into drops], ZhTF
 [Journal of Technical Physics] Vol III, Nr 5, 1933.
10. Bochkarev, V. Keirim-Marcus, I., L'vova, M., Pruslin, Ya.,
 Izmereniye aktivnosti istochnikov β - i γ -izlucheniya [Measure-
 ment of the Activity of β and γ Radiation Sources], Izd. AN
 SSSR, 1953.
11. Borishanskiy, V. M., K voprosu ob obobshchenii opytnykh dannykh
 po prekrashcheniyu pumyr'kovogo kipeniya v bol'shom ob'yeme
 zhidkosti [Generalization of Experimental Data on the Cessation
 of Nucleate Boiling in a Large Volume of Liquid], Trudy TsKTI
 [Trans. of the Central Turbine and Boiler Institute], Book 28,
 Mashgiz, 1955; ZhTF, 2, 1956.
12. Borishanskiy, V. M., Vliyaniye davleniya i svoystv zhidkosti na
 prekrashcheniye plenochnogo kipeniya, sb. "Voprosy teploobmena
 pri izmenenii agregatnogo sostoyaniya veshchestva" [Effect of
 Pressure and Properties of a Liquid on the Cessation of Film
 Boiling, Symposium: "Problems of Heat Transfer During Changes in
 the State of Aggregation of Substances"], Gosenergoizdat, 1953.
13. Brodermon, S. M., Baldina, O. M., Sorin, A. R. Issledovaniye
 tsirkulyatsii pri vysokom davlenii [Investigation of Circulation
 under High Pressure], "Sovetskoye kotloturbostro-yeniye" [Soviet
 Turbine and Boiler Construction], Nr 1-2, 1941.
14. Veksler, V. I., Ionizatsionnyye metody issledovaniya izlucheniya
 [Ionization Methods of Radiation Investigation], Gostekhnizdat,

1950.

15. Veber, K., Raspad strui zhidkosti, sb. "Dvigateli vnutrennego sgoraniya" [Break-up of Liquid Jet, Symposium: Internal Combustion Engines], Vol I, ONTI [United Sci. and Tech. Pub. Houses], 1936.
16. Vitman, L. A., Issledovaniye plotnosti orosheniya raspylennoy strui zhidkosti, sb. nauchnykh rabot inzh. f-ta Leningrad. sel'skokhoz. inst. [Investigation of the Spray Density of an Atomized Liquid Jet, Collection of Scientific Papers of Eng'g. Faculty of Leningrad Agric. Inst.], Vol XI, Sel'khozgiz, 1955.
17. Vitman, L. A., Raspylivaniye vyazkoy zhidkosti forsunkami net-sentrifuzhnogo tipa, sb. nauchnykh rabot inzh. f-ta Leningrad. inst. mekhanizatsii sel'skogo khozyaystva [Atomization of Viscous Liquid by Non-Centrifugal Type Spray Nozzles. Collection of Scientific Papers of Leningrad Inst. of Agric. Mechanization], Vol X, 1953.
18. Volynskiy, M. S., Izucheniye drobleniya kapel' v gazovom potoke [Investigation of Bubble Break-up in a Gas Flow], DAN SSSR [Proceedings of the USSR Academy of Sciences], Vol 68, Nr 2, 1949.
19. Voprosy teploobmena pri izmenenii agregatnogo sostoyaniya veshchestva, sb. statey pod red. S. S. Kutateladze [Problems of Heat Transfer During Changes in the State of Aggregation of Substances, symposium edited by S. S. Kutateladze], Gosenergoizdat, 1953.
20. Ganyan, G. S., Kharakteristicheskaya teoriya dvizheniya dvukhfaznoy smesi po vertikal'nym trubam [Characteristic Theory of the Motion of Two-Phase Mixtures in Vertical Tubes], "Neftyanoe

- khozyaistvo," *[Petroleum Economy]* Nr 8-9, 1950.
21. Gorodetskaya, A., Skorost' podnyatiya puzyr'kov v vode i vodnykh rastvorakh pri bol'shykh chislakh Re *[Ascent Velocity of Bubbles in Water and Aqueous Solutions at High Reynolds Numbers]*, *ZhFKh*, Vol XXIII, Ed 1, 1949.
 22. Gremilov, D. I., Issledovaniye dvizheniya paro-rtutnoy smesi v trubakh *[Investigation of the Motion of a Vapor-Mercury Mixture in Tubes]*, *Trudy TsKTI*, Book 23, 1952.
 23. Dement'yev, B. L., O vliyaniy diametra kolonki i davleniya na parosoderzhaniye vodyanogo ob'yema ustroystv s barbotazhem para cherez vodu *[Effect of Column Diameter and Pressure on the Steam Content of a Volume of Water in Equipment in Which Steam is Bubbled Through Water]*, "Teploenergetika," *[Thermal-Power Engineering]* Nr 4, 1957.
 24. Zysina-Molochan, L. M., and Kutateladze, S. S., K voprosu o vliyaniy davleniya na mekhanizm paroobrazovaniya v kipiyashchey zhidkosti *[Concerning the Effect of Pressure on the Mechanism of Vaporization in a Boiling Liquid]*, *ZhTF*, Nr 1, 1950.
 25. Ioffe, A. F., and Semenov, N. N., Kurs fiziki *[Physics Course]* Part IV, Gostekhizdat, 1933.
 26. Kazakova, Ye. A., O maksimal'nom teplovom potoke pri kipenii vody pod vysokim i sverkhvysokim davleniyami *[Maximum Heat Flux in Water Boiling Under High and Very High Pressures]*, Izv. AN SSSR, OTN *[Department of Technical Sciences]*, 9, 1950.
 27. Kapitsa, L. P., Vzhivoye techeniye tonkikh sloev vyazkoy zhidkosti *[Wave Flow of Thin Layers of a Viscous Liquid]*, *ZhETF* *[Journal of Experimental and Theoretical Physics]* Nr 1, 1948.
 28. Kolmogorov, A. N., O droblenii kapel' v turbulentnom potoke

- Drop Break-up in Turbulent Flow], DAN SSSR, Vol 66, Nr 5, 1949.
29. Konstantinov, N. N., Gidravlika dvukhfaznogo potoka i yeye primeneniye k raschetam erliftov, gidravlicheskiy zatvorov, i tsirkulyatsii v vertikal'no-vodotrubnykh parovykh kotlakh [Hydraulics of Two-Phase Flow and its Application to Design of Airlifts, Hydraulic Gates, and Circulation in Vertical Water-Tube Steam Boilers], Issledovaniye i primeneniye nefteproduktov [Research and Application of Petroleum Products], Nr 2, Gostoptekhnizdat [Pub. Hse. of Petrol. & Mineral-Fuel Industry], 1950.
30. Kosterin, S. I., Issledovaniye vliyaniya diametra i raspolzheniya truby na gidravlicheskiye soprotivleniye i strukturu techeniya gazo-zhidkostnykh smesey [Investigation of the Influence of the Diameter and Tube Position on Hydraulic Resistance and Flow Pattern of Gas-liquid Mixtures], Izv. AN SSSR, OTN, Nr 12, 1949.
31. Kuz'minykh, I. N., Rodionov, A. I., Gidrodinamicheskiye ispytaniya barbotazhnykh sitchatykh tarellok pri razlichnom ikh ustroystve [Hydrodynamic Tests of Bubble Sieve Plates of Different Design], Trudy Mosk. Khimiko-tekhnol. inst. im. D. I. Mendeleyeva [Trans. of the D. I. Mendeleyev Moscow Chemical Engineering Institute], Nr XVIII, 1954.
32. Kurbatov, A. V., Barbotazh i problema kriticheskikh nagruzok v paroseparatsii [Bubbling and the Problem of Critical Loads in Steam Separation], Trudy Moskovskogo energeticheskogo instituta, [Trans. of the Moscow Power Engineering Institute] Nr XI, Gosenergoizdat, 1953.
33. Krasyakova, L. Yu., Issledovaniye dvizheniya dvukhfaznoy smesi

- v gorizontal'noy trubke [Study of the Motion of a Two-Phase Mixture in a Horizontal Tube], ZhTF, Nr 4, 1952
34. Kutateladze, S. S., Dvizheniye dvukhfaznogo potoka v trubakh [Two-Phase Flow in Tubes], "Kotloturbostroyeniye," [Boiler and Turbine Design], Nr 6, 1947.
 35. Kutateladze, S. S., Dvizheniye paro-zhidkostnoy smesi v trubakh i obobshchennyye koordinaty dlya yego analiza [Motion of Vapor-Liquid Mixtures in Tubes, and Generalized Coordinates for its Analysis], "Kotloturbostroyeniye", Nr 2, 1946.
 36. Kutateladze, S. S., Teploperedacha pri kondensatsii i kipenii [Heat Transfer During Condensation and Boiling], Mashgiz, 1952.
 37. Kutateladze, S. S., Osnovy teorii teploperedachi pri izmenenii agregatnogo sostoyaniya [Bases of the Theory of Heat Transfer during Changes in the State of Aggregation], Mashgiz, 1939.
 38. Key and Lebi, Spravochnik fizika-eksperimentatora [Research Physicist's Handbook], IL, 1949.
 39. Laditskiy, V. P., Temperaturnyye usloviya raboty stenok gorizontal'no raspolozhennykh trub ispar'yayushchey poverkhnosti nagreva parovykh kotlov [Operating Temperature of the Walls of the Horizontal Tubes of the Vaporizing Heating Surfaces of Steam Boilers], Trudy TskTI, Book 10, Mashgiz, 1948.
 40. Ladyzhenskiy, R. M., Issledovaniye dvizheniya vozdušnogo puzyr'ka v vode pri vysokikh znacheniyakh Re [Investigation of the Motion of an Air Bubble in Water at High Re], ZhPKh, [Journal of Applied Chemistry], Vol XXVII, Nr 1, 1954.
 41. Levich, V. G., Fiziko-khimicheskaya gidrodinamika [Physico-chemical Hydrodynamics], Izd. AN SSSR, 1952.
 42. Loshkin, A. N., Krol', P. I., O mekhanizme kipeniya rtuti v

- elementakh rtutnogo parogenerators [Mechanism of Mercury Boiling in Elements of a Mercury-Vapor Generator], ZhTF, Vol VIII, Nr 21, 1938.
43. Loytsyanskiy, L. G., Mekhanika zhidkosti i gaza [Liquid and Gas Mechanics], Gostekhizdat, 1950.
44. Margulova, T. Kh., Eksperimental'noye issledovaniye otnositel'noy skorosti para pri barbotazhe ego cherez sloy vody pri sverkhvysokikh davleniyakh [Experimental Investigation of Relative Velocity of a Vapor Bubbling Through a Layer of Water at Super-High Pressures], Trudy Moskovskogo energeticheskogo instituta [Trans. Moscow Power Engineering Institute], Nr XI, Gosenergoizdat, 1953.
45. Meshcherskiy, I. V., Raboty po mekhanike tel peremennoy massy [Papers on the Mechanics of Bodies of Variable Mass], Gostekhizdat, 1952.
46. Miropol'skiy, Z. L. and Styrikovich, M. A., Primeneniye γ -luchey dlya izucheniya gidrodinamiki dvukhfaznykh sistem [The Use of γ -Rays in the Study of the Hydrodynamics of Two-Phase Systems], Izv. AN SSSR, OTN, Nr 9, 1955.
47. Molochin, M. A., Formy tekniya gazozhidkostnoy smesi v gorizontal'nykh trubakh [Flow Patterns of a Gas-Liquid Mixture in Horizontal Tubes], DAN SSSR, Vol 124, Nr 5, 1954.
48. Normy rascheta tsirkulyatsii vody v parovykh kotlakh [Standard Design Procedures for Water Circulation in Steam Boilers], Trudy TSKEI, Book 15, Mashin, 1950.
49. Ornatskiy, A. P., Vliyaniye skornosti zhidkosti na velichinu maksimal'noy teplovoy nagruzki pri vynuzhdennom potoke kipyashchey zhidkosti [Effect of Liquid Velocity on the Maximum Thermal

- Load in Forced Flow of a Boiling Liquid/, Trudy Inst. teplo-energetiki AN UKSSR [Trans. of the Thermal Power Engineering Institute of the UKSSR Academy of Sciences], 12, 1950.
50. Peterson, D. F., K voprosu ob otnositel'nom dvizhenii para i vody v trubakh parovykh kotlov [Concerning the Relative Motion of Steam and Water in Steam Boiler Tubes], "Sovetskoye kotlo-turbostroyeniye," Nr 4, 1936.
 51. Pletneva, N. A., Rebinder, P. A., Zakonomernosti ispareniya kapel' zhidkosti v sferoidal'nom sostoyanii [Laws Governing Vaporization of Liquid Drops in a Spheroidal State], ZhFKh, Vol XX, Nr 9, 1946.
 52. Pozin, M. Ye., and Tumarkina, Ye. S., O vliyani fizicheskikh svoystv zhidkosti na obrazovaniye podvizhnoy peny [Effect of the Physical Properties of a Liquid on the Formation of Movable Foam], ZhPKh, Vol XXVII, Nr 11, 1954.
 53. Pozin, M. Ye. and Tumarkina, Ye. S., O podavlenii peny khorosho rastvorimymi gazami [Suppression of Foam by Highly Soluble Gases], ZhPKh, Vol XXVII, Nr 11, 1954.
 54. Pomerantsev, V. V., Syrkin, S. N., K voprosu o mekhanizme yestestvennoy tsirkulyatsii v parovykh kotlakh [Concerning the Mechanism of Natural Circulation in Steam Boilers], Trudy TsKTI, 8, 1948.
 55. Reley, Teoriya zvuka [Theory of Sound], Vol 11, Gostekhizdat, 1944.
 56. Roddatis, K. F., Lokshin, V. A., Eksperimental'nye kharakteristiki yestestvennoy tsirkulyatsii pri vysokom davlenii [Experimental Characteristics of Natural Circulation at High Pressure], Izv. VTI, Nr 4, 1941.

57. Roddat's, K. P., Prizhailkovskiy, M. N., O temperaturnom rezhime metalla naklonnykh i obogrevayemykh trub Temperature Regime in the Metal of Inclined and Heated Tubes, Izv. VTI, 7, 1949.
58. Smirnov, N. I. and Polyuta, S. Ye., Istecheniye puzyr'kov vozdukha v zhidkuyu sredu Air Bubble Discharge into a Liquid Medium, ZhPKh, Vol XXII, Nr 11, 1949.
59. Smirnov, N. I. and Ruban, V. L., Skorost' dvizheniya kapel' v zavisimosti ot skorosti dvizheniya sredy Velocity of Drop Motion as a Function of the Velocity of Motion of the Medium, ZhPKh, Vol XXII, Nr 11, 1949.
60. Smirnov, N. I. and Ruban, V. L., Otnositel'naya skorost' dvizheniya kapel' v perekhodnoy oblasti Relative velocity of Drop Motion in the Transition Region, ZhPKh, Vol XXIV, Nr 1, 1951.
61. Sterman, L. S., Surkov, A. V., Ispol'zovaniye γ -luchey dlya opredeleniya ob'yemnogo napornogo parosoderzhaniya i istinnogo urovnya v apparate The Use of γ -Rays for Determination of the Volumetric Vapor Content in Terms of Pressure, and of the True Level in an Apparatus, Teploenergetika, 1955, Nr 8.
62. Styrikovich, M. A., V strukturnyye protsessy Processes Inside a Boiler, Gosenergolizdat, 1954.
63. Styrikovich, M. A., et al., Generatsiya para sverkhvysokikh parametrov Generating Super-High Parameter Steam, MEI, (Moscow Power Engineering Institute), ENIN, (Power Engineering Institute), 1951.
64. Styrikovich, M. A. and Polyakov, G. M., O kriticheskoy teplovoy nagruze pri kipenii zhidkosti v bol'shom ob'yeme Critical Thermal Load in the Boiling of Large Volumes of Liquid, Izv. AN SSSR, OTN, 5, 1951.

65. Styrikovich, M. A. and Kholodovskiy, G. Ye. Issledovaniye tsirkulyatsii v parogeneriruyushchikh trubakh pri vysokikh davleniyakh vodnogo para [Investigation of Circulation in Steam-Generating Tubes at High Steam Pressures], Izv. AN SSSR, OTN, 4, 1951.
66. Styrikovich, M. A. and Miropol'skiy, Z. L., Temperaturnyy rezhim gorizonta'nykh parogeneriruyushchikh trub pri vysokikh davleniyakh [Temperature Regime of Horizontal Vapor-Generating Tubes under High Pressures], Izv. AN SSSR, OTN, 4, 1951.
67. Styrikovich, M. A. and Shitsman, M. Ye. Temperaturnyy rezhim vertikal'nykh parogeneriruyushchikh trub pri sverkhvysokom davlenii, sb. "Teploobmen i gidrodinamika v kotlakh vysokogo davleniya" [Temperature Regime of Vertical Steam-Generating Tubes at Super-High Pressures, symposium "Heat Transfer and Hydrodynamics in High Pressure Boilers"], Izd. AN SSSR, 1954.
68. Teletov, S. G., Uravneniya gidrodinamiki dvukhfaznykh zhidkostey [Hydrodynamic Equations for Two-Phase Liquids], DAN SSSR Vol 4, 1945.
69. Teletov, S. G., O maksimal'nom razmere parovogo puzrya [Maximum Size of a Vapor Bubble], AN SSSR, Izv. Energ. Inst., Vol XI, 1940.
70. Tochilovskiy, B. I., O chastote vstryva puzry'kov v kipyaschuyu zhidkost' [Frequency of Bubble Release into a Boiling Liquid], Trudy Odesk. Tekhnol. Inst. pishchevoy i kholodil'noy prom. [Trans. of the Odessa Technological Institute of the Food and Refrigeration Industry], Vol V, Nr 1, 1952.
71. Frank-Kamenetskiy, L. A., Diffuziya i teploperedacha v khimicheskoy kinetike [Diffusion and Heat-Transfer in Chemical

- Kireevskiy, I. A., *ibid.*, 1954.
72. Chirkov, V. A., and Yudin, V. P., Kritis'ye teplos'yema v potoke nekippashchey vody dlya kol'tseвого zazora [Critical Conditions of Heat Removal in a Flow of Non-Boiling Water for an Annular Space], *ZhTF*, Nr 7, 1956.
 73. Shvab, V. A., Teoreticheskiye osnovy dvizheniya dvukhfaznogo potoka primer: del'no k raschetu tsirkulyatsionnogo kontura parovogo kotla [Elements of Two-Phase Flow Theory for the Design of Steam Boiler Circulation Loops], *Tomsk*, 1949.
 74. Behringer, Ph., *VDI Forschungsheft*, S. 365, 1934.
 75. Hadamard, *Comp. Rend.*, 192, 1735, 1911.
 76. Lane, W. R., Shatter of Drops in Streams of Air, *Ind. and Eng. Chemistry*, June, 1901.
 77. Miyagi Otoguro, The Motion of an Air Bubble Rising in Water, *Phil. Mag.*, Vol 50, 1925.
 78. Martinelli, Boller, *Transactions of the ASME*, 2, 1944.
 79. Peebles, F., and Garber, H., Studies on the Motion of Gas Bubbles in Liquids, *Chem. Eng. In.*, February, 1953.
 80. Ryberginski, *Bull. de Cracovie (A.)*, 1911, p 40.
 81. Troesch, H., *Chemi.-Ingenieur-Technik*, 6, 1954 (Liquid Atomization, Russian translation in mag. "Raketnaya tekhnika," [Rocket Technology], Nr 6, 1954).

UNCLASSIFIED

UNCLASSIFIED